Non-viral Transfection and Direct Reprogramming of Fibroblasts to Neurons and Glia:

Importance of Physical and Chemical Microenvironments

by

Andrew Frederick Adler

Department of Biomedical Engineering
Duke University

Date:_____

Approved:

_____
Kam W. Leong, Supervisor

_____
Ashutosh Chilkoti

_____
Charles A. Gersbach

_____
Brenton D. Hoffman

_____
Anne E. West

Dissertation submitted in partial fulfillment of
the requirements for the degree of Doctor
of Philosophy in the Department of
Biomedical Engineering in the Graduate School
of Duke University

2014

ABSTRACT

Non-viral Transfection and Direct Reprogramming of Fibroblasts to Neurons and Glia:

Importance of Physical and Chemical Microenvironments

by

Andrew Frederick Adler

Department of Biomedical Engineering
Duke University

Date:_____

Approved:

_____
Kam W. Leong, Supervisor

_____
Ashutosh Chilkoti

_____
Charles A. Gersbach

_____
Brenton D. Hoffman

_____
Anne E. West

An abstract of a dissertation submitted in partial fulfillment of
the requirements for the degree of Doctor
of Philosophy in the Department of
Biomedical Engineering in the Graduate School
of Duke University

2014

Abstract

The recent discovery that fibroblasts can be reprogrammed directly to functional neurons with lentivirus has reinvigorated the belief that autologous human cell therapies against many neurodegenerative diseases may be achievable in the near future. To increase the clinical translatability of this approach, we have developed a technique to perform this direct conversion without the use of virus. We transfected fibroblasts with plasmids condensed into non-viral nanoparticulate carriers with a bioerodible peptidomimetic polymer, pCBA-ABOL. Gene delivery with pCBA-ABOL was exceptionally effective and nontoxic, producing high transfection efficiencies and enabling serial dosing of plasmid cocktails. We delivered plasmids encoding neural lineage-instructive transcription factors to primary mouse embryonic fibroblasts (PMEFs), eliciting: drastic morphological changes, activation of endogenous neuronal transcription factor expression, neuronal promoter activity, and the appearance of neuronal proteins. Serial dosing of pCBA-ABOL complexes produced increasingly higher yields of these non-virally induced neurons (NiNs). The majority of NiNs fired action potentials under patch clamp. This is the first description of a method capable of directly inducing functional neuronal cells from fibroblasts without the use of virus.

We then moved on to further increase the yield of NiN generation, in an effort to produce a sufficient quantity of neurons for cell therapies. Informed by neurodevelopmental cues and by precedents set by the induced pluripotent stem cell (iPSC) field, we performed non-viral neuronal reprogramming in the presence of soluble microenvironmental factors that either inhibited GSK-3β and SMAD signaling, or

induced chronic membrane depolarization. Chronic depolarization doubled the number of cells expressing neuronal markers produced with glutamatergic as well as with dopaminergic transcription factor cocktails. Inhibition of GSK-3β and SMAD signaling similarly doubled the yield of glutamatergic NiNs, and enabled induction of neuronal markers and morphological transformation in human fibroblasts.

In addition to soluble microenvironmental factors, the physical microenvironment can also strongly influence various cellular phenotypes. This list includes many phenotypes related to endocytosis – the transit mechanism of nanoparticulate gene carriers entering cells during non-viral transfection. As such, we set out to determine if patterned physical substrate topography could be used to increase non-viral transfection. We employed a high-throughput screen of micropitted substrate topographies, and indeed found that larger, denser micropits could support significantly higher transfection efficiencies in fibroblasts compared to smooth substrates. The same topographies produced higher reverse transfection efficiencies, and greater siRNA-mediated knockdown of a reporter gene. The control of transfection with substrate topography is a new design parameter that could find broad application in *in vitro* non-viral reprogramming strategies, as well as in the intelligent design of nucleic acid-eluting scaffolds *in vivo*.

Encouraged by our success with direct neuronal reprogramming, and armed with a greater understanding of some microenvironmental mediators thereof, we attempted to produce non-virally-induced oligodendroglial progenitor cells (NiOPCs), which has been historically challenging for other investigators. We discovered the fibroblastic intracellular microenvironment is a significant barrier to the function of Olig2 – a master

regulator of OPC phenotype – in direct reprogramming. Fibroblasts do not express Olig2 chaperones which are normally expressed in OPCs, causing Olig2 to become sequestered in the cytoplasm of transfected PMEFs. We relieved this barrier through fusion of a strong nuclear localization sequence (NLS) to Olig2, which repartitioned Olig2-NLS from the cytoplasm to the nucleus in transfected fibroblasts. The use of Olig2-NLS in iOPC reprogramming cocktails resulted in a drastic improvement in the yield of OPC-specific marker expression. The improvement associated with Olig2-NLS was insufficient to elicit significant myelin protein expression with the non-viral system, but the yield of virally-induced oligodendrocyte-like cells (iOLs) was improved dramatically. Further enhancements will be required to generate fully-reprogrammed NiOPCs, but the increased efficiency of viral iOPC generation is immediately useful for disease modeling and potentially in cell replacement therapies if human cells can be converted for the first time using this technique. During direct reprogramming, CNS-specific transcription factors are delivered to foreign intracellular contexts as a rule, which may reduce their ability to function effectively; we have shown this can be a critical yet under-appreciated determinant of the success or failure of a direct reprogramming system.

Taken together, the technological and intellectual advancements we describe herein represent significant improvements to non-viral transfection and reprogramming systems. These techniques can find broad appeal to the many researchers and clinicians deploying these systems. More specifically, we present significant steps towards realization of the dream of safe and effective autologous cell therapies against devastating and currently-intractable neurodegenerative diseases.

This dissertation is dedicated to my parents,

Mark and Diane Adler,

and to my grandparents,

(Elsie and Norm Ek), and (Lois) and Fred Adler,

who together inspire(d), enable(d), and nurture(d) my love of exploration.

Table of Contents

List of Figures

Acknowledgements

This work could not have been started or completed without the support, sacrifice, stimulation, and humor of all of my friends, family, and colleagues – groups between which clear distinctions are often difficult to draw. First, let me acknowledge the unbroken emotional, intellectual, and financial support of my parents Mark and Diane; thank you for making all three of these sustenances freely available to me for my entire life. And to my brother, Rob: two out of three ain't bad! I love you all. I feel the same deep appreciation for the entirety of my family – grandparents, aunts, uncles, and cousins – thank you so much for the nurturing environment you have all provided to me.

Fittingly bridging the gap between my familial and scientific acknowledgments, I go on to attempt to express my gratitude to Prof. Kam Leong for his selfless patience, thoughtfulness, guidance, availability, and optimism, regardless of circumstance. You created an environment that allowed us to discover and create things that have never been seen before – for me there may be no greater joy. Similarly, the other members of my committee – Profs. Hoffman, Gersbach, Chilkoti, and West – have all been inspirational not only for their skilled performance of science, but even moreso for their obvious love and enjoyment of the process, and their willingness to share that excitement with me through always open doors and ears, and sometimes over open beers.

Thank you Prof. Reichert and CBTE for funding two years of my time at Duke. Thanks to Profs. Narasimhan, Shea, and Baldwin, and to your labs, for warmly and completely welcoming me into your scientific families. Thank you Carla Sturdivant, Kathy Barbour, Malathi Chellappan, and Joyce Franklin – without you none of us could

be here, and I certainly wouldn't have enjoyed my time at Duke as much as I have. Thank you to my fellow lab members, past and present, who made life fun, kept me rigorous, and pushed me to new areas of science that I now happily call home – especially Nicolas Christoforou, Karina Kulangara, and Megan Ho.

I want to particularly thank my friend and colleague Chris Grigsby, for being an integral part of both the professional and recreational aspects of what I will always consider to be some of the best years of my life. Similar thanks to Sarah MacEwan, Jon McDaniel, Alex Kent, Matt Novak, Jenny Gamboa, Katie Glass, Lauren Polstein, Megan Godsey, Leigh Atchison, and Allie Speidel. Lauren Polstein and Josh Black have also been fabulously invigorating new collaborators on the home stretch of my PhD – I hope to continue to work with you both for a long time. Thank you Julep Adler, for being my constant joyful and curious companion on this journey, all the way from NC to CA to MA, and for giving me perspective through your defiant happiness in the face of illness.

Finally, an insufficient thank you to Haruna Suzuki. Thank you for your positivity, kindness, scientific discussion, demented humor, and selfless love for me and Julep and your friends and everyone you know and meet and hear about. You are a courageously positive force in all of our lives, and a personal inspiration to me in every possible way.

Andy

Chapter 1: Introduction

1.1 Specific aims

The objective of this dissertation is to present new methods to increase the effectiveness of non-viral gene transfer and cellular reprogramming, as applied to the direct conversion of "terminally-differentiated" fibroblasts to neurons and glia. The generation of these non-virally induced neuronal (NiN), oligodendroglial progenitor cells (NiOPCs), and oligodendrocytes (NiOLs) is expected to lead to the first ethically-viable (non-embryonic) and safe (non-teratogenic and non-retroviral) autologous human cell sources for cell therapies against neurodegenerative disorders that currently lack curative treatment options. *The specific aims* developed in this dissertation are: **(1)** the first demonstration of non-viral direct conversion of fibroblasts to functional neuronal cells, **(2)** the improvement of iN yields with developmentally-inspired microenvironmental factors, **(3)** the first demonstration that physical substrate topography can be used to enhance non-viral gene transfer, and **(4)** the discovery and circumvention of a fibroblastic intracellular microenvironmental context that strongly represses their direct conversion to iOPCs. The results of these specific aims are summarized in Figure 1.

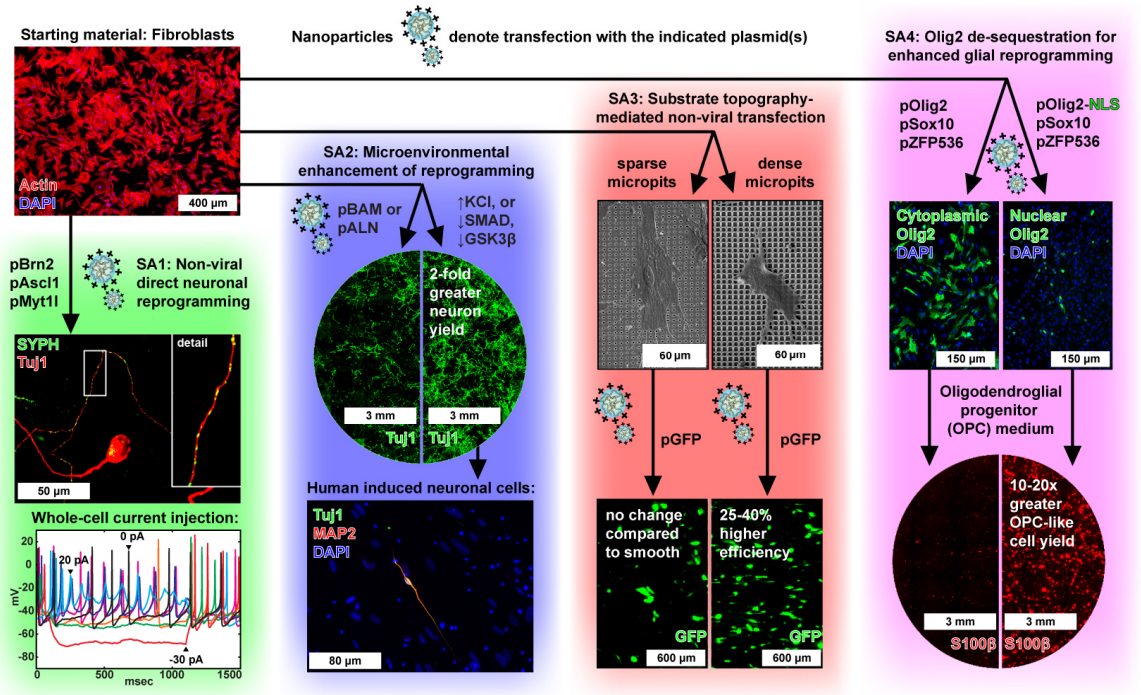

Figure 1. Summary of specific aims
SA1: Fibroblasts were directly converted to functional neurons without the use of virus. SA2: The efficiency of non-viral neuronal reprogramming was significantly improved with soluble microenvironmental factors that chronically depolarized the cells or inhibited SMAD and GSK-3β signaling. SA3: Micropitted substrate microtopographies that improve non-viral transfection were discovered with a high-throughput screening approach. SA4: Relief of cytoplasmic sequestration of Olig2 expressed ectopically in fibroblasts by genetic fusion with a nuclear localization sequence (NLS) greatly increases the induction of oligodendroglial markers during direct reprogramming.

1.1.1 Specific aim 1: Non-viral direct neuronal reprogramming

Hypothesis 1: Non-viral neuronal transdifferentiation of fibroblasts into neuronal cells that fire trains of action potentials can be achieved, and can benefit from multiple serial doses of transcription factor-encoding plasmid DNA to produce high conversion efficiencies. Poly(CBA-ABOL) is a uniquely nontoxic and effective non-viral gene carrier, and will be better-suited for this application than commercial reagents. **Chapter 3:** Here we demonstrated the feasibility of non-viral neuronal transdifferentiation. We modified the first published lentiviral direct neuronal reprogramming technique – the delivery of the glutamatergic neuronal transcription factors Brn2, Ascl1, and Myt1l

(BAM factors) to primary mouse embryonic fibroblasts (PMEFs) – with a non-viral nontoxic bioreducible polymeric nanoparticle gene transfer system. We optimized the polymer-to-DNA mass ratio and DNA dose to produce robust and nontoxic transgene expression in PMEFs. A multiple dose transfection scheme was then developed to maintain high levels of transgene expression during the transdifferentiation process, and the effectiveness of these multiple doses was quantified by the induced expression of neuron-specific tubulin 1 (Tuj1) protein. Non-virally-induced neuronal cells (NiNs) expressed a panel of other neuronal proteins and transgenic neuron-specific reporters. The most-mature NiNs were identified with a neuron-specific synapsin-RFP reporter lentivirus and were patch-clamped, revealing their ability to generate spontaneous and evoked trains of action potentials.

1.1.2 Specific aim 2: Improved direct neuronal reprogramming by control of extracellular microenvironments

Hypothesis 2: Extracellular microenvironmental factors can improve NiN yields. Specifically, chronic depolarization or inhibition of GSK-3β and SMAD signaling will increase the number of NiNs generated with the BAM or ALN cocktails. **Chapter 4:** With the proof-of-concept developed in SA1, we moved on to attempt the production of dopaminergic (DA) neurons, a clinically-relevant neuronal subtype with future utility in cell therapy against Parkinson's disease. Accordingly, we used the methods in SA1 with a dopaminergic transcription factor cocktail: Ascl1, Lmx1b, and Nurr1 (ALN factors). DA neurons are induced with less efficiency than are glutamatergic neurons, and the

human cells required for translation are significantly more refractory to conversion. Therefore, the method developed in SA1 was modified to increase reprogramming efficiency for both target neuron subtypes. Following transfection with the BAM or ALN factors, we significantly boosted the yield of NiNs with the inclusion of 30 mM KCl to chronically depolarize the cells, or with the inclusion of the small molecules LDN-193189, CHIR-99021, and SB-431542 to inhibit GSK-3β and SMAD signaling. The increased efficiency afforded by the small molecules was sufficient to encourage the activation of non-virally-induced neuronal markers and morphology from a human fibroblast source. Taken together with our recent demonstration that lentiviral BAM neuron yields can be significantly increased by reprogramming PMEFs cultured on micrograting substrate topography, these results reveal the importance of extracellular physical and chemical microenvironments during multiple forms of direct iN reprogramming.

1.1.3 Specific aim 3: Improved non-viral transfection by control of the physical cellular microenvironment

Hypothesis 3: High-throughput screening will identify micropitted topographies that enhance forward and reverse non-viral transfection and siRNA-mediated knockdown, compared to smooth substrates. **Chapter 5:** Here, we sought to determine whether non-viral transfection efficiency could be improved by culture on controlled physical substrate topographies. A high-throughput image analysis-based screening method was employed to discover substrate topographies in a combinatorial array that encouraged the

most efficient transfection of a GFP reporter plasmid in primary human fibroblasts. This screening method used an optimized formulation of Lipofectamine 2000 – the most ubiquitous non-viral transfection reagent – in order to provide the most impact to the field. "Hits" discovered with imaging of the combinatorial topographic array were validated with flow cytometry, and the interaction of fibroblasts with these patterns was investigated with scanning electron and confocal microscopy. The generality of topographic enhancement of transfection efficiency was demonstrated by the improved reverse transfection and siRNA-mediated knockdown of cells on patterned substrate topographies with Lipofectamine 2000, as well as the improved transfection of PMEFs with pCBA-ABOL. When taken with our demonstration of improved viral BAM iN yield on micrograting, we expect that non-viral transfection for neuronal reprogramming performed on topography could benefit from both enhancements synergistically.

1.1.4 Specific aim 4: Improved direct glial reprogramming via circumvention of an impermissive intracellular microenvironment

Hypothesis 4: Viral and non-viral iOPC generation is inefficient compared to iN generation, and therefore suffers from additional barriers to completion of this process. Cytoplasmic sequestration of Olig2 is one of these barriers, and re-localization of Olig2 into the nucleus in reprogramming PMEFs will increase the induction of OPC and OL markers. **Chapter 6:** SA1-SA3 demonstrate and suggest new means that could be used to generate NiNs at greater and greater efficiencies, but one of the potential weaknesses of a direct-to-neuron reprogramming strategy for cell therapy is that the iNs exit the cell cycle

immediately upon successful conversion. It may be also desirable to generate proliferative but committed progenitors, to ease the requirement for very high conversion efficiencies before human cell therapy can be attempted. To investigate this possibility, we attempted viral and non-viral conversion of PMEFs to induced oligodendroglial progenitor cells (iOPCs) using Sox10, Olig2, and ZFP536 (SOZ factors). We observed that Olig2 was expressed throughout the cytoplasm in PMEFs transfected with Olig2, and at times was excluded from the nucleus. Genetic fusion of a strong nuclear localization sequence redistributed Olig2 inside fibroblast nuclei, and greatly increased the induction of $S100\beta^{+}O4^{+}$ iOPC-like cells, and the efficiency of MBP^{+} (myelin basic protein) iOL generation with virus.

1.2 Organization statement

Chapter 2 of this dissertation is a review of relevant background information. There are four subsequent research chapters, organized as a series of manuscripts, which are based on published articles, or have been prepared in a format compatible with submission for publication in peer-reviewed journals. As such, there may be a degree of repetition in some introductory materials and experimental protocols. The final chapter is a brief summary and recontextualization of the research presented herein.

Chapter 2: Background Information

A portion of Chapter 2 appears in: Emerging links between surface nanotechnology and endocytosis: impact on nonviral gene delivery. Adler AF, Leong KW. Nano Today. 2010 Dec 1; 5(6):553-569.

The common thread throughout this dissertation is the use of non-viral transfection, with a specific aim towards safer autologous cell therapies against neurodegenerative disease. First we provide background pertaining to the first phase of this goal – non-viral transfection. Non-viral gene transfer vectors are a relatively mature and thoroughly-reviewed technology, so we place a new emphasis on the known and potential microenvironmental modulators of the process, which are important but under-appreciated factors compared to the design of the vectors themselves. We then move on to review the current state of gene and cell therapies applied against neurodegenerative disease, how the recent discovery of direct reprogramming from fibroblasts to neurons and glia might overcome problems associated with ES and iPSC-based therapies, and why the development of non-integrative methods is important for the full realization of this dream. Finally, we look towards neurodevelopment and to known microenvironmental effectors of direct reprogramming to pluripotency, in an attempt to find new means to improve the yields of neurons and glia produced via the direct conversion of fibroblasts.

2.1 Non-viral gene delivery

Gene transfer techniques and therapies have enjoyed steady interest due to their current and potential application against a diversity of human illnesses [1] including diabetes, hemophilia, peanut anaphylaxis, and cystic fibrosis. In an effort to increase transfection efficiency and specificity, researchers and physicians often turn to carrier systems to deliver engineered genetic material to target cells and tissues. Generally, such carriers fall into one of two broad categories – viral or non-viral vectors. Viruses are naturally professional gene therapists, and have been reengineered to carry a myriad of therapeutic gene sequences. Despite their high efficiency, there are a number of drawbacks associated with viral vectors: they are typically more immunogenic than their non-viral counterparts, limited in DNA packaging capacity, and if randomly integrative can introduce significant levels of genotoxicity. These potential issues motivate the ongoing search for suitable alternatives, frequently in the form of particulate polymer- and lipid-DNA complexes, which are less toxic, are able carry larger genes, and are amenable to formulation optimization to provide prolonged circulation, targeted delivery, and improved storage stability.

In spite of their wide application, the mechanisms whereby DNA complexes are able to traverse the cellular, lysosomal, and nuclear membrane barriers to then induce transgene expression are only recently being elucidated, often with contradictory results for seemingly similar carriers. Efficient cellular internalization of the carrier-DNA complex is crucial to non-viral gene transfer. Increasing consideration has been given to nanoscale particulate parameters including size, shape, ligand decoration, and surface charge. These parameters have been shown to dictate the extent and pathway of endocytic

uptake, and the subsequent ability of the DNA to arrive intact within the nucleus, able to induce transgene expression.

While clearly important for successful non-viral transfection, particulate parameters do not fully account for the differences in transfection efficiency in vitro and in vivo; particle- and cell-substrate interactions have also been demonstrated to influence the uptake and expression of particulate non-viral vectors. When delivered from a surface, the ability of non-viral particles to induce gene expression depends not only on their local concentration, but also on the tightness of their adsorption, the presence of extracellular matrix (ECM) proteins, and substrate surface chemistry. Substrates with micro- and nano-patterned topographies could also directly influence the endocytic behavior and transfectability of interacting cells by inducing changes in proliferation, spreading, morphology, cytoskeletal arrangement, differentiation, and protein expression. Though potential molecular links have been described by molecular biologists, little is known about the functional interactions between DNA complexes, cell substrates, focal adhesions, and the cytoskeletal and endocytic machineries; this presents an exciting opportunity for the design of particles and substrates that are able to probe and exploit beneficial aspects of endocytic processes.

While nanoscale particulate parameters continue to gain prominence, the contribution of nanoscale substrate-mediated effects on DNA complexes and cells that interact with them is generally ignored during non-viral gene carrier optimization. Here we highlight the body of evidence supporting the importance of nanoscale particulate parameters for gene delivery, and also prospect routes whereby nanoscale substrate parameters may influence the uptake, processing, and expression of nucleic acids

delivered by these particles. A full understanding of the interaction of cells with non-viral gene carriers depends not only on an awareness of particulate parameters and their implications on endocytosis and transgene expression, but also on a clear knowledge of the substrative microenvironmental context in which the particles are presented.

2.1.1 Barriers to gene transfer

DNA complexes must overcome a series of barriers to gain access to the membrane surface, cytoplasmic compartment, and nucleus of a target cell, and to translate transgenes into protein (Figure 2). As particles encounter each of these barriers, they are subject to a certain probability of success or failure in overcoming each. The product of the probabilities of success for each step in the journey is reflected in the transfection efficiency for a given system. Certain portions of the trip may be more limiting than others for a given carrier system. If an easily-crossed barrier is not subject to saturation and is upstream of a bottleneck barrier, increasing the efficiency of crossing the upstream barrier may help to increase the number of particles or plasmids that appear downstream of the limiting barrier.

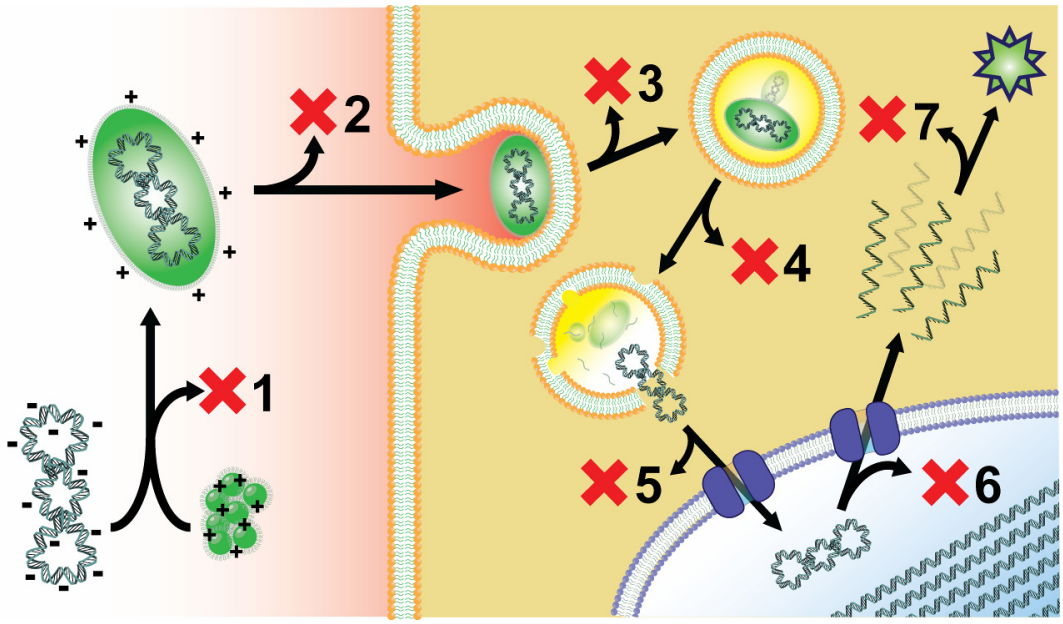

Figure 2. Barriers to non-viral gene delivery
(1) Transgenic DNA can be lost due to incomplete complexation with cationic polymer/lipid. (2) Complexes may be cleared from the circulation before they are able to bind to the cell surface. (3) Some of the complexes bound to the cell surface will not be internalized. (4) Following endocytosis, a portion of DNA may be degraded within the acidic late endosomes and lysosomes. (5) DNA successfully escaping the endosomal compartment may be further degraded by cytoplasmic DNAse. (6) A portion of the DNA reaching the nucleus may be unable to induce transcription. (7) Some of the exported mRNA may be incapable of translation into transgenic protein.

This probabilistic way of thinking about non-viral gene delivery is supported by a study finding that noncoding DNA can enhance the efficiency of transfection by polyethylenimine- (PEI) DNA complexes [2]. A constant quantity of reporter plasmid was diluted with noncoding "junk" DNA, followed by delivery of either one population of particles containing both coding and noncoding DNA, or co-delivery of two different particle populations – one containing coding DNA and one without. It is important to note that because the total amount of coding DNA remains the same in each case, the number of particles including coding DNA is increased in the case of particles formed with both coding and noncoding DNA. The mean expression per cell was not affected, but the number of expressing cells was increased when a larger number of coding

particles were delivered. The authors suggest that nuclear entry is a very inefficient process, so increasing the number of coding particles can overcome this bottleneck by increasing the number of opportunities for this rare event to occur.

The formation of DNA complexes usually proceeds by condensation of anionic DNA with cationic lipid (lipoplex) or polymer (polyplex); these interactions must be strong enough to keep particles stable during exposure to charged serum components. The next barriers facing systemically delivered particles are extracellular, and include: serum proteases and nucleases, variations in pH, opsonization, and clearance during passage through the kidneys and liver [3]. Upon arrival near the cell, complexes must associate with the cell surface, either through electrostatic interactions, physical concentration at the cell substrate via adsorption, or by ligand-receptor binding. Originally, it was thought that lipoplexes could then enter target cells by direct fusion with the cell membrane. It is now well-accepted that both nonspecifically- and ligand-bound complexes enter cells principally via endocytic processes [4], which we consider in detail in the following section.

After escape from the endocytic compartment, the complexes must gain entry to the nucleus, and unpack their DNA cargo. Upon arrival at this step, it becomes a liability for carriers to bind their cargo too tightly; overbinding prohibits access by the translational machinery (striking an appropriate balance between protection and release has been reviewed by Grigsby et al. [5]). Indeed, it is worth mentioning that translational inefficiencies may generally be one of the most rate-limiting obstacles in non-viral gene delivery. In one excellent exploration of this barrier, the efficiency of each step in transfection mediated by adenovirus and lipofectamine (LF) was compared [6-7]. LF

was shown to require a dose three thousand times higher than that delivered by adenovirus to support the same level of expression. Though LF encouraged higher levels of DNA uptake on a per-carrier basis, adenovirus was eight thousand times more efficient at completing transcription and translation of the transgenes delivered to the nucleus. Chemistry also appears to be important for this process; PEI polyplexes have been observed to unpack more efficiently compared to DOTAP lipoplexes following direct injection into the nucleus, lowering the translational barrier for this polyplex upon arrival in the nucleus [8].

2.1.2 Endocytic pathways

A basic discussion of relevant endocytic pathways is required to describe the uptake of non-viral vectors. All cells perform some form of endocytosis to maintain the homeostasis of intracellular species. Endocytosis is broadly divided here into clathrin- and caveolae-mediated endocytosis, and fluid-phase macropinocytosis (Figure 3). These three pathways are not inclusive of all the forms of endocytic uptake of non-viral carriers [9], but are the most studied in this context, and are our focus here.

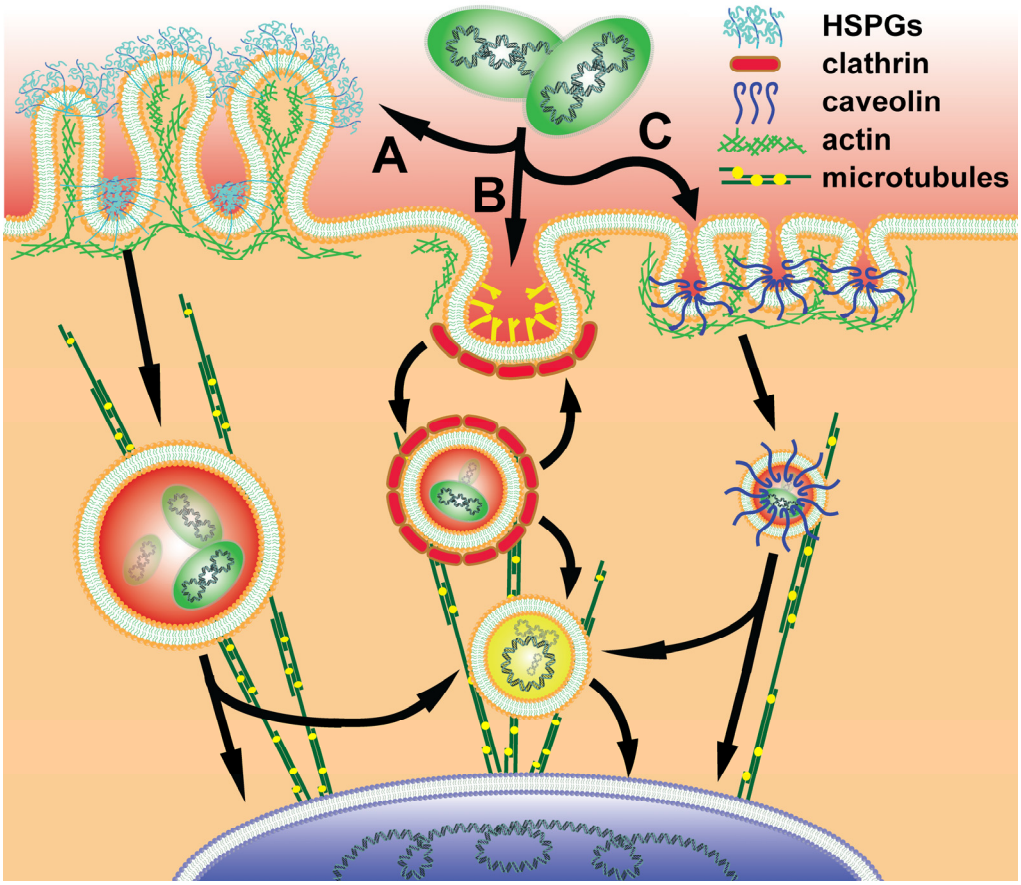

Figure 3. Endocytic pathways traversed by non-viral carriers
Cationic particles bind to anionic heparan sulfate proteoglycans (HSPGs) and may be internalized via macropinocytosis (A), a form of fluid-phase endocytosis. Macropinosomes are fluid-filled vesicles formed by actin-driven membrane ruffling; these vesicles may fuse with degradative late endosomes, or may be trafficked directly to the nucleus. Non-viral vectors can also be internalized by clathrin-mediated endocytosis (B), which progresses by receptor clustering, formation of the clathrin coat, and actin-driven internalization, forming early endosomes. Some early endosomes are recycled to the cell surface, while others are uncoated, acidified, and progress to late endosomes and lysosomes on their way to the nucleus. Caveolae-mediated endocytosis (C) proceeds by oligomerization of caveolin, actin-dependent internalization of caveolae to form cavicles, and merger with the degradative lysosomal compartment, or non-degradative trafficking to the nucleus via caveosomes. Each pathway relies on microtubules for rapid transport of endocytic vesicles.

Clathrin-mediated endocytosis is the most well-understood endocytic pathway [10], and is involved in nutrient uptake and signal transduction through internalization of ligand-bound receptors [3]. Low density lipoprotein (LDL), transferrin (Tf), and epidermal growth factor (EGF) are prototypic species transported via clathrin-mediated endocytosis. Upon receptor-ligand binding, the receptors cluster in clathrin-coated pits,

mediated by the adapter protein AP-2 [11]. Dynamin, a GTPase, then frees the coated pit into the cell interior, fusing with and forming early endosomes [4, 10]. Depending on the cargo molecule, early endosomes are either uncoated and trafficked to acidic lysosomes via microtubule transport, or shuttled back to the cell surface via recycling endosomes. Exposure to the acidic and degradative lysosomal compartment reduces the transfection efficiency of non-viral vectors. Therefore, enhanced escape from the acidic endosomes by the proton sponge effect [12], or by chemical and physical endosomolytic agents, have been pursued to help surmount this barrier [13]. Clathrin-mediated endocytosis is at times synonymous with "receptor-mediated endocytosis" in the literature, but this terminology has become antiquated with the discovery that other forms of endocytosis also proceed by ligand-receptor binding.

Caveolae-mediated endocytosis is associated with the uptake of glycosphingolipids, and is involved with transcytosis of serum proteins across endothelium [11]. Caveolae are caveolin-coated, cholesterol- and sphingolipid-enriched flask-shaped invaginations in the cell membrane. These structures are relatively static compared to clathrin-coated pits, and generally proceed via slower uptake kinetics compared to clathrin-mediated endocytosis [14]. Upon dynamin- and actin-mediated uptake, cavicles are shuttled toward the nucleus via microtubules. Importantly for non-viral gene delivery, certain forms of caveolae-mediated endocytosis are thought to avoid the degradative lysosomal compartment [15]. Caveolae-mediated endocytosis has been shown to be initiated by viruses binding to and clustering integrins, resulting in their uptake [16] in a manner similar to that observed in the ligand-receptor binding of clathrin-mediated endocytosis.

Macropinocytosis, a form of fluid-phase endocytosis, is the uptake of fluid and solutes by actin-driven ruffling of the plasma membrane. Macropinocytosis can be induced by platelet derived growth factor (PDGF) activating Rho-family GTPases, which trigger actin assembly and internalization of surrounding extracellular fluid [11]. Long-range transport of macropinosomes along microtubules is inhibited by nocodazole. The rate of macropinocytosis of a solute is typically proportional to its concentration in solution (giving non-saturable kinetics). Like caveolae-mediated endocytosis, particles endocytosed by macropinocytosis may bypass the lysosomal compartment, making it an attractive pathway for efficient non-viral gene delivery.

A number of studies have unambiguously implicated macropinocytosis and clathrin- and caveolae-mediated endocytosis as necessary processes for the uptake and subsequent expression of both poly- and lipoplexes. The contribution of each of these pathways also varies by cell type and cargo identity. The degradative processes following particle uptake vary by endocytic pathway and have been shown to be important barriers to non-viral gene delivery.

Clathrin-mediated endocytosis has been demonstrated to support transfection by lipoplexes through studies employing electron microscopy and co-localization with labeled transferrin [17]. Cells subject to inhibition of clathrin-mediated endocytosis by potassium or cholesterol depletion and those expressing dominant negative mutant Eps15 do not internalize lipoplexes, and subsequently support lower levels of transgene expression (wild-type Eps15 allows docking of AP-2 to the plasma membrane, which goes on to assemble clathrin-coated pits) [18]. Endocytosed lipoplexes eventually co-localize with acidic lysosomes stained with LysoTracker, providing evidence that

particles taken up by this pathways are subject to low pH [19]. The use of nocodazole to interfere with microtubule function has also been shown to increase the nuclear accumulation and transgene expression of lipoplexes [20]. The authors suggest that because nocodazole uncouples endosomes from their trafficking to the lysosomal compartment [21], lipoplexes are able to skirt degradative processing following endocytosis, thereby increasing their transfection efficiency.

The ability of a non-viral vector to escape from the endosomal compartment determines that carrier's transfection ability. Polyplexes and lipoplexes are believed to escape endosomes using different mechanisms. Carriers with a strong ability to buffer the influx of protons during endosome acidification increase the accumulation of H^+ and Cl^- ions and osmotic pressure within the vesicles, eventually leading to bursting and vector escape [10]. Inhibition of the activity of proton pumps decreases the transfection efficiency of PEI polyplexes [22], and endosomes have been observed to accumulate greater amounts of Cl^- and swelling after delivery of highly-buffering polyplexes [12]. In contrast to this "proton sponge effect", lipoplexes containing lipids that encourage formation of nonlamellar phases may escape endosomes through direct fusion and release into the cytosol [23]. Non-viral carriers must have the ability to escape the endocytic vesicles encountered along the endocytic pathway(s) they traverse.

A study relying on direct microscopic visualization has elucidated the relationship between endocytosis and transfection efficiency of PEI polyplexes, through observation of the uptake of polyplexes stained with YOYO-1 (a fluorescent DNA intercalator) by fibroblasts labeled with FM4-64 (a lipophilic stain which fluoresces red upon binding the outer leaf of cell membranes) [24]. Labeled particles were observed to co-localize

strongly with the membrane marker for endocytosis for the duration of the transfection process. Since endocytic uptake of the cell membrane and the macropinocytic uptake of extracellular fluid proceed by the same intracellular pathways, the polyplexes in this study were believed to be taken up by fluid-phase endocytosis. Given the co-localization persisted through maturation of the early endosomes into lysosomes, a large fraction of the complexes were sequestered in the endocytic compartment, with only a small population escaping to the nucleus to induce transgene expression.

Douglas et al. noted cell-line dependent differences in the endocytic processes of 293T, COS7, and CHO cells as the cause for varying levels of transfection using identical preparations of alginate-chitosan-DNA nanoparticles [25]. By measuring the variable inhibition of particle uptake by the clathrin-mediated inhibitor chlorpromazine and caveolin-mediated inhibitor genistein, the authors were able to determine that both routes were used for COS7 and 293T cells, whereas CHO cells endocytosed particles by a clathrin-independent mechanism. Furthermore, the induction of macropinocytosis by phorbol myristate acetate (PMA) did not result in an increase in complex internalization for any cell type. For COS7 and 293T cells, transfection was only supported by particles taken up by clathrin-mediated endocytosis, whereas CHO cells did not produce significant transgene product, possibly because they lack the mannose receptor indicated in the clathrin-mediated uptake of chitosan. In this case, clathrin-mediated endocytosis was thought to be superior because the particles were visualized escaping the acidic lysosomes, presumably via the proton sponge effect, whereas particles trafficked to non-degradative caveosomes lacked an escape mechanism and were therefore sequestered.

These results highlight the dependence of vector trafficking on particle chemistry and cell type.

Caveolae- and clathrin-mediated endocytosis have been demonstrated to be required for uptake and expression of polyplexes and lipoplexes, respectively, in a single study [14]. The internalization of DOTAP lipoplexes was inhibited by chlorpromazine and potassium depletion (clathrin-mediated) but was not affected by filipin and genistein (caveolae-mediated), and the uptake of PEI polyplexes was down-regulated by all four inhibitors. Transfection by DOTAP particles was also abolished by inhibitors of clathrin-mediated endocytosis, whereas transfection by PEI particles was only inhibited by removal of caveolae-mediated uptake. Rejman et al. suggest that PEI polyplexes (which are unable to fuse directly with endocytic vesicles due to a lack of lipid content) were only able to avoid degradation if trafficked via non-degradative caveolae-mediated endocytosis. On the other hand, the lipoplexes taken up by clathrin rapidly escaped the degradative pathway before acidification by direct fusion with the vesicle membranes.

Macropinocytosis is a major route of entry for positively charged complexes, particularly for those coated with arginine [26]. Membrane-bound negatively-charged heparan sulfates act as receptors for positively charged particles; liposomes modified with octaarginine co-localized with neutral dextran, a tracer of fluid-phase endocytosis [27]. The uptake of these particles was inhibited by amiloride, which interferes with a Na^+/H^+ exchanger required for macropinocytosis. The lipoplexes internalized by macropinocytosis did not co-localize with acidic lysosomes, lending support to macropinocytosis as an attractive non-degradative pathway for gene delivery.

2.1.3 Nanoparticulate parameters

As has been described, non-viral vectors can be transported to the cytoplasmic compartment by a diversity of endocytic mechanisms. Each of these pathways may support a different level of transfection mediated by a given lipo- or polyplex delivery system. An emerging paradigm for the design of effective gene carriers is the modification of particulate parameters to encourage entry via a preferable endocytic pathway. These parameters include size, shape, charge, chemistry, and ligand modification. These factors are often difficult to vary independently, so the contribution of each can be difficult to generalize. Furthermore, endocytic processes vary by cell type, so the behavior of particles in one culture system may not be predictive of another. For example, HepG2 cells lack endogenous caveolin and are therefore unable to internalize particles by caveolae-mediated endocytosis [28]. Some of the key findings of this section are summarized in Figure 4.

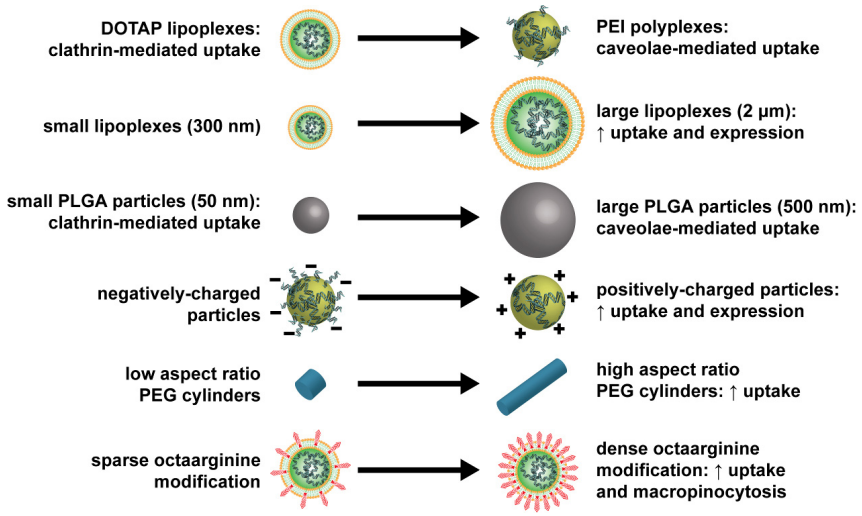

Figure 4. Typical strategies to overcome barriers to non-viral gene transfer
Tuning nanoparticle chemistry, size, surface charge, shape, and ligand density can alter the endocytic pathway and efficiency with which nanoparticles are taken up. Cell substrate parameters are often ignored in the design of non-viral transfection system.

2.1.3.1 Particle chemistry

Altering the chemistry of a particle can modulate its hydrophilicity, the tendency for it to fuse with endocytic vesicles, and its susceptibility to serum inhibition, all with implications for uptake and transfection efficiency. For instance, a comparison of six phosphatidylcholine lipoplexes with varying hydrophobic chain lengths revealed that those with short chains mediated much higher levels of transfection in endothelial cells, both in the presence and absence of serum [29]. X-ray diffraction showed the particles supported formation of an inverted cubic phase, which is believed to resemble the membrane structure produced during fusion between lipid bilayers [30]. Masotti et al. have shown identical particle sizes or charge ratios of DMRIE/Chol, Cellfectin, Lipofectamine, Lipofectamine 2000, Lipofectin, and Fugene lipoplexes induce transfection levels that vary over many orders of magnitude in rat glioma cells [31].

PEGylation of cyclodextrin polyplexes endowed the particles with enhanced stability in the presence of salt, but decreased their uptake and transfection efficiency in BHK-21 cells [32]. PEGylated PEI polyplexes were taken up to a similar extent as unmodified particles, but were unable to transfect cells as efficiently; the addition of PEG may have interfered with the proton sponge effect. Using EM and fluorescence microscopy, the authors observed that PEGylated particles remained separate and stable during their journey toward the nucleus and were unable to unpack their DNA cargo, whereas unmodified particles aggregated into larger masses, which released their DNA into the cytoplasm and the nucleus.

The molecular weight and degree of branching in PEI has been investigated in PEI/liposome/DNA complexes (polylipoplexes). Branched and linear PEI induced

similar levels of transfection, but PEI with lower molecular weight performed better than the larger PEI. Improvements in transfection efficiency with low over high molecular weight PEI have also been observed for pure PEI polyplexes [33]. PLGA nanoparticles made more hydrophilic with an increasing fraction of PVA emulsifier at their surface had a similar size and surface charge as more hydrophobic particles, but were taken up significantly less by smooth muscle cells [34].

2.1.3.2 Particle size

Nanoparticles are necessarily described by characteristic size parameters. It is important to note that DNA complex size can be a moving target, and is not completely defined by a single number. That is, particles often aggregate with time and, like polymers, require reporting of a polydispersity parameter for a full description of their size characteristics. Caution is warranted in comparison of particle sizes measured with different techniques and at different hydration states. For example, a particle's hydrodynamic diameter measured in solution with dynamic light scattering may differ significantly from the same particle measured after dehydration and visualization by TEM. The endocytic machinery and cell membrane have well-defined geometries and flexibility that may restrict entry of incompatibly large or small particles. Modifications and procedures to create or stabilize a target nanoparticle size can direct gene carriers to endocytic routes that are supportive of high expression levels.

A linear relationship between the size of DC/Chol/DOPE lipoplexes, uptake, and transfection efficiency was observed over a range of 300-2000 nm; this relationship held

true regardless of whether the particle size was changed by altering the cation to DNA charge ratio, or serum concentration [35]. Interestingly, particles formed in the presence of increasing serum concentration bound to cell membranes to the same extent, but larger particles were endocytosed much more efficiently. The size of DOTAP/DOPE lipoplexes can also be increased by pre-incubation with free PEG in solution prior to the onset of transfection [36]. PEG dehydrates and destabilizes lipid bilayers, leading to increased aggregation, fusion, and generation of micron-size particles from 500 – 800 nm nanoparticles. This increase in size led to an increase in cellular association and uptake of the particles in multiple cell types. Transfection efficiency also improved for micron-size particles, but the increase in uptake did not account for the difference observed, suggesting the larger particles may have been preferentially trafficked into a more favorable endocytic route.

Extrusion of various multilamellar vesicles through a 100 nm filter resulted in lower transfection efficiency, but the identity of the cationic lipids used had a stronger effect on transfection in Neuro2A cells [37]. Similarly, Li et al. observed an increase in uptake and transfection efficiency of DOTAP and Lipotap complexes when their size was increased with subsequent layer-by-layer self-assembly of positively charged gold nanoparticles with uncomplexed DNA on the surface of the lipoplexes [38]. Altered endocytic trafficking should be added to the authors' list of possible mechanisms whereby the larger particles increased transfection efficiency, which included elevated sedimentation, DNA payload, and charge-shielding. Larger, low molecular weight PEI polyplexes (590 nm) have also been observed to transfect NIH-3T3, HEK293, COS-7, CHO, HeLa, and Jurkat cells more efficiently than small high molecular weight

polyplexes (156 nm), though it is unclear what contribution size made relative to weaker DNA condensation for the larger particles [33].

Prabha et al. separated a bimodal preparation of PLGA nanoparticles into fractions with hydrodynamic diameters of 150 and 300 nm [39]. The smaller nanoparticles produced 27x higher transfection efficiency in COS-7 cells, despite similar levels of particle uptake by mass and slower DNA release by the smaller particles. However, it was revealed with calculation that the smaller particles were taken up 20x more efficiently by number. Therefore, it is difficult to determine if the increase in transfection efficiency was a result of differential trafficking, or simply due to an increase in particle count. Considering that non-viral carriers are typically delivered on a per-mass basis, increases particle count with decreasing diameter may influence transfection efficiency in many studies without notice. Other polymeric systems produce similar size-dependencies on uptake; only sub-micron polystyrene particles are efficiently taken up by Caco-2, HepG2, and Hepa 1-6 cells [40]. Very small (< 25 nm) particles may traffic through a unique non-clathrin- and non-caveolae pathway that could be interesting for non-viral gene delivery [41].

Particle size clearly affects the extent to which particles are taken up and are able to transfect target cells. Though many of the results presented here have suggested larger polymer and lipid particles (still in the submicron rage) are taken up more efficiently than smaller ones, some studies have claimed particles smaller than 100 nm offer good transfection efficiency, particularly when they must first pass through a capillary network (in vivo) [30]. Beyond controlling the extent of uptake, particle size has also been demonstrated to control the endocytic uptake pathway of nanoparticles [42]. In a

comparison of the uptake of fluorescent latex nanospheres by B16 cells, uptake was only observed for particles 50-500 nm in diameter, but not for 1 um particles. Inhibitors of clathrin-mediated endocytosis were less effective at blocking uptake of large particles, whereas inhibitors of uptake by caveolae were only effective against the uptake of 500 nm nanospheres. Small particles (50 – 100 nm) were taken up within 30 minutes and appeared in the lysosomal compartment, whereas larger particles were taken up over a span of hours and did not colocalize with the late endosomes. These results suggest that large particles may be preferentially trafficked through a slow, non-degradative, caveolae-mediated route, and may explain why larger lipoplexes often produce higher transfection efficiencies. It would be interesting to extend these results to other chemistries and surface charges to determine if the size cutoffs for each pathway are intrinsic to a particular geometry of the endocytic machinery.

2.1.3.3 Surface charge

Along with size, surface charge (zeta potential) is a ubiquitous particulate parameter that is important for the understanding of uptake mechanisms and transfection efficiency. Particles that may be of an appropriate size to traverse a desired endocytic pathway may not be able to access that pathway if cellular binding is diminished by a significantly negative zeta potential. Also, the stability of a particulate gene delivery system can often be predicted by its zeta potential.

It is generally believed that positively-charged nanoparticles perform better for in vitro transfection of cells through their enhanced binding to negatively-charged

proteoglycans on cell surfaces [27, 43]. Indeed, grafting polymerization of MMA onto carboxymethyl chitosan or chitosan hydrochloride can generate 150 nm nanoparticles with widely varying surface charge, leading to charge-dependent differences in endocytic uptake [44]. Particles with more-positive zeta potentials encouraged the highest rates of uptake in L02 and SMMC-7721 cells.

The dependence of uptake efficiency on surface charge is extendable to particles carrying genetic payloads. Optimization of a non-viral carrier often involves an empirical modification of the charge ratio (cationic polymer or lipid to anionic DNA) aimed to balance competing effects on cellular binding and uptake, DNA protection and release, and complex size and stability. Despite this wide parameter space for optimization, carriers with positive surface charges are often the most effective. This is likely due to increased binding to anionic cell surfaces, as well as more complete DNA complexation at high (+/-) charge ratios. Almofti et al. demonstrated that increasing the DNA content of DC-Chol-DOPE lipoplexes resulted in a decrease in zeta potential [45]. Particle size and liposome-liposome fusion were maximal at neutral charge ratios where the particles were unable to repel each other electrostatically, however transfection in A431 cells was greatest at a slightly positive charge ratio and was abolished by endocytic inhibitors. EPC-Chol lipoplexes modified with octaarginine demonstrate a similar dependence on surface charge; increasing densities of octaarginine produce increasingly cationic particles, leading to an increase in macropinocytosis, uptake, and transgene expression [26].

Though a positive zeta potential may be desirable to increase cellular uptake in vitro, positively charged particles may interact with negatively charged serum proteins in

vivo, leading to charge neutralization, opsonization, increased particle size, and clearance [46]. With this in mind, cationic particles can be pre-neutralized with plasma-compatible proteins to increase transfection efficiency [47-48]. Unlike their cationic precursors, BSA-neutralized particles do not accumulate extra protein or increase in size upon exposure to plasma, and are endocytosed more effectively than PEG-shielded liposomes [47]. The authors suggest this may be a consequence of the caveolae-mediated endocytosis of surface BSA by the albumin receptor gp60 [49].

2.1.3.4 Shape

Nonspherical particle shapes are only recently being evaluated for altered tissue distribution and cellular uptake. This may be due to a previous lack of readily available techniques for the synthesis of well-defined nonspherical particles [50]. A lithographic method called PRINT (Particle Replication In Non-wetting Templates) has been developed to produce particles with various shapes and surface charges [51-52]. These cationic poly(ethylene glycol)-based particles with different shapes but similar zeta potentials have dramatically different uptake kinetics in HeLa cells. Comparing cylinders with similar particle volume, 150 nm cylinders with aspect ratio of 3 were taken up much more rapidly than 200 nm cylinders with aspect ratio of 1. The uptake was abolished if the particles were rendered anionic by conversion of protonated surface amines to amides. The authors also interrogated the cells with a series of endocytic inhibitors, revealing important roles for clathrin- and caveolae-dependent endocytosis in the uptake of small particles. The high aspect ratio 150 nm cylinders may have been taken up efficiently due

to their utilization of all of the endocytic pathways probed. Highly elongated lipoplexes have also demonstrated improved efficiency in vivo [53], but the elongated structure has not been clearly correlated with improved transfection efficiency in vitro [54].

Alexander et al. have shown that polymeric micro-doughnuts are internalized much less efficiently than similarly-sized microspheres in a variety of non-phagocytic cell types [55]. This could be explained by the necessitation of a greater membrane curvature to engulf nonspherical particles of equal volumes [56]. Also, oblong nanoparticles with a minor axis that is smaller than nuclear membrane pores have been shown to transfect post-mitotic cells following cytoplasmic injection [57]. Taken together, these effects suggest particle shape could be engineered to investigate, avoid, or exploit various endocytic pathways and barriers to transfection by presentation of well-defined lengths and curvatures.

2.1.3.5 Ligand modification

Nanoparticles can also be targeted to specific arms of endocytosis through modification with species known to ligate endocytosable receptors, though this enormous body of work will not be the focus of this review. These strategies are particularly useful for targeting cell types that uniquely- or otherwise over-express a particular receptor. Many of the classic endocytic ligands have been added to the surface of DNA complexes to increase transfection efficiency, including EGF-modified PEI polyplexes [58-60] and transferrin-modified lipoplexes [61-63] targeted to clathrin-mediated endocytosis. As previously mentioned, heparan sulfate proteoglycans act as “nonspecific receptors” for

the binding of particles modified with arginine-rich peptides [64-65]. Arginine decoration can increase uptake by macropinocytosis [26] and clathrin-mediated endocytosis [66], depending on the orientation and concentration of the peptide on the particle surface. Interestingly, the uptake of octaarginine-modified particles can be switched from macropinocytosis to a caveolae-mediated pathway by substitution of only two of the peptide's residues [67].

2.2 Cell-substrate interactions

2.2.1 Impact of substrate chemistry on transfectability

As discussed above, cell-particle interactions are critically important for efficient uptake and transfection. Through these interactions, particle morphology and chemistry can either enable or prohibit entry into and expression from target cells. However, non-viral vectors not only interact with target cells, but also with the substrates on which the cells are cultured. While these particle-substrate interactions may quietly impact the success of many "forward" transfection systems, their effects are most apparent during reverse transfection (also referred to as substrate-mediated transfection). Reverse transfection differs from forward transfection in that cells are seeded on top of particles that have been previously immobilized onto a surface, rather than adding particles to previously seeded cells. Complex immobilization is thought to increase transfection efficiency by increasing the local concentration of DNA at the cell surface, and can out-perform bolus delivery at times [68-70]. In one such example, Okazaki et al. found that reverse transfection of DNA-spermine-pullulan complexes maintained better hMSC

viability, and produced a more intense and sustained expression of reporter transgene compared to forward transfection in the presence of serum - an important consideration for in vivo translation [71]. Substrate-mediated gene delivery also provides a simple method to locally deliver genetic material from the surface of porous implants. However, if the association of complexes with a substrate is too tight, endocytic uptake and transfection can suffer.

The context wherein adsorbed complexes are presented to cells can be modified with surface chemistry and the deposition of serum or ECM proteins. These modifications can alter transfection efficiency in a manner uncoupled from the extent of uptake, suggesting alternate processing for complexes presented in different substrative microenvironmental contexts. The consequences of altering the density and tightness of particle adsorption, as well as the benefit of matrix proteins, are presented in Figure 5. Furthermore, substrate-mediated transfection may change the rate-limiting barrier to expression. For instance, Bengali et al. report that internalization of lipoplexes is impaired but nuclear trafficking is improved in reverse compared to forward transfection. On the other hand, internalization of polyplexes was unaffected, but nuclear trafficking was impaired upon substrate-mediated rather than bolus delivery [72]. Reverse transfection may therefore be well-indicated for switching a bottleneck barrier to one that a certain particle type is more able to overcome.

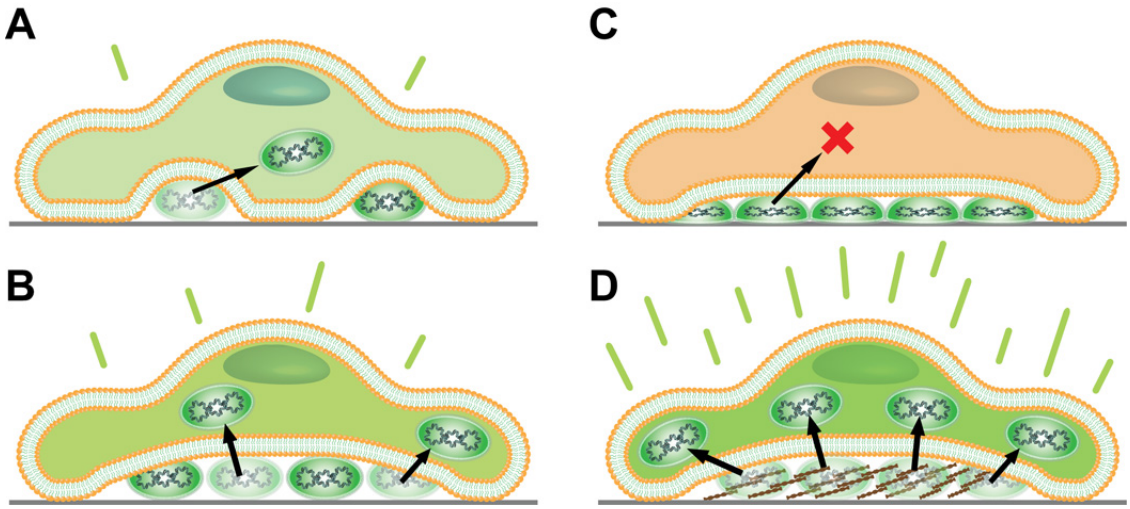

Figure 5. Effect of density and presentation of surface-bound complexes on the efficiency of reverse (substrate-mediated) transfection
(A) Low densities of adsorbed complexes lead to low levels of particle uptake and expression upon cell seeding. (B) Increasing the density of adsorbed complexes may lead to proportionally increased expression, but (C) over-tight immobilization of complexes renders cells unable to internalize bound complexes, and diminishes transgene expression. (D) Complexes co-immobilized with extracellular matrix components often support superior internalization and transfection by incompletely-understood mechanisms.

2.2.1.1 Concentration of DNA at the cell surface

The concentration of DNA at the cell surface has been suggested as a limiting factor in non-viral gene delivery [73]. For forward transfection, the delivery of complexes to the cell surface is typically a diffusion-limited process, whereas reverse transfection can pre-load complexes at high levels onto the cell-substrate interface through drying, electrostatic and hydrophobic interactions, or ligand-receptor binding. Similar to forward transfection, increasing the amount of DNA adsorbed to a surface during reverse transfection increases expression levels, up to a limit. PEI polyplexes with increasingly positive zeta potentials adhere in greater numbers to acellular intestinal submucosa that is rich in negatively charged glycosaminoglycans, leading to increased transgene expression in fibroblasts seeded in direct contact with the adsorbed complexes [74]. The size of printed lipoplex spots depends on the hydrophobicity of the substrate;

more hydrophobic substrates produce smaller spot sizes, higher local DNA concentrations, and elevated expression levels [75].

2.2.1.2 Strength and nature of complex adsorption

Aggregation may translate to weaker binding between complexes and their substrate [76]. Polyplexes formed from a block copolymer of cationic poly N,N-dimethylaminopropyl acrylamide and thermoresponsive N-isopropylacrylamide did not produce strong expression in forward transfection or when dried to the culture surface. However, heat-induced hydrophobic transition, aggregation, and deposition of the complexes onto the substrate produced expression levels rivaling that of PEI in conventional transfection; the authors suggested that dried complexes were too tightly attached to the surface for uptake to proceed [77]. The inclusion of an increasing amount of cationic peptide to lipoplex preparations also induced aggregation onto cell culture substrates, thereby increasing vector release, shifting to a non-lysosomal caveolar pathway, and enhancing transfection efficiency [76].

The balancing act between concentrating vector at the surface and facilitating cellular internalization is well-illustrated by the tethering of biotinylated polylysine complexes to a neutravidin-coated surface [78]. While the immobilization of particles increased with increasing biotinylation, the transfection efficiency was maximal for only a small amount of biotin functionalization; a low level of biotinylation encouraged complex deposition but was simultaneously permissive to internalization, whereas highly-biotinylated complexes were bound too tightly to the surface to be internalized. In

another study, stamping PEI complexes onto a layer of cells did not result in transfection unless the complexes were first released by an underlying pH-sensitive polymer layer [79].

Substrate surface chemistry can also have a marked effect on the immobilization and expression of non-viral vectors. Immobilization of Lipofectamine 2000 complexes onto self-assembled monolayers of alkanethiols with varying endgroups allowed the comparison of substrate-mediated gene delivery from surfaces with controlled ionization and hydrophilicity [80]. Surfaces with a high ratio of anionic (carboxylic) to neutral (hydroxyl) groups supported the highest levels of complex immobilization and transfection of NIH/3T3 fibroblasts. Hydrophobic decane surface chemistry also bound high levels of lipoplex, but did not transfect cells, putatively from over-tight complex-surface interactions. Inclusion of PEG-like moieties can also increase the transfection efficiency of PEI polyplexes adsorbed to monolayers of carboxylic endgroups [81]. This increase cannot be attributed to an increase in complex binding or release, but the size and shape of adsorbed complexes is markedly affected. The ionic association of complexes with a substrate may be preferable to hydrophobic association, because ionic interactions can be displaced upon introduction of serum proteins, freeing complexes for internalization during reverse transfection.

2.2.1.3 Co-presentation of adsorbed protein with non-viral vectors

Protein pre-adsorbed to surfaces used in reverse transfection can aid in the subsequent deposition of complexes. Adsorbed protein can also improve transgene

expression in a manner that is not fully explainable by increased immobilization or uptake. Complexes delivered with protein may maintain conformations favorable for cellular uptake, or may be differentially trafficked. Fibronectin deposited onto surfaces dramatically increased the reverse transfection efficiency of polyplexes in hMSCs, though cell adhesion and spreading were not apparently affected [69]. This suggests an active role of fibronectin in complex internalization. A similar effect was demonstrated with co-deposition of antibodies against various integrin subunits. Engagement of integrin subunits through adsorbed antibodies, particularly anti-CD29 (which engages the ubiquitously-expressed integrin β_1 [82]), resulted in an increase in transfection efficiency compared to control IgG for all of the cell types analyzed [83]. Intriguingly, placing RGD (an integrin-binding peptide sequence) directly on the surface of adsorbed PEI polyplexes leads to a decrease in transfection efficiency [84].

Fibronectin has been implicated elsewhere in the enhancement of substrate-mediated gene delivery [85]; drying a layer of fibronectin, collagen, laminin, FBS, BSA, and collagen was demonstrated to control the extent of PEI complex deposition, cellular association, endocytic internalization, and transfection efficiency following reverse transfection, whereas transgene expression was identical for all coating types following forward transfection. All coatings other than laminin mediated high levels of complex deposition. With the exception of FBS, complexes were found to be highly associated with the remaining coated surfaces (collagen, fibronectin, and BSA). Collagen and fibronectin had identically high levels of complex internalization compared to other coatings, but fibronectin supported a significantly higher level of transgene expression, suggesting differences in the trafficking of complexes internalized from collagen- and

fibronectin-coated surfaces. Uptake in this system depended more heavily on caveolae- than clathrin-mediated endocytosis, which may be a functional manifestation of the co-localization of fibronectin with integrin β_1 and caveolin in adhesion complexes [86] (discussed further in the next section). Similarly, substrates with adsorbed rather than dried FBS immobilized similar quantities of PEI and Lipofectamine 2000 complexes [70]. This FBS coating boosted the transgene expression of PEI 1500-fold compared to delivery from an uncoated surface. Expression of Lipofectamine 2000 from FBS-coated surfaces was unchanged, but the number of transfected cells was increased compared to uncoated substrates. Adsorption of fibronectin for improvement of substrate-mediated transfection has also been applied to 3D PLGA scaffolds for spinal cord regeneration [87-88].

2.2.2 Modulation of endocytic phenotype by substrate surface nanotechnology

The use of surface nanotechnology to modify particulate parameters has gained well-deserved attention in non-viral gene delivery, as these parameters are becoming increasingly well-understood modulators of uptake and transfection efficiency. Another approach worth considering is the engineering of desirable endocytic cellular phenotypes in target cells through substrate surface nanotechnology. A suite of parameters such as cell morphology, adhesion, proliferation, differentiation, and protein expression are tunable with substrate parameters including stiffness, chemistry, and physical topography (Figure 6). Cell biology offers hints towards mechanisms that may mediate useful

interactions between these substrate-mediated effects on cell phenotype, the endocytic machinery, and subsequent transfection. Further, perhaps the simplest method whereby substrate nanotopography could enhance the transgene expression of interacting cells would be by increasing the loading of non-viral carriers onto patterned surfaces through an increase in available surface area afforded by feature sidewalls. Cells stretched over substrate topography may also expose an increased proportion of their basal surface, creating a larger area for complexes to attach and to be internalized. In general these interactions have yet to be directly investigated and exploited for gene delivery. Advances in patterning technology have made micro- and nano-patterned substrates more widely available; the following is an exploratory discussion of how these substrates may already be affecting endocytosis and transfectability, despite a lack of explicit, functional studies.

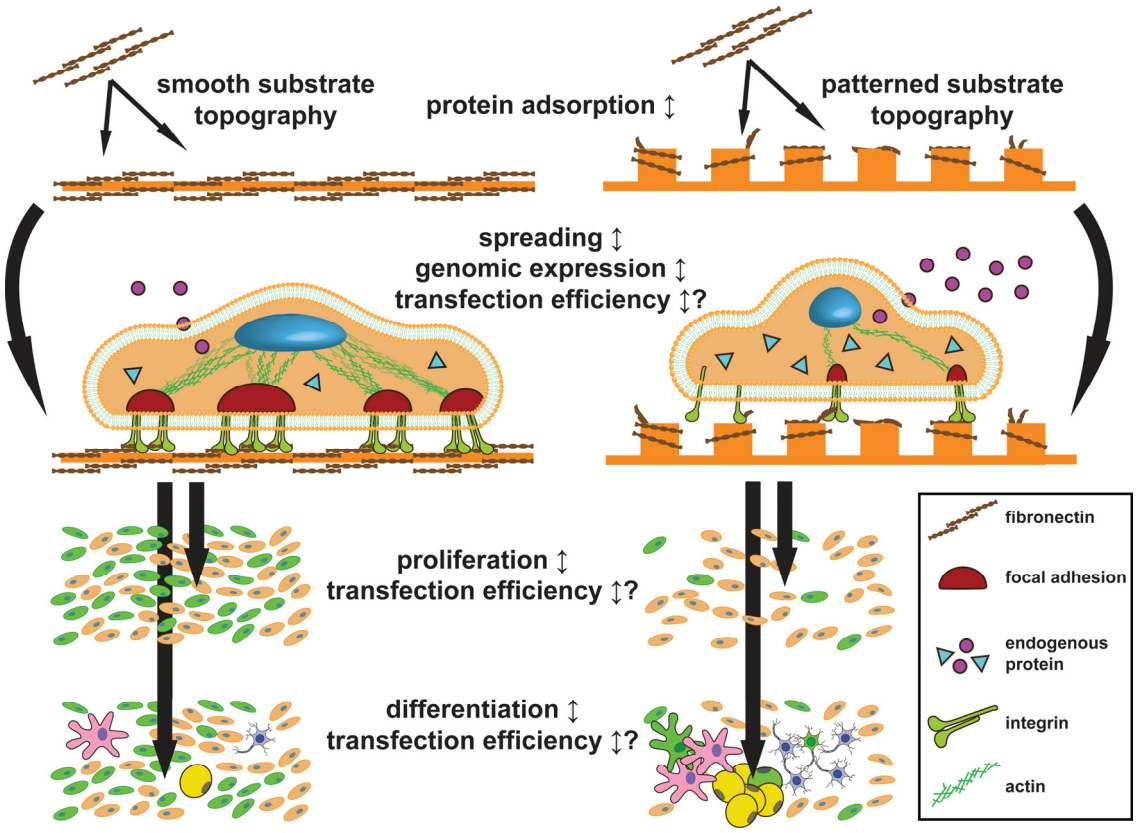

Figure 6. Topographical effects on cell phenotype may also impact non-viral gene transfer
The quantity and denaturation of matrix proteins adsorbed to patterns can be increased or decreased, depending on the specifics of the substrate topography and chemistry. These differences in the adsorbed protein layer mediate alterations in a number of cell phenotypes. Cells cultured on patterned topographies generally have decreased spreading and proliferation, reduced integrin clustering, and smaller focal adhesion complexes compared to smooth controls. Actin-mediated transduction of tension from integrin-nucleated focal adhesions to the nucleus alters the expression of a multitude of secreted and intracellular proteins; many of these proteins play a role in endocytosis, and therefore possibly in the endocytic uptake of non-viral carriers. Finally, patterned topography can control the differentiation state of many cell types, leading to concomitant alteration of transfectability.

2.2.2.1 Protein adsorption on nanofeatures

Cells interact with the substrates they are cultured on through integrins. Integrins are a family of transmembrane receptors that bind to an assortment of extracellular matrix proteins through shared RGD domains, including: fibronectin, laminin, collagen, and fibrinogen. Integrin binding and clustering initiates the assembly of adaptor proteins vinculin, talin, paxillin, and phosphorylative activation of focal adhesion kinase (FAK),

comprising the focal adhesion complex [89]. FAK goes on to provoke downstream effects such as cell movement and cytoskeletal contractility [90]. Therefore, cell-substrate interactions are mediated by the proteins that are deposited from solution onto to a given substrate, as actuated through integrin signaling. Substrate topography and chemistry alter the amount and conformation of integrin ligands, and may form the general basis for many if not all subsequent topographical effects on cell behavior.

Nano- and micro-scale topographies affect the amount and conformation of protein binding by presenting heterogeneous surface energies, altering exposed surface area, or restricting wettable area [91-92]. Nanoislands prepared by polymer demixing with heights of 14 nm supported 50% more fibronectin binding than 45 nm islands, despite a negligible change in exposed surface area [93]. Furthermore, the fibronectin preferentially adsorbed to the valleys between 14 nm islands. Similarly, 4 μm wide, 1 μm tall PDMS posts encouraged the adsorption of 50% more fibrinogen compared to smooth control despite only an 8% increase in surface area [94]. In contrast, higher aspect ratio PLGA support decreased fibrinogen adsorption [95].

The conformation of proteins adsorbed to surfaces also changes with physical patterning, which has implications for integrin binding. Adsorption of fibronectin to a nano-rough tantalum surface was increased compared to smooth tantalum, and the adsorbed layer's stiffness increased, accompanied by a decreased susceptibility to antibody interrogation, indicative of a more extended fibronectin conformation [96]. This result is echoed for fibronectin adsorbed to colloidally-roughened silica substrates [97]. The rearrangement of collagen into fibers on smooth substrates can also be hindered by nanocolumn patterning [98], and F-actin aligns on 2 nm- but not 4 nm- tall

ridges [99]. Globular proteins have been shown to retain their structure and biological activity on small, highly curved particles, whereas large proteins are denatured when forced to adsorb to such geometries [100-101]. These effects may be responsible for the differences observed for cells interacting with ECM adsorbed or secreted onto various nanopatterned substrates.

Altered protein conformation has also been directly implicated in the control of adherent cell behavior. Osteoblastic differentiation of MC3TC cells can be controlled by substrates that influence the conformation of adsorbed fibronectin [102]. Antibodies against specific fibronectin epitopes alter fibronectin binding when adsorbed to different substrate chemistries, subsequently affecting myoblast proliferation and differentiation [103]. Fibroblasts can sense the conformational change of fibronectin elicited by the subtle replacement of a substrate polymer's methylene groups with oxygen [104]. Cells are able to detect changes in substrate topography and chemistry through the high sensitivity of protein adsorption to these physical and chemical features.

2.2.2.2 Proliferation and endocytosis

Rapidly dividing cells are generally more susceptible to non-viral transfection, an effect generally attributed to greater access to the nucleus during cell division [4]. For example, low rates of proliferation elicited by contact-inhibition of epithelial cells leads to decreased lipoplex uptake and expression [105]. The decrease in transfectability with cellular confluence and age could also be due in part to decreased endocytosis in these cells. Indeed, late passage fibroblasts down-regulate the expression of amphiphysin-1, a

linker between the clathrin coat and dynamin, causing a decrease in receptor-mediated endocytosis that can be resurrected with reexpression of amphiphysin-1 [106-107]. Therefore, substrates that control cell proliferation are also expected to control cellular susceptibility to non-viral gene delivery.

Researchers have repeatedly noted changes in the metabolic and proliferative rates of cells cultured on patterned topographies. A decrease in proliferation for cells on micro- and nano-structures is most common, but increases are also observed [108]. For example, smooth muscle cells cultured on 350 nm wide gratings proliferated significantly slower, as measured by BrdU incorporation [109]. Fibroblasts cultured on quartz micropits with 7-25 μm diameters and 20-40 μm spacing proliferated most slowly for the smallest, most closely spaced pits [110]. There are some exceptions which report increased proliferation on patterns; connective tissue progenitor cells grown on 10 μm diameter, 6 μm high posts exited post-seeding lag phase days before cohorts cultured on smooth control PDMS [111]. Substrates eliciting elevated proliferation rates may therefore be beneficial for gene delivery.

2.2.2.3 Differentiation and endocytosis

The differentiation of certain cell types can be controlled with substrate topography and stiffness. Naïve hMSC are sensitive to nanotopography, encouraged by nanogratings to more readily commit to the neuronal lineage than by a chemical differentiation factor (retinoic acid) delivered to cells on a smooth substrate [112]. hMSCs are also sensitive to the stiffness of their substrate (a property that could be

modified locally with substrate topography), preferring osteogenic, myogenic, or neurogenic differentiation when cultured on gels with stiffnesses mimicking that of bone, muscle, or brain, respectively [113]. Mouse embryonic stem cells and osteoprogenitors can be maintained in undifferentiated phenotypes with culture on 2.4 μm tall, 1 μm diameter posts discovered by high-throughput screening of hundreds of micro-topographies [114-115].

The differentiation state of a cell population can determine the transfectability and endocytic phenotype of those cells. Non-viral transfection is notoriously difficult for neurons [116], macrophages [117], dendritic cells [118], and differentiated chondrocytes [119] and adipocytes [120]. Further, the expression of caveolae is up-regulated in terminally differentiated fat, endothelial, muscle, and transdifferentiated lens epithelial cells [121-122], and the uptake of LDL by clathrin-mediated endocytosis decreases with adipogenic differentiation of hMSCs [123]. hMSCs directed to the neuronal lineage by nanopatterns express less caveolin-1, and alter the expression profile of a number of integrin subunits [112]. In addition, the production of heparan sulfate proteoglycans (the ubiquitous receptors for cationic particles) is down-regulated with differentiation of myogenic satellite cells [124]. Given these differences in transfectability and endocytosis between various cell types, substrate nanotechnology-mediated differentiation is another tool that could be leveraged to engineer the non-viral expression of transgenes.

2.2.2.4 Expression of endocytic proteins

Irrespective of differentiation, cells cultured on patterned topography undergo genome-wide changes in the expression of proteins that are implicated in endocytosis. Changes in gene expression of cells on patterned topography are believed to be mediated, at least in part, by nuclear deformation. Many different cell types have been observed to align and elongate with nano- and micro-grooved topography. The lower size limit for this alignment may be cell type-specific, but has been demonstrated to be around 100 nm wide, 70 nm deep gratings for the early alignment of rat fibroblasts [125]. Smooth muscle cells [109] and hMSCs [112] also align and elongate on 350 nm PDMS gratings. Alignment of the cell membrane and cytoskeleton can translate force to the nucleus via intermediate filaments, and can result in nuclear alignment and deformation [126-129]. Stress applied to the nucleus alters histone deacetylation, chromatin condensation [130], and centromere arrangement [131], leading to global changes in gene expression.

The changes in protein expression on patterned topography include those explicitly implicated in endocytosis such as clathrin and caveolin, growth factors and cytokines that have established effects on endocytosis, matrix proteins that may alter cell-substrate interactions, and signaling proteins that are needed for endocytosis but are not necessarily as well understood in their mode of action. The latter category has recently been elucidated in an impressive manuscript where genomic libraries of siRNA were assessed for effects on the endocytosis of EGF and transferrin as directly observed with automated confocal microscopy [132]. The 4,609 genes affecting endocytosis can be cross-referenced with the handful of gene array studies that have been performed on cells interacting with patterned topography. For instance, human fibroblasts cultured on

micro-grooved quartz [126] and 13 nm polymer demixed islands [133-134] upregulated their expression of Grk6, integrin α_6, integrin β_5, the growth factor receptor tyrosine kinase Ryk, REP-2 (targets Rab5 to the plasma membrane for early endosome trafficking [135]), Jnk2, and many more; RNA interference with any of these proteins leads to changes in the uptake of EGF and transferrin or in the intracellular distribution of endosomes [132].

Dalby et al. have suggested that endocytosis is altered (qualitatively) for cells cultured on patterned topography. Human fibroblasts attempt to endocytose nanocolumns with 100 nm diameter and 160 nm height, as supported by increased dynamin and peripheral clathrin staining, and TEM visualization of nascent endocytic vesicles near columns [136]. Fibroblasts cultured on nanopits with similar dimensions formed clathrin tracks indicative of "high rates of endocytosis", and upregulated the expression of Epsin 2 [137], a stimulator of endocytic vesicle fissure from the plasma membrane [138].

Cytokines and growth factors are potent stimulators of cell function, and endocytosis is no exception. hMSCs cultured on patterned PMMA surfaces upregulated the expression of EGF and FGFb [112]. EGF can stimulate uptake of its own receptor as well as fluid phase endocytosis [139], and FGFb has been noted to downregulate the expression of surface-bound heparan sulfate proteoglycans [140]. Macrophages cultured on increasing nanograting widths increased their secretion of TNF-α [141], an inflammatory cytokine that accelerates clathrin-mediated endocytosis in Sertoli [142] and endothelial cells [143]. The expression of signals which increase endocytosis may be up-

regulated in cells interacting with patterns and act in an autocrine fashion, thereby altering the uptake of non-viral vectors.

2.2.2.5 Cell spreading and endocytosis

Cell spreading may be the best-described effect of culture on nano- and microtopographic surfaces. The heterogeneous presentation of extracellular matrix proteins adsorbed to topography supports varying degrees of integrin engagement. Adhesive substrates are predicted to sustain increased spreading with patterning (increased adhesive surface area), whereas non-adhesive substrates are expected to maintain better spreading if smooth (maintaining a minimal degree of cell deformation) [144]. Indeed, NIH/3T3 cells cultured on rough, super-hydrophobic silicon nanospikes were rounded, while those on rough, hydrophilic spikes were well-spread [145]. Fibroblasts [146] and endothelial cells [147] cultured on 13 nm tall polystyrene islands were more spread than those on flat control, and those cultured on 120 nm diameter, 100 nm depth pits in PMMA were much less spread than control [137]. This dependence of spreading on topography may be due to the altered ability of integrin to cluster for various substrates; gold nanospheres with RGD functionalization were deposited onto a passivated surface with well-defined spacing to study this possibility [148]. The nanospheres were small enough that only a single integrin could be expected to be able to bind to each. Cells grown on RGD spaced 108 nm apart had delayed spreading and a smaller projected area, compared to those on RGD spaced 58 nm apart.

The act of integrin engagement and spreading itself may have an immediate effect on endocytosis, before changes in protein synthesis could be expected (Figure 7, right). Caveolin-1 is a lynchpin of caveolar endocytosis, and convincing evidence has appeared implicating it in integrin signaling [149]. Integrin β_1 colocalizes with fibronectin and caveolin in focal adhesions [86], and its binding results in phosphorylation of caveolin-1 [150]. Caveolin-1 acts as a membrane adaptor protein to couple integrins to downstream signaling partners, and to facilitate integrin clustering by oligomerization [149]. Caveolin-1 knockouts are unable to internalize lipid rafts after detachment, and this behavior can be restored with subsequent reexpression of caveolin-1 [151]. Also, a loss of integrin-mediated adhesion results in the dramatic internalization of caveolae [152]. These studies demonstrate a strong link between integrin function and caveolar trafficking, but it is unclear what the functional implications are for the uptake of cargo molecules that are nearby or directly involved in this process.

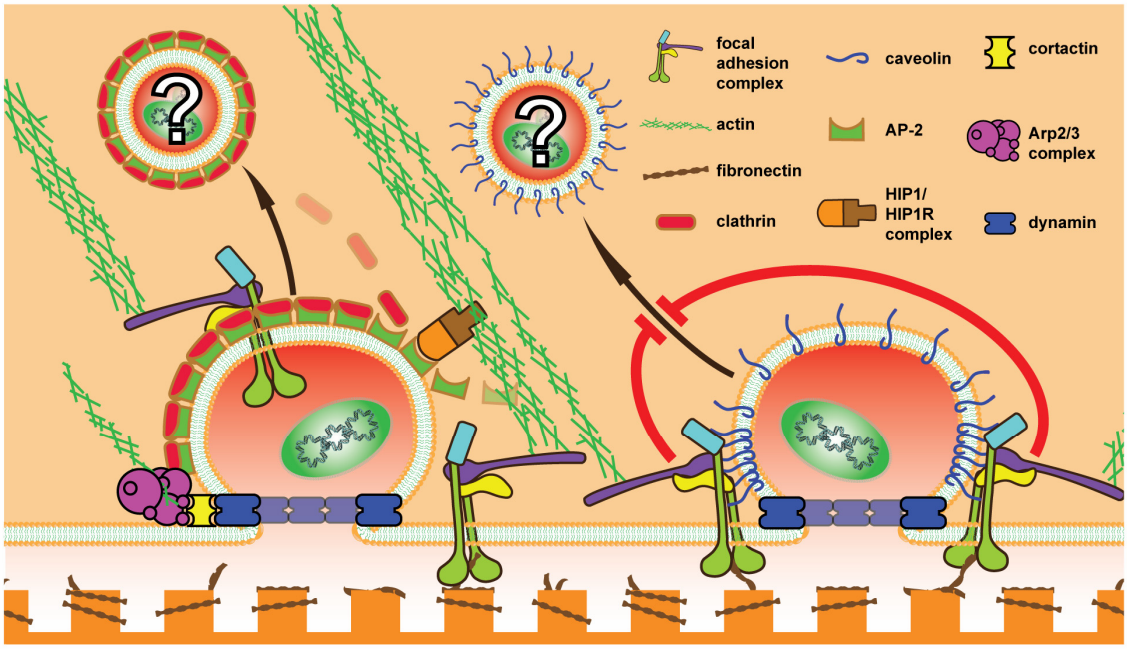

Figure 7. Two possible links between integrin engagement and nanoparticle uptake
(Left) Actin filaments localized to the cell surface by integrin-containing focal adhesions bind to the HIP1/HIP1R complex, which recruits AP-2 to assemble the clathrin coat on nascent vesicles. Cortactin is thought to induce and localize the polymerization of actin at internalizing vesicles by linking dynamin and the actin-nucleating complex Arp2/3. Integrin disassembly and internalization is a clathrin-mediated process, and high rates of this activity on patterned topography could compete with or augment complex uptake. (Right) Integrin engagement also results in local sequestration of caveolin-1 and stabilization of caveolae at the cell surface. Subsequent integrin release induces caveolae internalization, but it is unknown what effect this may have on the uptake of nearby gene carriers. Nanotopographical control of integrin engagement and turnover may be a useful tool in the study of these effects.

2.2.2.6 Endocytic turnover of focal adhesions

The formation, strengthening, contraction, and disassembly of focal adhesions allows cells to explore and move across their substrates. This cycle is controlled by substrate topography, as mediated through the availability of adsorbed integrin ligands. When integrins are not allowed to cluster, the small focal adhesions that form are unable to hold on upon contraction of the actin cytoskeleton [127], leading to a more rapid turnover of adhesions as the cell searches for stable contact [148]. Integrin clustering is likely affected by the adsorption of ECM to nano- and microtopography, producing differences in the size, strength, and number of adhesions formed on different structures.

Tall features restrict binding to the tops of patterns, small feature size (< 70 nm) prevents adhesions from forming at all, and large interfeature spacing reduces integrin clustering [89]. Indeed, fibroblasts cultured on 50 nm diameter pits have much smaller focal adhesions, and normal actin stress fibers are not formed [153]. On the other hand, shallow 30 μm diameter PMMA pits encourage a higher number of adhesions in hMSCs [154]. Furthermore, 350 nm PDMS gratings decrease the expression of vinculin in hMSCs compared to smooth control, and lower the cells' elastic moduli as measured by AFM, indicative of structural changes in the organization of the actin cytoskeleton [155].

These effects of topography on focal adhesion formation and turnover may be instructive of the situation in vivo; natural 3D extracellular matrices encourage the formation of small focal adhesions, while flattening the same matrix into two dimensions recovers large adhesions [156]. 3D fibrillar matrix also increases the rate of fibronectin remodeling [157]. This remodeling proceeds by caveolar endocytosis, as demonstrated with inhibition by low temperature, and siRNA against caveolin-1, genistein, β-cyclodextrin, and staursporin [158]. Substrate topography introduces a degree of three-dimensionality to the presentation of adsorbed proteins, and may therefore modulate this remodeling process.

A number of recently described molecular interactions have linked components of the focal adhesion complex and the endocytic and cytoskeletal machineries (Figure 7, left). Disassembly of focal adhesions is a clathrin-dependent endocytic process; clathrin and AP-2 colocalize with focal adhesions, and knockdown of clathrin, AP-2, and dynamin activity results in lowered integrin internalization [90]. As well, recently described proteins including cortactin, Abp1p, Hip1R, and intersectin-1 link actin-

nucleating enzymes such as Arp2/3 to their substrates [159-160], and recruit clathrin to the plasma membrane to stimulate its assembly and association with actin [161-162]. Actin contractility has indeed been suggested to drive the internalization of cholesterol-rich lipid rafts containing cationic complexes bound to proteoglycans [163]. Interestingly, inhibition of PKC with staurosporine inhibits uptake and expression of PEI complexes, but not their binding. These interactions suggest differences in the strength of integrin binding and the speed of integrin turnover induced by substrate topography can be expected to alter endocytic activity. This could manifest as a coincident uptake of complexes or as a downregulation of particle uptake through increased competition for the endocytic machinery by the process of integrin internalization.

2.3 Future therapies for neurodegenerative disease

Neurodegenerative diseases are responsible for an enormous proportion of global morbidity and mortality. Currently-approved treatments generally only manage symptoms, or at best slow disease progression. As a consequence of the high prevalence and poor prognoses of these diseases, the desire for and willingness to accept new gene- and cell-based therapies against neurodegeneration has been high for decades, with unfortunately little human benefit to show for it… yet. The groundbreaking discovery of iPSCs and the resulting upheaval of the dogmatic "irreversibility" of development has reignited the hope that curative autologous cell therapies for neurodegeneration can be realized. However, the teratogenic capacity of iPSCs may preclude or slow their wide approval for use in humans. Excitingly, the discovery of direct lineage conversion from

adult somatic cells to functional neurons and glia has significantly reduced if not eliminated safety concerns regarding teratogenicity, but much work remains to be done to produce sufficient quantities of cells for use in humans without the use of potentially dangerous integrative methods. In this section we review state-of-the-art gene and cell therapies against Alzheimer's disease (AD), Parkinson's disease (PD), and multiple sclerosis (MS), and describe how the rapidly-developing toolbox of direct reprogramming may be wielded to improve now-dire therapeutic outlooks, and how intelligently-selected microenvironmental factors may aid in this cause.

2.3.1 Current standard of care and prognosis

There are countless neurodegenerative diseases, but Alzheimer's, Parkinson's, and multiple sclerosis are, if not absolutely, among the most: costly, prevalent, debilitating, and deadly. These negative outcomes are a direct consequence of perhaps the most defining fact of our CNS – our neurons are as old as we are because they do not divide, and they are generally not replaced if lost (with rare exceptions – in the dentate gyrus, for example). This long persistence time provides us with a degree of permanence about our personalities and memories, but also poses a unique medical challenge when these cells and circuits die.

There are tens of thousands of highly-specified neuronal subtypes, each of which may theoretically be subject to a specific autoimmune or prion-mediated attack. These diseases can arise as a consequence of a highly penetrant familial mutation of a single gene, or as a sporatic idiopathic form that is presumably polygenic or otherwise

multifactorial. This diversity of etiologies makes cure development very difficult, particularly because patients are often undiagnosed until symptomatic, at which point neuronal death has typically progressed to a significant extent. Even with an accurate and timely diagnosis, there are no curative options for these diseases, only strategies for improved symptom management, or to slow progression. Developing curative treatments is becoming increasingly important, as our population shifts to a more aged demographic, and patients consequently suffer more from the neurodegenerative diseases which principally occur later in life [164].

Current estimates are that AD affects 5 million people in the US alone, and costs over $170 billion each year [165], with an additional 17.5 billion hours of unpaid care provided by friends and family yearly [166]. AD affects 10% of those over 65 years of age, and 50% of those over 85 [167], with a mean life expectancy of 7 years following diagnosis [168]. The major pathological change in AD is a loss of cholinergic neurons in the basal forebrain, with projections to the cortex and hippocampus [169], caused by accumulation of amyloid plaques. This eventually leads to widespread cortical neuron death, loss of memory, dementia, and eventual loss of organ functions, and to death of the patient. The only approved therapies for AD are neuroprotective cholinesterase inhibitors and NMDA receptor antagonists [170-171], which are only effective for a period of months to manage symptoms in a portion of patients.

Parkinson's disease is also highly prevalent in the aged; 1-2% of people over the age of 60 suffer from PD [164]. PD costs $11 billion per 500,000 affected Americans each year, with 1.5 million currently-diagnosed cases [172]. PD is a selective loss of dopaminergic neurons in the substantia nigra pars compacta of the ventral mesencephalon.

This loss lowers the dopamine levels in the dorsal striatum, with eventual deterioration of nigrostriatal projections [164]. This produces a gradual deterioration of motor function in the patient, leading to characteristic tremors, difficulty walking, and increasing disability. This eventually progresses to dementia, and a significantly increased risk of death from complications such as pneumonia [173]. Approved treatments manage symptoms and include: L-dopa, dopamine agonists, anticholinergics, MAO-B inhibitors (which block the breakdown of L-dopa), and deep brain stimulation (DBS) to treat tremors and medication-induced dyskinesia. The effectiveness of each of these treatments decreases over time, with a virtually inevitable symptomatic progression.

Multiple sclerosis has a worldwide prevalence of approximately 2.3 million, with 400,000 cases in the United States, carrying an average annual cost of $28 billion [174]. MS is an autoimmune inflammatory disease, which results from destruction of the myelin sheath insulating neurons in the brain and spinal cord. These lesions appear in multiple foci along the white matter tracts, and eventually result in death of the demyelinated axons, and motor deficit. After diagnosis, ambulation difficulty begins an average of 8 years later [174], and the employment rate of patients declines 3% each year [175]. There are many presentations of the disease, including relapsing-remitting and steadily-progressing forms. No treatment alters the course of primary progressive MS [176]. The progress of relapsing-remitting MS can be slowed but not reversed with aggressive immunomodulation via interferons [177], inhibition of T-cell proliferation [178], lymphocyte sequesteration [179], etc., and relapses are managed with corticosteroids [180], which does not alter the disease course. After immunosuppression fails, patients may elect for immunological ablation and hematopoietic stem cell transplantation in an

effort to induce tolerance rather than attack at lesion sites, which comes with a significant risk of implant-related mortality [181].

2.3.2 Gene therapies

Currently-approved medications for PD, AD, and MS collectively represent transformative advances for patient comfort, and some can extend symptomless months and even years, but they are not curative. The pipeline for discovering, implementing, and approving new drugs is extraordinarily slow and expensive, and animal models have not been predictive of success [182]. Current gene therapies for neurodegenerative disease generally aim to deliver neurotrophic factors to promote neuron survival, or enzymes that are known to be absent in patients with well-characterized deleterious genetic mutations. As a drug delivery technique, gene therapy promises more sustained therapeutic effects than small molecule drugs, as the gene products are produced actively by cells over a longer period of time – potentially for the entire life of the patient.

Viral vector-based gene therapies have largely coalesced into *ex vivo* lentiviral transduction into hematopoietic stem cells, and delivery of adeno-associated viruses *in vivo*, which can suffer from immune responses that limit efficacy [183]. Despite this concern, over 1800 gene therapy clinical trials have been completed worldwide [184], with an assortment of positive and negative outcomes. Most positively, lentivirus has been used to successfully treat X-linked adrenoleukodystrophy in two patients following immune ablation and reconstitution with genetically-corrected hematopoietic stem cells [185]. Sub-retinal injection of AAV expressing a corrected RPE65 gene has also

improved visual acuity in 5 patients with LCA2 3 years after treatment [186-187]. AAV is also beginning to show promise in the CNS. The use of AAV is particularly attractive for CNS gene therapy because AAVs infect non-dividing cells, can drive long-term expression from subtype-specific promoters, and can be serotyped to infect a particular neuronal or glial target [188]. The advent of recombinant AAV technology has allowed a number of human PD and AD trials to proceed [189-190], including focal delivery of AAV carrying neurotrophic factors (neurturin [191]) or enzymes for synthesis of dopamine (GAD [192], AADC [193]) for use in patients with PD [183], and delivery of NGF via infected fibroblasts to promote neuron survival in a major cholinergic center in patients with AD [194-195].

Despite these promising results, there are a number of safety and efficacy concerns associated with the use of viral vectors for gene therapy. Potential complications include retroviral insertional mutagenesis, phenotoxicity from prolonged transgene overexpression, immune response against capsid components, horizontal transmission from bodily fluids which remain infectious for a long period of time, and vertical transmission in the case of lentivirus [183]. For some specific examples – a trial to treat SCID-X1 in 5 patients with gammaretrovirus to correct the IL2RG gene was initially promising, but 4 of the patients developed T cell leukemia due to insertional mutagenesis and oncogene activation [196]. A patient treated for X-CGD with retrovirus died after the transgene was methylated and silenced [184, 197]. With gene therapy *in vivo*, the most proliferative (and potentially dangerous) clones may have a selective advantage [198]. Further, hepatocytes transduced with AAV have been shown to elicit a potent T cell-mediated killing response; such an immunological attack would not be

benign in the CNS [183]. Effective viral therapies may therefore require immunosuppressants [199]. There are also many examples of non-viral gene therapies against neurodegenerative disease [200], which typically avoid a majority of the genotoxicity and immune response associated with lentiviral and AAV therapy, respectively. For instance, there is currently an open Phase II trial for correction of MS by delivery of naked plasmid DNA vaccines encoding MBP [201-202], and naked VEGF plasmid has been injected to protect peripheral neurons in patients with diabetic neuropathy [203].

2.3.3 Cell replacement therapies

The approved drugs and gene therapy techniques described previously cannot replace neurons that have already been lost at a late stage of neurodegenerative disease – only alleviate symptoms of or slow their inevitable loss. However, cell replacement therapies have the potential to reverse neurodegeneration by replacing those lost cells with healthy equivalents, and as such have been a tantalizing target for decades. As described in this section, "cell therapy" is distinct from cell-based delivery of viral transgene products, which is occasionally used in conjunction with lentiviral or AAV neuroprotective strategies (such as a NGF delivery via infected fibroblasts). "Cell therapies" in this context aim to recapitulate all or the most critical complex function(s) of neurons or glia lost to degenerative processes – neurons for PD and AD, and oligodendroglial cells for MS.

There is some shared rationale for cell therapy against AD, PD, and MS. Generally speaking, idiopathic non-familial neurodegenerative diseases – which are polygenic or multifactorial – are more prevalent than their monogenic forms. Gene editing techniques, which can correct specifically-targeted (and known) diseased genes, are transformative for a small portion of the population with well-characterized singular defects, but are unable to treat the largest idiopathic proportion of the patient population. Neuroprotective gene therapies, as described in the previous section, can slow the progression of polygenic diseases, but the underlying degenerative processes continue. Embryonic, neural, and induced pluripotent stem cells (ESCs, NSCs, iPSCs) share a highly proliferative phenotype, and, with varying degrees of accuracy and efficiency, the ability to differentiate into functional neurons and glia. Stem and progenitor cell-derived neurons and glia may be able to correct neurodegenerative disease phenotypes without an understanding of the unique particularities of each patient's etiology. NPCs and NSCs have more limited division potentials than ESCs, but can be maintained in proliferative state in vitro [165, 204]. Grafted neurons and glia may replace tissue function directly, scavenge excitotoxic neurotransmitters, and support surrounding cells by the release of neurotrophins. These characteristics have allowed expansion of stem and progenitor cell sources to levels required for human trials, but also come with steep safety and, for embryo-derived tissues, ethical concerns, which may be insurmountable for widespread clinical translation.

Cholinergic neurons may be the best candidates for transplanted cell therapy in AD [170], but these are not the only neurons lost in AD, and as such replacement of only cholinergic neurons is not expected to restore full function to a patient. Cholinergic

differentiation from stem cells is difficult to achieve accurately, but is possible for a small proportion of the cells [169]. Cell therapy for AD is made more difficult by its multi-focal nature – implanted neurons would ideally be delivered and integrated into multiple sites across the brain for maximum recovery of function. Despite these hurdles, significant memory test recovery has been achieved after replacement of cholinergic neurons derived from ESCs in lesioned and aged animal models of AD [205-206]. The multifocal delivery required for improvement across an Alzheimerian brain could also be achieved by the widespread migratory capacity of neural progenitor cells [165]. iPSCs have also been differentiated to NSCs, and then to cholinergic neurons, and then implanted NSCs to provide phenotypic recovery in an animal model of AD [207].

PD results from disorder of a single small region of the brain, in a well-defined subtype of neuron – those which secrete dopamine. This is a best-case scenario for cell therapy in the CNS – delivery of relatively few cells at a single anatomically-defined focal point (the striatum or substantia nigra). At minimum, implanted dopaminergic neurons need only to secrete dopamine onto the striatum to provide some symptomatic relief. At best, implanted dopaminergic neurons would integrate with their appropriate afferent and efferent connections along the nigrostriatal pathway, thereby recapitulating the normal feedback circuits required for proper dopamine regulation.

Initial allogeneic transplantation of DA neurons from fetal ventral mesencephalic tissue into the striata of PD patients showed some clinical benefits [208-211], but the improvement was modest and results were mixed across several trials [212-213]. Societal concerns of using fetal tissue as a cell source and low yields of DA neurons from the tissue presented additional challenges [165]. Motivated by these results and a desire to

improve yields of pure DA neurons for transplantation, investigators have developed protocols for dopaminergic differentiation from ESCs that are much more efficient than other neural subtypes [169]. iPSCs have also been successfully differentiated to functional dopaminergic neurons, and implanted in a lesioned animal model of PD, with restoration of some motor function [214].

Cell replacement therapy for multiple sclerosis shares some of the same challenges faced in cell therapy for AD, as well as some of the advantages of cell therapy for PD. Like AD, MS is widespread and multifocal, with inflammatory lesions appearing throughout all of the white matter tracts. However, like PD, the target cells to be replaced are well-defined – the oligodendrocyte progenitor cell (OPC), or myelinating oligodendrocyte (OL). Though a multifocal disease, the motivation for cell replacement therapy in MS is very strong [215]. For progressive MS, standard medications fail in an early stage, with uniform downhill progression. Transplanted OPCs or OLs can migrate rapidly to sites of injury and inflammation [216-217] where they can act to inhibit inflammation, protect neurons with neurotrophins, and participate directly in remyelination. Transplanted OPCs have superior remyelination capacity than OLs [218], presumably because individual OPCs can each produce multiple OLs. Various transplanted OPC cell sources can remyelinate model lesions in the adult CNS [219]. Perhaps most excitingly, human iPSC-derived OPCs have been shown to migrate, disseminate, and myelinate across the entire neuroaxis of congenitally hypomyelinated animals *in vivo* [220].

For each of these implantation strategies in AD, PD, and MS, it is not fully clear what implications the underlying disorder may have on long term graft survival,

particularly considering there may be a prion component to these diseases [221-222]. Transgenic and lesioned animal models often do not fully capture the sensitivity implanted neurons may have to the disordered microenvironment in patients with non-familial disease. Supporting this notion, remyelination is a constantly active process in human MS tissues [223]. The failure of endogenous OPCs to fully myelinate axons in chronic MS [224] may reflect an impermissive extracellular microenvironment, potentially mediated by chondroitin sulfate proteoglycans and hyaluronan at lesion sites [225]. Despite the potential for impermissive microenvironmental effects at diseased implant sites, there is some evidence for the functional superiority of transplanted OPCs over older resident OPCs [215, 226].

These results are a clear indication of the potential cell replacement therapies hold for regenerative medicine. The discovery of iPSCs by Yamanaka in 2006 [227] removed the greatest ethical and practical barriers to stem cell access, and provided the first feasible opportunity to produce autologous neurons and glial cells. Autologous iPSC-derived neurons and glia have a clear advantage for cell replacement over fetal and embryonic sources, in that they should theoretically not require immune suppression upon implantation. Unfortunately, the exciting functional improvements afforded by differentiated ESCs, NSCs, and iPSCs are tempered by a host of safety concerns. iPSCs can incur genotoxic integrations when produced with integrative viral methods, and their autologous immunological privilege is not always absolute. We discuss these concerns next.

The danger of uncommitted progenitors and stem cells is now appreciated as a real one, following human implantation trials. In one example, a boy implanted with

fetal NSCs to treat a congenital ataxia developed a donor-derived tumor 4 years later [228]. Animal models also agree that, even with efficient differentiation techniques, ESCs carry the potential for phenotypic instability and can retain tumorigenicity after implantation [229]. Besides incomplete differentiation, *inaccurate* differentiation of ESCs and NPCs is problematic as well. Graft-induced dyskinesias are a common complication following cell replacement therapies for PD, and may result from unintended co-transplantation of serotonergic cells [164, 230-231]. The same concerns arise from the use of iPSCs [232], with the added concern that the use of viruses in their derivation can induce copy-number variation [233] – a structural mutation that may underlie complex heritable diseases [234], including those of the nervous system [235] – and insertional activation of oncogenes [236]. Finally, it is somewhat surprising to note that implanted syngeneic undifferentiated iPSCs are immunogenic [237], though it remains to be seen if the same is true for xeno-free and fully-differentiated cells [164].

Though the concerns associated with the continuously-proliferative phenotype of iPSCs are inherent to their identity as self-renewing stem cells, their safety profile could be improved through the removal of viral transduction during their creation. As such, there has been a significant effort devoted to the removal of virus and vector sequences for the generation of more clinically-translatable iPSCs [238]. Transfection with episomal plasmids [239] or direct transcription factor protein delivery [240] can generate integration-free iPSCs, but at very low efficiencies. Plasmid DNA transfected with lipoplexes [241], polyplexes [242], or electroporation [243] can also produce integration-free iPSCs (with screening) at comparatively higher efficiencies. Repeated transfection of mRNA with modified ribonucleotides avoids integration and is less immunogenic than

unmodified mRNA [244], and can generate iPSCs at an even higher efficiency than retrovirus [245]. Transposase- [246-247] and cre recombinase-based [248] insertion/excision of reprogramming factors can remove reprogramming factors after conversion has been completed, and will benefit from ongoing advancements in safe harbor-targeted, rather than random, insertion [249-250]. Taken together, these results are definitive evidence that efficient but less-safe integrative viral techniques are not obligate for the successful generation of iPSCs.

2.3.4 Direct somatic cell reprogramming

We have described how cell replacement is expected to deliver improved future therapeutics over current "gold standard" drug-based treatments, how iPSCs are an ethical and immunological improvement over ESC sources for cell replacement therapies, and how iPSC safety can be improved with the use of non-viral reprogramming systems. From a therapeutic perspective, the biggest remaining problem is the unrestricted proliferative nature of iPSCs. The ability to directly generate functional neurons and glia from an autologous adult cell source while completely avoiding a teratogenic pluripotent stage, preferably without the use of virus, would be the "ideal" cell source to be wielded on behalf of millions of patients with intractable neurodegenerative disease.

2.3.4.1 Directly-inducible CNS cell types

In 2010, Wernig et al. succeeded in delivering three neuronal transcription factors (TFs) – Brn2, Ascl1, and Myt1l (BAM factors) – with lentivirus, to convert mouse

fibroblasts directly into functional neuronal cells [251], referred to as induced neuronal cells (iNs). Human cells were converted subsequently with the addition of NeuroD1 [252]. These iNs generated action potentials and formed functional synapses when co-cultured with primary cortical neurons or glia. Like the first report of iPSC generation, this discovery represented a paradigm shift for cell biologists and cell therapists alike, demonstrating the first clear direct conversion of somatic cells from one germ layer to another. As a source for cell replacement therapy, cells produced via direct somatic reprogramming with terminal fate-determining factors likely have a marked safety advantage over iPSCs, in that they do not rely on oncogenes for induction, and are not expected to proliferate indefinitely *in vivo*.

Since its inception, the neuronal transdifferentiation field has expanded rapidly. The use of new transcription factor cocktails has generated induced human dopaminergic neuronal cells (iDAs) which are capable of releasing dopamine and providing phenotypic rescue in animal models of PD [253-257], as well as cholinergic motor neuronal cells (iMNs) [258]. Fibroblasts from patients with familial Alzheimer's disease [259], hepatocytes [260], astrocytes [257], and pericytes [261] have all been directly induced to a functional neuronal phenotype. Further, cells have been infected with lentiviral miRNA/TF cocktails [262-263], or only with a shRNA construct targeting a single gene to de-restrict miRNA-mediated interference with REST function, to convert fibroblasts to functional neurons [264].

Direct neuronal reprogramming is more efficient than iPSC generation, but iPSCs still have the logistical (though not necessarily medical) advantage of a proliferative phenotype, which eases scale-up to the quantities required for animal and human trials.

However, accurate and efficient differentiation of ESCs and iPSCs remains a challenge, particularly for astro- and oligodendroglial targets [164, 265], so only a fraction of those expanded iPSCs would be therapeutically-beneficial as implants – "It can be summarized that, after a decade of research […], robust and reproducible differentiation protocols have not been established" [164]. For these reasons, the subsequent discovery of transcription factor cocktails that can reprogram fibroblasts to lineage-committed but expandable NPCs [266-267] and OPCs [268-269] is particularly exciting. With defined growth factor support these cells can be expanded many times, and upon mitogen removal efficiently differentiate into functional neurons and myelinogenic glia. iOPCs and iNPCs are expected to have more limited proliferation and lineage restrictions *in vivo* than iPSCs or ESCs [220, 270], and are likely much safer as a consequence.

Beyond their utility in cell replacement therapies, these induced neurons and glia will also find utility as test beds for drug discovery. Before the discovery of iNs, there was no way to drug diseased, aged, and accurately-specified human neurons *in vitro*. Neurons harvested post-mortem often reflect a diseased endpoint phenotype, which is likely not the most amenable to therapeutic intervention. One example of the promise of this new modeling technique is the derivation of functional neurons from fibroblasts taken from patients with familial Alzheimer's disease. These neurons recapitulated diseased processing of APP and Aβ [259]. Similarly, neurons generated from fibroblasts carrying a neuroligin-3 mutation associated with autism demonstrated a diseased synaptic phenotype [271].

2.3.4.2 Direct neuronal reprogramming *in vivo*

Some of the most recent developments in direct neuronal reprogramming have demonstrated direct conversion *in vivo*. The success of these techniques may be particularly important for certain types of clinical reprogramming. The panoply of neuronal subtype specificity is based not only on the molecular identity, morphology, and electrophysiology of individual cells, but also on their anatomic location and connectivity with others – these are exclusively *in vivo* traits which, if necessary for positive therapeutic outcome, may be particularly difficult to recapitulate fully with *ex vivo* reprogramming and subsequent transplantation [272].

Encouragingly, reactive glial cells have been reprogrammed to neurons *in vivo* with lentiviral delivery of NeuroD1 in an animal model of AD [273]. Implanted pre-infected dox-inducible fibroblasts and striatal astrocytes could also convert to neurons *in situ* [274]. Furthermore, resident postmitotic neurons could be reprogrammed with electroporation of Fezf2 from one subtype and cortical layer to another [275], and accurately reprogram the afferent/efferent connectivity of L4 neocortical neurons (which make local intracortical connections and do not project axons to subcortical structures) to that of L5B neurons (which project through the striatum to the pons and spinal cord) [276]. These results are proof-of principle that *in vivo* cues may be supportive and sufficient to guide more complex subtype-specific anatomical integration and function of iNs than can be attempted *in vitro*.

2.3.4.3 Non-integrative direct reprogramming

To date, all the neuronal transdifferentiation success has been achieved using viral, and almost exclusively integrative, delivery strategies. These iNs are invaluable for neuronal disease recapitulation, drug discovery, and exploring the emerging biology of direct reprogramming. However, the concern of genotoxic integration of viral payloads into the host genome hinders the clinical translatability of lentiviral iNs [164, 184, 236], just as it does lentiviral iPSCs, and encourages the search for efficient non-integrative methods to generate these cells.

For the moment, the list of non-integrative direct reprogramming methods in the CNS is considerably shorter than that for iPSC generation, as the field is just beginning to emerge. Cytoplasmic Sendai viruses have been deployed to generate iNPCs via brief expression of the Yamanaka factors, including the oncogene c-Myc [277]. Adenoviral delivery of Ascl1, Brn2, and Ngn2 was used to reprogram fibroblasts to iNs, without evidence of integration [278]. There are ongoing trials to convert resident astrocytes to dopaminergic neurons in a non-human primate model of PD with *in vivo* delivery of Ascl1, Nurr1, and Lmx1b via AAV [279]. iNPCs were also generated by lipofection of Sox2 and Pax6 plasmids into adult human fibroblasts, which could be differentiated into multiple neuronal subtypes, and were electrophysiologically-capable [280]. To date, our report of polymeric nanoparticle-mediated reprogramming of fibroblasts to iNs with Ascl1, Brn2, and Myt1l (described in Chapter 3), is the only published protocol for non-viral direct generation of neurons [281]. These successes clearly demonstrate that various clinically-relevant cell types can be produced via direct reprogramming without integration, and without virus.

2.4 Microenvironmental effects on direct reprogramming

Though the published non-viral methods for iN and iNPC production are encouraging, the efficiency of these processes is currently lower than that of their viral counterparts. Even viral direct reprogramming can suffer low conversion yields – in particular, induced motor neurons [258] and iOPCs [268] initially suffered from drastically lower efficiencies than Ascl1, Brn2, Myt1l glutamatergic neuron induction [251]. The field is therefore well-motivated to investigate and understand the unique contextual barriers to reprogramming for each specific transcription factor cocktail and starting cell source, as well as any barriers shared by all cells converting from the mesodermal to ectodermal lineage.

Setting aside the practical issues of transcription factor- and cell-delivery for a moment, the many questions faced by the field can perhaps be summarized generally as: Why are certain transcription factor cocktails more efficient at reprogramming the same cell source, and why are certain cell sources more amenable to reprogramming with the same factors [282]? It could be that there are inherently "powerful" pioneer transcription factors, which are particularly capable at binding condensed chromatin and efficiently recruiting transcriptional and epigenetic-modifying machinery [283]. It could also be that target genes for a particular desired phenotype may be potently occluded (or primed) epigenetically [284] in a given starting cell source. These "intracellular microenvironmental factors" have been the best-studied to this point in the short history of direct neuronal reprogramming.

Extracellular microenvironmental factors are less-understood in the context of direct neuronal reprogramming. Ordinary culture systems may not provide appropriate

physio-chemical cues for the survival and maturation of newly born neurons [164], which are exposed to a variety of spatio-temporally varying electrical and soluble cues to prompt differentiation, maturation, and survival *in vivo*, not to mention any intermediate transient phenotypes which lay between fibroblast and neuron. Interestingly, it is becoming clear that at least some of the processes of normal neurodevelopment are traversed by induced neurons. For instance, the sequential activation of endogenous Ascl1, Brn2, Myt1l, then NeuroD1 expression in reprogramming human neurons is the same as that seen *in vivo* [285]. Furthermore, the genomic binding sites of Ascl1 in fibroblasts overlap closely with those in ESC-derived NPCs [272]. As such, informed appropriation of developmentally-inspired microenvironmental cues may provide an excellent entry point for the discovery of new techniques to improve direct reprogramming yields and to accurately guide subtype specification. In the following sections we explore how microenvironmental encouragement and transcription factor-mediated forcing could act synergistically.

2.4.1 The epigenome

Cells expressing the same set of ectopic transcription factors do not always reprogram to the same fate – epigenetic modifications are required as well, as demonstrated by the reprogramming of mitotic germ cells into neurons *in vivo* only upon removal of a histone remodeling complex component [286]. The stability of a differentiated phenotype is the result of a combination of cis-acting factors such as methylation, posttranslational histone modifications, and nucleosome positioning, and

trans-acting factors including transcription factors, coactivators, noncoding RNA, and chromatin remodeling complexes [283]. Epigenetic modifications can therefore act as potent inhibitors to reprogramming speed and success.

Some of the earliest evidence for the importance of epigenetic modifications in direct reprogramming came from studies of myogenesis in non-muscle cells via cell fusion or transfection. Pretreatment of HeLa cells with 5-azaC, a global DNA methyltransferase inhibitor, allowed their reprogrammed via fusion with myotubes [287]. 5-azaC can also induce spontaneous muscle differentiation in fibroblasts, and the demethylated genomic DNA from these cells could induce muscle phenotypes in other cells [288]. MyoD, the "master regulator" of skeletal muscle induction was discovered shortly thereafter [289]. MyoD-mediated reprogramming is dependent on the intracellular microenvironment; on its own, MyoD is unable to fully convert cells from non-mesoderm lineages [290].

These early reprogramming experiments with MyoD were indicating that the pre-existing state of a starting cell source is crucial to the success or failure of complete transdifferentiation. The induced expression of a gene is dependent on permittivity both in cis and in trans. One of the most elegant examples of this came from the transfection of epigenetically blank or "naive" bacterial artificial chromosomes (BACs) of myogenic genes that are normally silent (occluded, either in trans or in cis) in fibroblasts. Whereas the endogenous copies of these genes (Myf5/6) were silent, BACs transfected into fibroblasts induced Myf5/6 expression and a muscle phenotype, meaning the fibroblastic intracellular microenvironment was entirely supportive of expression in trans. However, when transgenic mice were generated carrying the Myf5/6 BAC, both the endogenous

and BAC copies of the gene were silent. Myf5/6 BACs transfected in at an early stage of development were also silenced. These results suggest the Myf5/6 locus is cis-silenced during development, which is a prerequisite for maintenance of a non-muscle phenotype in fibroblasts [284].

The importance of epigenetic states has also been well-documented in the iPSC field. Small molecular inhibitors of DNA methyltransferases, histone deacetylases, and demethylases have all been found to be able to increase iPSC generation efficiency, and at times to substitute for some of the Yamanaka transcription factors [291-292]. The ability of only a small percentage of cells to surmount all of the barriers to reprogramming has been a point of particular interest to the field. There has been debate over two hypotheses with respect to the method whereby these rare cells become iPSCs: stochastic induction of pluripotency (perhaps reflecting brief access to a critical promoter during cell division), or deterministic acquisition of pluripotency from an "elite" cohort of cells. The current state of understanding is that fibroblasts reprogram to iPSCs via distinct intermediate stages, each with a variable recalcitrance to progression towards the next [293]. One of these intermediate stages may be a hyperproliferative phenotype, which is acquired stochastically with Yamanaka factor induction, but once obtained progresses deterministically to full pluripotency, and is parent to 99% of iPSC clones [294].

The details of the epigenetic changes required for a fibroblast to become a neuron are not well known. The differences in reprogramming efficiency towards various neuronal subtypes may reflect necessary activation of a particularly stubborn cis- or trans-occluded gene during reprogramming. Interestingly, a complex combination of

chromatin marks identified by ChIP predicts both the permissiveness to Ascl1 binding in non-neuronal cells, and the efficiency of their reprogramming to iNs [282]. Fortunately, it seems that stable and complex cell fates can often be fully-instructed by a remarkably short list of master regulators (Ascl1 is sufficient to generate functional albeit slowly-maturing neurons from fibroblasts [251], and Ngn2 alone can produce functional motor neurons [295], for example). Therefore, improvements in transdifferentiation may come from selecting maximally-permissive starting cell sources for a given master regulator, and further microenvironmental destabilization of existing transcriptional programs to discourage converting cells from falling into undesirable valleys on Waddington's "epigenetic landscape" [285] during the reprogramming process.

Necessary destabilization of starting cell programs may be why the efficiency of neuronal reprogramming is proportional to viral titer [285], and by extension potentially why non-viral methods generally produce lower yields. Supra-physiological doses of ectopic reprogramming factors may outcompete endogenous transcription factors for ubiquitous E protein cofactors such as Tcf3, which are required for lineage-specific bHLH factors (like MyoD and Ascl1) to bind to DNA [283, 296]. Other factors may act in trans to compete with ectopic factors; Foxo3, for instance, shares many targets with Ascl1, and inhibits Ascl1's ability to reprogram fibroblasts [297]. High levels of Oct4 and Klf4, with lower levels of c-Myc and Sox2, is the best combination for iPSC generation [292]. It is also possible that the increased iN generation efficiency with high levels of ectopic factor expression may reflect an improved activation of the endogenous loci via epigenetic remodeling, irrespective of increased levels of direct downstream transactivation.

The advent of synthetic CRISPR/Cas9 transcription factors may help to elucidate the relative contributions of stable activation of endogenous master transcription factor loci from the supraphysiological expression of the downstream targets of those factors. CRISPR/Cas9 transcription factors directly activate target endogenous loci, evidently even when occluded by heterochromatin [298], but currently induce lower overall levels of protein expression than is produced from conventional plasmids. It therefore remains to be determined if equal amounts of endogenous and ectopic transcription factor expression result in greater reprogramming for those activated endogenously by CRISPR/Cas9, which would indicate that epigenetic de-repression of the endogenous loci may be one of the principal barriers to successful direct reprogramming.

2.4.2 Soluble factors

Normal development relies on a host of soluble factors to specify and pattern the differentiation of all cell types. For just a few examples: FGF, TGF, Shh, and Wnt signaling specify germ layers - TGFβ and BMP-4 to mesoderm, and ectodermin to ectoderm, often utilizing cross-antagonism to support stable fates [299]. Neural subtype patterning is guided in a similar way by soluble factors - for instance FGF8, TGFβ3, and Shh specify a dopaminergic neuronal fate from progenitors. These developmental cues have been used to improve both the derivation of specific neuronal subtypes from progenitor cells, as well as to increase the yields of neurons induced by direct reprogramming.

Dorsomorphin, a BMP inhibitor, drastically increased the yield of induced cholinergic motor neurons from human fibroblasts, and their survival depended on the support of the essential motor neuron trophic factors BDNF, GDNF, and NT-3 [295]. Inhibition of BMP, SMAD, and GSK-3β (involved in TGFβ signaling [300]) with small molecules also improved the yield of glutamatergic neurons [301]. Interestingly, similar small molecule cocktails have previously worked to improve the yield of iPSCs [302] and induced cardiomyocytes [303-304]. For iPSCs, it is believed that the small molecules encourage the obligatory mesenchymal to epithelial transition (MET), but it's not known if a similar transition is required for iN formation [292]. Ngn2 and Ascl1 both have a repressive GSK-3β phosphorylation site [285], which may act to diminish their activity during reprogramming. Forced post-translational modification of master regulators may be a fruitful area of exploration; the transactivating activity of Sox10 (the master iOPC instructive factor), for example, can be increased by mutating inhibitory SUMOylation sites [305], an effect that could potentially also be mimicked by soluble SUMOylation inhibitors during reprogramming [306].

The complex milieu of trophic factors secreted by neurons and glia likely contain as-yet undefined factors that could aid in neuronal reprogramming. Differentiation of ESCs is aided, for example, by co-culture with PA6 stromal cells, which improve the yield of dopaminergic [307] and cholinergic motor neurons [308], presumably by paracrine effects. Retinoic acid (RA) is one of the better-defined of these pro-neural soluble factors. RA is critical for normal neurodevelopment [309], induces neuronal differentiation from ESCs [310], and lentiviral addition of an RA receptor to fibroblasts with soluble RA supplementation can improve the subsequent yield of iNs produced by

Ascl1, Brn2, and Ngn2 [278]. *In vivo* reprogramming of resident progenitors with Ngn2 has also been demonstrated to be sensitive to the presence of growth factors, and on the anatomic location the reprogramming is performed. In the striatum, delivery of growth factors (FGF2 and EGF) and Ngn2 induced few neurons at the site of a stab injury, whereas in the neocortex Ngn2 induced a large number of immature neurons, with few lasting to maturity, and distinct gene expression profiles observed for each [311]. Reduced oxygen tension compared to atmospheric (as is normally the case *in vivo*) also improves iN yield [312]. These are clear demonstrations of the strong impact that soluble microenvironmental cues can have on direct reprogramming.

2.4.3 Calcium signaling

Membrane depolarization could also complement efficient transcription factor delivery by encouraging favorable epigenetic modifications in converting cells, and resilient phenotypes in the resulting iNs, likely via Ca^{2+} signaling. This notion is informed by normal developmental processes. *In vivo*, electrical activity is one of the signals migrating progenitors and immature neurons use to recognize and stop at their final destination, and to initiate axono- and synaptogenesis, as coded via voltage-sensitive calcium influx [313]. Electrical activity also serves to balance excitatory and inhibitory subtype specification [314]. *In vitro*, hippocampal neural progenitor cells differentiate more efficiently upon chronic depolarization by high extracellular levels of KCl [315]. Nurr1, a dopaminergic reprogramming factor [257], can be rapidly activated by neurotransmitters, membrane depolarization, and intracellular Ca^{2+} [316]. Furthermore,

prolonged membrane depolarization with KCl has been recently demonstrated to enhance midbrain dopamine neuron differentiation from progenitor cells via epigenetic histone modifications [317]. In this system, high extracellular KCl but not NaCl increased the number of TH^+ neurons, increased DAT-mediated dopamine uptake, and increased access of Nurr1 to the TH and DAT promoters by dissociating MeCP2 and corepressors HDAC1 and CoREST [317].

In normal development, approximately half of all immature neurons die via apoptosis; this process is necessary to arrive at an appropriate final level of innervation density [318-319]. During this apoptotic phase, the availability of neurotrophic factors and afferent input determines which neurons survive and which do not [318]. Treatment with TTX (a sodium channel blocker) can kill 50% of neurons in culture by 2 weeks, via ablation of spontaneous electrical activity [320]. Applying chronic depolarization with high extracellular KCl can rescue 100% survival in these cultures [321], an effect that is believed to mimic spontaneous activity-mediated opening of voltage-sensitive Ca^{2+} channels [318, 320]. This increase in survivability does not appear to depend on paracrine effects; the same improvements were observed in low-density cultures [322-323]. KCl-mediated influx of Ca^{2+} can transfer neurons among one of four distinct intracellular calcium ($[Ca^{2+}]_i$) states: too little $[Ca^{2+}]_i$ to be rescued by neurotrophins, normal $[Ca^{2+}]_i$ where they are subject to normal apoptotic processes, high $[Ca^{2+}]_i$ where they do not require neurotrophic support, and very high $[Ca^{2+}]_i$ which can be excitotoxic [324]. It appears high extracellular KCl can transport neurons to the third category [324]. The most obvious link between intracellular Ca^{2+}, transcription, and survival may be the CaMKII pathway [318].

As applied to direct neuronal reprogramming, chronic depolarization could be used to encourage the emergence of a particular subtype, or to improve neuronal yield in general via increased survivability. Interestingly, GSK-3β is inhibited via CaMKII-mediated phosphorylation [325]. Non-phosphorylatable GSK-3β mutants can promote neuronal apoptosis, whereas a peptide including the phosphorylation site protects neurons [325]. These results suggest there may be a close link between Ca^{2+}-mediated survival in primary neuronal cultures, and small molecule-mediated improvements in induced neuron yields via GSK-3β inhibition. Beyond survivability, depolarization may also act to encourage the activation of endogenous transcription factor loci; activators of Ascl1 expression have been shown to induce CaMKII binding at the Ascl1 promoter, which may be further encouraged by high $[Ca^{2+}]_i$ [326].

2.4.4 Cell-substrate interactions

Just as substrate-mediated changes in endocytic phenotypes may have consequences for non-viral transfection, known cell-substrate interactions can also likely impact both the efficiency of direct somatic reprogramming, as well as the phenotype of the cells produced. Many of these effects appear to act via some of the same epigenetic and signaling processes operating in normal development which we have already described. As such, neuro-supportive effects of physical nano- and microtopographies could be wielded synergistically with the delivery of appropriate lineage instructive transcription factors in a supportive chemical microenvironment to improve the yield and specification of non-viral iNs towards therapeutically-useful levels.

For an example of physical microenvironmental improvement of reprogramming via epigenetic modification, microgratings have been shown to increase the generation efficiency of iPSCs, via histone deacetylase (HDAC) inhibition [327]. HDAC inhibition by VPA has also been shown to increase the yield of neurons differentiated from NPCs at the expense of the glial lineage, via upregulation of NeuroD1 [328] (one of the critical transcription factors for generation of human glutamatergic iNs [252]). Similarly, iPSCs cultured on gratings upregulated TUJ1 and NeuroD1 expression [329]. ESCs cultured on nanofibers upregulated TUJ1 expression compared to smooth substrates, but required further encouragement by ectopic Ngn1 expression to extend neurites [330]. In another study, anisotropic substrate topographies produced more $TUJ1^+$ and $MAP2^+$ neuronal cells from differentiating ESCs and NPCs, whereas anisotropic substrates favored glial differentiation [331]. Topographic cues have also been used to: increase the yield of oligodendrocytes from NSCs [332], accelerate neurite outgrowth of motor neurons [333], and to encourage a neuronal phenotype in MSCs [112].

Beyond physical topography, other substrate-mediated effects may be important for iN generation. ECM factors provide nanotopographical cues, but also can control the content of soluble and immobilized growth factors [334], which can have a potent impact on neuronal differentiation [335]. Scaffold-mediated encouragement of neuronal differentiation in NSCs can be blocked by inhibition of integrin β_1 [336]. Similarly, an observation of increased neuronal differentiation of MSCs on soft substrates was due specifically to caveolae-mediated internalization of integrin β_1 [337]. Taken together, these results suggest that the control of cell-substrate interactions may provide a potent means to guide and encourage direct neuronal reprogramming.

Chapter 3: Non-viral Direct Conversion of Primary Mouse Embryonic Fibroblasts to Neuronal Cells

A portion of Chapter 3 appears in: Nonviral direct conversion of primary mouse embryonic fibroblasts to neuronal cells. Adler AF, Grigsby CL, Kulangara K, Wang H, Yasuda R, Leong KW. Molecular Therapy – Nucleic Acids. 2012 Jul; 1(7):e32.

3.1 Summary

Transdifferentiation, where differentiated cells are reprogrammed into another lineage without going through an intermediate proliferative stem cell-like stage, is the next frontier of regenerative medicine. Wernig et al. first described the direct conversion of fibroblasts into functional induced neuronal cells (iNs). Subsequent reports of transdifferentiation into clinically relevant neuronal subtypes have further endorsed the prospect of autologous cell therapy for neurodegenerative disorders. So far, all published neuronal transdifferentiation protocols rely on lentiviruses, which hinders their clinical translation. Instead, we delivered plasmids encoding neuronal transcription factors (Brn2, Ascl1, Myt1l) to primary mouse embryonic fibroblasts with a bioreducible linear poly(amidoamine). The low toxicity and high transfection efficiency of this gene carrier allowed repeated dosing to sustain high transgene expression levels. Serial 0.5 μg cm^{-2} doses of reprogramming factors delivered at 48-hour intervals produced up to 7.6% $Tuj1^{+}$ (neuron-specific class III beta-tubulin) cells, a subset of which expressed MAP2 (microtubule-associated protein 2), tau, and synaptophysin. Transgenic fibroblasts reported NeuroD6 and doublecortin expression as early as day 6 post-transfection, and

Tau expression by day 12. A synapsin-RFP reporter helped identify mature, electrophysiologically active cells, with 24/26 patch-clamped RFP^+ cells firing action potentials. Some non-virally-induced neuronal cells (NiNs) were observed firing multiple and spontaneous action potentials. This study demonstrates the feasibility of non-viral neuronal transdifferentiation, and may be amenable to other transdifferentiation processes.

3.2 Rationale and Significance

Neuronal transdifferentiation has revived the dream of future therapies that truly alter the course of neurodegenerative disease which currently have only palliative treatment options. iNs are non-proliferative [258, 260], and are therefore far less likely to generate teratomas after implantation compared to iPSC-derived neurons, which can also produce immunogenic intermediates from syngeneic sources [237]. The successful demonstration of iMN [258] and iDA [254] engraftment and functional improvement in animal models of Parkinson's [255-256] suggests the goal of cell-replacement therapies using iNs for a number of neurodegenerative diseases is within reach. This type of approach is made even more attractive by the difficulty of adult neural stem cell isolation [338]. The benefit-to-risk ratio of neuroprotective adeno-associated virus (AAV) gene therapy to combat PD has already been deemed high enough to warrant clinical trials [339], so the introduction of ethically and technically viable autologous non-viral sources of neuronal cells should be of great and immediate therapeutic value. The reduced risk of insertional mutagenesis with a non-viral approach should push the barrier to entry for a variety of neurodegenerative therapies even lower. Further, the demonstration of NiN

generation would support the feasibility of non-viral approaches to the other known forms of direct reprogramming, for the generation of β-cells, macrophages, cardiomyocytes, and hepatocytes [340-345]. In addition to cell therapy, direct neuronal reprogramming also provides a unique opportunity to model disease through the generation of neurons that recapitulate pathological phenotypes from patients with neurodevelopmental, psychiatric, and neurodegenerative disorders [346-347]. New enhancements to the reprogramming process, as we expect to discover through completion of this work, can also be applied to generate these model cell types at higher efficiencies to facilitate drug screening.

A critical finding of viral neuronal transdifferentiation studies is that the epigenetic and transcriptional programs of the source cells are largely (but not completely) erased and rewritten in favor of a stable neuronal state [260], which persists even when exogenous transcription factor (TF) expression is discontinued. Endogenous neuronal TFs are activated and continue to be expressed after a relatively brief pulse of doxycycline (dox)-inducible ectopic transgene expression is shut down by dox withdrawal [253-254]. This, taken with the rapidness and high efficiency of iN generation, and the published success of non-viral iPSC generation [243, 348-351], suggested to us that neuronal transdifferentiation could be achieved with a clinically-advantageous transient non-viral gene delivery strategy, which we report herein. We hypothesized that multiple doses of reprogramming factors would be beneficial to generate non-virally-induced neuronal cells (NiNs) at high efficiencies. Predicting that non-viral transdifferentiation would be less efficient than the viral systems, we elected to begin with primary mouse embryonic fibroblasts (PMEFs) as a starting material; PMEFs are

putatively the somatic cell type most-susceptible to neuronal transdifferentiation [251, 260].

3.3 Methods

Molecular cloning and plasmid purification

The reporter vectors pmax-GFP (3486 bp, Amaxa, Cologne, Germany) and VR1255C (6413 bp, Vical, San Diego, CA), which respectively express GFP and luciferase under control of the CMV promoter, were used for flow cytometric measurement of transfection efficiency. pmax-Brn2 (4154 bp), pmax-Ascl1 (3497 bp), and pmax-Myt1l (6359 bp), which express the mouse transcription factors Brn2, Ascl1, and Myt1l, respectively, under control of the CMV promoter, were generated by first excising the GFP coding sequence from pmax-GFP with SacI digestion, blunting by DNA polymerase I Klenow fragment, NheI-HF digestion (NEB, Ipswich, MA), and gel extraction (QIAquick Gel Extraction Kit, QIAGEN, Hilden, Germany). Then, Brn2, Ascl1, and Myt1l inserts were prepared by digestion of the lentiviral vectors Tet-O-FUW-Brn2 (Addgene 27151), Tet-O-FUW-Ascl1 (Addgene 27150), and Tet-O-FUW-Myt1l (Addgene 27152) with EcoRV and NheI-HF (NEB) and gel extraction, and were subsequently ligated into the empty pmax vector with T4 DNA ligase (NEB). When used together, these three plasmids are abbreviated as pmax-BAM. pUNO1-mAscl1 (3892 bp, InvivoGen, San Diego, CA) and pUNO1-mMyt1lb (6744 bp, InvivoGen), expressing mouse Ascl1 and Myt1l under control of the EF1α/HTLV promoter, were used in conjunction with pmax-Brn2, and when used together are abbreviated as pUNO-

AM/pmax-B. A summary of these plasmid cocktails is presented in Figure 8. Plasmids were propagated in *Escherichia coli* DH5α (Invitrogen, Carlsbad, CA) and purified with EndoFree Plasmid Mega and Maxi kits (QIAGEN). Plasmid DNA concentrations were quantified by measurement of absorbance at 260 nm with a NanoDrop ND-1000 Spectrophotometer (Thermo Scientific, Waltham, MA).

Production and purification of lentiviral synapsin reporter

Stbl3 bacteria (Invitrogen) were transformed with pLV-hSyn-RFP [352] (Addgene 22909) according to the manufacturer's protocol. Plasmid DNA was propagated and purified using the EndoFree Maxiprep kit (QIAGEN). For the lentiviral production, HEK293T cells were seeded in 75 cm^2 dishes, cultured in DMEM (Invitrogen) containing 10% Premium Select FBS (Atlanta Biologicals, Lawrenceville, GA) and 1% penicillin-streptomycin (Invitrogen), and were transfected by the calcium phosphate technique with the following plasmids: 16.9 μg of pMD2.G (Addgene plasmid 12259) 31.3 μg of psPAX2 (Addgene plasmid 12260) and 48.2 μg of pLV-hSyn-RFP. The medium was changed after 14 h. 72 h after transfection, the medium was collected in 50 mL tubes, centrifuged, and filtered through a 0.45μm filter to remove cell and membrane debris. The supernatant was then concentrated to 100x in Amicon Ultra centrifugal filter tubes, (Millipore, Billerica, MA) and the concentrated virus was stored at -80^oC. PMEFs in 2 cm^2 wells were infected with 1 μL of 100x viral concentrate in PMEF medium 5 days before patch clamping.

Poly(CBA-ABOL) synthesis and polyplex formation

Poly(CBA-ABOL) was synthesized by Michael polyaddition of 3.67 g N,N-cystaminebisacrylamide (CBA) (Polysciences, Warrington, PA) and 1.26 g 4-amino-1-butanol (ABOL) (Sigma-Aldrich, Saint Louis, MO) as described by Lin et al. [353] The reaction product was purified by dialysis (3.5 kDa cutoff) in acidic deionized water (pH 4) and then lyophilized. The polymer was collected in its HCl-salt form (1.63 g, 33% yield), and its structure validated by ^{1}H NMR (in D_2O) on a Varian Mercury 300 MHz NMR Spectrometer. p(CBA-ABOL)/DNA nanocomplexes (polyplexes) were synthesized at a polymer:DNA mass ratio of 45:1, which was selected based on a preliminary optimization of GFP expression in primary mouse embryonic fibroblasts (PMEFs) (results not shown). Polyplexes were prepared by adding a HEPES buffer solution (20 mM HEPES, 5 wt % glucose, pH 7.4) of p(CBA-ABOL) (900 μg/mL) to a HEPES buffer solution (20 mM HEPES, 5 wt % glucose, pH 7.4) of plasmid DNA (75 μg/mL), followed immediately by vortexing for 20 seconds. Reaction sizes ranged from 5 to 15 μg of plasmid DNA. Average p(CBA-ABOL)/pmax-BAM polyplex diameter was 102.5 nm ± 3.7 nm, and zeta potential was +23.5 mV ± 1.5 mV (mean ± SEM, n = 3), as measured with a Zetasizer Nano ZS (Malvern Instruments Ltd, Malvern, UK).

Cell culture and transfection

40,000 cells (80,000 cells) passage six (eight) PMEF-HLs (Millipore, Billerica, MA) were seeded per well in 24-well TCPS plates (BD, Franklin Lakes, NJ) at 37 °C and 5% CO_2 in complete PMEF medium: Dulbecco's Modified Eagle's Medium with 4.5 g/L glucose (GIBCO 11960-044) (Invitrogen), 10% Premium Select FBS (Atlanta

Biologicals), 25 μg mL^{-1} gentamicin (Invitrogen), and 1x GlutaMAX, non-essential amino acids, sodium pyruvate, and β-mercaptoethanol (Invitrogen). In the case of electrophysiology and most immunofluorochemistry experiments, 12 mm BD BioCoat poly-D-lysine/laminin-coated glass coverslips were placed in the bottom of TCPS wells prior to cell seeding. 24 hours after seeding, PMEFs were transfected with either: reporter plasmids for flow cytometry, or pmax-BAM or pUNO-AM/pmax-B plasmid cocktails for induced neuronal transdifferentiation. BAM factor plasmids were delivered at an equimolar ratio in all cases. A 2:1 ratio of Lipofectamine 2000 (Invitrogen) volume (μL) to DNA mass (μg) was used for flow cytometry experiments, in accordance with the manufacturer's protocol. All transfections were carried out in serum- and antibiotic-free OptiMEM (Invitrogen). OptiMEM was replaced with complete PMEF medium four hours after the onset of transfection. Serial transfections for neuronal transdifferentiation proceeded as depicted in (Figure 9). 48 hours after the final transfection was completed, PMEF medium was replaced with N3 neural induction medium containing: DMEM/F-12 (Invitrogen), 25 μg mL^{-1} bovine insulin (Gemini Bio-Products, West Sacramento, CA), 50 μg mL^{-1} human apo-transferrin, 30 nM sodium selenite, 20 nM progesterone, 100 μM putrescine (Sigma-Aldrich), 10 ng mL^{-1} human bFGF2 (Stemgent, Cambridge, MA), and 25 μg mL^{-1} gentamicin (Invitrogen). Transgenic PMEFs were dissected carefully away from neural tissue in E14.5 'NeuroD6-Cre'x'LoxP-RFP' (NC-Ai9 line, gift from Kristin Baldwin, TSRI), doublecortin-RFP (gift from Deborah Silver, Duke University), and TauEGFP (gift from Marius Wernig, Stanford University) mice, cultured, and transfected as described previously.

Viability assay

The quantification of PMEF viability following transfection was duplexed with flow cytometry experiments. 24 hours after the onset of the final transfection with pmax-GFP, cells were incubated for four hours with fresh PMEF medium containing alamarBlue (Invitrogen) in accordance with the manufacturer's protocol. Metabolic reduction of alamarBlue was monitored at 570 nm/590 nm excitation/emission using a BMG Labtech FLUOStar Optima plate reader (Ortenberg, Germany). AlamarBlue-containing medium was then removed, and the cells were prepared for flow cytometry.

Flow cytometry

24 hours after completion of the final transfection with pmax-GFP, PMEFs were washed briefly with PBS without Ca^{2+} and Mg^{2+} (Mediatech, Washington, DC), and released from TCPS surfaces with 0.25% Trypsin-EDTA (Invitrogen). The trypsin was inactivated with serum-containing medium and the cells were centrifuged at 4 °C, resuspended in ice-cold PBS, centrifuged again, and resuspended in PBS containing 1% PFA (EMS, Hatfield, PA). Cells were then filtered through 40 μm nylon cell strainers (BD) and analyzed with a BD FACSCanto II flow cytometer. PMEFs transfected with the non-fluorescent VR1255C plasmid served as negative controls for each equivalent pmax-GFP dose, with gates set such that 1% of these cells were considered GFP^+. The recorded median fluorescent intensities of GFP^+ cells (MFI_{GFP}) were linearized according to an assumption of ideal logarithmic amplifier behavior, and normalized by the median fluorescent intensity of negative control cells (MFI_{NC}) to calculate the reported % MFI change: $100\%*(MFI_{GFP} - MFI_{NC})/MFI_{NC}$.

Real-time RT-PCR

Comparative C_T real-time RT-PCR was performed in 20 μL reactions using the QuantiTect SYBR Green RT-PCR Kit (QIAGEN) with 10 ng of starting mRNA isolated with RNeasy and QIAshredder kits (QIAGEN) from cells transfected with pmax-BAM factors. mRNA concentrations were quantified with a NanoDrop ND-1000 Spectrophotometer (Thermo Scientific). PCR proceeded for 40 cycles in an ABI 7300 Real-Time PCR System (Carlsbad, CA). Target mRNA levels were normalized to endogenous GAPDH references, and presented as a fold-change increase relative to expression levels from untransfected PMEF mRNA collected 48 hours after seeding. Correct RT-PCR target amplicon lengths for exogenous pmax-BAM factors were verified with gel electrophoresis in a separate experiment. Primers (IDT, Coralville, Iowa) were as follows: Ascl1 forward (GCTGCAAACGCCGGCTCAAC); Ascl1 reverse (GCGGATGTACTCGACCGCCG); Ascl1 Endo forward (TGGCGGGTTCTCCGGTCTCGT); Ascl1 Endo reverse (TCCCCATTTGACGTCGTTGGCGA); Brn2 forward (CCATCGTACATGCCGAGCCGC); Brn2 reverse (GCGCGGTGATCCACTGGTGAG); Myt1l forward (CGGGTGTGATGGAACCGGCC); Myt1l reverse (GCCCTGTGCAGCCTGGAGTG); GAPDH forward (ACGGCCGCATCTTCTTGTGCA); GAPDH reverse (TTCTCGGCCTTGACTGTGCCG).

Immunofluorochemistry and image analysis

Transfected cells were washed briefly with PBS containing Ca^{2+} and Mg^{2+} (Mediatech), and fixed with 4% PFA (EMS) at RT for 20 minutes. Cells were then incubated for two hours at room temperature (RT) in blocking buffer containing 0.2% Triton X-100, 3% w/v BSA, 10% goat serum (Sigma-Aldrich), and combinations of the following primary antibodies with rabbit anti-Tuj1 (Covance, 1:500): mouse anti-MAP2 (Sigma-Aldrich, 1:500), mouse anti-synaptophysin (BD, 1:100), or mouse anti-Tau (BD, 1:50). The cells were then washed three times with PBS, and incubated for one hour at RT in blocking buffer containing Alexa Fluor 488 goat anti-mouse IgG and Alexa Fluor 594 goat anti-rabbit IgG (Invitrogen), washed three times with PBS, and imaged with a Nikon Eclipse TE2000-U inverted fluorescence microscope (Tokyo, Japan) with a ProScanII motorized stage (Prior Scientific, Rockland, MA).

To quantify the relationship between $Tuj1^+$ cell generation and the number of serial BAM factor transfections, PMEFs were transfected in TCPS wells, stained for Tuj1, and scanned to produce large mosaic images of each complete culture area. These mosaics were processed with a FIJI (Fiji Is Just ImageJ, http://fiji.sc) macro to: automatically and uniformly threshold each image according to local contrast, exclude small debris, and to count the number of $Tuj1^+$ cells in each well. These counts were then divided by the number of PMEFs seeded in each well to calculate % $Tuj1^+$ cell generation efficiencies.

Electrophysiology

Non-virally-induced neuronal cells cultured on poly-D-lysine/laminin-coated glass coverslips (BD) were identified for patch clamp analysis by synapsin promoter-driven RFP expression [352] after 12-17 days of culture in N3 medium. One dose of p(CBA-ABOL)/BAM factors produced synapsin-RFP^+ cells that were too sparse to find readily with the patch clamping apparatus, and five doses kept unconverted PMEFs in serum-containing medium for an additional 4 days compared to three doses, allowing a layer of cells to develop on the back of the coverslips, which made it more difficult to affix samples securely to our patching setup. So, we elected to patch cells that received three doses. Micropipettes had resistances between 3-7 MΩ, and were filled with internal solution containing: 130 mM $KMeSO_3$, 10 mM HEPES, 10 mM sodium phosphocreatine, 4 mM $MgCl_2$, 4 mM Na_2ATP, 0.4 mM Na_2GTP, 3 mM sodium L-ascorbic acid, with pH 7.24 and an osmolarity of 290 mM. The cells were perfused with artificial cerebral spinal fluid (ACSF) saturated with 5% O_2 and 95% CO_2 and containing: 130 mM NaCl, 2.5 mM KCl, 2 mM $NaHCO_3$, 1.25 mM NaH_2PO_4, 25 mM glucose, 2 mM $CaCl_2$, and 2 mM $MgCl_2$. Giga-ohm membrane seals were formed under voltage-clamp conditions. Action potentials were then recorded using an Axon Multiclamp 700B Microelectrode Amplifier (Molecular Devices, Sunnyvale, CA) by stepwise whole-cell current clamp injections, and analyzed with custom in-house MATLAB programs.

3.4 Results

Poly(CBA-ABOL)/DNA polyplexes mediate non-toxic and highly-efficient transfection of a GFP-reporter plasmid in PMEFs

Of the three primary mouse embryonic fibroblast (PMEF) cell sources screened (PMEF-HL, PMEF-NL, and PMEF-CFL (Millipore)), we found PMEF HLs to be the most-efficiently transfected with p(CBA-ABOL)/DNA polyplexes (data not shown) and used them in all subsequent experiments. Fluorescence microscopy revealed that a 1.0 μg dose of pmax-GFP in p(CBA-ABOL) polyplexes produced high transfection efficiencies without noticeable toxicity (Figure 10a). 2.0 μg doses also gave high transfection efficiencies, with some visibly rounded and dead cells, and 4.0 μg was grossly toxic. 1.0 μg of pmax-GFP delivered with p(CBA-ABOL) transfected cells more efficiently than the same dose delivered with Lipofectamine 2000.

One and two doses of 1.0 μg pmax-GFP in p(CBA-ABOL) polyplexes were almost entirely nontoxic compared to untransfected controls, and a second transfection 48 hours later did not compound toxicity up to 2.0 μg (Figure 10b). Lipofectamine 2000 was significantly more toxic than p(CBA-ABOL) when delivering the same DNA dose, and its toxicity compounded with a second serial dose.

Flow cytometric quantification of GFP expression confirmed a high transfection efficiency for 1.0 and 2.0 μg pmax-GFP doses in p(CBA-ABOL) polyplexes, significantly higher than with Lipofectamine 2000 lipoplexes (Figure 10c). Further, a second dose maintained a high percentage of cells expressing GFP for an additional two days; without re-transfection, the percentage of GFP^+ cells fell relatively by 15 and 28% for 1.0 and 2.0 μg pmax-GFP in p(CBA-ABOL) polyplexes, respectively (results not

shown). Though 1.0 and 2.0 μg doses of pmax-GFP in p(CBA-ABOL) polyplexes elicited similar percentages of GFP^+ cells, the median fluorescence intensity (MFI) change of GFP^+ cells over non-fluorescent negative controls revealed that cells transfected with a 2.0 μg DNA dose had significantly higher GFP expression levels (Figure 10d).

Poly(CBA-ABOL)/DNA polyplexes elicit potent but transient expression of neuronal reprogramming factor mRNAs

An equimolar ratio of 1.0 μg pmax-BAM neuronal reprogramming factors in p(CBA-ABOL) polyplexes was delivered to PMEFs according to the scheme in (Figure 9). 24 hours after the initial transfection, each of the exogenous BAM factor transcripts were expressed at levels that were orders of magnitude higher than non-transfected PMEFs (Figure 11). Ectopic expression of pmax-BAM factors diminished by approximately two orders of magnitude by day 10 of culture in N3 medium as the plasmids were silenced and/or degraded, for both one and three doses. Endogenous Ascl1 was activated in some cells by day 10 in N3 medium, as measured with primers targeted against an untranslated region (UTR) of the endogenous transcript not present in the exogenous transcript. Tuj1 and MAP2 transcripts were quantified but not detectably increased by transfection (results not shown).

Serial non-viral delivery of neuronal reprogramming factors generates Tuj1$^+$ cells efficiently

One dose of 1.0 μg pmax-BAM neuronal reprogramming factors in p(CBA-ABOL) polyplexes produced rare and isolated Tuj1$^+$ cells, while three and particularly five doses generated networks of Tuj1$^+$ cells showing varying degrees of neuronal and fibroblastic morphologies (Figure 12a). Neuron-like Tuj1$^+$ processes increased in length and complexity with increased culture time in N3 medium. Untransfected PMEFs were not reactive to antibodies against Tuj1. Automated microscopy and image analysis of large culture regions (Figure 12b) were used to quantify the efficiency of Tuj1$^+$ conversion relative to the number of PMEFs seeded (Figure 12c). Five doses produced significantly more Tuj1$^+$ cells than one or three doses. The increase in efficiency with dose is visually evident in the mosaic images of 24-well plates (Figure 12b).

Non-virally-induced neuronal cells express pan-neuronal cytoskeletal and synaptic proteins

After observing the feasibility of neuronal transdifferentiation using the BAM factors, we added an additional set of plasmids to give the best chance of producing NiNs with active membrane properties. The CMV promoter is generally inactive in cortical neurons [354], and it is not known if or at what point this silencing could occur during neuronal transdifferentiation. We therefore added a parallel plasmid cocktail with serial transfections of 2.0 μg pUNO-AM/pmax-B factors, which utilize the EF1α/HTLV promoter for Ascl1 and Myt1l expression instead of the CMV promoter in pmax-BAM

plasmids, and would potentially take advantage of increased expression levels with 2.0 μg of plasmid compared to 1.0 μg.

Distal enrichment of tau (Figure 13, top row), characteristic of neurons, was visible for a subset of $Tuj1^+$ cells (center and right panels). $Tuj1^+$ cells with fibroblastic morphologies were not tau^+ (red cells, left panel). $Tuj1^+$ cells with neuronal morphology were also reactive to MAP2 antibodies (second row). Synaptophysin punctae were visible in a subset of $Tuj1^+$ cells, a protein characteristic of synaptic vesicles (third row). Synapsin-RFP was also visible in long, branching processes. Synapsin-RFP^+ cells were less common than any of those detected by immunofluorescence. Though comparatively uncommon, synapsin-RFP^+ processes were present at sufficient densities and lengths to intersect with neighboring cells (fourth row), particularly for those transfected with the pUNO-AM/pmax-B cocktail (right panel). A worst case estimate of synapsin-RFP^+ cells counted compared to $Tuj1^+$ cells quantified in Figure 12c provides that approximately 0.1% - 1% of $Tuj1^+$ cells are also synapsin-RFP^+ for three doses of 1.0 μg pmax-BAM factors. It is instructive to note that this is less efficient than our lentiviral derivation of iNs using the same TFs and cell source, with 66% synapsin-RFP^+ cells generated from those plated, as detected by FACS (not shown).

We also produced NiNs from three additional PMEF sources, which were dissected from E14.5 transgenic mice reporting NeuroD6, doublecortin (DCX), or tau promoter activity via GFP or RFP. NeuroD6-RFP^+ cells were observed as early as day 4 in N3 medium, and rapidly increased in neurite complexity with further culture (Figure 14a). DCX-RFP^+ cells (Figure 14b) also appeared at day 4 in N3 medium, and similarly

increased in complexity with time. TauEGFP$^+$ cells with clear neuronal morphology took longer to appear, at approximately day 12 of neurogenic culture.

Non-virally-induced neuronal cells with synapsin I promoter activity are electrophysiologically active and complex

Given the increased heterogeneity in maturity and completeness of NiNs compared to conventional iNs, we expected that upstream markers of neurogenesis, such as tau [251] or MAP2 promoter activity [257], would likely be less useful in NiNs for predicting active membrane properties. Accordingly, we transduced NiNs with a lentiviral reporter driving expression of RFP under the control of the highly neuron-specific synapsin I promoter [355-356], in order to help us identify the most-mature NiNs for electrophysiological characterization. This lentivirus may have a natural tropism for excitatory cortical neurons [352], which are similar to the predominant subtype generated by ectopic BAM expression in PMEFs [251].

The presence of synapsin-RFP in long processes of NiNs was used to identify cells for electrophysiological recording. 12/13 synapsin-RFP$^+$ cells produced with three doses of 1.0 μg pmax-BAM factors fired single action potentials in response to depolarizing current injection as shown in (Figure 15a,b). These cells had an average resting membrane potential of -46.3 ± 2.2 mV (mean ± SEM, n = 12), and an average input resistance of 1.7 ± 0.3 GΩ (mean ± SEM, n = 11). 12/13 synapsin-RFP$^+$ cells produced with three doses of 2.0 μg pUNO-AM/pmax-B factors fired at least one action potential in response to depolarizing current injection. Further, 5/13 of these cells fired multiple action potentials as shown in (Figure 15c,d), and 7/13 fired single action

potentials. One cell was observed firing spontaneous trains of action potentials (Figure 15d, 0 pA), and rebound action potentials were also recorded (Figure 15c,d). These cells had an average resting membrane potential of -41.7 ± 2.4 mV (mean ± SEM, n = 12), and an average input resistance of 1.5 ± 0.2 GΩ (mean ± SEM, n = 12). Results are for recordings with freely-fluctuating resting membrane potentials, though maintaining the cells at ~ -65 mV with holding current between recordings did occasionally result in more-clearly defined trains of action potentials. Qualitatively, we observed that cells firing trains of action potentials tended to be larger and expressed synapsin-RFP more-intensely than those firing only once.

3.5 Discussion

Our aim in this study was to demonstrate direct neuronal transdifferentiation without viral delivery of TFs, in an effort to bring this exciting new field one step closer to clinical translation. We hypothesized that multiple doses of reprogramming factors would be required to generate non-virally-induced neuronal cells (NiNs) efficiently. Predicting that non-viral transdifferentiation would be less efficient than the viral systems, we elected to use primary mouse embryonic fibroblasts (PMEFs) as a starting material; PMEFs are putatively the somatic cell type most-susceptible to neuronal transdifferentiation [251, 260].

We delivered the three neuronal reprogramming factors Brn2, Ascl1, and Myt1l (BAM) in separate non-viral plasmids. Accordingly, we expect the proportion of cells that receive and express all three transgenes to be lower than that of those expressing

only one or two [357]. The fraction of cells co-expressing all three can be roughly calculated by considering the fraction of cells positive for a single reporter, and raising it to the power n = number of transgenes that must be co-expressed. This worst-case is mitigated somewhat by our inclusion of all three factors in the same polyplexes, such that they are co-endocytosed, but it is helpful to realize the large benefit high transfection efficiencies have on co-expression of multiple plasmids. For example, if a population is transfected with 20% efficiency for one of three separate genes, approximately $100\%*(0.2)^3 = 0.8\%$ will be positive for all three factors. An 80% transfection efficiency would produce $100\%*(0.8)^3 = 51\%$ triple-positive cells (a 60-fold increase). This is particularly important if serial dosing is required, which will compound the effect.

Previous reports have clearly demonstrated the importance of co-expression of all three BAM factors to produce iNs with mature electrophysiological phenotypes [251], which we expected to occur for a subset of cells transfected with our system. Improvement in transfection efficiency should result in nonlinear improvement in the appearance of NiNs firing multiple action potentials. p(CBA-ABOL) is a highly-efficient and non-toxic gene carrier that is rapidly degraded upon delivery to the reducing intracellular environment, for favorable unpacking of the polyplex [353]. In our hands, p(CBA-ABOL) outperforms most commercially-available transfection reagents *in vitro*. The high efficiency and low cytotoxicity of this gene carrier is key to the success of the current study, as serial multiple-plasmid transfections are helpful for efficient NiN generation.

Optimization of PMEF transfection demonstrated that p(CBA-ABOL) polyplexes are nontoxic for doses that elicit very efficient transgene expression (Figure 10b,c). A 2.0

μg dose was identified as the highest dose suitable for serial delivery without toxicity concerns. p(CBA-ABOL) is more efficient and less toxic than Lipofectamine 2000, which we deemed to be inappropriate for multiple dose delivery due to its compounding toxicity. We have previously observed a sharp threshold for p(CBA-ABOL) efficacy, near 0.5 μg. To avoid inconsistent transfection and significant toxicity, our operating range for these experiments was therefore 1.0 to 2.0 μg. Maintenance of high transfection efficiencies upon administration of a second dose is likely due to re-transfection of fibroblasts silencing the transgene(s), as well as from transfection of newly-divided PMEFs replacing those lost to toxicity. The increase in expression levels for 2.0 μg compared to 1.0 μg (Figure 10d) is important, particularly if there is a threshold level of transcription factor that must be expressed in a given cell to "pioneer" heterochromatin or to outcompete a fibroblastic epigenetic program to "throw the switch" on transdifferentiation [358-359].

Using 1.0 μg of pmax-BAM factors, we observed dramatic ectopic expression of BAM factor mRNA (Figure 11) and endogenous activation of Ascl1, but no upregulation of MAP2 or Tuj1 mRNA. However, the presence of Tuj1 and MAP2 at the protein level (Figure 13) highlights the necessity of FACS enrichment via a neuronal reporter or single-cell PCR [360] when attempting to analyze iN mRNA amidst a background of unconverted cells. The exogenous BAM factors were silenced to a large extent by day 10 in N3 medium, supporting the use of this technique as a transient expression system. Further transgene silencing is expected to continue with increased time in culture. Integration of non-viral DNA vectors occurs rarely [348, 350, 361], but direct

transdifferentiation is superior to iPSC systems in this regard, in that sporadic BAM factor reactivation would lead to growth arrest, rather than tumorigenic proliferation.

The morphological heterogeneity of $Tuj1^+$ cells generated by our technique (Figure 12a) is further confirmation of $Tuj1^+$ as an early or promiscuous marker of induced neurogenesis [359]. However, a subset of these cells have more complete neuronal morphologies and phenotypes, and increasing the number of $Tuj1^+$ cells is therefore likely predictive of an increased number of more-mature NiNs at downstream analysis points, and is hence useful for screening experiments without the use of transgenic neuronal reporter cells. The nonlinear improvement in the efficiency of Tuj1 induction with an increasing number of serial transfections (Figure 12b,c) may be a consequence of the re-transfection of individual cells that did not initially express sufficient transcription factor to surpass the threshold required for transdifferentiation, and also of the potential continued proliferation and subsequent transfection of unconverted PMEFs. It seems likely that additional doses could further increase the efficiency of $Tuj1^+$ cell generation.

In accordance with the mixture of fibroblastic and neuron-like $Tuj1^+$ cell morphologies, immunofluorochemistry revealed a similar heterogeneity in the expression of pan-neuronal markers (Figure 13). Delivering separate transcription factors with both pmax-BAM and pUNO-AM/pmax-B plasmids resulted in some more-mature NiNs that expressed MAP2, distal tau enrichment, Tuj1, synaptophysin punctae, and had synapsin promoter activity, as well as some less-mature cells that expressed a subset of these markers. These less-complete neuron-like cells may have received an inappropriate timing, amount, or mixture of transcription factors, or may have been on their way to

becoming fully-reprogrammed NiNs. The initiation of transgenic NeuroD6 and DCX reporter activity was rapid and co-incident with a rapid increase in arbor complexity (Figure 14), commensurate with their normal developmental roles in axo- and neurogenesis, respectively [362]. Though heterogeneous on the population level, the presence of non-virally-induced markers of maturing neuronal cells (persistent transgenic reporter activation, synapsin promoter activity, synaptophysin punctae) indicated the likely neuronal electrophysiological properties of these cells.

The synapsin-RFP reporter was excellent at predicting which cells would fire action potentials, with 24/26 patched cells firing at least once (Figure 15). These cells had heterogeneous resting membrane potentials, action potential thresholds, action potential amplitudes, and number of action potentials. We observed action potentials after hyperpolarization (Figure 15c), and spontaneous action potentials (Figure 15d) for NiNs generated with 2.0 μg pUNO-AM/pmax-B factors. These heterogeneous active membrane properties are likely a consequence of the myriad combinations of BAM factors the cells receive during non-viral transdifferentiation, producing NiNs in different stages of maturity and completion.

NiNs generated with pmax-BAM factors were electrophysiologically similar to iNs produced with lentiviral transduction of Ascl1 only [251]. Ascl1 is the only member of the BAM factors that is able to generate cells with active membrane responses on its own. As such, if a population of cells tends to receive a supra-threshold dose of only one of the transcription factors, $Ascl1^{+}$ cells may be the only ones detected as synapsin-RFP^{+}. pmax-BAM vectors may be silenced before an expression time has been reached that is sufficient for Brn2 or Myt1l to act, or more-prevalent pmax-Ascl1 transcript may have

out-competed pmax-Brn2 and -Myt1l for translational machinery [363]. The 2.0 µg dose of pUNO-AM/pmax-B factors may have elicited higher (or more balanced) overall expression levels compared to 1.0 µg of pmax-BAM factors. The use of separate plasmids would allow simple alteration of BAM plasmid ratios to correct such an imbalance, if necessary.

3.6 Conclusion and future perspectives

These results are the first example of non-viral direct neuronal transdifferentiation. We believe this method will prove useful in the non-viral production of other subtypes of neuronal cells, as well as to provide an accessible means of generating iNs without lentivirus. Lentiviral protocols have demonstrated that adult human cells may be intrinsically more resistant to neuronal transdifferentiation than are mouse fibroblasts, and as such our non-viral approach can benefit from further increases in efficiency as it is deployed in human cells. The effectiveness of the non-viral technique may improve as polycistronic vectors for iN generation become more readily available [257, 259], which, by removing redundant plasmid backbone sequences could increase the effective dose of each factor, and ensure co-expression of all factors in transfected cells. The recent discovery that small molecules can greatly boost the efficiency of neuronal transdifferentiation is also expected to help reach this goal [364]. Subtype-specific human NiN generation will likely require a longer pulse of ectopic expression [254], which may further rely on the unique non-toxicity of p(CBA-ABOL). Though the non-integrative requirement for *ex vivo* generation of non-proliferative therapeutic NiNs is relaxed

compared to iPSCs, mRNA vectors will be of interest, and may need to be delivered even more frequently to maintain a sufficient duration and levels of ectopic expression. The reduced risk of insertion mutagenesis with non-viral reprogramming approaches should lower the entry barrier for cell therapy against a variety of neurological diseases. Further, our demonstration of NiN generation suggests that other forms of non-viral inter-lineage transdifferentiation may be feasible [340-344].

3.7 Figures

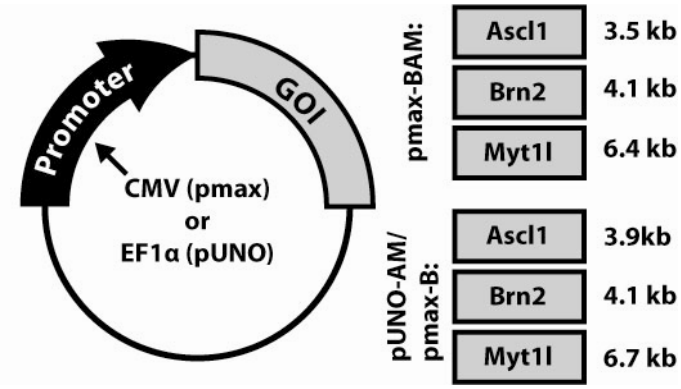

Figure 8. Non-viral vectors generated for direct reprogramming of fibroblasts to glutamatergic neurons
Coding sequences for mouse Ascl1, Brn2, and Myt1l (BAM) transcription factors were inserted into the pmax and pUNO backbones, under control of the CMV and EF1α-HTLV promoters, respectively. Cocktails of BAM factor-encoding plasmids were delivered at an equimolar ratio.

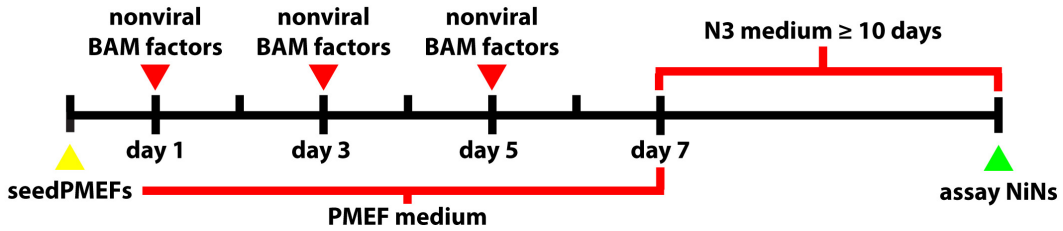

Figure 9. Non-virally-induced neuron (NiN) generation scheme
On day zero, PMEFs were seeded on TCPS wells or poly-D-lysine/laminin-coated glass coverslips in complete medium containing serum. 24 hours later, the first transfection was performed. One to four additional doses were then administered every 48 hours. Beginning 48 hours after administration of the final dose, the cells were cultured for a minimum of 10 additional days before assay in serum-free N3 neural induction medium containing FGF2, which was replaced every 48 hours, or every 24 hours beyond day 10 in N3 for longer-term experiments.

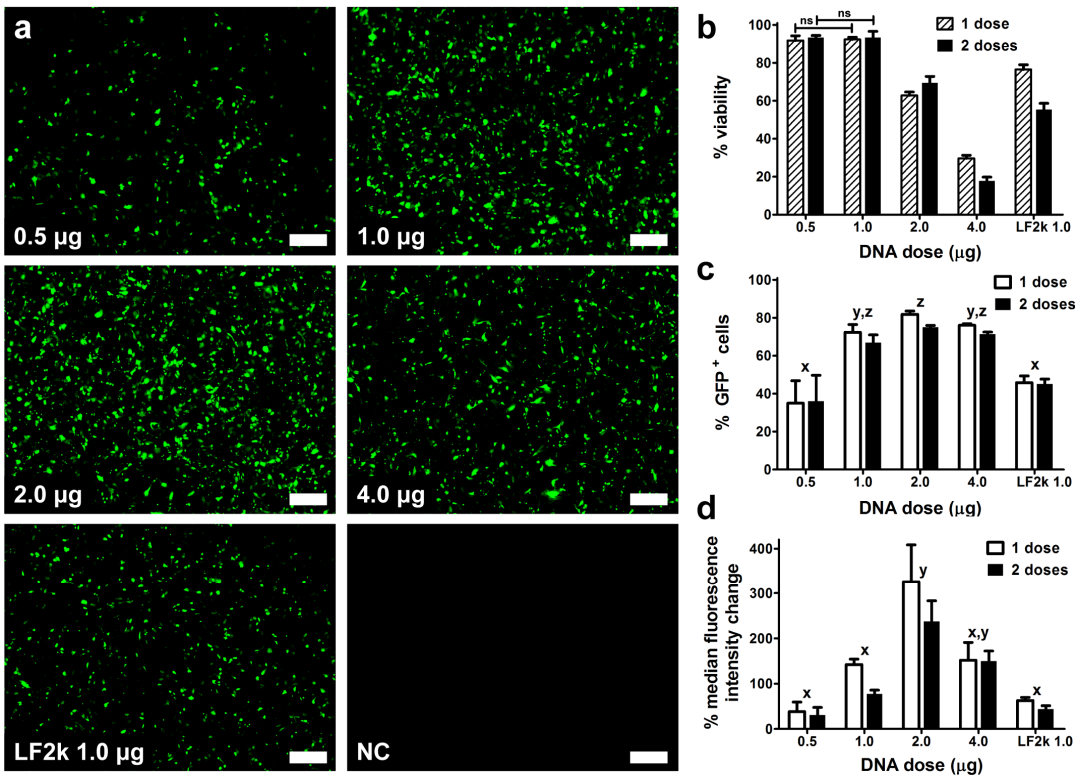

Figure 10. Optimization of non-viral GFP reporter plasmid transfection in PMEFs
(a) Fluorescence micrographs of PMEFs transfected with increasing doses of DNA in p(CBA-ABOL)/pmax-GFP polyplexes (500 µm scale bars), with 1.0 µg of pmax-GFP delivered with Lipofectamine 2000 (LF2k) included for comparison. Images were taken 24 hours after transfection. (b) AlamarBlue toxicity assay multiplexed with (c) flow cytometric measurement of GFP transfection efficiency and (d) % median fluorescence intensity increase of GFP^+ cells compared to non-fluorescent control transfections for one and two doses of p(CBA-ABOL)/pmax-GFP polyplexes, assayed 24h after transfection. 1.0 µg of pmax-GFP delivered with Lipofectamine 2000 (LF2k) is again included for comparison. Error bars represent SEM of three separate experiments performed in triplicate. Two-way ANOVA were performed with $P < 0.05$ considered significant. The main effect of DNA mass was significant in (b-d), and the main effect of DNA dose # was significant in (b). Letters (x,y,z) not shared between columns denote significant comparisons between DNA masses by Tukey post-hoc tests ($P < 0.05$) of one-way ANOVA across DNA masses, with data from one and two doses pooled in (c) and (d), due to absence of a main effect of dose # by two-way ANOVA. All comparisons of viability (b) across DNA mass within a given dose # were significant, other than those between 0.5 and 1.0 µg pmax-GFP in p(CBA-ABOL) polyplexes (marked ns – not significant).

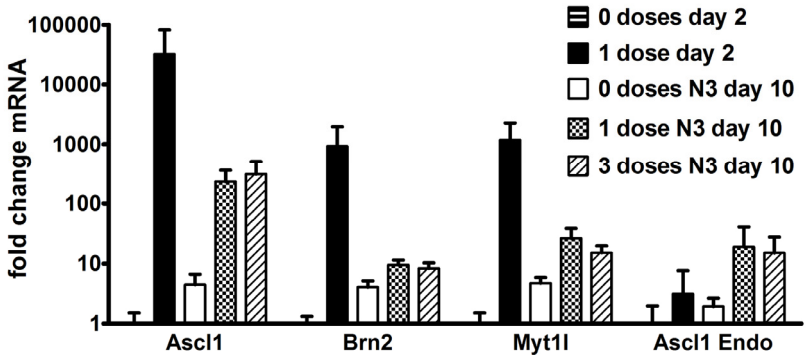

Figure 11. Ectopic and endogenous reprogramming factor transcript in transdifferentiating PMEFs
PMEFs were transfected with one or three doses of 1.0 µg pmax-BAM (Brn2, Ascl1, Myt1l) factors complexed with p(CBA-ABOL), and total mRNA was collected 24h after transfection (day 2) or after 10 days of culture in N3 and analyzed with RT-qPCR. Error bars represent the range of transcript produced by the standard deviation about a mean C_T value (n = 3).

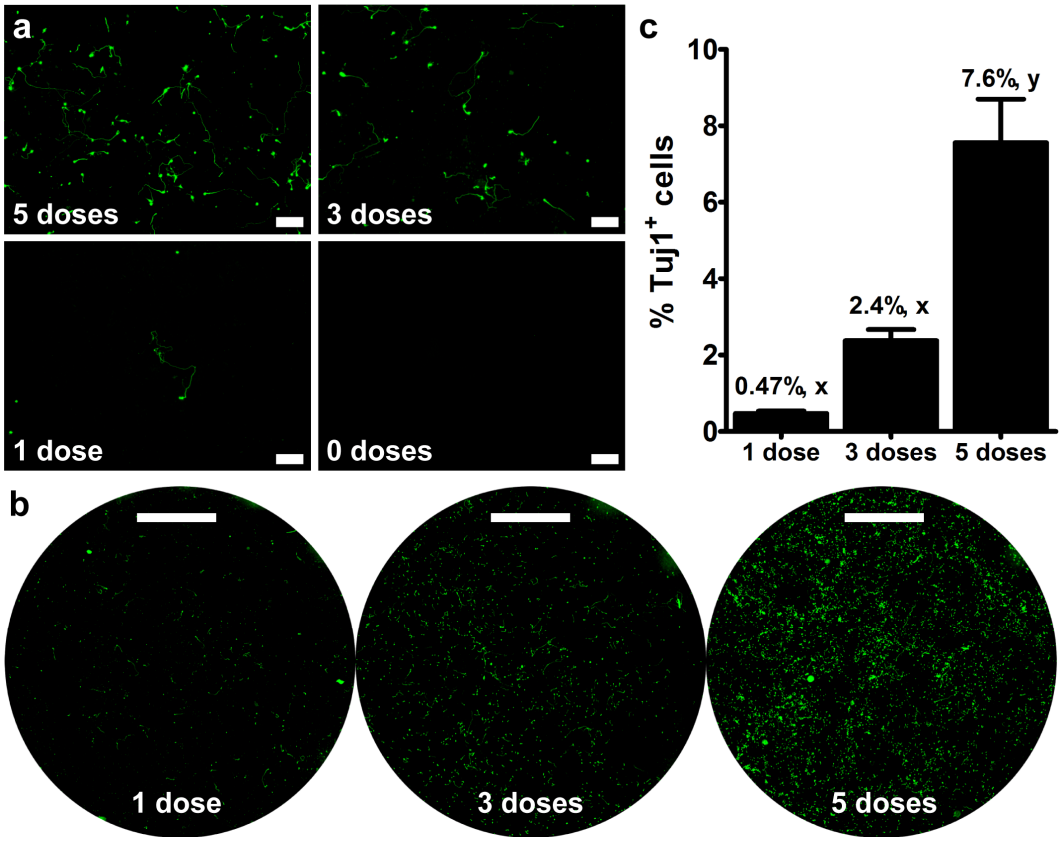

Figure 12. Tuj1 induction in cells transfected with multiple doses of reprogramming factors
(a) Tuj1 stain of cells transfected with one to five doses of 1.0 µg pmax-BAM factors in p(CBA-ABOL) polyplexes after a minimum of 14 days in N3 medium following transfection. 200 µm scale bars. (b) Large mosaic images of the entire culture area (2.5 mm scale bar) acquired for image analysis-based quantification of the number of Tuj1+ cells normalized to the number of PMEFs seeded (c), after a minimum of 10 days in N3 following transfection. Letters (x,y) not shared between columns denote significant comparisons by Tukey post-hoc tests of a one-way ANOVA ($P < 0.05$). Error bars represent the SEM of three separate experiments performed in triplicate.

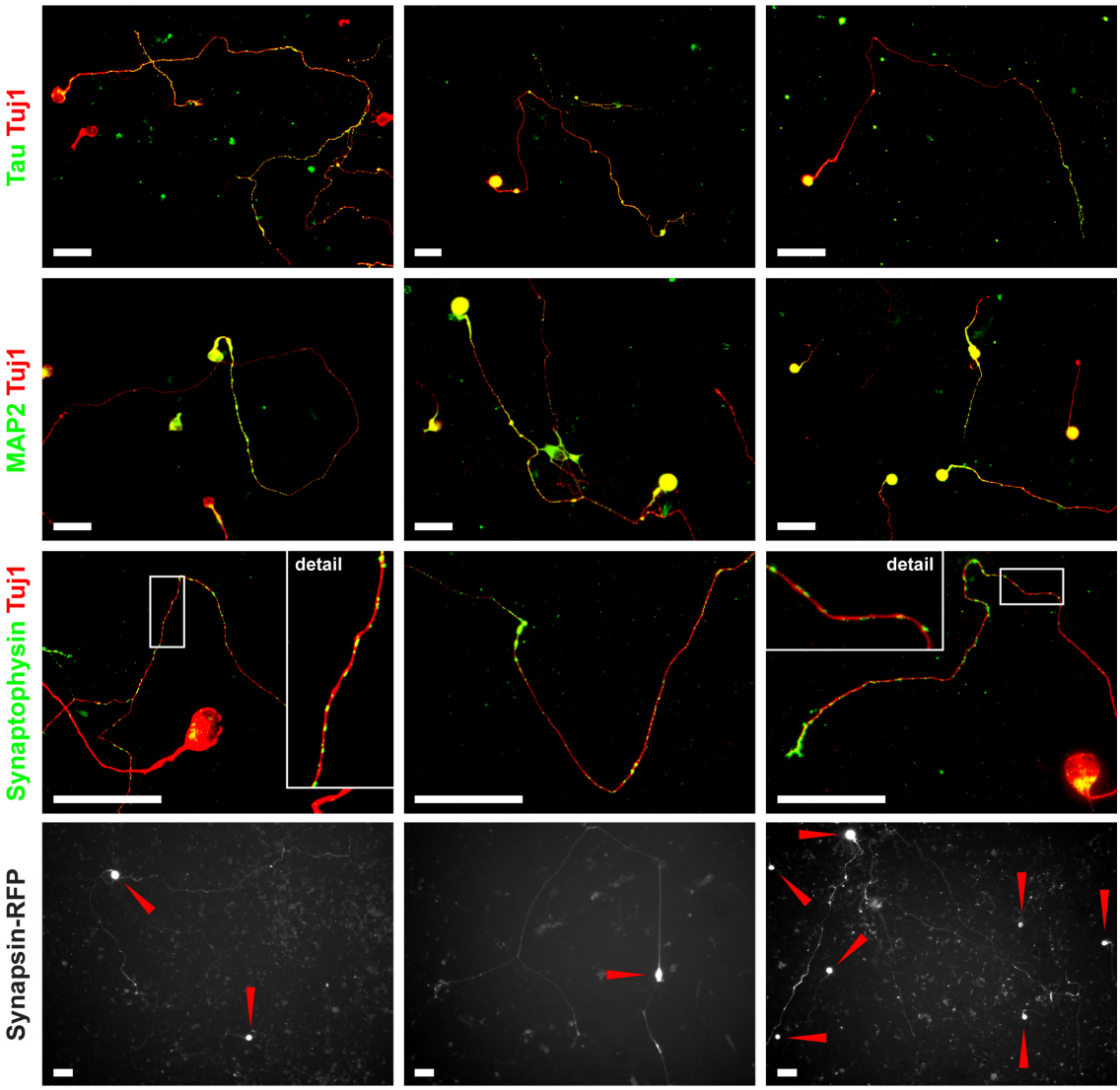

Figure 13. Neuron-specific immunofluorochemistry and synapsin reporter activity in NiNs
All scale bars are 50 µm. Tau stain (first row): three doses of 1.0 µg pmax-BAM factors, ≥ 10 days in N3 medium, on TCPS. MAP2 stain (second row): three doses of 1.0 µg pmax-BAM factors (left panel), or 2.0 µg pUNO-AM/pmax-B factors (center and right panels), 16 days in N3, on poly-D-lysine/laminin-coated coverslips. Synaptophysin stain (third row): five (left and center panels) or three (right panel) doses of 1.0 µg pmax-BAM factors, 17 days in N3, on PDL/laminin-coated coverslips. Expression of RFP under control of the synapsin promoter (fourth row): three doses of 1.0 µg pmax-BAM factors (left and center panels), or 2.0 µg pUNO-AM/pmax-B factors (right panel), ≥ 10 days in N3, on PDL/laminin-coated coverslips. Synapsin-RFP images have not been false-colored red, in order to maximize visual contrast for thin cellular processes. Arrows indicate synapsin-RFP^{+} cell bodies.

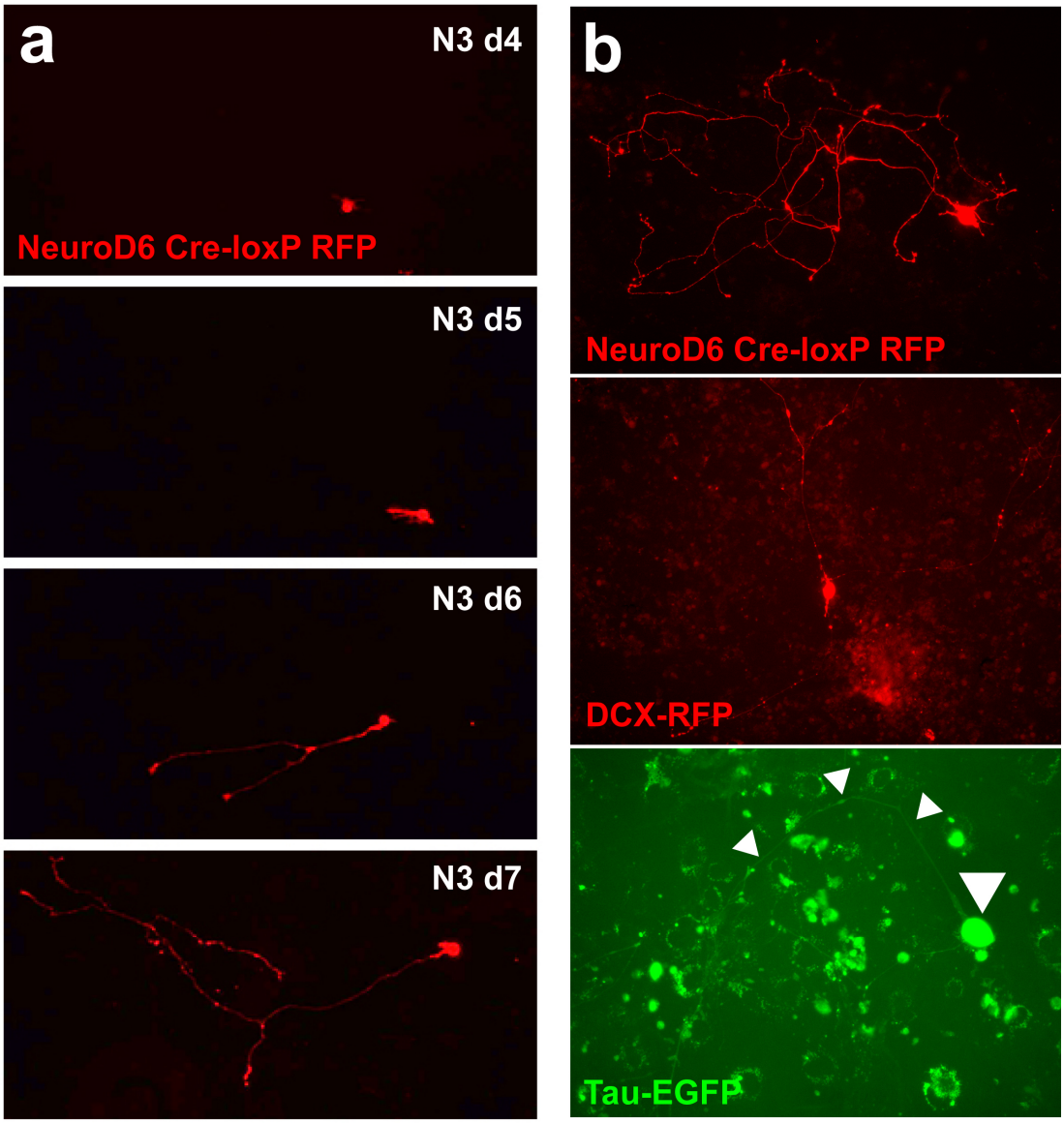

Figure 14. Transgenic PMEF reporter activation in NiNs
(a) RFP^+ NiN at day four of culture in N3 following transfection of NeuroD6 Cre-loxP RFP PMEFs with pUNO-AM/pmax-B. An increase in neurite extension and complexity was observed with each subsequent day in culture. Images depict a single representative NiN imaged repeatedly over seven days. (b) Neurite complexity in NeuroD6 Cre-loxP RFP^+, DCX-RFP^+, or Tau-$EGFP^+$ NiNs at day 10, 8, and 18, respectively. Contrast has been enhanced to reveal dim GFP^+ neurites in Tau-$EGFP^+$ NiN neurites (small arrows) emerging from a brighter GFP^+ soma (large arrow).

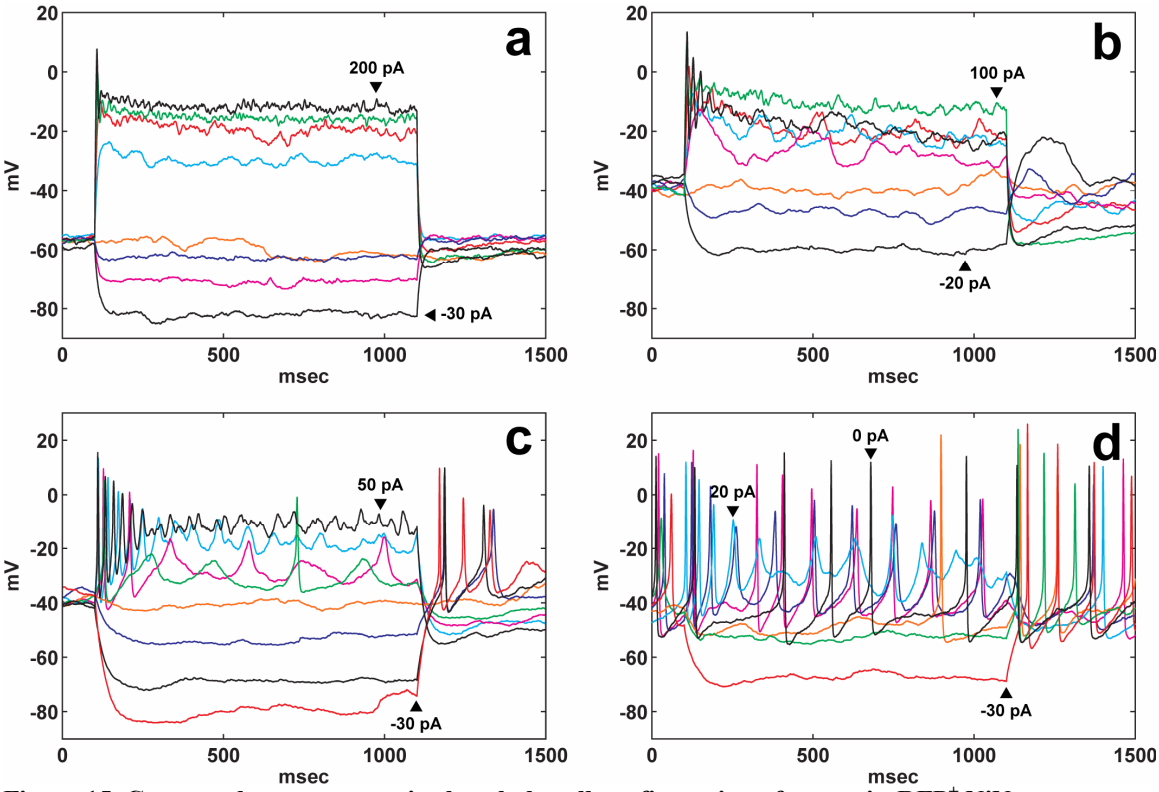

Figure 15. Current clamp response in the whole-cell configuration of synapsin-RFP^{+} NiNs
(a) and (b) are traces of cells that received three doses of 1.0 µg pmax-BAM factors, after 16-17 days of culture in N3 medium, on poly-D-lysine/laminin-coated coverslips. (c) and (d) are traces of cells that received three doses of 2.0 µg pUNO-AM/pmax-B factors, on day 12 of culture in N3, on poly-D-lysine/laminin-coated coverslips.

Chapter 4: Non-viral Neuronal Reprogramming can be Enhanced with Small Molecules and Chronic Depolarization

4.1 Summary

Since Wernig's original description of lentiviral direct reprogramming of fibroblasts to functional glutamatergic neurons in 2010 [251], the field has expanded to include the generation of neural and oligodendroglial progenitors [267-268], photoreceptors [365], dopaminergic [253, 255-256, 366], GABAergic [273], and spinal motor neurons [258, 295], and many others, from a variety of human and murine cell types of various ages and disease states. As applied to future cell therapies against myriad intractable neurodegenerative diseases, each of these techniques share a strong impetus for increased reprogramming efficiency. To that end, small molecule cocktails have been tested in and demonstrated to greatly enhance the efficiency of viral neuronal reprogramming [364]. In an effort to improve the clinical translatability of neuronal reprogramming, we have previously developed a safer non-integrative, non-viral method based on nanoparticulate transfection of lineage-instructive transcription factor-encoding plasmids, to produce functional neurons from mouse fibroblasts [281]. In this report we extend our non-viral technique by the use of small molecules and chronic depolarization to double our yields of glutamatergic neurons, as well as to enable the non-viral induction of a neuronal phenotype in human fibroblasts. We also report the first non-virally induced dopaminergic neuron-like cells that co-express tyrosine hydroxylase, TUJ1, and MAP2. We provide evidence that chronic depolarization can improve both dopaminergic and

pan-neuronal conversion efficiencies, but that small molecular inhibition of GSK-3β and SMAD signaling may increase pan-neuronal reprogramming efficiency particularly in reprogramming cocktails containing Ascl1. The use of chronic depolarization to guide direct reprogramming is a new strategy that may find general application in other subtypes of neuronal transdifferentiation. Each of these advances brings the goal of safe, efficient, autologous cell therapies for human neurodegenerative diseases closer to reality.

4.2 Rationale and Significance

Our success in Chapter 3 suggested that the generation of human NiNs, mouse NiDAs, and mouse NiMNs would be possible to some extent when our non-viral BAM NiN transdifferentiation protocol is respectively applied to human fibroblasts, or to mouse fibroblasts with a dopaminergic or motor neuron transcription factor cocktail. It is important to consider, however, that lentiviral protocols have demonstrated that human cells are inherently more resistant to neuronal transdifferentiation than are embryonic mouse cells [367], and as such our non-viral approach may require further increases in efficiency as it is deployed therein. Similarly, dopaminergic iN generation requires a longer pulse of ectopic TF expression than does glutamatergic iN creation [254], which may further benefit from the unique non-toxicity of p(CBA-ABOL) for serial transfection.

When the scalability of p(CBA-ABOL) synthesis is taken together with successful demonstration of iMN [258] and iDA [254] engraftment and iDA functional improvement in animal models of Parkinson's disease [255-256], the goal of various cell-replacement therapies using iNs for a variety of neurodegenerative diseases seems

attainable. Parkinson's disease is particularly focal and gradual, and is therefore attractive target for cell therapy, due to the relatively small quantity of iDAs that would be required to produce a therapeutic benefit. For example, if a non-viral method could produce functional dopaminergic neurons with five 1 μg doses at a 7.5% efficiency, only ~ 0.5% of a typical p(CBA-ABOL) synthesis and ~ 1% of a Plasmid Giga Kit product would be required to generate enough neurons to produce phenotype correction in a Parkinsonian rat [255]. The benefit-to-risk ratio of neuroprotective AAV gene therapy to combat PD is already deemed high enough to warrant clinical trials in humans [339], so the introduction of an ethically and technically viable autologous non-viral source of neuronal cells would be of great therapeutic value.

We hypothesized the effectiveness of the non-viral technique would improve with use of polycistronic vectors for iN generation [257, 259], which by removing redundant plasmid backbone sequences could increase the effective dose of each factor, and ensure co-expression of all factors in transfected cells. Consistent with the heterogeneity in neuronal properties observed in SA2, we have observed wide cell-to-cell differences in expression of reporter plasmids co-transfected into PMEFs. To ensure co-expression of all necessary dopaminergic transcription factors in each cell transfected, we used an Ascl1-Lmx1b-Nurr1 polycistronic insert that has been proven in lentiviral dopaminergic transdifferentiation of mouse astrocytes and fibroblasts [257], in our non-viral system.

We also chose to evaluate recently-discovered small molecules which can greatly boost the efficiency of lentiviral glutamatergic iN [364] and iMN [295] reprogramming. This approach draws on previous results that demonstrate inhibition of SMAD and GSK-3β signaling drives more-efficient neuronal differentiation of hES and iPSCs [368-369].

Adding small molecules SB-431542, CHIR-99021, and noggin for 2 weeks increased the purity and efficiency of neuronal transdifferentiation in human fibroblasts by 17- and 25-fold, respectively [364]. The addition of FSK and DM to iMN reprogramming media also reduces the number of transcription factors required from seven [258] to one [295], making the approach significantly more amenable for a non-viral transfection strategy, as it does not rely on rare co-expression of many plasmids in single cells.

We further proposed to utilize chronic depolarization of transdifferentiating neuronal cells in an effort to encourage their survival and/or dopaminergic specification. This is a new strategy that is informed by many developmental examples that indicate an intimate connection between electrochemical stimulation and neuronal development in general [313-314, 319], and dopaminergic specification in particular [317]. We were interested to determine if these interactions are also applicable in direct neuronal reprogramming, which appears to co-opt some of the biochemical circuits utilized in normal development [285]. The use of chronic depolarization and small molecular enhancers of reprogramming to boost the efficiency of our non-viral system will push iN yields towards therapeutically-useful levels. Further, generalizing the technique to other neuronal subtypes will extend the impact of non-viral neuronal reprogramming, and further develop our understanding of the relative importance of general barriers to delivery compared to barriers that are highly specific for a particular transcription factor cocktail or reprogramming target.

4.3 Methods

Plasmids, molecular cloning, and plasmid purification.

The reporter vectors pmax-GFP (3486 bp, Amaxa, Cologne, Germany) and VR1255C (6413 bp, Vical, San Diego, CA), which respectively express GFP and luciferase under control of the CMV promoter, were used as a positive transfection control (GFP), and a no-reprogramming negative control (pLuc).

pEF-Ascl1 (6539 bp), pEF-Lmx1b (6947 bp), pEF-Nurr1 (7625 bp), and pEF-polyALN (9560 bp) which carry human ORFs, or a polycistronic 2A-linked cassette with all three ALN factors, were expressed under control of the EF1α promoter in the pEF-DEST51 vector, and were gifts from Russ Addis (University of Pennsylvania, PA). When used together, the separate ALN-expressing vectors are abbreviated pEF-ALN. pUNO1-mAscl1 (3892 bp, InvivoGen, San Diego, CA, expressing mouse Ascl1 and under control of the EF1α/HTLV promoter, was occasionally used in conjunction with pEF-Lmx1b and pEF-Nurr1, and when used together are abbreviated as pEF-(A)LN. A summary of these dopaminergic plasmid cocktails is presented in Figure 16.

pCIG2-mNgn2-6XMyc (7282 bp), which expresses myc-tagged mouse Ngn2 followed by IRES-GFP under control of the CAG promoter, was a gift from Franck Polleux (The Scripps Research Institute, CA). pmax-Ngn2 (3683 bp), which expresses mouse Ngn2 under control of the CMV promoter, was generated by excision of the Ngn2 ORF from pCIG2-mNgn2 digested with PstI and EcoRI (NEB, Ipswich, MA), and ligation into pmaxCloning (Amaxa) digested with PstI and EcoRI.

Plasmids were propagated in *Escherichia coli* DH5α (Invitrogen, Carlsbad, CA) and purified with EndoFree Plasmid Mega and Maxi kits (QIAGEN). Plasmid DNA

concentrations were quantified by measurement of absorbance at 260 nm with a NanoDrop ND-1000 Spectrophotometer (Thermo Scientific, Waltham, MA).

Poly(CBA-ABOL) synthesis and polyplex formation

Poly(CBA-ABOL) was synthesized by Michael polyaddition of 3.67 g N,N-cystaminebisacrylamide (CBA) (Polysciences, Warrington, PA) and 1.26 g 4-amino-1-butanol (ABOL) (Sigma-Aldrich, Saint Louis, MO) as described by Lin et al [353]. The reaction product was purified by dialysis (3.5 kDa cutoff) in acidic deionized water (pH 4) and then lyophilized. The polymer was collected in its HCl-salt form (1.63 g, 33% yield), and its structure validated by ^{1}H NMR (in D_2O) on a Varian Mercury 300 MHz NMR Spectrometer. p(CBA-ABOL)/DNA nanocomplexes (polyplexes) were synthesized at a polymer:DNA mass ratio of 45:1, which was selected based on a preliminary optimization of GFP expression in primary mouse embryonic fibroblasts (PMEFs) (results not shown). Polyplexes were prepared by adding a HEPES buffer solution (20 mM HEPES, 5 wt % glucose, pH 7.4) of p(CBA-ABOL) (900 μg/mL) to a HEPES buffer solution (20 mM HEPES, 5 wt % glucose, pH 7.4) of plasmid DNA (75 μg/mL), followed immediately by vortexing for 20 seconds. Reaction sizes ranged from 5 to 15 μg of plasmid DNA.

Cell culture and transfection

PMEF CD1s were dissected carefully away from neural tissue in E14.5 mice. 80,000 PMEF-HLs (Millipore, Billerica, MA) or PMEF-CD1s, or 60,000 MRC-5 fetal human fibroblasts (ATCC) were seeded per well in 24-well TCPS plates (BD, Franklin

Lakes, NJ) at 37 °C and 5% CO_2 in complete PMEF medium: Dulbecco's Modified Eagle's Medium with 4.5 g/L glucose (GIBCO 11960-044) (Invitrogen), 10% Premium Select FBS (Atlanta Biologicals), 25 μg mL^{-1} gentamicin (Invitrogen), and 1x GlutaMAX, non-essential amino acids, sodium pyruvate, and β-mercaptoethanol (Invitrogen). For the ECM study, PMEF-HLs were additionally seeded on BD BioCoat poly-D-lysine/laminin or human fibronectin-coated plates.

PMEFs were transfected with either: GFP as a positive transfection control, pLuc as a no-reprogramming control, or pUNO-AM/pmax-B, pEF-ALN, pEF-polyALN, pEF-(A)LN, pCIG2-mNgn2-6XMyc, or pmax-Ngn2 plasmid cocktails for induced neuronal transdifferentiation. Separate BAM and ALN factor plasmids were delivered at an equimolar ratio in all cases. All transfections were carried out in serum- and antibiotic-free OptiMEM (Invitrogen). OptiMEM was replaced with complete PMEF medium four hours after the onset of transfection. Serial transfections were performed every 48 hours, with complete PMEF media between.

48 hours after the final transfection was completed, complete PMEF medium was replaced with neurogenic medium. BAM-transfected cells were placed in N3 neural induction medium containing: DMEM/F-12, 1x N2 supplement, 1x B27 supplement (Invitrogen), 10 ng mL^{-1} human bFGF2 (Stemgent, Cambridge, MA), and 25 μg mL^{-1} gentamicin (Invitrogen). ALN-transfected cells were placed in dopaminergic induction medium containing: DMEM/F-12, 1x N2 supplement, 1x B27 supplement (Invitrogen), and 25 μg mL^{-1} gentamicin (Invitrogen), with 10 ng mL^{-1} human bFGF2 (Stemgent) and 25 ng mL^{-1} FGF8 (R&D) for 1 week, followed by withdrawal of bFGF and FGF8. Ngn2-transfected cells were placed in C2 neural induction medium containing:

DMEM:F12:Neurobasal (2:2:1), 0.8% N2 supplement, 0.4% B27 supplement (Invitrogen), 1 μM dorsomorphin, 10 μM forskolin (Stemgent), and 25 μg mL^{-1} gentamicin (Invitrogen).

For chronic depolarization experiments, OptiMEM from the final transfection was replaced with PMEF medium containing an additional 30 mM KCl or NaCl, or 1 mM TEACl (Sigma), and two days later were maintained in neurogenic media containing these factors for the remainder of the experiments. For small molecular inhibition of GSK-3β and SMAD signaling, OptiMEM from the final transfection was replaced with PMEF medium containing 10 μM SB-431542, 0.5 μM LDN-193189 (Sigma), and 2 μM CHIR99021 (Stemgent), and two days later were maintained in neurogenic media containing these factors for 10 days, followed by their withdrawal.

Immunofluorochemistry

Transfected cells were washed briefly with PBS containing Ca^{2+} and Mg^{2+} (Mediatech), and fixed with 4% PFA (EMS) at RT for 20 minutes. Cells were then incubated for 2 hours at room temperature (or 18 hours at 4C for Ascl1) in blocking buffer containing 0.2% Triton X-100, 3% w/v BSA, 10% goat or fetal bovine serum (Sigma-Aldrich), and combinations of the following primary antibodies: rabbit anti-Tuj1 (Covance, 1:500), mouse anti-MAP2 (BD, 1:500), goat anti-Ascl1 (Santa Cruz 48449, 1:500), rabbit anti-Ngn2 (Millipore AB5682, 1:500), FITC-conjugated mouse anti-V5 (Life Technologies R963-25, 1:500), rabbit anti-TH (Pel-Freez, 1:500). The cells were then washed three times with PBS, and if necessary incubated for one hour at RT in blocking buffer containing appropriate AlexaFluor 488 or 594 secondary antibodies

(1:200, Invitrogen), washed three times with PBS, and imaged with a Nikon Eclipse TE2000-U inverted fluorescence microscope (Tokyo, Japan) with a ProScanII motorized stage (Prior Scientific, Rockland, MA).

Image analysis

To quantify $Tuj1^+$, $MAP2^+$, and TH^+ cell generation, PMEFs were transfected in TCPS wells, stained, and scanned to produce large mosaic images of each complete culture area. Tuj1 and MAP2 mosaics were processed with a FIJI (Fiji Is Just ImageJ, http://fiji.sc) macro to: automatically and uniformly threshold each image according to local contrast, exclude small debris, overlay thresholded TUJ1 and MAP2 channels, and to count the number of double-positive cells in each well. Because TH+ cells were present at a frequency similar to that of debris particles indistinguishable via automated ImageJ analysis, large well scans were counted manually in their entirety for TH^+ cells with neuronal morphology by an experimenter blinded to the experimental condition.

4.4 Results

NiN yield is increased with exposure to chronic depolarization during reprogramming

In PMEF CD1s transfected with three 1 μg doses of pUNO-AM/pmax-B, a greater number of $TUJ1^+$, $MAP2^+$, and double-positive cells were each evident with KCl exposure at N3 day 10, and neurite complexity was not evidently affected (Figure 17). To quantify this effect, we performed large area automated image analysis (Figure 18a) to

count the number of total cells (Figure 18b) (including unconverted PMEFs), and $MAP2^{+}TUJ1^{+}$ double-positive NiNs (Figure 18c) at N3 day 10. The total final cell number was unchanged with 30 mM KCl or non-depolarizing 30 mM NaCl osmotic control, compared to normal N3 media formulation (Figure 18b). $TUJ1^{+}MAP2^{+}$ NiN yield was more than doubled with 30 mM KCl exposure compared to normal media, and was unchanged with 30 mM NaCl (Figure 18c). Unlike PMEF CD1s, exposure to 30 mM KCl was toxic to PMEF HLs during transfection with a 1 μg dose of pUNO-AM/pmax-B, diminishing the number of surviving cells at N3 day 10 by half compared to normal media (Figure 19a). Depolarization instead with 1 mM TEACl, a K^{+} channel blocker, rescued a 30% enhancement in NiN yield from PMEF HLs, compared to normal media (Figure 19b).

NiN yield is increased with exposure to small molecular inhibitors of GSK-3β and SMAD signaling during reprogramming

The yield of NiNs generated from PMEF HLs with a 1 μg dose of pUNO-AM/pmax-B was increased by reprogramming in the presence of small molecules LDN-193189, CHIR-99021, and SB-431542 small molecules (SMs) inhibiting GSK-3β and SMAD signaling for 10 days immediately following non-viral transfection (Figure 20). A greater number of $TUJ1^{+}$, $MAP2^{+}$, and double-positive cells were each evident with SM exposure at N3 day 14, and neurite complexity was not evidently affected. To quantify this effect, we performed large area automated image analysis to count the number $MAP2^{+}TUJ1^{+}$ double-positive NiNs at N3 day 14 (Figure 21a). NiN yield was more than doubled with exposure to SMs compared to normal media, and PMEF HLs

transfected with luciferase (pLuc) did not express neuronal markers (Figure 21b). Exposure to the SM cocktail doubled the efficiency of NiN generation when PMEF HLs were transfected with a 1 μg dose of pUNO-BAM on TCPS, PDL/laminin-, or human fibronectin-coated substrates, and analyzed for MAP2 and TUJ1 positivity at N3 day 10 (Figure 22). Human fetal lung fibroblasts (MRC-5) transfected with a 1 μg dose of pUNO-AM/pmax-B adopted neuronal morphology and co-expressed TUJ1 and MAP2 at N3 day 14, only if reprogrammed in the presence of SMs for ten days (Figure 23); neuronal markers were not expressed in the absence of SMs during reprogramming, or in pLuc-transfected MRC-5s.

Non-viral induction of TH^+ cell yield is inefficient, but can be improved with chronic depolarization

PMEF CD1s transfected with three 1 μg doses of polycistronic ALN (pEF-poly ALN) or separate ALN factors (pEF-ALN) both generated rare TH^+ cells (Figure 24). pEF-poly ALN cells were rarely $MAP2^+$ and had atypically large and multinuclear "soma", whereas pEF-ALN TH^+ cells were generally also $MAP2^+$ and exhibited a soma and mononuclear phenotype more typical of published iDAs. Addition of 30 mM KCl did not evidently alter NiDA morphology in either case (Figure 24), but more than doubled the yield of TH^+ cells generated from pEF-ALN transfected cells (Figure 25).

Ascl1 is sensitive to 3' modification when used for neuronal reprogramming

PMEFs transfected with individual ALN factors carrying a 3' V5 tag fusion were stained with an anti-V5 antibody, revealing the expected proper nuclear localization of

Lmx1b-V5 and Nurr1-V5, whereas Ascl1-V5 was sequestered in bright punctae near the nuclear envelope (Figure 26). Delivery of a tagless wild-type Ascl1 via the pUNO-Ascl1 construct restores an even nuclear expression localization of Ascl1. Replacement of pEF-Ascl1-V5 with pUNO-Ascl1 in the ALN cocktail, denoted as pEF-(A)LN, produced an order of magnitude improvement in the yield of $TUJ1^+$ cells detected at N3 day 10 (Figure 27). The number of rare TH^+ and double-positive cells was also increased, but to a lesser extent than TUJ1. Untransfected PMEFs did not express detectable TH or TUJ1.

Pan-neuronal but not TH^+ cell yield is increased by inhibition of GSK-3β and SMAD during reprogramming with ALN factors

The yield of $TUJ1^+$ cells generated with a 1 μg dose of pEF-(A)LN plasmids could be increased over 80% by reprogramming in the presence of small molecules LDN-193189, CHIR-99021, and SB-431542 (SM) inhibiting GSK-3β and SMAD signaling for 10 days immediately following non-viral transfection, but the number of TH+ cells was not affected (Figure 29). Neurite complexity was reduced at this timepoint because the small molecules were not yet withdrawn (Figure 28).

Non-viral neuronal reprogramming does not depend exclusively on Ascl1

PMEFs transfected with a plasmid expressing Neurogenin 2 (Ngn2) under control of either the CMV (Figure 30, left column) or CAG promoter (Figure 30, right column) expressed abundant Ngn2 at day 2 following transfection (Figure 30, top row), but comparatively rare $MAP2^+TUJ1^+$ NiNs converted and survived to day 11 of culture in iMN media containing FSK, DM, and neurotrophic factors (Figure 30, bottom row).

CAG-driven Ngn2 expression did not guarantee neuronal conversion in surviving cells at day 11, as evident by the presence of IRES-GFP^{+}TUJ^{-} cells.

4.5 Discussion

In PMEF CD1s collected freshly from embryos, addition of 30 mM KCl did not impair BAM NiN neurite outgrowth (Figure 17) and was not toxic to the starting fibroblasts (Figure 18a), but dramatically improved the yield of NiNs collected at the end of the experiment, compared to normal N3 medium (Figure 18b). Non-depolarizing NaCl did not produce a difference in NiN yield. This suggests depolarization by elevated [Ca^{2+}] (which continues as long as high [K^{+}] is present [318]), rather than elevated osmotic pressure or [Cl^{-}], mediated an increase in either reprogramming efficiency or NiN survival after conversion.

We are currently unable to distinguish between these potential impacts on survival or conversion efficiency, but both are supported by the literature. For instance, depolarization can increase the survival of neural progenitors following injury [370]. Chronic depolarization can also dissociate repressive REST from target loci in differentiating dopaminergic progenitors, and can increase the yield of dopaminergic neurons produced [317]. Direct knockdown of REST has also recently been shown to be sufficient to reprogram fibroblasts into functional neurons [264]. Increased intracellular Ca^{2+}, as can occur via depolarization of voltage-gated Ca^{2+} channels, is a well-known improver of primary neuron survivability both *in vitro* [320, 322-324] and *in vivo* [371]. Activity also continues to control the identity of neurons post-natally - in one example,

acting as a switch to induce a dopaminergic phenotype in the brain of adult rats [372]. Perhaps most strikingly, increased intracellular Ca^{2+} entry (as occurs through voltage-gated Ca^{2+} channels with depolarization) has recently been shown to activate calcineurin to dephosphorylate and inhibit SMAD1/5/8 (the same targets of the small molecules shown to improve viral iN yield [364]), thereby increasing neural induction from NPCs [373]. Taking all of these precedents together, we believe chronic depolarization contributes to increased NiN yield via either: a switch to a subtype that better survives low density cultures, improved survivability without a concurrent subtype switch, an increased number of initial successfully-converted neurons, or a combination thereof.

A commercial fibroblast source (PMEF HLs) was sensitive to increased osmotic pressure – KCl toxicity significantly reduced the number of surviving cells at the end of the reprogramming experiment (Figure 19a). Interestingly, despite the sensitivity to high [KCl], depolarization of these cells with TEACl (a K^+ channel blocker) during reprogramming with BAM factors recovered an enhancement of BAM factor NiN yield (Figure 19b). We are interested therefore to evaluate KCl and TEACl for improved NiN generation in additional PMEF sources, particularly for those collected at various developmental stages, with an aim to correlate the degree of improvement afforded by chronic depolarization to concurrent epigenetic or developmental events.

Electrical activity acts as a critical switch to stop neuron migration and differentiate to a mature "GABA-inhibitory" phenotype, via increased expression of a Cl^- channel [374]. Various fibroblast sources may be more or less epigenetically-primed to track these normal expression patterns neurons follow in development, and presumably when induced *in vitro*. These differences would likely affect intracellular Ca^{2+} levels, and

consequently the sensitivity to, and utility of, chronic depolarization. It may also be possible to further delineate the relative contribution of depolarization to NiN induction and survivability by adding and withdrawing KCl at various stages of the reprogramming process, while continuously monitoring the induction kinetics of transgenic markers such as NeuroD6- or DCX-RFP, as described in Chapter 3. We also intend to re-evaluate the electrophysiological competence of these cells. Chronic depolarization can retard synaptic network formation in primary neuron cultures, but which can then recover and develop normally upon withdrawal of high [KCl] [320].

We next evaluated a slightly modified version of a small molecule cocktail with published success improving viral iPSC and neural induction [302, 375] and viral iN [364] derivation from PMEF sources for its ability to increase BAM NiN generation efficiency in PMEF HLs. These molecules inhibit BMP- and TGFβ-dependent EMT pathways in normal development via inhibition of SMAD and GSK-3β signaling. The details of their mechanisms of action in direct reprogramming are unclear, but they are generally believed to destabilize EMT differentiation programs, leaving MET and neuronal differentiation more likely [285]. Furthermore, Ascl1 may be inhibited via a GSK-3β phosphorylation site [285]; inhibition of GSK-3β may therefore act to directly de-repress Ascl1. As previously reported, it was necessary to withdraw the small molecules for four days to de-restrict neurite branching via CHIR [364]. With small molecule withdrawal, neurite complexity was similar to that observed in normal N3 medium (Figure 20). The addition of small molecules more than doubled BAM NiN yield at the end of the reprogramming period (Figure 21).

The production of BAM NiNs in the presence or absence of small molecules was not affected by PDL/laminin- or fibronectin-coated surfaces (Figure 22). We stopped these experiments at an earlier timepoint due to the known pro-survival effects ECM can have on neurons [376], in an effort to focus on the induction phase of iN generation. As such, it appears the early stage of NiN reprogramming may be more potently affected by GSK-3β and SMAD signaling than substrate ECM. Based on reports of enhanced transfection on hFN surfaces [69, 82-83], and our own experience, we expected that the PMEFs on hFN would be transfected to a greater extent and efficiency than on uncoated. Though GFP controls were qualitatively more transfected on hFN than TCPS (results not shown), the efficiency of iN generation was unaffected. As such, further improving transfection of the already-efficient pCBA-ABOL particles in PMEFs may not be as significant a barrier to reprogramming in the BAM NiN system as those barriers surmounted by the small molecule cocktail. This may not be the case for more difficult transfection targets, such as primary human fibroblasts.

We also observed that the improvement in BAM NiN yield from PMEFs with small molecule exposure was recapitulated in primary human fibroblasts. Without SMs, we observed no co-expression of TUJ1 and MAP2 from fetal lung fibroblasts transfected with the BAM factors, but 10 days of small molecule exposure was sufficient to induce at least immature human NiNs (Figure 23). To our knowledge this is the first report of non-viral human neuronal reprogramming. We next intend to evaluate the electrophysiological competence of these hNiNs, and to reprogram adult human fibroblasts. This effort may also benefit from possible synergy between the KCl- and small molecule-mediated improvements in NiN yield.

We next moved on to determine if the enhancements provided by the SMs and depolarization could be translated to more efficient production of NiDAs, which was expected to be more difficult than BAM NiN production, as dox-withdrawal experiments have shown that a longer pulse of ectopic dopaminergic factors is required for successful reprogramming [254]. The small molecule cocktail may encourage all forms of neuronal reprogramming, or operate specifically on one or more of the BAM factors, or their downstream targets. We began with a polycistronic dopaminergic vector that expresses Ascl1, Lmx1b, and Nurr1 from a single ORF, with transcription factor coding regions linked by 2A sequences, which release as individual proteins at nearly stoichiometric levels during translation [377-378]. These linker sequences are generally superior to the use of internal ribosomal entry sites (IRES), which drive significantly lower expression than from typical 5' cap initiation of translation. We hypothesized this would reduce some of the heterogeneity observed in Chapter 3, by ensuring co-expression of all three ALNs in every transfected cell.

Both polycistronic ALN and separate ALN factors were able to induce tyrosine hydroxylase (TH, an enzyme required for biosynthesis of dopamine) expression and morphological changes in transfected PMEFs (Figure 24). Surprisingly, the polycistronic ALN construct produced TH^+ cells that generally did not also express MAP2, and also had large multinuclear "soma", with thin neurite-like processes. The lack of MAP2 expression in these cells suggested they were not fully reprogrammed neurons, and that potentially only the dopaminergic transcription factors Lmx1b and Nurr1 were at work in these cells. Considering the potent and rapid growth arrest observed with Ascl1 expression in fibroblasts destined to become BAM factor neurons [251-252], the

appearance of multinuclear soma may further suggest reduced activity of Ascl1 as delivered via the polycistronic ALN construct. Separate ALN plasmids, on the other hand, produced iDA-like cells that expressed MAP2 and had more compact and mononuclear soma.

The efficiency of TH^+ cell production was improved by chronic KCl depolarization from PMEFs transfected with separate ALN plasmids, but the efficiency of the polycistronic vector was unaffected (Figure 25). The overall efficiency of NiDA generation was one to two orders of magnitude lower than that of BAM NiN generation. The polycistronic ALN construct may be less efficient due to lower overall expression levels and efficiency due to more difficult nuclear entry of large plasmids – an effect previously noted for a large polycistronic construct producing decreased iPSC-derivation efficiency compared to separate factors [379]. These results may imply that co-transfection is less of a barrier than are low overall expression levels. This result is despite the observation that viral delivery of the same construct is able to efficiently induce iDA formation from PMEFs and astrocytes [257].

We next worked to determine the source of the apparently impaired function of Ascl1 in the polycistronic ALN vector. We began by staining for proper nuclear localization of the separate ALN vectors, each of which carried a 3' V5 fusion tag. Lmx1b-V5 and Nurr1-V5 were localized to the nucleus, whereas Ascl1-V5 appeared to be sequestered in punctae near the nuclear envelope (Figure 26). The tagless Ascl1 vector used for BAM NiN in Chapter 3 was more efficient at transfecting PMEFs, and expressed Ascl1 throughout PMEF nuclei. Replacement of the V5-tagged Ascl1 with untagged Ascl1 produced an order of magnitude greater induction of TUJ1 in ALN-

transfected cells (Figure 27). When taken with the published success of the polycistronic ALN vector (with a 3' 2A sequence on Ascl1) delivered from lentivirus, we believe 3' Ascl1 fusions are functional but less stable or active than native Ascl1, and that when combined with lower expression duration or levels with non-viral delivery, may be accordingly less able to reprogram PMEFs. The reduction in Ascl1 transfection efficiency from pEF compared to pUNO, despite sharing the same promoter, may also be a consequence of the larger size of the pEF backbone. In all subsequent experiments we designed plasmids that were as small as possible.

The persistent difficulty of activating highly efficient TH^+ expression with the separate (A)LN factors presented us with an opportunity to study whether the improvements observed with GSK-3β and SMAD inhibition in BAM NiNs could be generalized to improve the efficiency of NiDA generation. Small molecules increased the yield of $TUJ1^+$ cells to the same extent we previously observed, but did not similarly improve the yield of TH^+ or $TUJ1^+TH^+$ cells (Figure 28, Figure 29). This suggests that the small molecule cocktail may be impacting Ascl1 or its downstream pan-neuronal targets independent of the dopaminergic transcriptional networks activated by the dopaminergic lineage-instructive Lmx1b and Nurr1 factors. This notion of transcription-factor-specific small molecule interactions is further supported by a recent report of a unique and synergistic interaction between Ngn2, forskolin, and dorsomorphin for viral iMN induction; no improvement or similar interaction was observed with Ascl1 [295]. These specific interactions may reflect various supportive and cross-repressive soluble cues in the maturation of the myriad neural subtypes in normal development.

Next, we set out to determine if the powerful pioneer activity of Ascl1 [282] and uniquely brief period of its ectopic expression required for neuronal conversion [252] are solely responsible for the success of our non-viral BAM iN system. We chose to evaluate the most efficient currently published lentiviral system that does not use Ascl1 – the reprogramming of PMEFs and human fibroblasts to iMNs with Ngn2 in the presence of forskolin, dorsomorphin, and neurotrophic factors [295]. We were able to induce robust nuclear non-viral expression of Ngn2, but only relatively rare $MAP2^{+}TUJ1^{+}$ cells appeared (Figure 30). This is the first example of non-viral neuronal reprogramming without Ascl1. With an IRES-GFP construct we were able to monitor live iN arborization as it matured rapidly and extensively at approximately day 6, followed soon thereafter by cell death in the next few days. We were therefore unable to culture putative NiMNs long enough to observe maturation of motor neuron-specific markers such as Isl1/2 and Hb9.

Considering the excellent survival and high yields we can produce with the non-viral BAM factors, our iMN results suggest that each iN subtype may be variably sensitive to extended culture. One potential explanation may be differential expression of ion channels one neuronal subtype relative to another; motor neurons may be particularly susceptible to death by excitotoxicity. Or, iMNs may be more prone to programmed death by apoptosis, as occurs to a great extent in normal development to maintain a proper innervation density [318-319]. The higher efficiency viral iMN cultures may also secrete and benefit from neuroprotective autocrine effects. We and many others have observed improved culture viability and iN complexity with half-volume rather than full-volume media changes, which potentially maintains the presence of some as-yet

undescribed critical conditioned media component(s). Culturing NiMNs in glia- or neuron-conditioned media may help to improve survivability.

4.6 Conclusion and future perspectives

Our aim was to extend our success producing BAM NiNs to a human cell source, as well as to other neuronal subtypes, and to determine if the efficiency of these processes could be improved with small molecules and chronic depolarization, towards the production of iNs that are therapeutically attractive. The use of chronic depolarization to improve NiN induction and/or survivability is a new technique that can be readily evaluated in any lab performing neuronal reprogramming. In accordance with the many neural subtypes that depend on depolarization for accurate specification and survival during normal development, we observed an improvement in both dopaminergic and pan-neuronal marker expression with culture in medium containing high KCl; this may suggest the technique can be further generalized to other forms of neural reprogramming. We look forward to evaluating the technique in lentiviral systems that suffer from unexplained low efficiencies. To delineate the contribution of KCl to the neural induction versus survival phases of the experiments, we will use PMEF reporter lines as described in Chapter 3, add and remove KCl at various times, and employ longitudinal single-cell imaging.

We have demonstrated that Brüstle's cocktail of small molecules [364] can also be used to greatly improve the yield of $TUJ1^{+}MAP2^{+}$ NiNs, in particular for cocktails including Ascl1. It remains for us to evaluate potential synergy between chronic

depolarization and small molecules for NiDA induction with the (A)LN cocktail; KCl may act on the dopaminergic TFs Lmx1b and Nurr1 to improve TH^+ induction, and the small molecules on Ascl1 for general enhancement of neural induction and survival. With further increases in NiDA efficiency we will be able to evaluate the functional characteristics of these cells. The small molecules also enabled us to produce the first human BAM NiNs, which is a significant proof-of-concept advance that brings us closer to the goal of transformative autologous cell therapies for neurodegenerative disease.

A critical finding of this chapter is that the successful deployment of each transcription factor cocktail seems to require the surmounting of a mixture of shared and unique barriers. To over-simplify for the purpose of illustration: all forms of non-viral neuronal reprogramming can benefit from the high transfection efficiencies afforded by pCBA-ABOL, a large subset may benefit from pro-survival effects of chronic depolarization, NiMNs may benefit from NMDAR inhibitors to prevent excitotoxicity, and potentially only NiN cocktails including Ascl1 may benefit from inclusion of GSK-3β and SMAD inhibitors. Rapid development of the field will require an understanding and ability to detect and circumnavigate each of the potential barriers.

The most poorly-understood of these barriers may be the variable epigenetic availability of critical target loci in the starting cell source. There has been a recent attempt to mechanistically describe the difference in BAM iN induction efficiency between various cell sources, which finds that the susceptibility to reprogramming by Ascl1 appears to depend on a complex trivalent chromatin state [282]. Each target iN type may have a similar "ideal" set of chromatin marks that may previously exist and/or appear gradually in reprogramming cells.

Each of the endogenous BAM factor genes activate in around 48 hours of lentiviral induction [380], which is also readily achieved with non-viral delivery. If kinetically-limited epigenetic changes are required to allow stable activation of endogenous gene circuits, transient transfection may be less-readily able to achieve efficient reprogramming (for example in non-viral dopaminergic neuron reprogramming). Slow epigenetic or stochastically-unlikely pioneer events may be responsible for the differences in reprogramming speed and efficiency reported for various forms of reprogramming. iPSCs for example, require perhaps the longest continuous induction of ectopic factors, presumably because their epigenetic landscape must be reverted to the greatest extent to prime for the rapid induction that occurs with subsequent differentiation into all possible lineages.

Difficult forms of non-viral reprogramming may therefore benefit from CRISPR/Cas9-based synthetic transcription factor activation of endogenous loci, which appear to have pioneer activity of their own [298], which some natural lineage-instructive TFs may lack in a fibroblastic context (Brn2 in the absence of Ascl1, for example [282]). This approach could make the largest impact in low-efficiency reprogramming cocktails that include transcription factors with demonstrable difficulty binding to their targets in the starting cell source. Future dCas9 systems carrying chromatin-remodeling enzymes may also help to precisely define and surgically excise the epigenetic barriers to reprogramming without repeated and laborious protein engineering, potentially providing a strong therapeutic rationale for the nascent field of "epigenetic editing" [381-382].

A current restriction on the full potential of CRISPR/Cas9-based epigenetic modifiers for reprogramming may be the generally-desired single-site specificity of

dCas9 targeting; ideally the epigenetic modifiers could be simultaneously targeted with a library of gRNAs across all of the consensus binding sites for the lineage-specifying transcription factors. This could speed slow forms of reprogramming by specifically removing repressive marks on all target loci, thereby allowing the ectopic (or dCas9-activated endogenous) transcription factors to act on their targets freely. Transfection of gRNA libraries into transgenic reporter PMEFs, followed by FACS purification of rapidly- or completely-reprogrammed cells, and a compilation of the gRNAs sequenced from those successful cells may identify epigenetic "hot spots" that are particularly critical for successful reprogramming.

Having demonstrated the large impact *chemical* microenvironments can exert on NiN generation, and our lab's experience with the power substrate topography can have on cell phenotype, we were also interested to determine if the *physical* microenvironment might have a positive effect on non-viral transfection, and direct neuronal reprogramming. We have considered this question in two independent parts, in order to isolate the relative contribution of topography to each. In Biomaterials, we recently demonstrated that substrate topography can encourage the viral neuronal reprogramming of fibroblasts to neurons [383]. Briefly, we found that viral reprogramming of PMEFs with the BAM factors on micron-scale gratings could increase iN yields by 35-60%, as well as affect neurite branching and global gene expression patterns. These effects may be transduced by mechanotransductive modulation of GSK-3β [384] and SMAD activity by YAP/TAZ. In Chapter 5, we go on to demonstrate that substrate topography can also increase non-viral transfection efficiency in fibroblasts more generally, which could be applied to any form of plasmid-based non-viral reprogramming.

4.7 Figures

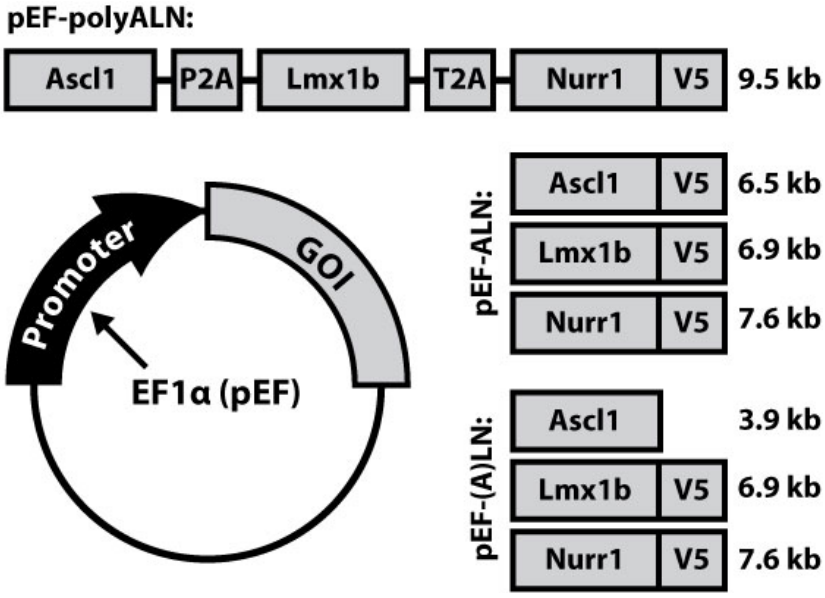

Figure 16. Non-viral vectors generated for direct reprogramming of fibroblasts to dopaminergic neurons

Coding sequences for human Ascl1, Lmx1b, and Nurr1 (ALN) transcription factors were inserted into the pEF-DEST1 backbone, under control of the EF1α promoter, either separately or as a single polycistronic 2A-linked construct (pEF-poly ALN), with 3' V5 tags. pUNO-Ascl1 was used with pEF-Lmx1b and pEF-Nurr1 as a tagless version of Ascl1, denoted pEF-(A)LN. The separate ALN factor-encoding plasmid cocktails (pEF-ALN and pEF-(A)LN) were delivered at equimolar ratios.

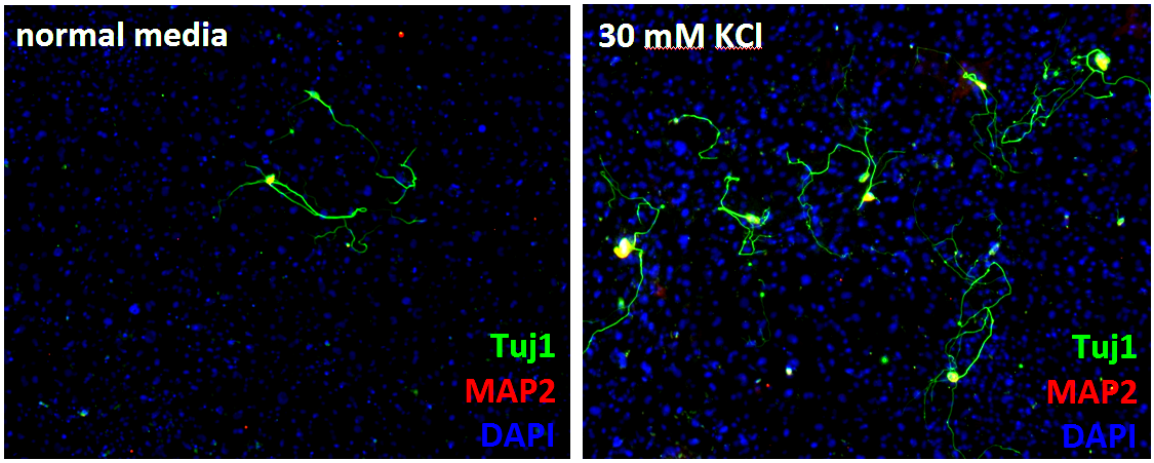

Figure 17. NiNs produced with and without chronic exposure to depolarizing concentrations of KCl

The appearance of NiNs at N3 day 10 produced with three 1 µg doses of pUNO-AM/pmax-B with and without exposure to 30 mM KCl immediately following non-viral transfection, for the duration of reprogramming.

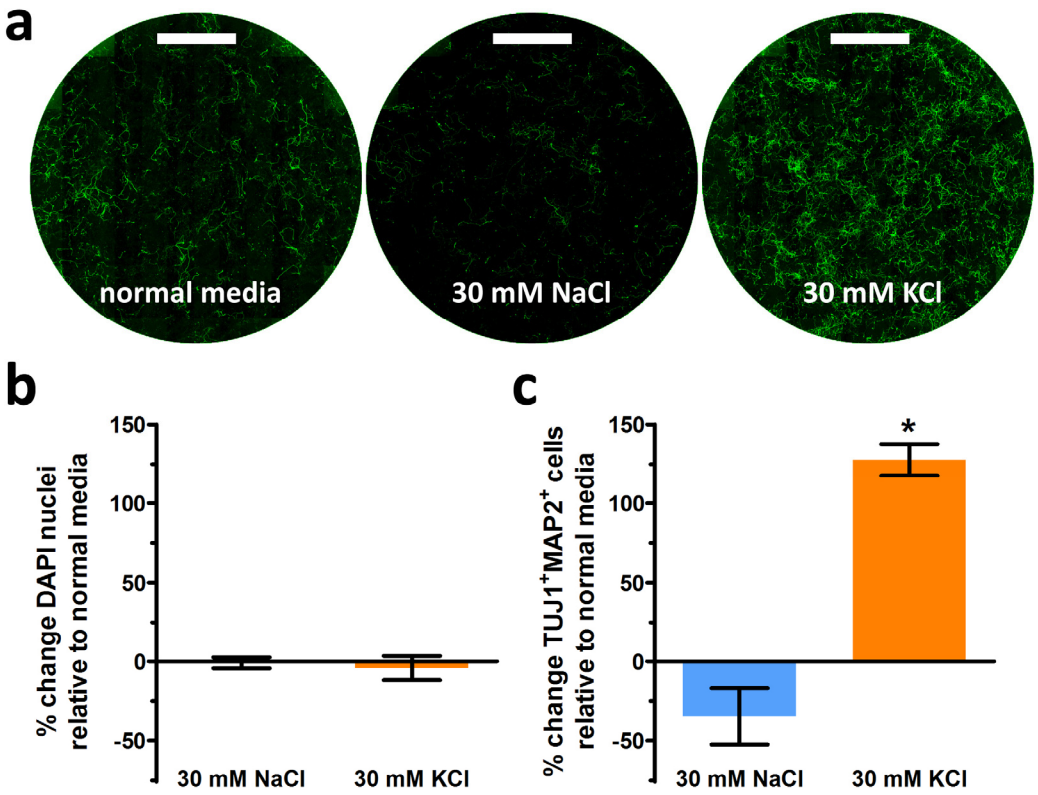

Figure 18. Quantification of NiN yield from PMEFs with and without chronic depolarization by KCl
(a) Large area scans of TUJ1 expression at N3 day 10 following three 1 µg doses of pUNO-AM/pmax-B in PMEFs (2.5 mm scale bar). (b) Total final cell number with 30 mM KCl or non-depolarizing 30 mM NaCl osmotic control, compared to normal N3 media formulation. (c) $TUJ1^{+}MAP2^{+}$ NiN yield was more than doubled with 30 mM KCl exposure compared to normal media, and was unchanged with 30 mM NaCl. Cell counts were generated with large area image analysis; bars represent mean ± SEM of three separate experiments performed in triplicate.

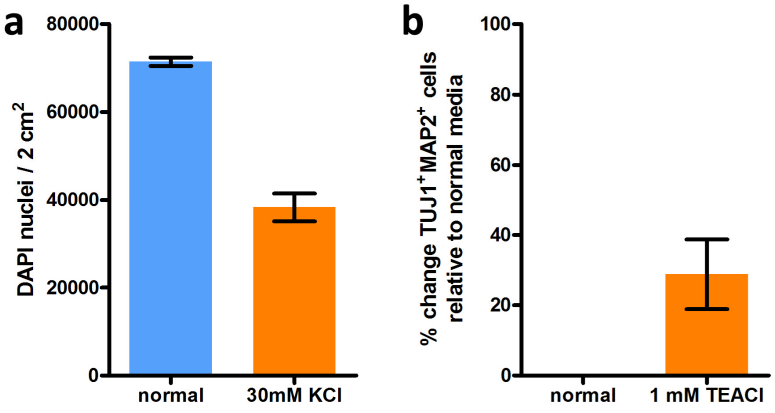

Figure 19. Quantification of NiN yield from a commercial MEF source with and without chronic depolarization by TEACl
(a) Number of surviving PMEF HLs at N3 day 10 following a 1 µg dose of pUNO-AM/pmax-B, in the presence or absence of 30 mM KCl. (b) NiN yield at N3 day 10 following reprogramming in the presence or absence of 1 mM TEACl (K^{+} channel blocker). Cell counts were generated with large area image analysis, error bars represent SEM, n = 3.

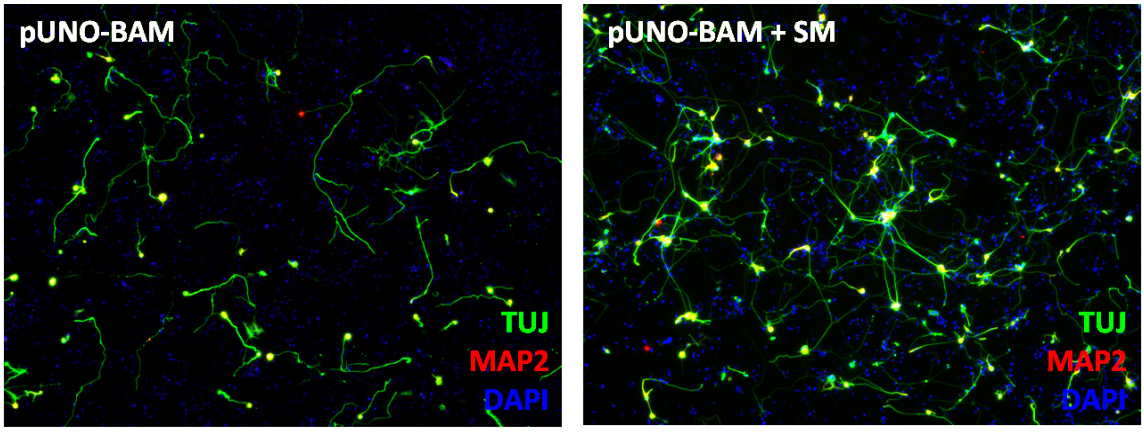

Figure 20. NiNs produced with and without inhibition of GSK-3β and SMAD signaling
The appearance of NiNs at N3 day 14 generated with a 1 µg dose of pUNO-AM/pmax-B in the presence or absence of small molecules LDN-193189, CHIR-99021, and SB-431542 (SM) for 10 days immediately following non-viral transfection.

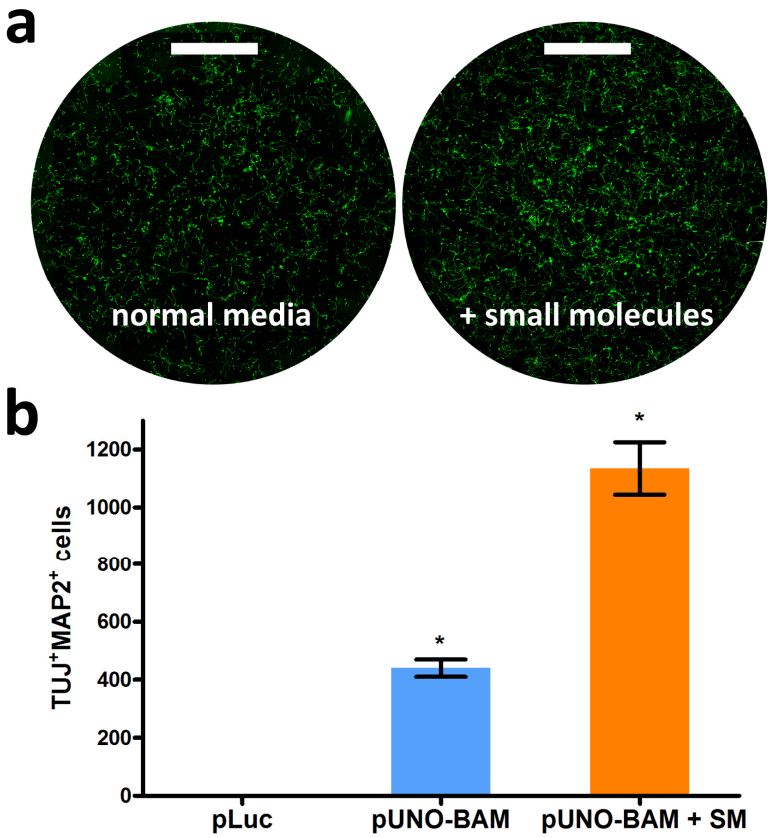

Figure 21. Quantification of NiN yield with and without inhibition of GSK-3β and SMAD signaling
(a) Large area scans of TUJ1 expression at N3 day 14 following a 1 µg dose of pUNO-AM/pmax-B in PMEFs (2.5 mm scale bar). (b) $TUJ1^{+}MAP2^{+}$ NiN yield at N3 day 14 with exposure to LDN-193189, CHIR-99021, and SB-431542 (SM) compared to normal media. Cell counts were generated with large area image analysis; bars represent mean ± SEM of three separate experiments performed in triplicate.

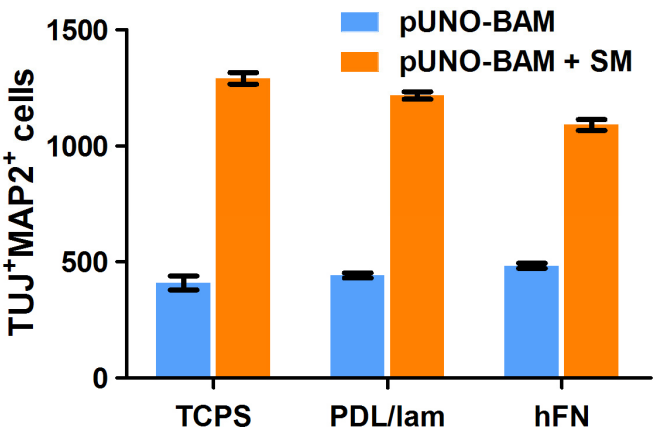

Figure 22. Quantification of NiN yield on various substrate ECMs with and without inhibition of GSK-3β and SMAD signaling
NiN yield at N3 day 10 from PMEFs transfected with 1 µg pUNO-BAM when reprogrammed on TCPS, PDL/laminin, or human fibronectin, in the presence or absence of LDN-193189, CHIR-99021, and SB-431542 (SM). Cell counts were generated with large area image analysis, error bars represent SEM, n = 3.

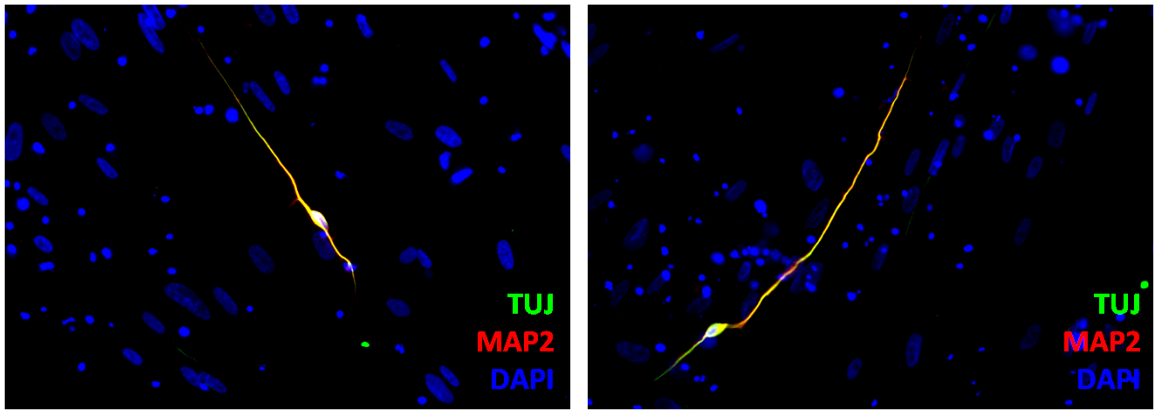

Figure 23. Expression of neuronal markers in human NiNs produced with inhibition of GSK-3β and SMAD signaling
Expression of TUJ1 and MAP2 at N3 day 14 in NiNs produced from human fetal fibroblasts (MRC-5) transfected with a 1 µg dose of pUNO-AM/pmax-B and reprogrammed in the presence of LDN-193189, CHIR-99021, and SB-431542 (SM) for ten days.

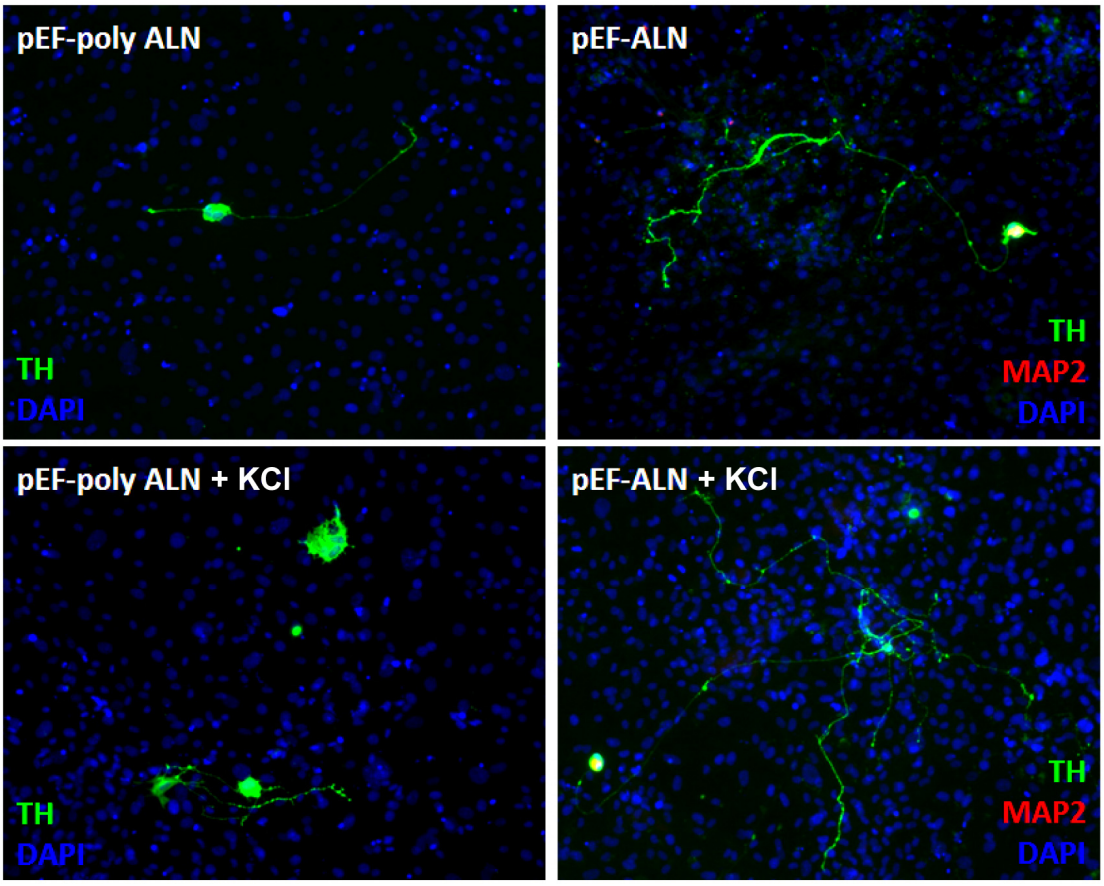

Figure 24. Expression of tyrosine hydroxylase (TH) in PMEFs transfected with a cocktail of ALN plasmids, or a polycistronic ALN construct
Induction of TH^+ cells at iDA medium day 10 in PMEF CD1s transfected with three 1 µg doses of polycistronic ALN (pEF-poly ALN) or separate ALN plasmids (pEF-ALN). pEF-poly ALN-transfected cells were generally not $MAP2^+$.

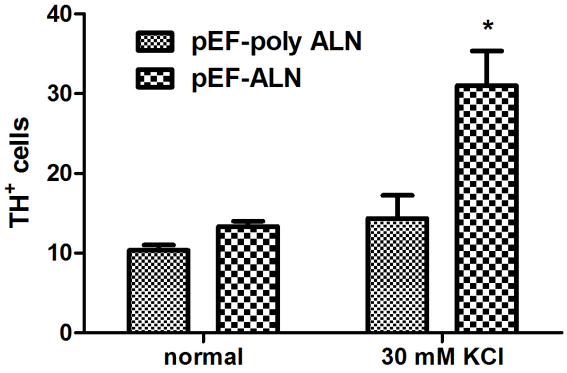

Figure 25. Quantification of TH^+ cells produced with separate or polycistronic ALN factors in presence of KCl
TH^+ yield at iDA medium day 10 following three 1 µg doses of pEF-poly ALN or pEF-ALN in PMEF CD1s, with or without 30 mM KCl. Cell counts were generated with large area image analysis, error bars represent SEM, n = 3.

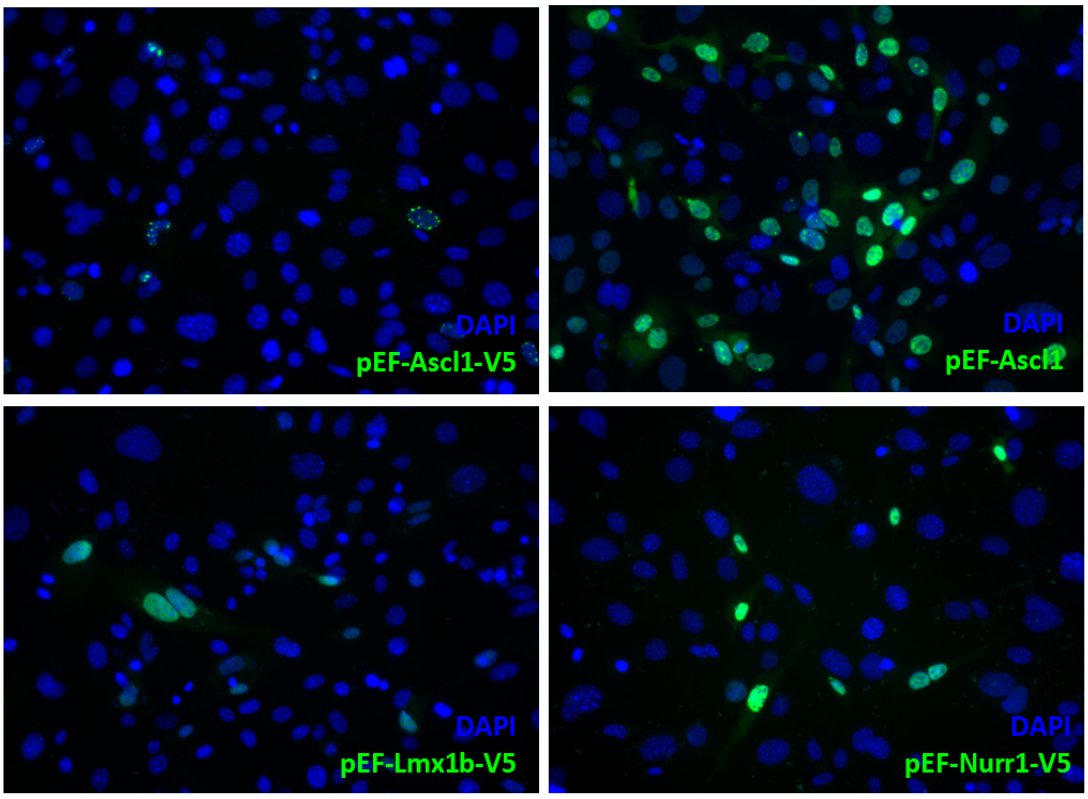

Figure 26. Localization of Ascl1, Lmx1b, and Nurr1 with 3' V5 tags, and tagless Ascl1
Staining in PMEFs two days after transfection with V5-tagged (top left) or wild-type Ascl1 (top right), and V5 tagged Lmx1b and Nurr1 (bottom row). V5 stains were performed with an anti-V5 antibody, and wild-type Ascl1 stain with an anti-Ascl1 antibody.

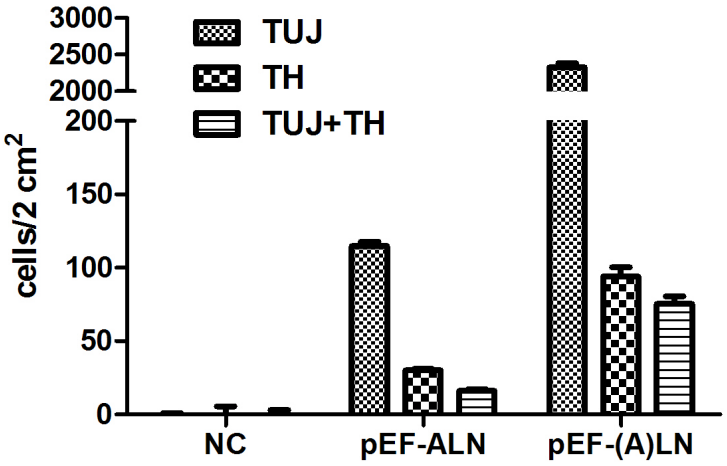

Figure 27. Quantification of cells expressing TUJ and TH upon removal of V5 tag from Ascl1
Yield of TH^+ and $TUJ1^+$ cells from V5-tagged ALN factors (pEF-ALN) or ALN factors with tagless Ascl1 (pEF-(A)LN) at N3 day 10. Cells were counted with large area image analysis, error bars represent SEM, n = 3.

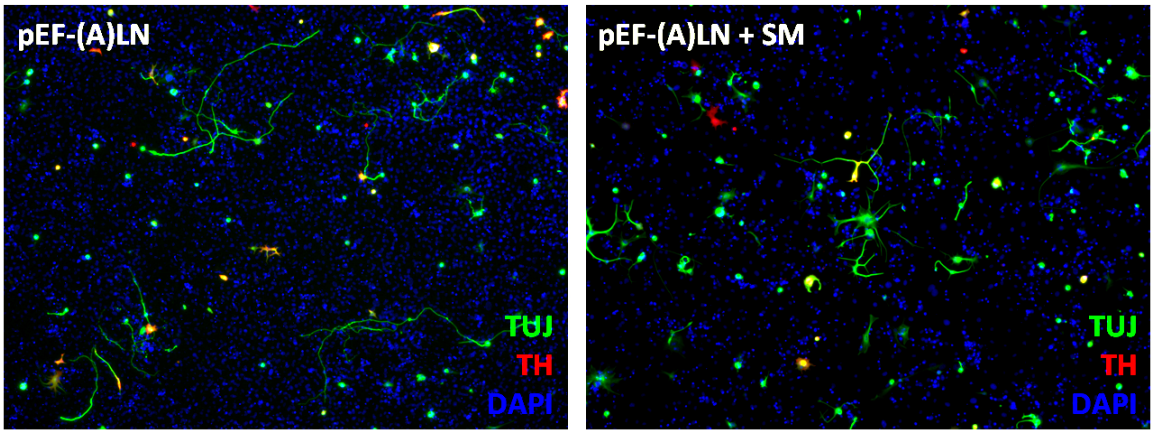

Figure 28. TH and TUJ1 expression in (A)LN-transfected PMEFs with and without exposure to small molecules inhibiting GSK-3β and SMAD signaling
The expression of $TUJ1^+$ and TH^+ in PMEF HLs transfected with a 1 µg dose of pEF-(A)LN plasmids by reprogramming in the presence of small molecules LDN-193189, CHIR-99021, and SB-431542 (SM) inhibiting GSK-3β and SMAD signaling for 10 days immediately following non-viral transfection.

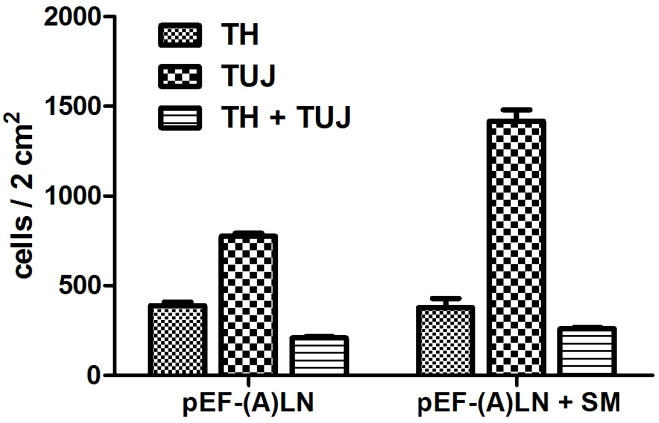

Figure 29. Quantification of $TUJ1^+$ yield in pEF-(A)LN transfected PMEFs with or without exposure to small molecular inhibitors of GSK-3β and SMAD signaling
$TUJ1^+$ and TH^+ cell yield in PMEF HLs transfected with a 1 µg dose of pEF-(A)LN plasmids with or without exposure to LDN-193189, CHIR-99021, and SB-431542 (SM). Cell counts were generated with large area image analysis, error bars represent SEM, n = 3.

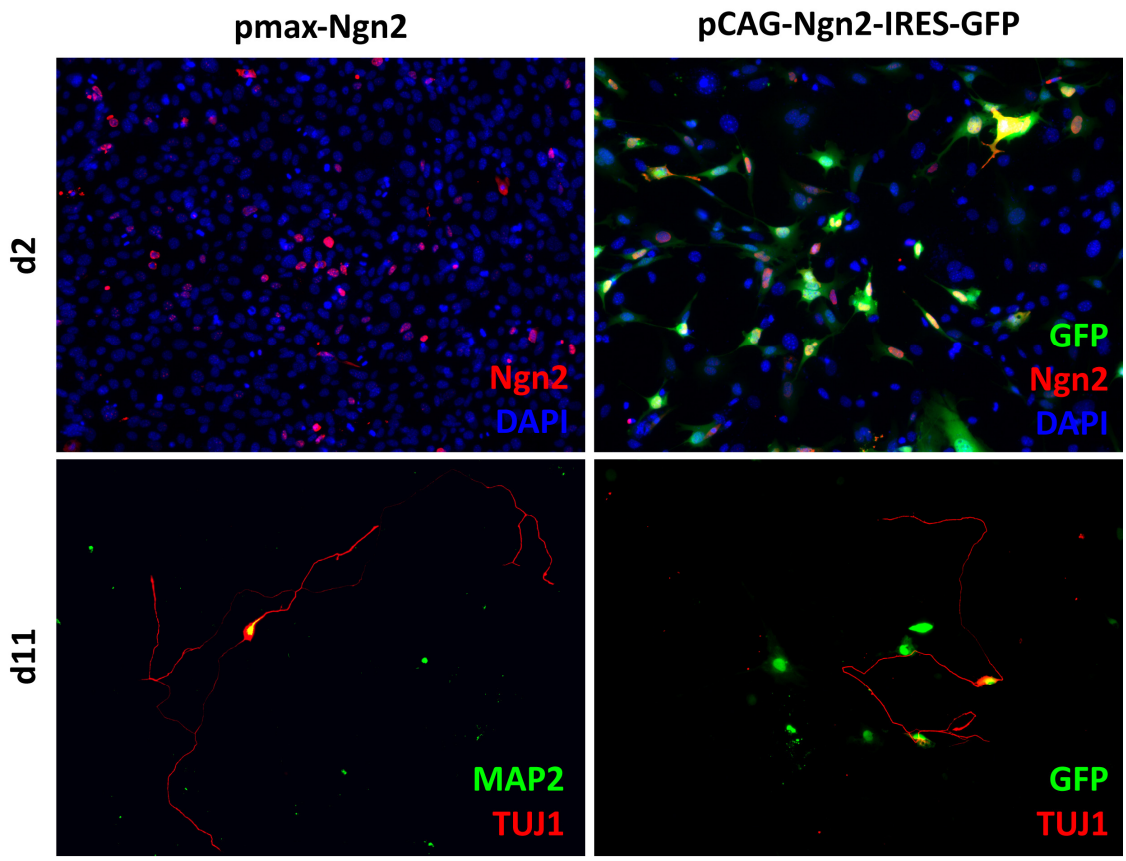

Figure 30. Transgene and neuronal marker expression in PMEFs transfected with Neurogenin 2
Expression of Neurogenin 2 (Ngn2) and GFP in PMEFs transfected with a plasmid expressing Ngn2 under control of the CMV (top left) or CAG promoter (top right) and stained two days following transfection. MAP2 and TUJ1 expression at day 11 of culture in iMN medium (bottom row).

Chapter 5: High-Throughput Screening of Microscale Pitted Substrate Topographies for Enhanced Non-viral Transfection Efficiency in Primary Human Fibroblasts

A portion of Chapter 5 appears in: High-throughput screening of microscale pitted substrate topographies for enhanced nonviral transfection efficiency in primary human fibroblasts. Adler AF, Speidel AT, Christoforou N, Kolind K, Foss M, Leong KW. Biomaterials. 2011 May;32(14):3611-9.

5.1 Summary

Optimization of non-viral gene delivery typically focuses on the design of particulate carriers that are endowed with desirable membrane targeting, internalization, and endosomal escape properties. Topographical control of cell transfectability, however, remains a largely unexplored parameter. Emerging literature has highlighted the influence of cell-topography interactions on many cell phenotypes, including protein expression and cytoskeletal behaviors implicated in endocytosis, the principal means of nanoparticulate gene carrier internalization. Using high-throughput screening of primary human dermal fibroblasts cultured on a combinatorial library of microscale topographies, we have demonstrated an improvement in non-viral lipoplex transfection efficiency for cells cultured on dense micropit patterns compared to smooth substrates, as verified with flow cytometry. A 25% increase in GFP transfection efficiency was observed, independent of proliferation, accompanied by SEM and confocal microscopy to help explain the phenomenon qualitatively. This improvement was also observed in a reverse

transfection format, as well as in cells transfected with cationic polyplexes. Further, the micropit-mediated enhancement of siRNA knockdown and low-dose plasmid delivery was evaluated. These findings encourage researchers to investigate substrate topography as a new design consideration for the optimization of non-viral transfection systems.

5.2 Rationale and Significance

We have previously presented a method whereby physical substrate topography could be used to increase the yield of NiNs produced from PMEFs with lentiviral delivery of the BAM factors, either by encouraging the reprogramming process itself, or by improving iN survival [383]. We expect a similar improvement may be possible with NiN reprogramming. Here, we use similar micropatterned substrates in an attempt to increase the efficiency of transfection – the first step of non-viral reprogramming, in adult human fibroblasts, the eventual cell source needed for transdifferentiation-based cell therapies. Beyond neuronal reprogramming, topographical cues influence many cell phenotypes including proliferation, spreading, cytoskeletal organization, and endocytosis [108-110]. We hypothesize therefore that substrates with nano- and micropatterned topographies may also influence the transfectability of interacting cells. We endeavor to understand the functional relationship between substrate topography, focal adhesion formation, cytoskeletal tension, endocytosis, and transfectability. We demonstrate topographical control of transfection in this chapter, first with bolus delivery of Lipofectamine 2000 (LF2k) complexes to primary normal dermal human fibroblasts (NHDFs) cultured on a combinatorial library of well-defined micropitted topographies.

Topography-mediated enhancement of non-viral gene transfer can find utility in transfected cell arrays, *ex vivo* cell therapy approaches, and in the intelligent design of gene-eluting scaffolds. Cell culture substrates for *in vitro* use are typically smooth by default, whereas implantable gene-eluting scaffolds often impart tunable porosity (and therefore topography) via electrospinning [385], polymer chemistry, or porogen inclusion [386] to promote cell penetration and enhance mass transfer of entrapped therapeutics.

The microenvironment at implant surfaces is critically important to efficient transfection; the inclusion of soluble factors, adsorption of ECM molecules, modulation of cell-cell interactions, and tuning of mechanical stress are all currently leveraged towards the improvement of transfection efficiency [387]. Scaffold surface topography is an additional design parameter that may be optimized to bolster *in situ* genetic manipulation of infiltrating cells.

The use of pitted topography may also facilitate maintenance of a detectable level of knockdown with a diminished dose of siRNA or pDNA in transfected cell arrays. Even modest improvements in transfected cell array efficiency and miniaturization can significantly reduce the cost and quantity of reagents and cells required to perform these assays, encouraging researchers to embrace the technology to accelerate discovery. Topographically-enhanced transfection is particularly attractive for *ex vivo* cell therapy systems (such as direct neuronal reprogramming), where increases in transfection efficiency will translate to improved therapeutic benefit in the form of more successfully-transdifferentiated cells.

5.3 Methods

Preparation of 13 x 13 pattern topographical library

Topographical libraries (arrays) were prepared as described in [388], using a standard lithography process. Briefly, a resist without hard bake was etched with Cl_2, HBr and NF_3 to produce sidewall angles of 85° with etch rate non-uniformity of 2–3% (max–min). After removal of the resist and cleaning, the surface was sputter- coated with 100 nm of tantalum at a rate of 50 nm min^{-1}, producing a 13 x 13 master library of post topographies. To create substrates for cell culture, Sylgard 184 polydimethylsiloxane (PDMS) (Dow Corning, Midland, MI) was mixed at a curing agent/base ratio of 1.05/10 w/w, degassed in a vacuum chamber, cast onto the metal master, and cured overnight at 47°C. PDMS arrays were peeled from the metal master and used for cell culture. These arrays were composed of 10 distinct pit morphologies (A-J) with: pit size (X) and edge-to-edge spacing (Y) iterated combinatorially through values of 1, 2, 4, and 6 μm (Figure 31), a uniform depth of 2.4 μm, and with 3×3 mm^2 patterned area for each. Pattern K did not support robust NHDF adhesion, and was excluded from all analyses. Smooth control regions were present in the middle of the array, and in the boundaries between patterns. Large area (2×2 cm^2) metal masters of the single patterns F(X,Y) = F(1,4) and F(4,1) were also produced following the same lithographical process to facilitate analysis by flow cytometry and luciferase assay. Pitted PDMS replicates of these "single-pattern" substrates, as well as smooth PDMS substrates produced from smooth silicon wafers, were stamped into 2 cm^2 circular disks, affixed to the bottom of 24-well tissue culture plates (Falcon, Heidelberg, Germany) with 50 μL PDMS, and cured overnight.

Cell culture

Adult normal human dermal fibroblasts (NHDFs) (Lonza, Basel, Switzerland) were cultured in high glucose Dulbecco's Modified Eagle's Medium (GIBCO 11960-044) (Invitrogen, Carlsbad, CA) supplemented with 20% Premium Select FBS (Atlanta Biologicals, Lawrenceville, GA), 25 μg mL^{-1} gentamicin (Invitrogen), and 1x GlutaMAX, non-essential amino acids, sodium pyruvate, and β-mercaptoethanol (Invitrogen), at 37°C and 5% CO_2. NHDFs were passaged a maximum of six times prior to experimentation. PDMS substrates were washed with 70% ethanol and air-dried twice, then washed with sterile deionized (DI) water and air-dried twice again. 25 μg mL^{-1} human plasma fibronectin (BD, Franklin Lakes, NJ) in DI water was adsorbed to PDMS substrates for 1 hour at room temperature (RT) before seeding NHDFs at a density of 7,500 cells cm^{-2} for quantitative analyses, and 3,750 cells cm^{-2} for visualization by SEM and confocal microscopy.

Plasmid DNA

pmaxGFP (Amaxa, Cologne, Germany) and VR1255 (Vical, San Diego, CA) plasmids expressing green fluorescent protein (GFP) and luciferase reporters under control of the CMV promoter were propagated in *Escherichia coli* DH5α and purified with the EndoFree Plasmid Giga Kit (Qiagen, Hilden, Germany). Plasmid DNA concentrations were quantified by measurement of absorbance at 260 nm with a NanoDrop ND-1000 Spectrophotometer (Thermo Scientific, Waltham, MA).

Transfection protocol

24 hours after seeding on topographical libraries or single-pattern substrates, NHDFs were transfected with a 2:1 ratio of Lipofectamine 2000 (Invitrogen) volume (μL) to pmaxGFP or VR1255 DNA mass (μg) at a dose of 1 μg plasmid cm^{-2} in serum- and antibiotic-free OptiMEM (Invitrogen), according to the manufacturer's protocol. Transfection medium was replaced with complete medium 4 hours after the onset of transfection. Mass ratio and DNA dose were selected based on a preliminary optimization of luciferase expression levels in NHDFs cultured on smooth substrates (results not shown).

Proliferation assay

Proliferation of cells on topographical libraries was quantified with the BrdU (5-bromo-2-deoxyuridine) incorporation assay, which labels the nuclei of cells that have undergone mitosis. Following removal of the transfection medium, cells were incubated for 20 hours with 15 μM BrdU (Invitrogen) in complete media. Cells were then washed briefly with Cellgro phosphate-buffered saline (PBS) containing Ca^{2+} and Mg^{2+} (Mediatech, Washington, DC), and fixed with 4% paraformaldehyde (PFA) (EMS, Hatfield, PA) at 4°C for 30 minutes. Genomic DNA was denatured with 2M HCl (Sigma-Aldrich, Saint Louis, MO) for 10 minutes at RT and 20 minutes at 37°C, immediately followed by a 5 minute wash with 0.1 M borate buffer (Thermo Scientific), and a 30 minute RT incubation in blocking buffer containing 0.2% Triton X-100, 3% w/v BSA, and 10% goat serum (Sigma-Aldrich). BrdU incorporation was detected by 12 hour incubation at 4°C with anti-BrdU-AF594 mAb (1:100 dilution, Invitrogen), and 15

minute RT DAPI counterstain (1:5000, Invitrogen). Between each staining step, cells were washed three times for five minutes at RT with PBS containing 0.2% Triton X-100 and 1% BSA.

Automated fluorescence imaging and analysis of topographical library

24 hours after the onset of transfection, NHDFs were washed briefly with PBS containing Ca^{2+} and Mg^{2+}, and fixed with 4% PFA (EMS) at 4°C for 30 minutes. Cell spreading was visualized with a 30 minute RT phalloidin-AF594 (1:200, Invitrogen) stain, and nuclei with 15 minute DAPI (1:5000, Invitrogen) stain at RT, with three five-minute PBS washes before and after each. Following staining, arrays were mounted face-down on Nunc single-well OmniTrays (Thermo Scientific) with Fluoro-Gel (EMS).

Transfection efficiency (GFP, green), cell spreading (phalloidin, red), and cell number (DAPI, blue) data were collected from three independent arrays, while proliferation data (BrdU, red; DAPI, blue) were collected from another three, using a Nikon Eclipse TE2000-U fluorescence inverted microscope fitted with appropriate filters and ProScanII robotic stage and autofocus controllers (Prior). Each array was scanned automatically using NIS-Elements software (Nikon, Tokyo, Japan), with autofocus performed in every field, and a constant exposure time for each channel within a given array, producing large high-resolution composite images for each fluorophore.

Adobe Photoshop CS3 (Adobe Systems, San Jose, CA) was used to overlay a black grid onto an image of an array, outlining the boundaries of each patterned region within that array (Figure 32). This masked image was then used to define regions of interest (ROIs) in ImageJ (NIH). First, a threshold was set to differentiate the background

in each region from the black mask. The "Analyze particles" command was then used to detect and store each patterned area as a unique ROI. The original (unmasked) images were then re-thresholded and analyzed with a custom ImageJ macro, which sequentially stepped through each ROI and utilized the "Analyze particles" command to count the number of $BrdU^+$ nuclei, $DAPI^+$ nuclei, and GFP^+ cells, or quantified the area fraction of each region stained with phalloidin. Particles that were significantly smaller than cells or nuclei were excluded from the relevant quantifications with the "Particle size" setting within "Analyze particles".

Flow cytometry of cells on single-patterned substrates

24 hours after the onset of transfection with pmaxGFP-containing complexes (48 hours after cell seeding), NHDFs cultured on F(1,4), F(4,1), and smooth PDMS substrates in quadruplicate were washed briefly with PBS containing Ca^{2+} and Mg^{2+}, released from substrate surfaces with 0.25% Trypsin-EDTA (Invitrogen), centrifuged, and resuspended in propidium iodide (PI) (1:1000, Invitrogen) to stain dead cells. Cells were then filtered through 40 μm nylon cell strainers (BD) and analyzed with a BD FACSCanto II flow cytometer. Single-positive PI^+ and GFP^+ cells were used to adjust spectral compensation. Non-transfected NHDFs cultured on smooth PDMS served as negative control, with 1% of these cells considered GFP^+.

Luciferase assay

24 hours after the onset of transfection with VR1255-containing complexes, NHDFs cultured on F(1,4), F(4,1), and smooth PDMS substrates in triplicate were

washed briefly with PBS containing Ca^{2+} and Mg^{2+}, and lysed with: 500 μL Glo Lysis Buffer (Promega, Fitchburd, WI), a -80°C freeze-thaw cycle, and scraping. Non-transfected cells served as negative control. 100 μL of each lysate was then combined with 100 μL Steady-Glo Luciferase Assay Substrate (Promega) in an opaque 96-well plate (Thermo Scientific). Luminescence signals were normalized to the total dsDNA content in each lysate measured by Quant-iT PicoGreen assay (Invitrogen), according to the manufacturer's protocol. A standard curve of cell number to PicoGreen signal was linear in the required dynamic range. Luminescence integrated over 7 seconds (luciferase) and fluorescence (PicoGreen) values were collected at RT following 5 minute incubations using a BMG Labtech FLUOStar Optima plate reader.

Confocal laser scanning microscopy

To visualize NHDFs protruding into pits, the cells were stably transduced with fluorescent cytoskeletal fusion proteins Lifeact-mRFPRuby (F-actin) [389] and α-actinin-GFP [390] (Addgene plasmid 11908) which were previously cloned into the lentiviral vector FUGW, and delivered with replication-deficient 2^{nd} generation lentiviruses (packaging vectors psPAX2 (Addgene plasmid 12260) and pMD2.G (Addgene plasmid 12259)). Lentiviral transduction was used in place of immunohistochemistry to minimize sample handling. The stably-transduced NHDFs were cultured on patterns F(1,4) and F(4,1) for 24 hours, washed with PBS containing Ca^{2+} and Mg^{2+}, fixed for 20 minutes in 4% PFA at 4°C, mounted face-down in Fluoro-Gel (EMS) on #1.5 coverslips (VWR, West Chester, PA), and visualized with the 63× oil immersion objective of a Zeiss LSM 510 inverted confocal microscope.

SEM

Cells cultured on single-pattern substrates were washed briefly with PBS containing Ca^{2+} and Mg^{2+}, and dehydrated with a graded ethanol series. The cell samples were then dried with a Pelco CPD2 critical point drier, and sputter coated with a 10 nm layer of gold using a Denton Desk IV Vacuum Sputter Unit. Single-pattern substrates without cells were cleaned with 70% ethanol, freeze-fractured with liquid nitrogen, and sputter-coated with 10 nm of gold. All samples were then examined with an FEI XL30 scanning electron microscope.

Real-time RT-PCR

Comparative C_T real-time RT-PCR was performed in 20 μL reactions using the QuantiTect SYBR Green RT-PCR Kit (QIAGEN) with 10 ng of starting mRNA isolated with RNeasy and QIAshredder kits (QIAGEN) from cells cultured on smooth or micropitted substrates. mRNA concentrations were quantified with a NanoDrop ND-1000 Spectrophotometer (Thermo Scientific). PCR proceeded for 40 cycles in an ABI 7300 Real-Time PCR System (Carlsbad, CA). Target mRNA levels were normalized to endogenous GAPDH references, and presented as a fold-change increase on topography relative to smooth substrates, collected 48 hours after seeding. Primers used (IDT, Coralville, Iowa) were as follows: CAV1 forward (TGG GCC CAG GAC GCG TTT TC), CAV1 reverse (GAT GTC CCT GCG CAG CTC CC), CLTC forward (CCA TAA CCC CCG ACA GCG CC), CLTC reverse (CCC ACC ACA CGA TTT TGC TGT GC), ITGB1 forward (TGT CTG TGC TGA GCA TAA AGA ATG TGT), ITGB1 reverse (GCG TGT CCC ATT TGG CAT TCA TTT), ITGAV forward (CTT AAA GGC AGA

TGG CAA GG), ITGAV reverse (AAA TGG TGA TGG GAG TGA GC), HSPG2 (perlecan) forward (CAC AGC AAG CCA AAT GCG CTG G), HSPG2 reverse (ACT CCA GCG TGT CTA CCA CAG CC), GAPDH forward (CGT ATT GGG CGC CTG GTC ACC), GAPDH reverse (TGG CAT GGA CTG TGG TCA TGA GT).

Statistics

Statistical treatment and graphing of data were performed using Prism (GraphPad Software, La Jolla, CA). For comparisons of multiple pairs, ANOVA with Tukey post-test was performed, with p-values < 0.05 considered significant. For post-normalization comparisons to smooth substrates, one-sample t-test was performed, with p-values < 0.05 considered significant. Error bars represent the standard deviation of three independent experiments.

5.4 Results

Transfection efficiency, morphology, and proliferation of fibroblasts on topographical libraries

High-throughput parallel screening of 160 pitted topographies revealed a significant 25% enhancement of GFP transfection efficiency for cells cultured on patterns with small interfeature spacings (Y = 1, 2 μm) compared to smooth regions (Figure 34a). This enhancement decreased and disappeared as the pits became spaced further apart; that is, as they more closely approximated a smooth surface. Regions with large pits (X) increased transfection efficiency more modestly, while patterns with small pits supported

identical transfection efficiencies as smooth regions. Pit morphologies A-J had no significant impact on transfection efficiency (results not shown). Topography-mediated enhancement of transfection was significant compared to smooth regions within each array, as well as between the averages of three normalized arrays presented in Figure 34. Examples of these differences are visible in representative widefield fluorescence images presented in Figure 33.

Cell spreading was quantified as the area occupied by actin on each pattern normalized by the number of cells in that region (Figure 34b). Spreading showed a trend opposite that observed for transfection efficiency; NHDFs on large, closely spaced pits were significantly less spread than those on small, distal pits, and on smooth regions. Regions with large, closely-spaced pits were also observed to encourage cell alignment. The strong influence of pitted topography on NHDF morphology is also evident in Figure 33.

Pit size had no effect on the number of cells in each patterned region after transfection. However, features with closely-spaced pits had slightly but significantly fewer cells than those with large interfeature distances (Figure 34c). No combination of pit size or spacing supported a significantly different number of cells than found on smooth regions. No significant differences in proliferation rates were observed for NHDFs cultured on topographical libraries (Figure 34).

Flow cytometry on single-patterned substrates

Refer to Figure 35 for freeze fracture cross sections of F(1,4) and F(4,1), the topographies selected for this experiment. Without normalization, an average of 55.0 ±

3.5% NHDFs cultured on smooth PDMS were GFP-positive following non-viral transfection, whereas an average of 68.3 ± 2.7% of cells cultured on pattern F(4,1) and 57.8 ± 3.6% on pattern F(1,4) were successfully transfected across all three experiments (95% confidence intervals). Normalization to the transfection efficiency of cells on smooth PDMS in each experiment gives a significant 24.4% average enhancement of transfection efficiency for cells cultured on F(4,1), compared to F(1,4) and smooth substrates (Figure 36a). Reverse transfection with Lipofectamine 2000 was also increased 35% (Figure 36b), and forward transfection with pCBA-ABOL/DNA nanoparticles was increased 15% by culture on F(4,1) compared to F(1,4) and smooth substrates (Figure 37).

Luciferase assay

Luciferase activity normalized to total cellular DNA was not significantly different for NHDFs transfected on smooth, F(1,4), or F(4,1) patterned topographies (data not shown). Cells transfected with luciferase were 4,000 times more luminescent than no-transfection negative controls.

SEM

Inspection of NHDFs cultured on pitted topography with SEM revealed NHDFs cultured on pattern F(4,1) were less spread, and more aligned than those on pattern F(1,4) (Figure 39). The cells were also observed to drastically deform the walls of the 4 μm pits, sometimes with a single thin process. For both patterns, cells could be seen extending

portions of their membrane over the edge of open pits. Freeze fracture of the patterns revealed a uniform pit depth of 2.4 μm (Figure 35).

Confocal microscopy

Cytoskeletal fusion proteins expressed in NHDFs were observed protruding 2.4 μm below the rest of the basal membrane plane from cells cultured on both 4 and 1 μm pits (Figure 40). Cells cultured on 4 μm pits appeared as "waves" in the XY and XZ planes, because both the apical and basal membrane descended into pits. This is in contrast to cells on 1 μm pits, which only extended their basal membrane to pit bottoms. Further, in many of the cells cultured on 1 μm pits, there were no protrusions visible.

siRNA knockdown in cells transfected on micropits

Positive controls (GFP DNA only, on TCPS) were 20% and 7% GFP^+ for adsorbed 500 μg cm^{-2} and bolus 75 ng cm^{-2} doses, respectively (not shown). 4 μm pits increased the fraction of GFP^+ cells co-transfected with bolus lipoplexes containing GFP pDNA and non-targeted negative control siRNA by 44% (Figure 38, solid bars). α-GFP siRNA was efficient at knocking down GFP expression on all substrates (Figure 38, hatched).

qPCR comparison of cells on micropits versus smooth topography

A preliminary screen of transcript expression of genes implicated in endocytosis reveals cells cultured on micropitted topography upregulate integrin α_v and possibly β_1

(Figure 41), components of the vitronectin receptor (vitronectin is a principal ECM component in serum) $\alpha_v\beta_3$, and fibronectin receptor $\alpha_5\beta_1$ respectively.

5.5 Discussion

In this study, our goal was to test the hypothesis that substrate topographies, which have been shown to affect many cell phenotypes, also have an influence on transfectability. High-throughput microscopy of primary NHDFs cultured on topographical arrays revealed that cells on large, closely spaced pits were transfected a significant 25% more efficiently than those on smooth surfaces, while small, distally-spaced pits did not significantly alter GFP expression (Figure 34a). Flow cytometric analysis of NHDFs cultured on single patterns verified the prediction made by screening (Figure 36). When taken with the increased GFP expression, total siRNA-mediated knockdown was greater on 4 μm pits than on 1 μm pits or smooth substrates (Figure 38). These effects are applicable to scaffold-mediated gene delivery, which can be thought of as a mixture of bolus- and substrate-mediated delivery, and to reverse-transfected cell arrays. The bolus LF2k delivery used previously (Figure 36a) was an optimized dose (1 μg); it is interesting to note that transfections with a lower (suboptimal) dose of plasmid (150 ng) are enhanced to a greater extent by micropitted topography (Figure 38). pCBA-ABOL is an extremely efficient gene carrier - as such it may not benefit as greatly from topographical enhancements if the transfection is already nearly "saturated" on smooth substrates (Figure 37). To our knowledge, these results represent the first demonstration of a topographic control of transfection.

Additional experiments and measurements were performed in an effort to understand why cells cultured on patterned topography were transfected more efficiently. NHDFs that were least-spread were most efficiently transfected (Figure 33, Figure 34a,b). Visible deformation of pattern F(4,1) but not of pattern F(1,4) implies cells may experience a different effective surface stiffness and intracellular tension on each topography (Figure 39).

Cytoskeletal tension and cell spreading have been repeatedly demonstrated to modulate genome-wide changes in protein expression levels and patterns, including many involved in endocytosis, including: clathrin, epsin 2, caveolin-1, REP-2, and integrins [133-134, 137, 391]. Actin contraction, a process required for formation and strengthening of focal adhesions on integrin ligands during spreading, has been suggested to drive the internalization of cholesterol-rich lipid rafts containing cationic complexes bound to proteoglycans [163].

Emerging research suggests cell spreading may have a direct impact on endocytic processes. The formation, maturation, contraction, and disassembly of focal adhesions allow cells to spread over and move across their substrates. The speed of this cycle is controllable with substrate topography, as mediated through the heterogeneous spatial availability of adsorbed integrin ligands [89, 148]. A loss of integrin-mediated adhesion results in dramatic internalization of caveolae [152]. Disassembly of focal adhesions is a clathrin-dependent endocytic process; clathrin colocalizes with focal adhesions as nucleated by actin fibers, and knockdown of clathrin activity results in diminished integrin internalization [90]. These studies demonstrate strong links between integrin function and caveolae- and clathrin-mediated trafficking. These links could manifest as a

coincident uptake of complexes or as a downregulation of particle uptake through competition for the endocytic machinery by altered integrin presentation and internalization on patterned topographies. As such, enhanced transfection efficiency of NHDFs cultured on patterned topography may be a downstream consequence of altered endocytic uptake and/or intracellular trafficking.

Substrate stiffness has been previously demonstrated to control transfectability, with stiffer substrates supporting more efficient transfection, putatively a consequence of enhanced proliferation on stiff surfaces [392]. Similarly, dense presentation of integrin ligands has also been shown to improve gene transfer through increased proliferation [393]. In our study however, neither pit spacing nor size had a significant impact on cell density or proliferation compared to smooth substrates (Figure 34c,d), indicating differences in cell division are not responsible for the enhanced transfection efficiency. Regions with large pit spacing had a greater number of cells than those with small spacing after transfection (Figure 34c); when taken with the observation that proliferation is unchanged this suggests either decreased initial attachment, or survival, during transfection on more discontinuous surfaces.

Luciferase expression levels were not detectably altered with transfection on the patterns that increased the percentage of GFP-expressing cells. This result may reflect the difference in how the reporter signals are weighted in each case - weakly GFP^+ cells are counted with equal importance as those that saturate the photodetectors when quantified with thresholded fluorescence microscopy or flow cytometry. In contrast, luciferase assays weight highly-expressing cells more heavily than weakly-positive cells. Therefore, patterned topography may be exerting its influence on cells that express only a few copies

of reporter - that is, on cells that are very near to the positive/negative threshold. Alternatively, luciferase expression could be more toxic than GFP in NHDFs, leading to greater cell death in luciferase-positive cells. Increased transfection efficiency without an associated increase in transfection level is desirable at times, particularly for transfected cell arrays, where over-expression can be a significant problem if it doesn't reflect a natural phenotype *in vivo* [394].

Detailed microscopic examination of cells cultured on patterned topography reveals more possibilities to explain the increase in transfection efficiency. SEM images demonstrate NHDFs stretch their membrane over open pits as they move across their substrates, thereby exposing their basal surface to complex-containing medium (Figure 40). It is reasonable to expect this process to occur more often, and for a larger proportion of the cell membrane, on surfaces with large, dense pits. Including sidewall surfaces, dense pits have an increased effective surface area than sparse patterns or smooth surfaces; pattern F(4,1) has ~ 2.4× and 1.8× greater effective surface area than smooth and F(1,4) substrates, respectively. This potentially increases the amount of fibronectin that is able to adsorb to pitted surfaces, and the amount of non-viral vector that can adsorb during transfection. Substrate-mediated gene delivery has at times been demonstrated to be more effective than bolus delivery [68-70]; if cells can interact with this increased substrate surface area, they may have access to a larger amount of complexes, increasing their probability of being successfully transfected. Confocal microscopy revealed that NHDFs were indeed capable of reaching the bottom of both 1 and 4 μm pits, though the cells were more able to do so for 4 μm pits, which may have contributed to their enhanced transfection.

qPCR also demonstrated that integrin α_v expression is upregulated in NHDFs on pitted topographies (Figure 41). This may be a compensatory mechanism for diminished attachment, or a response to increased availability of the ligands through increased effective surface area. Perlecan, a matrix heparan sulfate proteoglycan (HSPG), is expressed by dermal fibroblasts [395], and can bind to integrin β_3 and β_1 through an RGD domain in its core protein [396]. HSPGs are polyanionic, and serve as nonspecific receptors for cationic gene carriers [397]. Integrin $\alpha_v\beta_5$ functions in endocytosis and degradation of matrix-bound vitronectin by human skin fibroblasts [398], a process that is inhibited by heparin (a soluble anionic HSPG competitor), suggesting integrin receptors and HSPGs are involved in endocytosis of vitronectin [399]. Syndecan-1 (a transmembrane HSPG) expression increases transfection efficiency [400], co-precipitates with integrin β_5 [401], and acts as a co-receptor with $\alpha_v\beta_3$ to initiate cell spreading [402]. Further, engagement of integrin subunits through adsorbed antibodies against the dominant integrins expressed by a cell subtype increase transfection efficiency of adsorbed Lipofectamine 2000 [83]. Non-viral gene therapy approaches have also targeted the α_v family in biomimetic approaches mimicking the natural hijacking of these integrins by AAV in receptor-mediated endocytosis to infect cells [403]. Taken together, these links suggest altered integrin expression on microtopography may be affecting the endocytosis of co-receptor HSPGs and any associated cationic nanoparticulate cargo.

Cell culture substrates for *in vitro* use are typically smooth by default, whereas implantable gene-eluting scaffolds often impart tunable porosity (and therefore topography) via electrospinning [385], polymer chemistry, or porogen inclusion [386] to promote cell penetration and enhance mass transfer of entrapped therapeutics. The

microenvironment at implant surfaces is critically important to efficient transfection; the inclusion of soluble factors, adsorption of ECM molecules, maintenance of cell-cell interactions, and tuning of mechanical stress are all currently leveraged towards the improvement of transfection efficiency [387]. Scaffold surface topography is an additional design parameter that may be optimized to bolster *in situ* genetic manipulation of infiltrating cells.

Ultimately, our goal is to understand the functional relationship between substrate topography, focal adhesion formation, cytoskeletal tension, endocytosis, and transfectability. We elected to take the first step with demonstration of the most downstream effect, transfectability, using bolus delivery of ubiquitous Lipofectamine 2000 complexes to primary human fibroblasts cultured on a combinatorial library of well-defined pitted topographies. Transfection is a multi-step process with many known and unknown modulators, including some that are evidently tunable with substrate topography. Discovery of topographies that increase transfection efficiency in primary human fibroblasts is another example of the power of high-throughput screening, complimenting the previous use of this technique to discover substrates with desirable stem and progenitor cell maintenance [114] or differentiation [388] effects and cytoskeletal changes in primary fibroblasts [404].

5.6 Conclusion and future perspectives

We have performed a systematic screen of non-viral transfection efficiency on microtopographic substrates, and discovered a significant enhancement of transfection

efficiencies for primary human fibroblasts cultured on densely-pitted surfaces compared to smooth. This improvement could not be attributed to an altered proliferation rate for cells on pitted substrates, and represents the first demonstration of a topographic influence on non-viral gene transfer. Topographic modulation of transfection is a new and therefore under-appreciated factor to consider when creating gene delivery systems.

Understanding the mechanism responsible for this enhancement could allow us to determine the generality of the effect. Substrate topography may enhance transfection efficiency by encouraging the endocytic uptake of nanoparticulate carriers. This effect could be quantified by transfection of NHDFs with rhodamine-labeled GFP-encoding DNA. And, to begin to determine the relative contribution of endocytosis, protein synthesis/degradation, and exocytic processes in topography-mediated transfection, the experiments could be repeated by first transfecting cells on topography, then trypsinizing and replating onto smooth substrates, and analyzing with flow cytometry a day later.

Our main future interest in topography-mediated transfection is to apply the technology to a therapeutic system, such as NiN generation. Combination of topography-mediated transfection with topography-mediated enhancement of the iN reprogramming process [383] could lead to a synergistic improvement in NiN yields. Heirarchical topographies, which include both nano- and microtopographical features [331], could simultaneously take advantage of the neuro-inducing effects nanotopography has on progenitor and stem cells [330], as well as of the improvements in transfectability and iN survival and/or induction efficiency on microtopography [383]. Synthesizing the results of Chapters 3-5, we can conclude that physical and chemical microenvironmental factors

each have an important place in the design of effective non-viral direct neuronal reprogramming strategies.

5.7 Figures

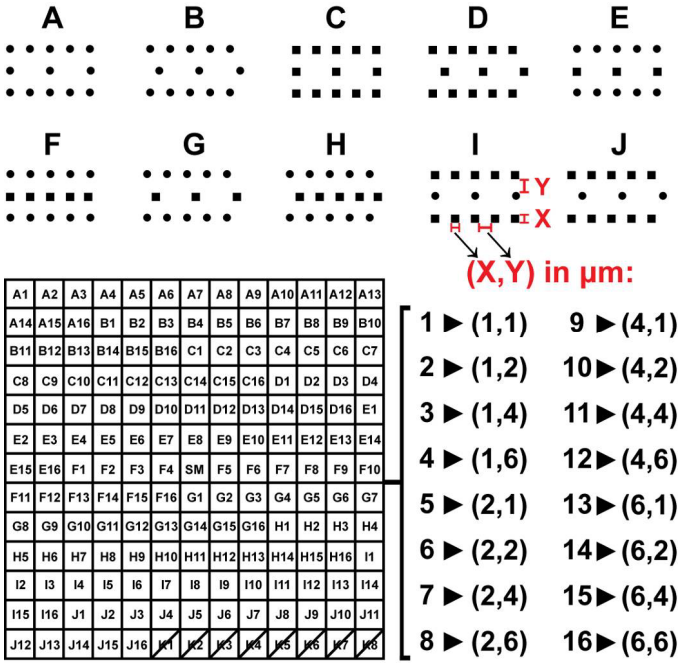

Figure 31. Topographical library details
10 pit morphologies (A–J) were replicated with 16 different combinations of size (X, 1–6 µm) and spacing (Y, 1–6 µm), giving 160 unique patterned PDMS substrates for cell growth, each with a uniform pit depth of 2.4 µm. Smooth regions were present in the center of the array (SM), and in the regions between patterns. Pattern K was excluded due to poor cell attachment.

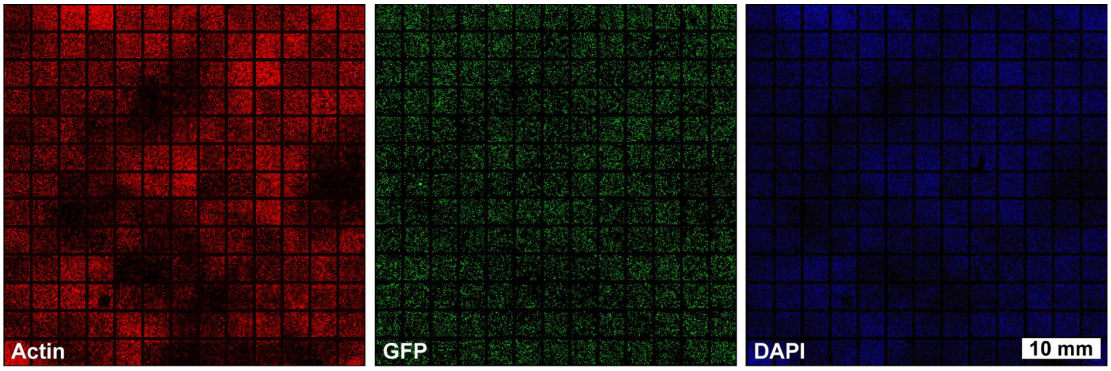

Figure 32. Fluorescence micrographs of NHDFs transfected on topographical libraries
Masked large-area scans of transfected topographical arrays, with visible GFP transgenic protein (green), actin (phalloidin stain, red), and nuclei (DAPI, blue).

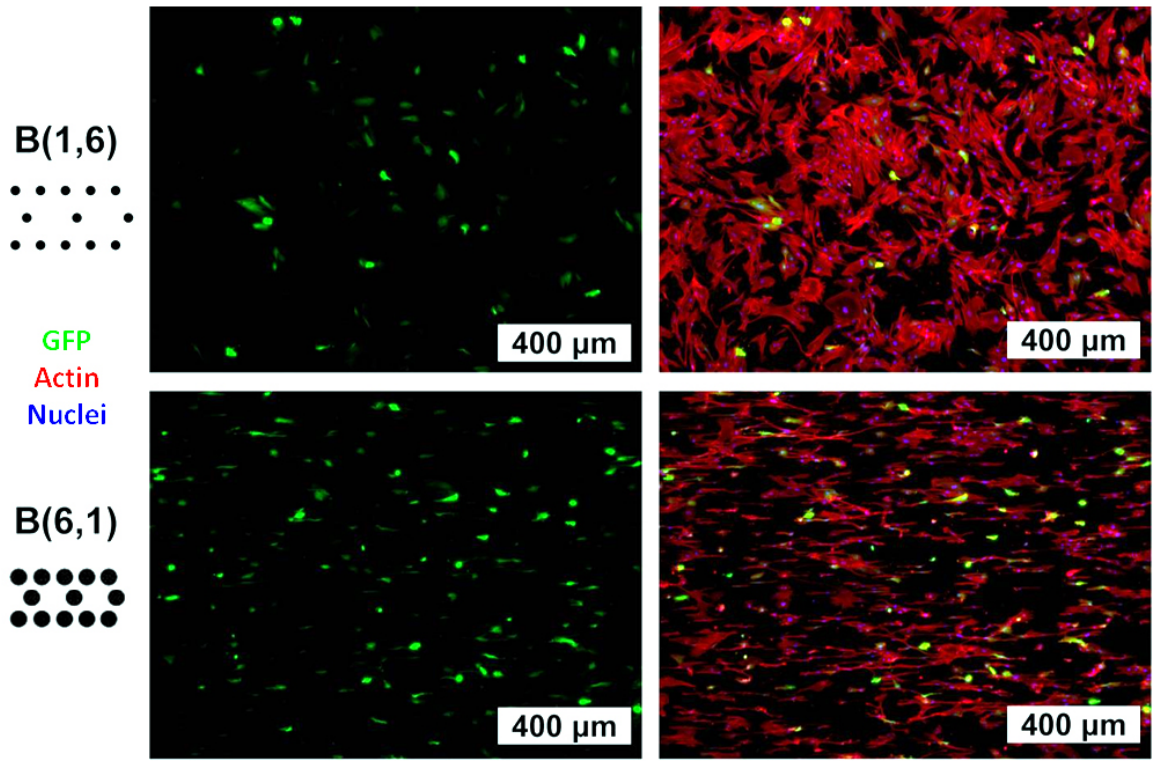

Figure 33. Fluorescence micrographs of NHDFs transfected on topographical libraries (detail)
Patterns with small interfeature spacing (B(6,1)) supported higher transfection efficiency, greater alignment, and less spreading than those with large interfeature spacing (B(1,6)).

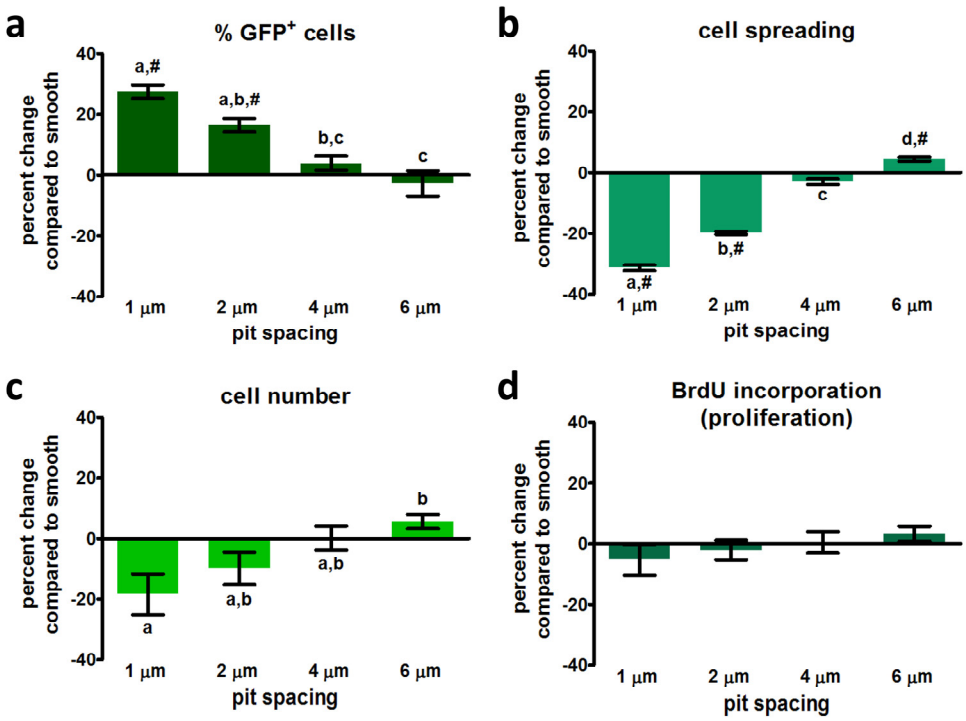

Figure 34. Transfection, spreading, attachment, and proliferation of NHDFs on topographical libraries

(a) Transfection efficiency, (b) spreading, (c) cell number, and (d) proliferation of NHDFs cultured on topographical PDMS libraries as normalized to values taken from smooth regions in each array. Data are grouped across pit morphologies A-J by pit spacing (Y). Error bars represent the SEM of three independent experiments. Letters above bars (w-z) denote significance between columns by Tukey post-hoc testing of one-way ANOVA ($P < 0.05$) and symbols (#) denote significance compared to smooth regions by single sample t-test ($P < 0.05$). (a) Small interfeature spacing (Y = 1 µm) produced a 25% increase in transfection efficiency compared to smooth regions. (b) Pits spaced far apart (large Y) supported the highest levels of spreading. (c) Patterns with large interfeature spacing (Y = 6 µm) contained 25% more cells than those with small interfeature spacing (Y = 1 µm). (d) No significant dependence of proliferation on feature spacing was detected, suggesting increased cell number on features with large interfeature spacing may reflect increased initial attachment or survival.

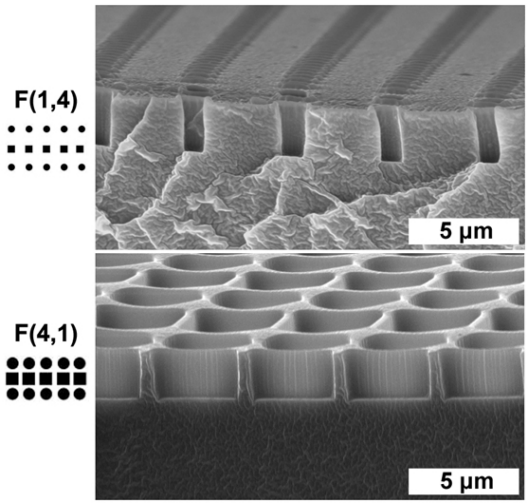

Figure 35. Freeze fracture SEM of patterns used for flow cytometry experiments

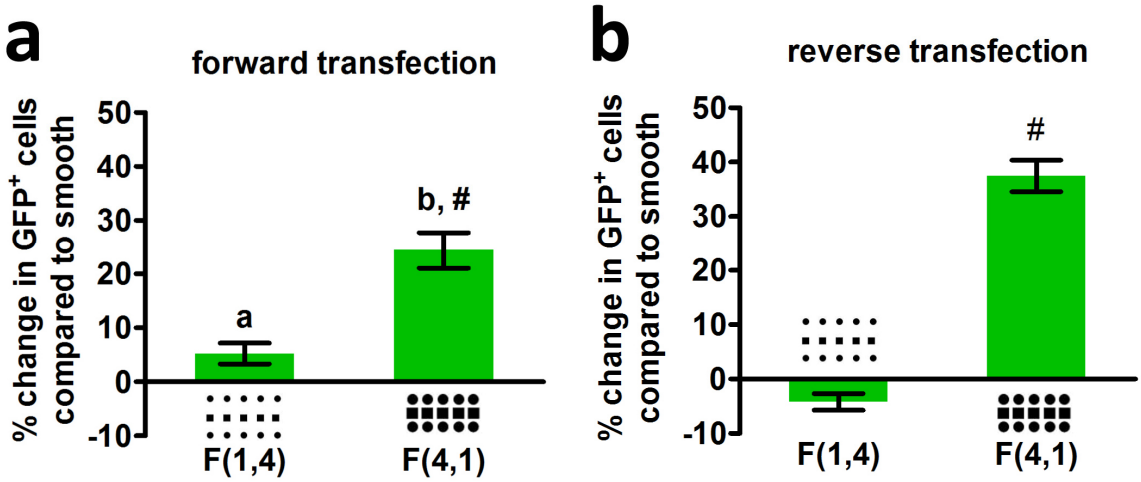

Figure 36. Flow cytometric quantification of transfection on micropits
(a) Flow cytometry corroborates the results presented in FIGURE XXX; F(4,1), a pattern with small interfeature spacing (1 μm), supported 25% higher transfection efficiency than smooth PDMS and F(1,4), a substrate with large interfeature spacing (4 μm). (b) Reverse transfection is enhanced to an even greater extent on dense micropits. Error bars represent SEM (n = 3). Letters (a,b) not shared between columns denote significant comparisons between pitted substrates by Tukey post-hoc tests ($P < 0.05$) of one-way ANOVA, and symbols (#) denote significant differences compared to smooth substrates by single sample t-test ($P < 0.05$).

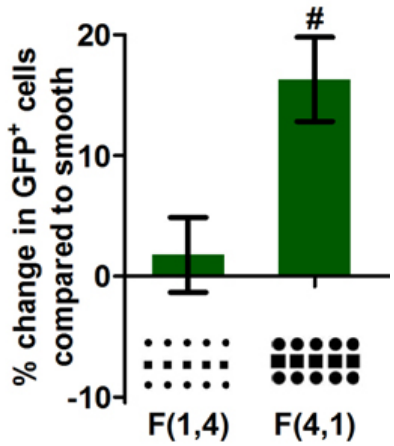

Figure 37. Microtopographical increase of pCBA-ABOL polyplex transfection efficiency in PMEFs
Dense micropits (F(4,1)) significantly increase the efficiency of pCBA-ABOL transfection in PMEFs. Error bars represent SEM (n = 3). Symbols (#) denote significant differences compared to smooth substrates by single sample t-test ($P < 0.05$).

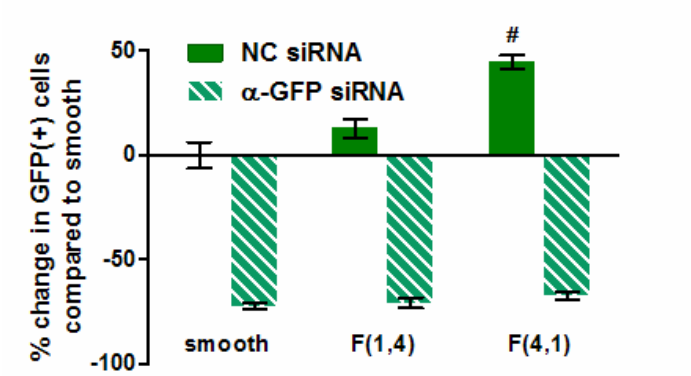

Figure 38. Microtopographical increases in siRNA knockdown
The transfection efficiency of low doses of DNA (solid bars), and siRNA knockdown (difference between solid and hatched bars) are enhanced by patterned topographies with small interfeature spacing ((F(4,1)) compared to smooth substrates. Error bars represent SEM (n = 3). Symbols (#) represent significant comparisons between substrates by Tukey post-hoc testing following one-way ANOVA ($P < 0.05$).

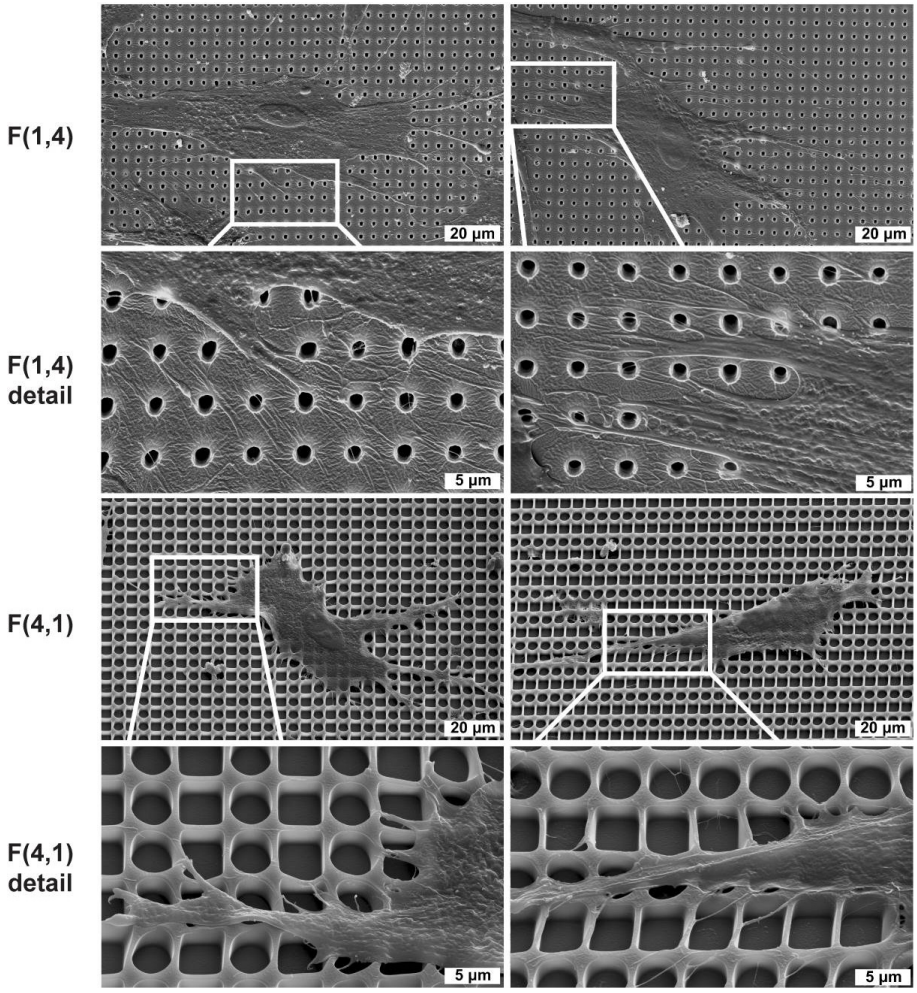

Figure 39. SEM of NHDFs interacting with pitted topography
As imaged with 30° tilt. NHDFs cultured on F(1,4) are more spread than those cultured on F(4,1). Regions of the cell membranes were stretched over open pits on both patterns. Cells cultured on F(4,1) dramatically deform pit sidewalls.

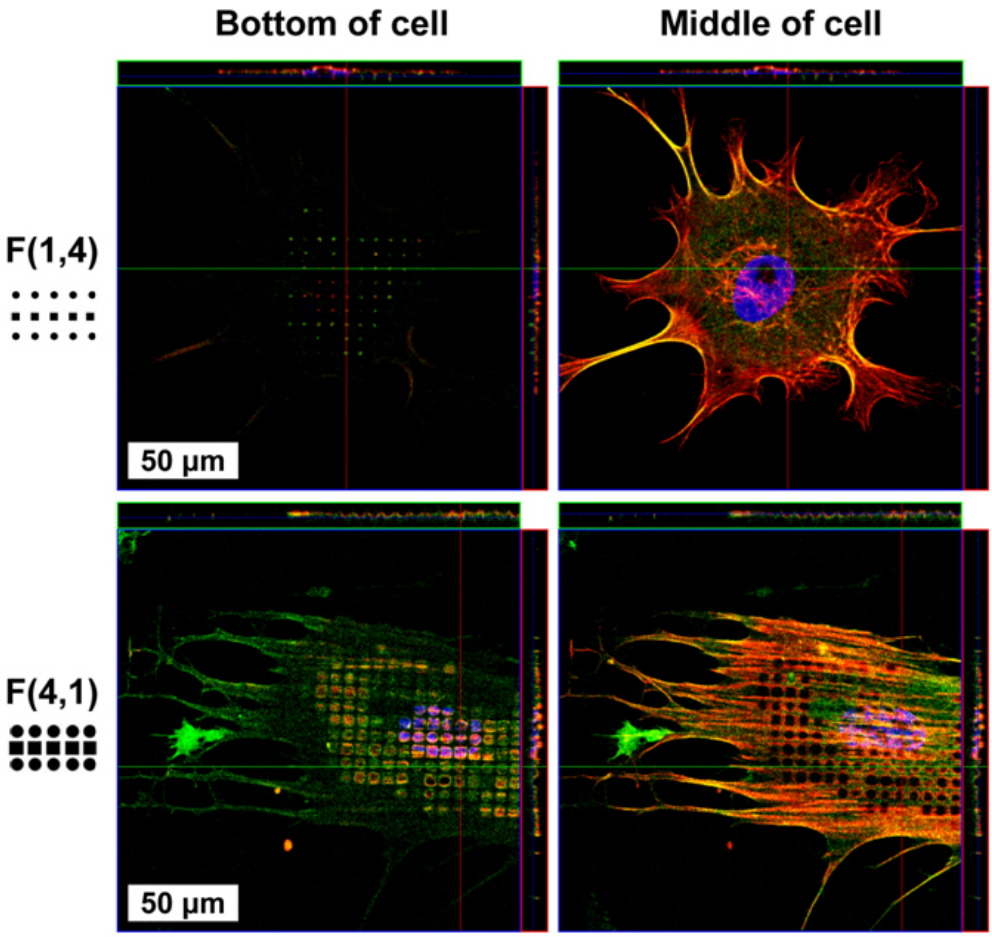

Figure 40. Confocal microscopy of NHDFs interacting with pitted topography
NHDFs explore the bottom of 1 and 4 µm diameter pits, with visible α-actinin (green), actin filaments (red), and nuclei (blue). The appearance of "holes" in the cell membrane of cells cultured on pattern F(4,1) is a consequence of the apical and basal cell surfaces bending below the focal plane, whereas cells on F(1,4) only reached the bottom of pits with their basal membrane.

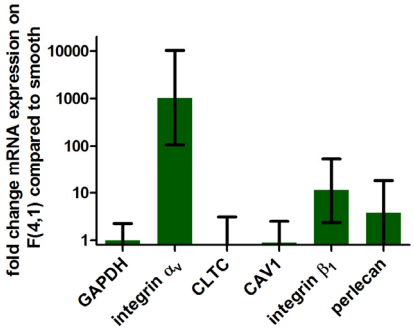

Figure 41. mRNA expression of NHDFs on micropits compared to those on smooth substrates
Preliminary RT-qPCR quantification of mRNA transcript from cells cultured on F(4,1) compared to smooth patterns, normalized to GAPDH. Integrin α_V expression was elevated on micropitted topographies. No significant changes were detected for the endocytic genes clathrin heavy chain (CLTC), caveolin 1 (CAV1), or perlecan. Error bars represent the range of transcript produced by the standard deviation about a mean C_T value (n = 3).

Chapter 6: Cytoplasmic Sequestration of Olig2 is a Significant Barrier to the Direct Reprogramming of Fibroblasts to Oligodendrocyte Progenitor Cells

6.1 Summary

Demyelinating diseases are a devastating burden on human health and healthcare, with currently no curative therapeutic options. Autologous replacement of oligodendrocyte progenitor cells (OPCs) derived via direct reprogramming has the potential to drastically improve therapeutic outlook [268-269]. Ideally, integrative transcription factor delivery methods can be replaced with safer non-viral methods. As such, we delivered combinations of transcription factors expressed during OPC development: Sox10, Olig2, and ZFP536 (SOZ factors) to fibroblasts via transfection with pCBA-ABOL, or dox-inducible lentiviruses (as a positive control), in an effort to produce iOPCs capable of proliferating in response to PDGF, and of differentiating to oligodendrocytes. Cells expressing the SOZ factors were cultured for a period of one to three weeks in OPC proliferation media, and then stained for the proliferative OPC markers S100β and O4, or differentiated with T3 for one week to oligodendrocyte-like cells and stained for myelin proteins MBP and MOG. During this process we discovered that the cytoplasmic sequestration of wildtype Olig2 in PMEFs is a critical barrier to the induction of an OPC phenotype in fibroblasts. We appended the SV40 nuclear localization sequence (NLS) to the N-terminus of Olig2, which redistributed the transcription factor from the cytoplasm to the nucleus. When delivered in the SOZ factor cocktail virally and non-virally, Olig2-NLS produced a many-fold improvement in the

number of cells expressing iOPC markers over wildtype Olig2, and induced a vast improvement in the number of myelin-producing iOLs generated by viral transduction. Our discovery and surmounting of this previously-unknown barrier to reprogramming is expected to make derivation of human iOPCs more achievable, and to serve as a template approach for other forms of reprogramming that may suffer from cytoplasmic sequestration of a lineage-instructive transcription factor.

6.2 Rationale and Significance

Much like Alzheimer's and Parkinson's diseases, and ALS (against which we are working to develop non-viral strategies to produce autologous replacements for dying cortical, dopaminergic, and motor neurons respectively), MS is a crippling and deadly neurodegenerative disease with currently no curative treatment options for the most common progressive forms [176], though immunomodulation can modestly slow the deterioration in relapsing-remitting cases [177-179]. MS is caused by the autoimmune attack of myelin sheath-producing oligodendrocytes (OLs), leading to deterioration of the insulating myelin layer on axons throughout the CNS and eventual neuron death.

Two reports have recently appeared which describe the generation of induced oligodendroglial progenitor cells (iOPCs) with lentiviral delivery of OPC lineage specifying factors [268-269]. With mitogenic stimulation these iOPCs can be maintained and expanded in a proliferative phenotype for many passages, and can then be differentiated with T3 into oligodendrocytes capable of compactly myelinating axons of dorsal root ganglia collected from shiverer mice (which are incapable of producing

normal myelin sheaths due to deletion of a portion of the MBP gene). Encouragingly, OPCs differentiated from human iPSCs have been shown to migrate through and myelinate the brains of mice with congenital hypomyelination (shiverer) with a single intracranial injection, without tumor formation or heterotropic nonglial differentiation [220], thereby firmly establishing cell replacement as a promising treatment option for MS. Compared to iPSC-derived OPCs, directly-reprogrammed iOPCs would have the advantage of being syngenic with the patient, and not derived from potentially teratogenic pluripotent intermediates [405].

The generation of autologous OPCs from adult human sources is particularly attractive for human cell therapy, because the proliferative pre-differentiation phase of iOPCs could be exploited to increase the amount of cells that can be produced from however many cells are initially reprogrammed. This is particularly true for non-viral iOPC generation; regardless of the initial reprogramming efficiency, the proliferative phase could be used to generate a sufficiently large source of safer autologous OLs. Compared to iPSCs, autologous OPCs are expected to be less tumorigenic due to their exclusive commitment to the glial lineage and reliance on PDGF for continued proliferation. Furthermore, OPC generation from iPSCs currently takes 110-150 days (in addition to the time required to generate the iPSCs) [220] – a daunting prospect for clinical scale-up. iOPCs, on the other hand, require less than a month from induction to differentiation into oligodendrocytes [268-269].

Non-viral induction of myelin genes has been previously attempted, unfortunately with no activation of endogenous myelin gene expression [406]. However, the researchers: attempted to simultaneously deliver seven transcription factors non-virally,

only allowed the cells to reprogram for seven days before analysis, and included Nkx2.2, which is dispensable for and may unpredictably affect iOPC generation [268] via complex suppression/activation of Olig2 [407-408], and Ascl1, which may have strongly arrested cell division in this context [409] as it is now known Ascl1 levels need to oscillate to maintain the proliferative phenotype observed in $Ascl1^{+}$ NPCs [410]. Armed with the knowledge that iOPCs may require at least 14 days to reprogram in the lentiviral system, as well as with a smaller list of essential transcription factors (Sox10, Olig2, and ZFP536) we also ambitiously attempted non-viral iOPC production in the PMEFs that we are able to transfect very efficiently with pCBA-ABOL [281]. As we discussed in Chapter 4, we were aware that each direct reprogramming cocktail may face unique barriers that may hinder complete conversion to the desired fate; this awareness sensitized us to recognize a previously undescribed but evidently critically important barrier to both viral and non-viral iOPC generation: cell type-dependent nuclear import of Olig2 – one of the master regulators of iOPC generation that is shared between the two currently known iOPC cocktails.

6.3 Methods

Plasmids, molecular cloning, and plasmid purification.

The reporter vectors pmax-GFP (3486 bp, Amaxa, Cologne, Germany) and VR1255C (6413 bp, Vical, San Diego, CA), which respectively express GFP and luciferase under control of the CMV promoter, were used as a positive transfection control (GFP), and a no-reprogramming negative control (pLuc). pORF-Sox10 (4642 bp),

pORF-Olig2 (4213 bp), and pORF-ZFP536 (7150 bp), which carry mouse ORFs under control of the EF1α promoter, were generated by digestion of Tet-O-FUW-Sox10, Tet-O-FUW-Olig2, and Tet-O-FUW-ZFP536 (gifts from Marius Wernig, Stanford University) with EcoRI (NEB), and ligation into pORF-mcs (Invivogen, San Diego, CA) digested with EcoRI.

pORF-Olig2-NLS (4237 bp) was generated by PCR-amplification of Olig2 from TetO-FUW-Olig2, with primers that added flanking 5' and 3' EcoRI restriction enzyme sites, as well as a 5' Kozak sequence followed by an ATG start codon and SV40 NLS sequence (NLS sequence: 5'-CCC AAG AAG AAG AGG AAG GTG GGC-3'). The forward PCR primer sequence was 5'-CAG CAG GAA TTC GCC ACC ATG CCC AAG AAG AAG AGG AAG GTG GGC GAC TCG GAC GCC AGC-3' and the reverse PCR primer sequence was 5'-CAG CAG GAA TTC TCA CTT GGC GTC GGA G-3'. Tet-O-FUW-Olig2-NLS was produced by digestion of pORF-Olig2-NLS with EcoRI, and insertion into Tet-O-FUW-Ascl1 digested with EcoRI. A summary of the non-viral SOZ and SOZ-NLS plasmid cocktails is presented in Figure 42.

Plasmids were propagated in *Escherichia coli* DH5α (Invitrogen, Carlsbad, CA) and purified with EndoFree Plasmid Mega and Maxi kits (QIAGEN). Plasmid DNA concentrations were quantified by measurement of absorbance at 260 nm with a NanoDrop ND-1000 Spectrophotometer (Thermo Scientific, Waltham, MA).

Poly(CBA-ABOL) synthesis and polyplex formation

Poly(CBA-ABOL) was synthesized by Michael polyaddition of 3.67 g N,N-cystaminebisacrylamide (CBA) (Polysciences, Warrington, PA) and 1.26 g 4-amino-1-

butanol (ABOL) (Sigma-Aldrich, Saint Louis, MO) as described by Lin et al.[353] The reaction product was purified by dialysis (3.5 kDa cutoff) in acidic deionized water (pH 4) and then lyophilized. The polymer was collected in its HCl-salt form (1.63 g, 33% yield), and its structure validated by ^{1}H NMR (in D_2O) on a Varian Mercury 300 MHz NMR Spectrometer. p(CBA-ABOL)/DNA nanocomplexes (polyplexes) were synthesized at a polymer:DNA mass ratio of 45:1, which was selected based on a preliminary optimization of GFP expression in primary mouse embryonic fibroblasts (PMEFs) (results not shown). Polyplexes were prepared by adding a HEPES buffer solution (20 mM HEPES, 5 wt % glucose, pH 7.4) of p(CBA-ABOL) (900 μg/mL) to a HEPES buffer solution (20 mM HEPES, 5 wt % glucose, pH 7.4) of plasmid DNA (75 μg/mL), followed immediately by vortexing for 20 seconds. Reaction sizes ranged from 5 to 15 μg of plasmid DNA.

Cell culture and transfection or transduction

80,000 PMEF-HLs for non-viral (Millipore, Billerica, MA), or 40,000 PMEF-HLs for viral were seeded per well in 24-well TCPS plates (BD, Franklin Lakes, NJ) at 37 °C and 5% CO_2 in complete PMEF medium: Dulbecco's Modified Eagle's Medium with 4.5 g/L glucose (GIBCO 11960-044) (Invitrogen), 10% Premium Select FBS (Atlanta Biologicals), 25 μg mL^{-1} gentamicin (Invitrogen), and 1x GlutaMAX, non-essential amino acids, sodium pyruvate, and β-mercaptoethanol (Invitrogen).

PMEFs were transfected with either: GFP as a positive transfection control, pLuc as a no-reprogramming control, or cocktails of pORF-Sox10, pORF-Olig2, pORF-ZFP536 (SOZ factors) for induced oligodendroglial progenitor transdifferentiation.

Cocktails containing Olig2 with the SV40 NLS sequence have "-NLS" appended to their name (SOZ-NLS, for example). SOZ factor plasmids were delivered at an equal mass ratio in all cases. All transfections were carried out in serum- and antibiotic-free OptiMEM (Invitrogen). OptiMEM was replaced with complete PMEF medium four hours after the onset of transfection. Serial transfections were performed every 48 hours, with complete PMEF media between.

Viral transduction of the SOZ or SOZ-NLS factors was performed 24 hours after PMEF seeding in medium with 8 μg mL^{-1} sequabrene (Sigma), using replication-deficient 2nd generation lentiviruses (packaging vectors psPAX2 (Addgene plasmid 12260) and pMD2.G (Addgene plasmid 12259)), in combination with Tet-O-FUW-Sox10, Tet-O-FUW-Olig2, and Tet-O-FUW-ZFP536. 24 hours after transduction, PMEF medium was replaced with PMEF medium containing 2 μg mL^{-1} doxycycline (Sigma).

48 hours after the final transfection was completed, or 48 hours after viral transduction, complete PMEF medium was replaced with OPC proliferation medium: DMEM 11960 (Invitrogen) containing 100 μg mL^{-1} human transferrin, 100 μg mL^{-1} bovine serum albumin, 16 μg mL^{-1} putrescine, 60 ng mL^{-1} progesterone, 40 ng mL^{-1} sodium selenite, 5 μg mL^{-1} *N*-acetyl-L-cysteine, 10 ng mL^{-1} D-biotin (Sigma), 4.2 μg mL^{-1} forskolin (Stemgent), 5 μg mL^{-1} bovine insulin (Gemini Biosystems), 1x B27 supplement without vitamin A, 1x GlutaMAX, 1x sodium pyruvate, 25 μg mL^{-1} gentamicin (Invitrogen), 1x Trace Elements (Cellgro), 10 ng mL^{-1} CNTF, 10 ng mL^{-1} PDGF-AA, and 1 ng mL^{-1} NT-3 (PeproTech). After 21 days of culture in proliferation medium, iOPCs were switched to differentiation medium. Differentiation medium was the same as proliferation medium, with addition of 40 ng mL^{-1} triiodothyronine (T3,

Sigma) and absence of PDGF-AA and NT-3. Viral OPC proliferation and differentiation medium contained 2 μg mL^{-1} doxycycline (Sigma).

Immunofluorochemistry

Transfected cells were washed briefly with PBS containing Ca^{2+} and Mg^{2+} (Mediatech), and fixed with 4% PFA (EMS) at RT for 15 minutes. Cells were then permeabilized for 10 minutes in 0.2% Triton X-100, washed twice, blocked for an hour in 10% donkey, goat, or fetal bovine serum, and incubated for 2 hours at room temperature (or 18 hours at 4C for myelin antibodies) in blocking buffer containing 10% goat or fetal bovine serum (Sigma-Aldrich) and combinations of the following primary antibodies: mouse IgM anti-A2B5 (R&D MAB141, 1:200), mouse IgM anti-O4 (R&D MAB1326), rabbit anti-S100β (Abcam ab52642, 1:500), goat anti-Sox10 (Santa Cruz sc-17342, 1:500), goat anti-Olig2 (Santa Cruz sc-19969, 1:500), rat anti-MBP (Abcam ab7349, 1:100), goat anti-MOG (R&D AF2439, 1:50). The cells were then washed three times with PBS, and incubated for one hour at RT in blocking buffer containing appropriate AlexaFluor 488 or 594 anti-IgG or anti-IgM secondary antibodies (1:500, Invitrogen), washed three times with PBS, and imaged with a Nikon Eclipse TE2000-U inverted fluorescence microscope (Tokyo, Japan) with a ProScanII motorized stage (Prior Scientific, Rockland, MA).

Image analysis

To quantify $S100\beta^{+}$ and $O4^{+}$ cell generation, PMEFs were transfected in TCPS wells, stained, and scanned to produce large mosaic images of each complete culture area.

S100β and O4 mosaics were processed with a FIJI (Fiji Is Just ImageJ, http://fiji.sc) macro to: automatically and uniformly threshold each image according to local contrast, exclude small debris, overlay thresholded S100β and O4 channels, and to count the number of single- and double-positive cells in each well.

6.4 Results

Olig2 requires a synthetic nuclear localization sequence to efficiently traffic to the nucleus in fibroblasts

To check expression, transfection efficiency, and proper nuclear localization of the master OPC transcription factors Sox10 and Olig2 cloned into the non-viral pORF vectors, PMEFs were transfected using pCBA-ABOL with pORF-Sox10 or pORF-Olig2. PMEFs were then stained at day two post transfection for Sox10 and Olig2 expression. Sox10 was located in the nucleus, whereas Olig2 was largely cytoplasmic, with some nuclear expression. A subset of $Olig2^{+}$ cells excluded Olig2 from their nuclear compartment, evident as a "hole" coincident with DAPI staining of the nucleus (Figure 43, left). To determine the effect on nuclear localization from addition of the SV40 NLS to Olig2, pORF-Olig2-NLS and pORF-Olig2 were transfected into MEFs, and imaged at day 2. Addition of NLS repartitioned virtually all visible Olig2 from the cytoplasm to the nucleus (Figure 43, right). The same repartitioning was observed when Olig2 or Olig2-NLS were delivered with lentiviral transduction (not shown).

The addition of NLS to Olig2 dramatically increases the expression of OPC markers in PMEFs expressing ectopic SOZ factors

PMEFs were transfected with 1 μg of pORF-SOZ and pORF-SOZ-NLS cocktails, cultured in OPC proliferation media for a period of 7 to 21 days, and exposed to T3-containing media for 7 days. A subset of PMEFs transfected with equimolar mixtures of SOZ factors drastically altered their morphology and expressed OPC lineage markers (Figure 44). SOZ-NLS qualitatively produced the highest efficiency of S100β induction at day 14 in OPC proliferation medium, and produced the most compact $O4^+$ cells (Figure 44, lower right panel).

The increase in S100β and O4 positivity was significant as measured by large area image analysis (Figure 45). Without the addition of SV40 NLS to Olig2, both pORF-SO and pORF-SOZ factor cocktails were ineffective at generating $O4^+$ and $S100\beta^+$ cells compared to delivery of Sox10 alone. ZFP536 increased the expression of S100β in all cases tested. The fusion of SV40 NLS to Olig2 increased the expression of S100β over 15-fold, O4 5-fold, and double-positive cells 20-fold for the pORF-SO and pORF-SOZ factor cocktails.

The number of $S100\beta^+$ and $O4^+$ cells increased from day 7 to day 14 in OPC proliferation media for all combinations of SOZ factors other than pORF-Olig2 delivered alone (Figure 46). SOZ factor combinations with the highest fraction of Sox10 produced the greatest number of $O4^+$ cells. Olig2 and Olig2-NLS were unable to induce OPC marker expression in the absence of Sox10. PMEFs transfected with luciferase (pLuc) did not express OPC markers.

Addition of NLS to Olig2 increases the yield of iOLs produced with viral delivery of SOZ factors

Rare PMEFs transfected non-virally with pORF-SOZ-NLS factors and exposed to T3 for 7 days expressed MOG, but the morphology and expression pattern of these MOG^+ cells was not typical of primary oligodendrocytes (Figure 47). PMEFs virally transduced and differentiated in parallel with SOZ or SOZ-NLS factors co-expressed MBP and MOG with the stellate morphology expected of primary myelinating oligodendrocytes. Large area image analysis reveals that viral SOZ factors without NLS produced what appeared to be clusters of iOLs arising from colonies proliferated from single successfully-reprogrammed iOPCs, while inclusion of Olig2-NLS produced a much denser field of iOLs (Figure 48).

6.5 Discussion

iOPCs are an attractive target for viral and non-viral reprogramming. Their proliferative yet glia-committed phenotype simultaneously diminishes their potential for tumorigenicity compared to iPSCs, while being expandable to provide a therapeutic quantify of cells for transplantation. In a pioneering description of iOPC generation from fibroblasts, Wernig *et al.* demonstrated SO and SOZ efficiently activate OPC markers with lentivirus, but SOZ was the only combination that produced myelinating OLs [268] – as such, we focused on this combination. Both of the currently-published iOPC protocols are encouraging for their complete recapitulation of all measured functions of bona-fide OLs, but the efficiency of iOPC generation is markedly lower than neuronal

reprogramming protocols. This presents a particularly exciting opportunity and steep challenge for non-viral generation of OPCs; successful non-viral OPC reprogramming will be more difficult than non-viral neuronal reprogramming, but any successfully-reprogrammed cells could be greatly expanded for therapeutic deployment.

OPCs express a variety of lineage-specific markers throughout their normal development and differentiation. Fast-dividing early OPCs express A2B5, slow-dividing late OPCs express S100β and begin to express O4 [411]. Mature OLs express MBP, MOG, and may continue to express O4 [411]. We were able to detect each of these markers with immunostaining in non-viral iOPC-like cells transfected with the SOZ factors. However, for the most part NiOPC-like cells had abnormally large, spread morphologies when compared to primary OPCs. Accordingly, $O4^+$ NiOPC-like cells did not proliferate significantly in response to mitogen stimulation following FACS purification (not shown). Furthermore, MBP^+ and MOG^+ cells were exceedingly rare, and also had morphologies that were dissimilar to that of primary OLs (Figure 47). MBP^+ and MOG^+ NiOPC-like cells were never double-positive. Taken together, these results suggest these NiOPC-like cells are only partially reprogrammed.

Considering the incomplete reprogramming of these NiOPC-like cells, it is surprising to note the gradual appearance of $O4^+$ and $S100\beta^+$ cells between days seven and 14 post-transfection (Figure 46) – a period during which the ectopic SOZ factors are expected to be silenced. These cells may gradually find a pseudostable fate that is neither OPC nor PMEF, and may be entirely synthetic. It is important to keep this "synthetic cell" possibility in mind when determining the "success" of reprogramming based on appearance of markers that are exquisitely unique to the target cell type in normal

development – these markers may appear during reprogramming as direct or indirect transactivants of the ectopic transcription factors, and waves of downstream markers may appear at the "normal" point they would be expected *in vivo*, in cells that are nevertheless unable to perform the required therapeutic function (myelination of axons, in this case). Indeed, single-cell expression analysis of iPSCs in the process of converting have revealed that many distinct intermediate stages can exist between starting fibroblasts and the final reprogrammed phenotype, each with a different resistance to proceeding on to the next [293]. These intermediates are a (meta)stable fate in their own rite, and can persist for some time without fully committing to the desired final functional form.

Viral iOPCs, on the other hand, were $A2B5^+$, $S100\beta^+$, $O4^+$, and MBP^+ and MOG^+ upon differentiation with T3, and single cells were generally co-stained for all markers analyzed. Viral iOPCs and iOLs assumed morphologies typical of proliferative OPCs and myelinating primary OLs, respectively. We generated iOPCs with SOZ factors at an efficiency that was comparable to that which has been previously reported [268-269].

During validation of molecular cloning of the non-viral SOZ factors, we observed a cytoplasmic localization of Olig2 that is not typical of that in primary OPCs (Figure 43, left). Olig2 has a cryptic NLS which is only exposed and active upon interaction with chaperone proteins, none of which are normally expressed in fibroblasts [407]. Considering the central importance of Olig2 in both published iOPC derivation protocols, and the fact that transcription factors must be physically located in the nucleus to initiate or repress transcription on target genomic DNA, we hypothesized cytoplasmic sequestration of Olig2 may be a previously unknown barrier to iOPC generation.

With an aim to translocate Olig2 to the nucleus in PMEFs, we first considered small molecules which can globally inhibit the active export of transcription factors from the nucleus (leptomycin B, for example). However, Sox10 activity is known to be dependent on continuously active nucleoplasmic shuttling [412]. An indiscriminate inhibitor of nuclear export would likely therefore impair the activity of Sox10, the other master regulator of OPC reprogramming. Adding chaperone transcription factors to the cocktail is another possibility to carry ectopic Olig2 into the nucleus, but this is not ideal for non-viral reprogramming, as it diminishes the total mass of the other plasmids that can be delivered in the cocktail. We had already noted that co-delivery of three plasmids decreases the mass of Sox10 plasmid to levels near the cutoff threshold of its ability to induce O4 positivity in PMEFs (not shown). Furthermore, the Olig2 chaperone transcription factor Nkx2.2 may inhibit viral iOPC generation [268]; other chaperone proteins may have similarly unpredictable and undesirable side effects.

Transgenic mice with an N-terminal Olig2 fusion have been previously described to be developmentally normal [410]; this suggests the function of Olig2 may not critically depend on interactions at the N-terminus. We therefore elected to append the strong SV40 NLS to the N-terminus of Olig2 to encourage nuclear entry without the assistance of chaperone proteins. With addition of the NLS, Olig2 delivered both virally and non-virally to PMEFs was repartitioned from the cytoplasm almost exclusively to the nucleus (Figure 43, right). Consequently, the number of $S100\beta^+$ and $O4^+$ cells was dramatically increased at day 14 post introduction of the SOZ factors with non-viral (and viral, not shown) delivery of cocktails containing Olig2-NLS, as well as expression of other OPC lineage-specific markers (Figure 44, Figure 45). The additional activation afforded by

nuclear localization of Olig2 was not sufficient to induce complete reprogramming of NiOPCs as measured by MBP and MOG positivity, but the yield of MBP^+ viral OLs was increased markedly (Figure 48). We were unable to increase the number of non-virally induced MBP^+MOG^+ cells with three serial transfections of SOZ-NLS factors, nor with further addition of miRNAs highly and uniquely expressed in OPCs, or reprogramming in the presence of small molecules that remove repressive epigenetic marks from mature myelin genes [406] (results not shown). Non-viral transfection with SOZ factors in general, or with the EF1α promoter specifically, may produce expression that is currently of an insufficient duration, stability, and/or intensity to completely reprogram PMEs to iOPCs. The addition of NLS to the non-viral SOZ cocktail may lower the barrier of conversion from fibroblasts to an intermediate fate [293], through which viral SOZ-NLS transduced cells can pass on to the iOPC fate efficiently, but non-virally transfected cells cannot.

6.6 Conclusion and future perspectives

We have demonstrated that relief of cytoplasmic sequestration of Olig2 is sufficient to dramatically increase the non-virally-induced expression of OPC lineage markers, and to increase viral iOL yield. To our knowledge this is the first demonstration of a strongly repressive host cell context "in trans", which can be circumvented during direct reprogramming via the intelligent reengineering of a master transcription factor. Therefore, the failure of a cell to reprogram may not always be a consequence of insurmountable epigenetic barriers, but also potentially due to the absence of critical

cofactors [283]. The generation of fibroblast-OPC heterokaryons could be instructive to determine which genes are not transactivated in the fibroblast nuclei. Manipulation of the ground state of starting cell sources is an almost completely unsolved barrier to direct reprogramming in the CNS [285].

Optimistically, the increased yield of viral iOLs with the use of Olig2-NLS may help to allow iOPC reprogramming from human fibroblast sources for the first time. These results serve not only as a specific notice to researchers performing any form of direct reprogramming to ensure proper nuclear localization of transcription factors rather than only expression by Western blot, but also more broadly to consider other potential cell-type-specific contextual inhibitors of transcription factor function such as post-translational modifications, chaperone interactions, and extracellular signaling. Two related examples are the demonstrated requirement for Ascl1's pioneer activity before Brn2 can bind to its genomic targets during BAM NiN generation [282], and that the ability of Ngn2 to reprogram cells *in vivo* has been shown to depend on the local milieu of growth factors [311].

Our present inability to fully convert iOPCs without lentivirus implies there are one or more additional barriers preventing non-viral iOPC generation. This is likely a consequence of delivery, as the viral and non-viral experiments were performed entirely in parallel from an identical cell source. Minicircle vectors avoid silencing and may help to maintain longer-term expression [351]. The use of orthogonally-inducible lentiviral systems could also help determine the order, duration, and level of TF expression that is required for complete iOPC reprogramming, and to better predict whether transient non-viral transfection will be able to achieve the required thresholds. Assuming epigenetic

repression in cis is a barrier to non-viral iOPC generation, CRISPR/Cas9 synthetic TFs [298] should also be evaluated for their ability to activate more stable expression from the endogenous SOZ loci than ectopic factors delivered via plasmid DNA.

Appending a strong NLS to Olig2 is only one example of an "intelligently designed" synthetic transcription factor for use in reprogramming - there are many other design possibilities that remain to be explored in the context of direct reprogramming. For example, appending VP16/64/160 transactivation domains to increase transcription factor potency (as has been done to enhance iPSC reprogramming [413]), or specifically mutating or applying directed evolution to wild-type transcription factors to alter known or as-yet-undiscovered critical post-translational modification sites (such as those used for inhibitory SUMOylation of Sox10 [305]), may further improve the efficiency of these difficult forms of direct reprogramming. Interestingly, VP16-Olig2 fusions act as dominant-negative mutants, presumably because of Olig2's normal role as a transcriptional repressor [408]. OPCs also respond strongly to topographical cues, even in the absence of biochemical signals provided by an actual axon, to initiate differentiation and myelination of nanofibers [414]. The stage is therefore well-set to explore a rich parameter space of intra- and extracellular microenvironmental factors to push non-viral iOPC generation over its remaining barriers to complete conversion, towards deployment in safer future cell replacement therapies against MS.

6.7 Figures

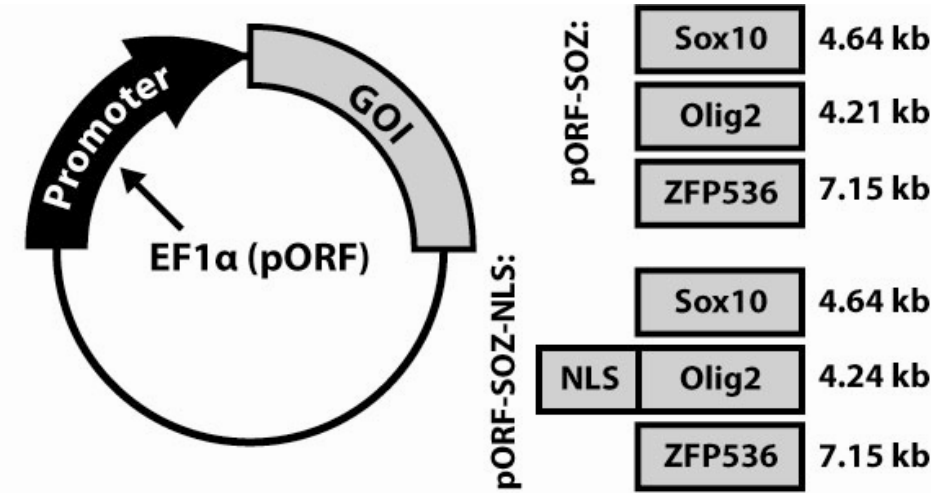

Figure 42. Non-viral vectors for direct reprogramming of fibroblasts to oligodendroglial progenitors
Coding sequences for mouse Sox10 (S), Olig2 (O), and ZFP536 (Z) transcription factors were inserted into the pORF backbone under control of the EF1α-HTLV promoter, or the dox-inducible Tet-O-FUW lentiviral backbone. The SV40 nuclear localization sequence was cloned 5' of the coding sequence of Olig2, producing Olig2-NLS. Cocktails of SOZ factor-encoding plasmids were delivered at an equimolar ratio.

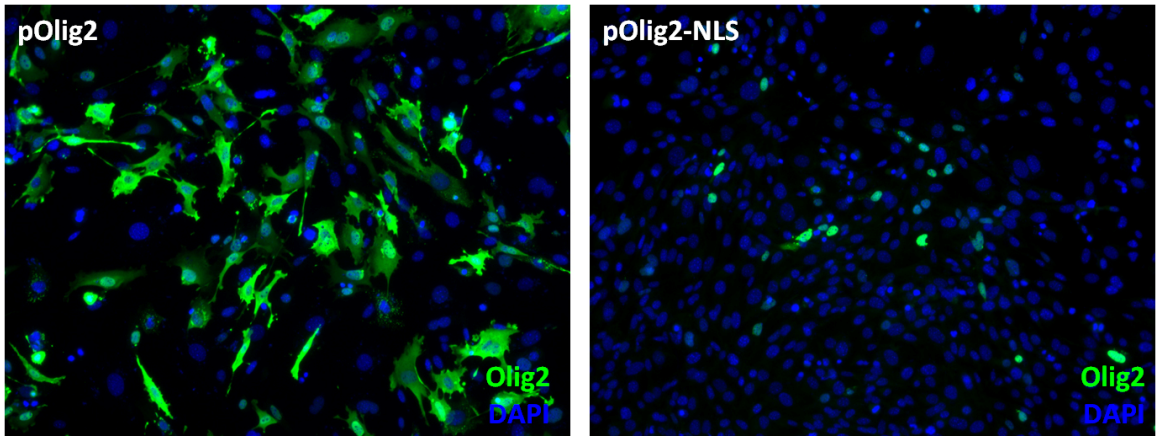

Figure 43. Olig2 expression in fibroblasts transfected with and without 5' addition of the SV40 NLS
Olig2 expression as visualized by immunofluorochemistry at day 2 post-non-viral transfection. Wild-type Olig2 transfected into PMEFs is primarily located in the cytoplasm, and is excluded from the nucleus in some cells (left). 5' addition of the SV40 nuclear localization sequence (NLS) repartitions Olig2 exclusively to the nucleus in PMEFs.

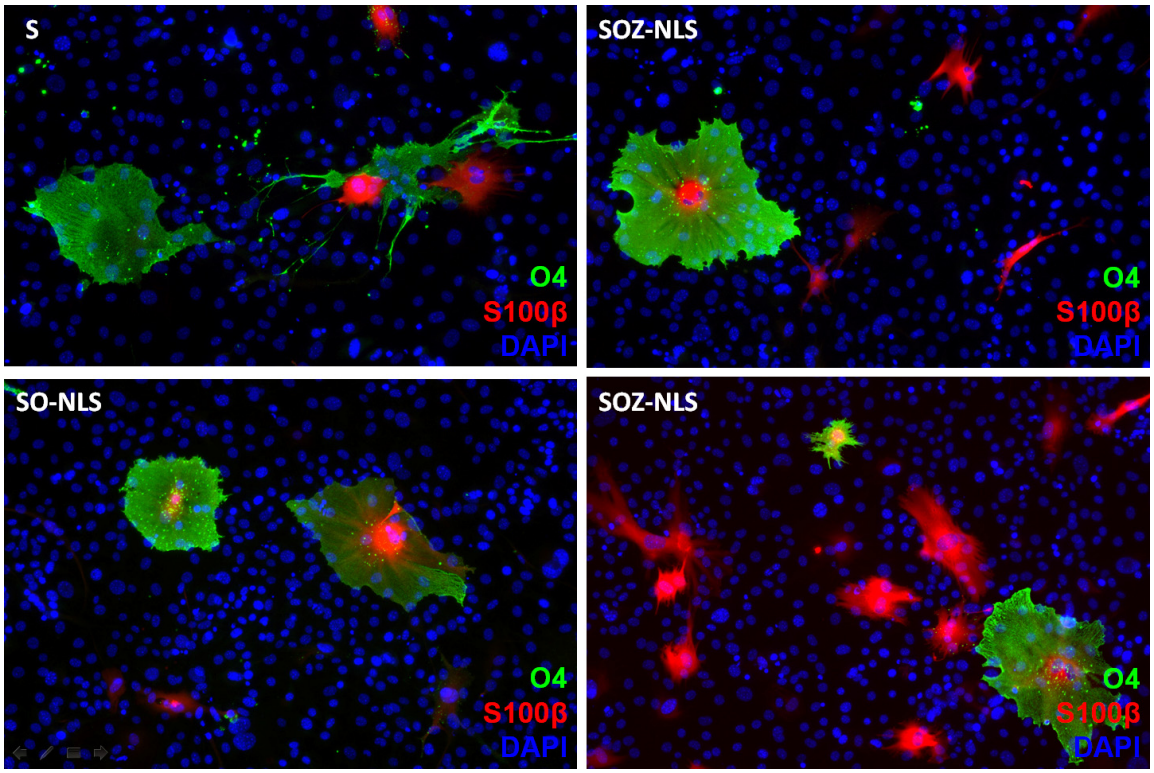

Figure 44. OPC marker expression in PMEFs non-virally transfected with SOZ factors
S100β (red) and O4 (green) expression as visualized by immunofluorochemistry at day 14 OPC proliferation media, following non-viral transfection of 1 μg pORF-SOZ or pORF-SOZ-NLS factors, with DAPI-labeled nuclei (blue). A subset of PMEFs transfected with equimolar mixtures of Sox10 (S), Olig2-NLS (O-NLS), and ZFP536 (Z) plasmids drastically altered their morphology and expressed OPC lineage markers. SOZ-NLS produced the highest efficiency of S100β induction at day 14 in OPC proliferation medium, and produced the most compact $O4^+$ cells (lower right panel).

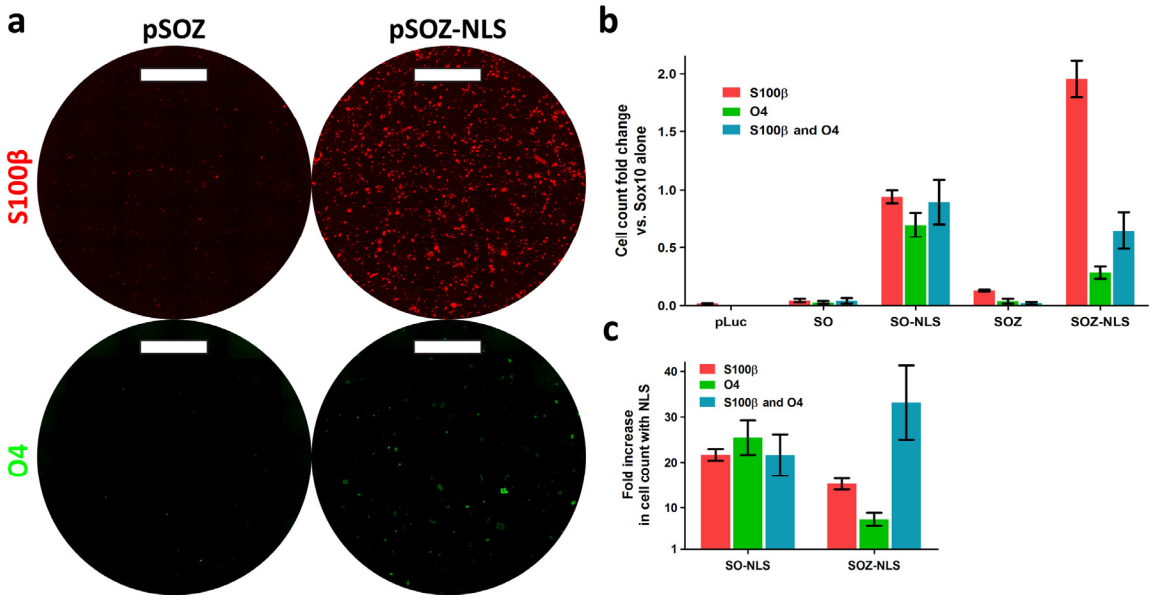

Figure 45. Quantification of OPC marker expression in PMEFs non-virally transfected with SOZ and SOZ-NLS factors

Large area scans of S100β and O4 expression at day 14 in OPC proliferation media following a 1 µg dose of pORF-SOZ or pORF-SOZ-NLS in PMEFs (2.5 mm scale bar). (b) Quantification of $S100\beta^+$ and $O4^+$ cells at day 14 of OPC proliferation media culture. Without the addition of SV40 NLS to Olig2, both combinations of OPC transcription factors were ineffective at generating $O4^+$ and $S100\beta^+$ cells compared to delivery of Sox10 alone. ZFP536 increased the expression of S100β in all cases. (c) The inclusion of NLS increased the expression of S100β over 15-fold, O4 5-fold, and double-positive cells 20-fold. PMEFs transfected with luciferase (pLuc) did not express OPC markers. Cell counts were generated with large area image analysis; bars represent mean ± SEM of three separate experiments performed in triplicate.

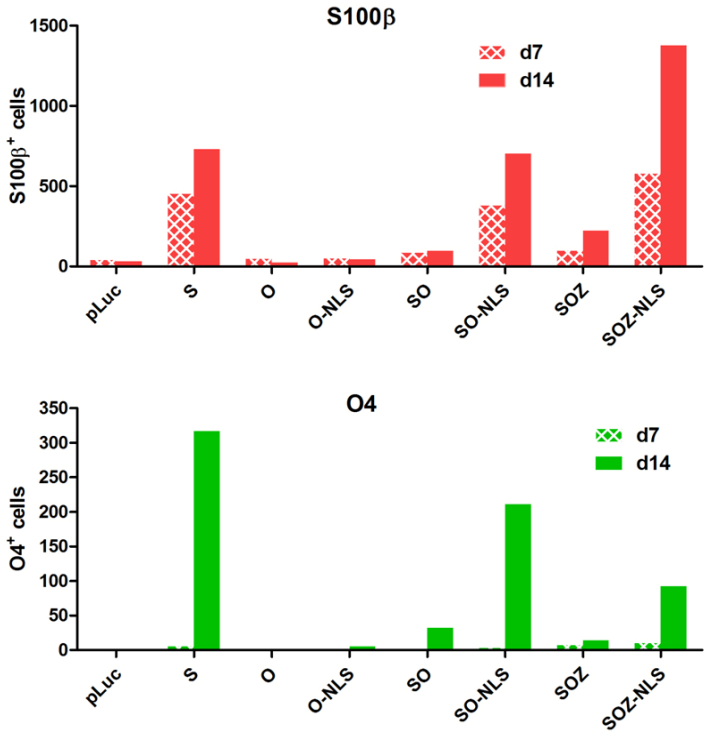

Figure 46. Time course of OPC marker expression one to two weeks following SOZ factor transfection

Quantification of the increase in $S100\beta^+$ and $O4^+$ cells between day seven and 14 of culture in OPC proliferation medium. Combinations with the highest fraction of Sox10 produced the greatest number of $O4^+$ cells. Olig2 and Olig2-NLS were unable to induce OPC marker expression in the absence of Sox10. PMEFs transfected with luciferase (pLuc) did not express OPC markers. Cell counts were generated with large area image analysis.

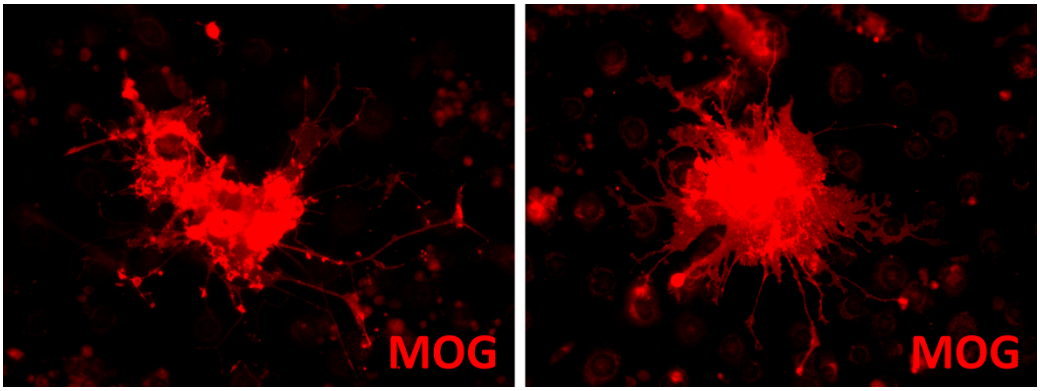

Figure 47. Expression of MOG in PMEFs transfected with SOZ-NLS factors and exposed to T3

MOG expression as visualized by immunofluorochemistry in PMEFs non-virally transfected with SOZ-NLS, cultured in OPC proliferation medium for 21 days, and exposed to T3 differentiation medium for 7 days.

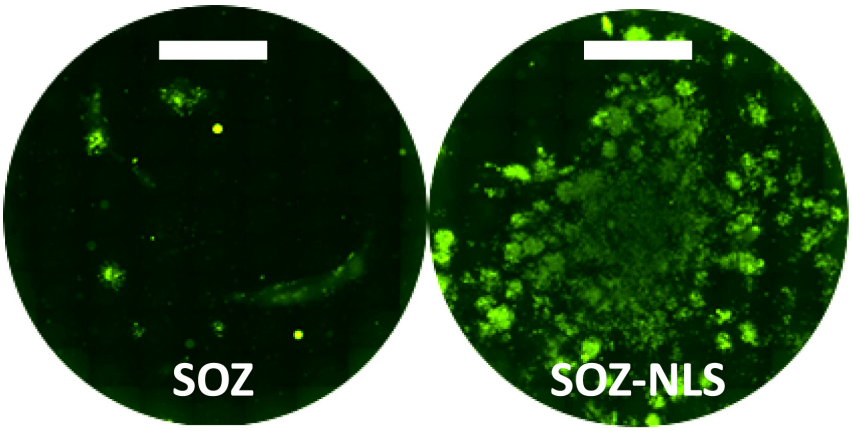

Figure 48. Myelin protein expression in PMEFs virally transduced with SOZ and SOZ-NLS factors
Large area scans of MBP expression at day seven of culture in T3 differentiation media following viral transduction of SOZ or SOZ-NLS factors and 21 days of culture in OPC proliferation medium (2.5 mm scale bar). Figure produced in equal collaboration with Karina Kulangara.

Chapter 7: Summary and Synthesis

7.1 Non-viral direct neuronal reprogramming

In Chapter 3, we provided data that strongly supports *Hypothesis 1: Non-viral neuronal transdifferentiation of fibroblasts into neuronal cells that fire trains of action potentials can be achieved.* With multiple transfections of transcription factor-encoding plasmids we produced immature NiNs at an efficiency similar to that of published lentiviral BAM-factor iN generation protocols, and a proportion of those NiNs went on to mature into an electrophysiologically-active phenotype. To our knowledge this is the first demonstration of non-viral direct somatic reprogramming across germ layers (complete myoblast reprogramming with MyoD is restricted to mesodermal starting cells), and is therefore an important proof-of-concept which demonstrates the feasibility of safer non-integrative direct neuronal reprogramming. If the history of the iPSC field is predictive of future iN developments, the safety profile of iN generation can and will be improved even further by replacement of plasmid DNA (which integrates very rarely) with completely non-integrative mRNA, siRNA, miRNA, protein-transduction, and entirely small molecule-based techniques.

NiN generation with BAM factors is an accessible technique; though pCBA-ABOL transfection improves the yield of iNs compared to commercial carriers, labs with non-viral transfection experience should be able to rapidly produce neurons from MEF sources with their transfection reagent of choice. This advance over viral delivery will lower the barrier to entry for many biomaterials labs, which already have experience

studying the differentiation of ESCs and iPSCs into CNS lineages in a variety of microenvironmental contexts, but due to the risk of teratoma formation may have lacked a strong therapeutic rationale for the near future. Our demonstration of successful NiN reprogramming can therefore act as a bridge between the neurobiologists who are now delving into the biology of direct reprogramming, and the tissue- and bio-engineers who are well-equipped to deploy these cells in their most translatable forms. Non-viral neuronal reprogramming may also re-invigorate the design of non-viral transfection agents with a new question: What can be done to re-transfect partially-converted intermediate cell fates stuck between fibroblast and neuronal phenotypes, particularly those which may have arrested division? Subsequent mRNA/miRNA/siRNA transfections, which do not depend on nuclear entry, may be a good answer to this open question.

Gene-eluting implantable scaffolds for nerve regeneration in the PNS and CNS are just two examples which could be modified from a neuro-protective to a cell-replacement paradigm with substitution of the plasmids delivered. We expect there will be an explosion of work performed to study the interaction of iNs, iNPCs, and iOPCs with biomaterials, both to improve the efficiency of their generation, as well as to deliver the cells in a supportive context *in vivo*. We have provided the first examples of these microenvironmental mediators of transfection and iN generation and/or survivability in Chapters 4-6.

7.2 Extracellular microenvironment and non-viral direct reprogramming

In Chapter 4 we provided evidence in support of *Hypothesis 2: Microenvironmental factors can improve iN yield.* We demonstrated that defined chemical microenvironments can improve the yield of non-viral iNs for both a glutamatergic and dopaminergic cocktail of transcription factors, either by inducing chronic depolarization, or by manipulating SMAD and GSK-3β signaling with small molecules. Chemical control of microenvironment with these same approaches elicits similar pro-survival and pro-neuronal changes in normal development and in differentiating iPSCs. This adds to growing support across the field of direct neuronal reprogramming that seems to suggest emerging iNs may be subject to some of the same developmental cues and controls as newborn primary neurons. We expect that our extension of these techniques to non-viral neuronal reprogramming will provoke any translational bioengineers who adopt our NiN production scheme in Chapter 3 to look towards normal neurodevelopment to discover new means to further improve and instruct NiN reprogramming, especially for difficult target subtypes that may nevertheless be particularly attractive for cell replacement therapies.

The physical microenvironment imparted by substrate topography is another powerful mediator of cell phenotype *in vitro*, but its role in normal development is difficult to study *in vivo*. Cell replacement strategies for neurodegenerative diseases typically enjoy the benefit of a slow disease progression, and may therefore readily adopt *ex vivo* iN generation schemes, which could potentially gain from topographical

enhancements of this process. Similarly, implantable scaffolds for iN delivery or *in vivo* induction could include surface topographies that encourage transfection and iN conversion and survival. In Chapter 5 we go on to show that microtopography can improve the non-viral transfection efficiency of fibroblasts, in support of *Hypothesis 3: High-throughput screening will identify micropitted topographies that enhance transfection compared to smooth substrates.* Our lab has also further demonstrated that microtopographies can enhance both the yield and purity of iNs produced with lentiviral transduction.

We are currently investigating potential synergy between these substrate-mediated effects on transfection and iN generation via non-viral direct neuronal reprogramming on patterned micro- and nanotopographies. Topography could also be intelligently designed to guide neurite extension of iNs in such a way that they are more likely to encounter desirable circuits *in vivo* or other converting iNs *in vitro*, to encourage a particular electrical microenvironmental connectivity that might enhance subtype specification, integration, or survival, potentially via some of the same beneficial depolarization-mediated effects we described in Chapter 4.

7.3 Intracellular microenvironment and non-viral direct reprogramming

Drawing a distinction between extra- and intracellular microenvironment may be largely semantic – extracellular signaling is transduced and reflected inside the cell, and cells actively secrete and modify extracellular factors. In this case however, we use

"intracellular microenvironment" as shorthand to encapsulate the overall epigenetic and transcriptional phenotype of naïve and mid-reprogramming fibroblasts, which may be impermissive to completion of the transdifferentiation process. To this point, researchers have largely ignored the status of the starting cell type, which may drastically impact reprogramming. Consideration of the differences in efficiency for various starting and target cell types highlights perhaps the most exciting and fundamental questions in the field of direct reprogramming: What keeps somatic cell fates stable, and how can we precisely break down and rebuild those stable programs to produce the cells desperately needed for therapeutic cell replacement? For the most part, all cells contain the same genomic DNA, so the most fundamental "switch" in a reprogrammed cell occurs at the epigenetic level. However, it is generally unclear whether resistance to reprogramming is principally a consequence of epigenetic silencing in cis, insufficient transgene delivery levels or duration, or the presence (absence) of suppressive (supportive) trans-acting factors.

We investigated this idea in Chapter 6 with *Hypothesis 4: Viral and non-viral iOPC generation is inefficient compared to iN generation, and may therefore suffer from additional barriers to complete reprogramming*. We found that the published iOPC generation protocols indeed suffer from a lack of chaperone factors to carry Olig2 into fibroblastic nuclei. We relieved this barrier via fusion of a constitutive NLS to Olig2, which greatly improved the induction of OPC markers. The appended NLS was sufficient to greatly improve the yield of oligodendrocytes from a lentiviral reprogramming approach, but one or more barriers to non-viral iOPC generation remain.

Our discovery of a strongly repressive fibroblastic intracellular context will not only improve iOPC derivation efficiencies specifically, but can also serve as a general notice to the field to search for other non-permissive intracellular contexts, whether they be acting in cis or trans. We have demonstrated proof-of-concept that trans repressors of transcription factor function can be overcome via protein engineering. Currently, the strategies for overcoming epigenetic cis repressors are generally limited to global epigenetic modifiers, or biasing stochastic epigenetic changes towards a desired fate with supraphysiological levels of ectopic transcription factor expression. In the future, the nascent field of "epigenetic editing" may be able to more-precisely manipulate epigenetic marks at the loci most critical for successful reprogramming. Safe translation of these techniques as deployed against neurodegenerative disease can draw benefit from consideration of the enhanced non-viral transfection and reprogramming methods we have developed in this dissertation.

7.4 Closing remarks

Safe direct reprogramming of readily-obtained somatic cells to the neuronal and glial cell types lost in neurodegenerative disease could provide patients with the most realistic hope for curative therapies to date. The direct conversion of fibroblasts to neurons and glia is not likely a naturally-occurring process, but it does appear to follow some of the normal "rules" of development. In the pursuit of efficient generation of these cells, we should therefore look to and respect development, while remaining suspicious of starting cell programs which have evolved to resist change. We must be willing and

able to re-engineer the intracellular and extracellular contexts before, during, and after reprogramming, to allow the desired natural transcriptional programs to take hold and remain healthy. The most permissive microenvironments for iN conversion and survival may be quite similar to those encountered by primary progenitors, neurons, and glia during their journey through development. In this dissertation we have demonstrated that such physical and chemical microenvironments can be potently repressive, or wielded to encourage the direct reprogramming of neurons and glia. This sets the stage for a new field of therapeutically-fruitful research, which can draw equally from neurobiology and bioengineering: the development of *in vitro* and *in vivo* systems for close recapitulation of dynamic developmentally-inspired soluble and biophysical cues during non-integrative direct neuronal and glial reprogramming.

References

1. Ratko, T.A., et al., *Clinical gene therapy for nonmalignant disease.* The American Journal of Medicine, 2003. **115**(7): p. 560-569.

2. van Gaal, E.V.B., et al., *Junk DNA enhances pEI-based non-viral gene delivery.* International Journal of Pharmaceutics. **In Press, Corrected Proof**.

3. Belting, M., S. Sandgren, and A. Wittrup, *Nuclear delivery of macromolecules: barriers and carriers.* Advanced Drug Delivery Reviews, 2005. **57**(4): p. 505-527.

4. Medina-Kauwe, L.K., J. Xie, and S. Hamm-Alvarez, *Intracellular trafficking of nonviral vectors.* Gene Therapy, 2005. **12**(24): p. 1734-1751.

5. Grigsby, C.L. and K.W. Leong, *Balancing protection and release of DNA: tools to address a bottleneck of non-viral gene delivery.* Journal of the Royal Society Interface. **7**(Suppl 1): p. S67-S82.

6. Hama, S., et al., *Quantitative and mechanism-based investigation of post-nuclear delivery events between adenovirus and lipoplex.* Nucleic Acids Res, 2007. **35**(5): p. 1533-43.

7. Kogure, K., et al., *Multifunctional envelope-type nano device (MEND) as a non-viral gene delivery system.* Adv Drug Deliv Rev, 2008. **60**(4-5): p. 559-71.

8. Pollard, H.l.n., et al., *Polyethylenimine but Not Cationic Lipids Promotes Transgene Delivery to the Nucleus in Mammalian Cells.* Journal of Biological Chemistry, 1998. **273**(13): p. 7507-7511.

9. Payne, C.K., et al., *Internalization and trafficking of cell surface proteoglycans and proteoglycan-binding ligands.* Traffic, 2007. **8**(4): p. 389-401.

10. Lechardeur, D., A.S. Verkman, and G.L. Lukacs, *Intracellular routing of plasmid DNA during non-viral gene transfer.* Advanced Drug Delivery Reviews, 2005. **57**(5): p. 755-767.

11. Conner, S.D. and S.L. Schmid, *Regulated portals of entry into the cell.* Nature, 2003. **422**(6927): p. 37-44.

12. Sonawane, N.D., F.C. Szoka, Jr., and A.S. Verkman, *Chloride accumulation and swelling in endosomes enhances DNA transfer by polyamine-DNA polyplexes.* J Biol Chem, 2003. **278**(45): p. 44826-31.

13. Wagner, E., *Effects of membrane-active agents in gene delivery.* Journal of Controlled Release, 1998. **53**(1-3): p. 155-158.

14. Rejman, J., A. Bragonzi, and M. Conese, *Role of clathrin- and caveolae-mediated endocytosis in gene transfer mediated by lipo- and polyplexes.* Mol Ther, 2005. **12**(3): p. 468-74.

15. Pelkmans, L., et al., *Caveolin-Stabilized Membrane Domains as Multifunctional Transport and Sorting Devices in Endocytic Membrane Traffic.* Cell, 2004. **118**(6): p. 767-780.

16. Pelkmans, L., *Secrets of caveolae- and lipid raft-mediated endocytosis revealed by mammalian viruses.* Biochimica et Biophysica Acta (BBA) - Molecular Cell Research, 2005. **1746**(3): p. 295-304.

17. Hoekstra, D., et al., *Gene delivery by cationic lipids: in and out of an endosome.* Biochem Soc Trans, 2007. **35**(Pt 1): p. 68-71.

18. Zuhorn, I.S., R. Kalicharan, and D. Hoekstra, *Lipoplex-mediated transfection of mammalian cells occurs through the cholesterol-dependent clathrin-mediated pathway of endocytosis.* Journal of Biological Chemistry, 2002. **277**(20): p. 18021-18028.

19. Zuhorn, I.S., et al., *Phase behavior of cationic amphiphiles and their mixtures with helper lipid influences lipoplex shape, DNA translocation, and transfection efficiency.* Biophys J, 2002. **83**(4): p. 2096-108.

20. Lindberg, J., et al., *Nocodazole treatment of CV-1 cells enhances nuclear/perinuclear accumulation of lipid-DNA complexes and increases gene expression.* Pharm Res, 2001. **18**(2): p. 246-9.

21. HammAlvarez, S.F., et al., *Paclitaxel and nocodazole differentially alter endocytosis in cultured cells.* Pharmaceutical Research, 1996. **13**(11): p. 1647-1656.

22. Akinc, A., et al., *Exploring polyethylenimine-mediated DNA transfection and the proton sponge hypothesis.* The Journal of Gene Medicine, 2005. **7**(5): p. 657-663.

23. Wrobel, I. and D. Collins, *Fusion of Cationic Liposomes with Mammalian-Cells Occurs after Endocytosis.* Biochimica Et Biophysica Acta-Biomembranes, 1995. **1235**(2): p. 296-304.

24. Rémy-Kristensen, A., et al., *Role of endocytosis in the transfection of L929 fibroblasts by polyethylenimine/DNA complexes.* Biochimica et Biophysica Acta (BBA) - Biomembranes, 2001. **1514**(1): p. 21-32.

25. Douglas, K.L., C.A. Piccirillo, and M. Tabrizian, *Cell line-dependent internalization pathways and intracellular trafficking determine transfection efficiency of nanoparticle vectors.* European Journal of Pharmaceutics and Biopharmaceutics, 2008. **68**(3): p. 676-687.

26. Khalil, I.A., et al., *High density of octaarginine stimulates macropinocytosis leading to efficient intracellular trafficking for gene expression.* J Biol Chem, 2006. **281**(6): p. 3544-51.

27. Hess, G.T., et al., *Cellular binding, motion, and internalization of synthetic gene delivery polymers.* Biochimica et Biophysica Acta (BBA) - Molecular Cell Research, 2007. **1773**(10): p. 1583-1588.

28. Fujimoto, T., et al., *Isoforms of caveolin-1 and caveolar structure.* J Cell Sci, 2000. **113**(19): p. 3509-3517.

29. Tenchov, B.G., et al., *Modulation of a membrane lipid lamellar-nonlamellar phase transition by cationic lipids: A measure for transfection efficiency.* Biochimica et Biophysica Acta (BBA) - Biomembranes, 2008. **1778**(10): p. 2405-2412.

30. Ma, B., et al., *Lipoplex morphologies and their influences on transfection efficiency in gene delivery.* Journal of Controlled Release, 2007. **123**(3): p. 184-194.

31. Masotti, A., et al., *Comparison of different commercially available cationic liposome-DNA lipoplexes: Parameters influencing toxicity and transfection efficiency.* Colloids and Surfaces B: Biointerfaces, 2009. **68**(2): p. 136-144.

32. Mishra, S., P. Webster, and M.E. Davis, *PEGylation significantly affects cellular uptake and intracellular trafficking of non-viral gene delivery particles.* European Journal of Cell Biology, 2004. **83**(3): p. 97-111.

33. Kunath, K., et al., *Low-molecular-weight polyethylenimine as a non-viral vector for DNA delivery: comparison of physicochemical properties, transfection efficiency and in vivo distribution with high-molecular-weight polyethylenimine.* Journal of Controlled Release, 2003. **89**(1): p. 113-125.

34. Sahoo, S.K., et al., *Residual polyvinyl alcohol associated with poly (D,L-lactide-co-glycolide) nanoparticles affects their physical properties and cellular uptake.* Journal of Controlled Release, 2002. **82**(1): p. 105-114.

35. Almofti, M.R., et al., *Lipoplex size determines lipofection efficiency with or without serum.* Molecular Membrane Biology, 2003. **20**(1): p. 35-43.

36. Ross, P.C. and S.W. Hui, *Polyethylene glycol enhances lipoplex-cell association and lipofection.* Biochimica et Biophysica Acta (BBA) - Biomembranes, 1999. **1421**(2): p. 273-283.

37. Ramezani, M., et al., *The influence of size, lipid composition and bilayer fluidity of cationic liposomes on the transfection efficiency of nanolipoplexes.* Colloids and Surfaces B: Biointerfaces, 2009. **72**(1): p. 1-5.

38. Li, D., et al., *The enhancement of transfection efficiency of cationic liposomes by didodecyldimethylammonium bromide coated gold nanoparticles.* Biomaterials, 2010. **31**(7): p. 1850-1857.

39. Prabha, S., et al., *Size-dependency of nanoparticle-mediated gene transfection: studies with fractionated nanoparticles.* International Journal of Pharmaceutics, 2002. **244**(1-2): p. 105-115.

40. Zauner, W., N.A. Farrow, and A.M.R. Haines, *In vitro uptake of polystyrene microspheres: effect of particle size, cell line and cell density.* Journal of Controlled Release, 2001. **71**(1): p. 39-51.

41. Lai, S.K., et al., *Privileged delivery of polymer nanoparticles to the perinuclear region of live cells via a non-clathrin, non-degradative pathway.* Biomaterials, 2007. **28**(18): p. 2876-84.

42. Rejman, J., et al., *Size-dependent internalization of particles via the pathways of clathrin- and caveolae-mediated endocytosis.* Biochem J, 2004. **377**(Pt 1): p. 159-69.

43. Wiethoff, C.M., et al., *Compositional effects of cationic lipid/DNA delivery systems on transgene expression in cell culture.* Journal of Pharmaceutical Sciences, 2004. **93**(1): p. 108-123.

44. He, C., et al., *Effects of particle size and surface charge on cellular uptake and biodistribution of polymeric nanoparticles.* Biomaterials. **In Press, Corrected Proof**.

45. Radwan Almofti, M., et al., *Cationic liposome-mediated gene delivery: Biophysical study and mechanism of internalization.* Archives of Biochemistry and Biophysics, 2003. **410**(2): p. 246-253.

46. Liu, D.X., *Biological factors involved in blood clearance of liposomes by liver.* Advanced Drug Delivery Reviews, 1997. **24**(2-3): p. 201-213.

47. Jung, S.H., et al., *Increased stability in plasma and enhanced cellular uptake of thermally denatured albumin-coated liposomes.* Colloids and Surfaces B: Biointerfaces, 2010. **76**(2): p. 434-440.

48. Caracciolo, G., et al., *Surface adsorption of protein corona controls the cell internalization mechanism of DC-Chol-DOPE/DNA lipoplexes in serum.* Biochimica et Biophysica Acta (BBA) - Biomembranes. **In Press, Corrected Proof**.

49. Schnitzer, J.E., *Caveolae: from basic trafficking mechanisms to targeting transcytosis for tissue-specific drug and gene delivery in vivo.* Advanced Drug Delivery Reviews, 2001. **49**(3): p. 265-280.

50. Champion, J.A., Y.K. Katare, and S. Mitragotri, *Particle shape: A new design parameter for micro- and nanoscale drug delivery carriers.* Journal of Controlled Release, 2007. **121**(1-2): p. 3-9.

51. Gratton, S.E.A., et al., *Nanofabricated particles for engineered drug therapies: A preliminary biodistribution study of PRINT(TM) nanoparticles.* Journal of Controlled Release, 2007. **121**(1-2): p. 10-18.

52. Gratton, S.E.A., et al., *The effect of particle design on cellular internalization pathways.* Proceedings of the National Academy of Sciences of the United States of America, 2008. **105**(33): p. 11613-11618.

53. Sternberg, B., et al., *Ultrastructural characterization of cationic liposome-DNA complexes showing enhanced stability in serum and high transfection activity in vivo.* Biochimica et Biophysica Acta (BBA) - Biomembranes, 1998. **1375**(1-2): p. 23-35.

54. Xu, Y., et al., *Physicochemical Characterization and Purification of Cationic Lipoplexes.* Biophysical Journal, 1999. **77**(1): p. 341-353.

55. Alexander, L., et al., *Dunking doughnuts into cells--selective cellular translocation and in vivo analysis of polymeric micro-doughnuts.* Chem Commun (Camb), 2008(30): p. 3507-9.

56. Decuzzi, P. and M. Ferrari, *The Receptor-Mediated Endocytosis of Nonspherical Particles.* Biophysical Journal, 2008. **94**(10): p. 3790-3797.

57. Liu, G., et al., *Nanoparticles of compacted DNA transfect postmitotic cells.* J Biol Chem, 2003. **278**(35): p. 32578-86.

58. Blessing, T., et al., *Different strategies for formation of pegylated EGF-conjugated PEI/DNA complexes for targeted gene delivery.* Bioconjug Chem, 2001. **12**(4): p. 529-37.

59. Kloeckner, J., et al., *DNA polyplexes based on degradable oligoethylenimine-derivatives: combination with EGF receptor targeting and endosomal release functions.* J Control Release, 2006. **116**(2): p. 115-22.

60. Wolschek, M.F., et al., *Specific systemic nonviral gene delivery to human hepatocellular carcinoma xenografts in SCID mice.* Hepatology, 2002. **36**(5): p. 1106-14.

61. Girão da Cruz, M.T., S. Simões, and M.C. Pedroso de Lima, *Improving lipoplex-mediated gene transfer into C6 glioma cells and primary neurons.* Experimental Neurology, 2004. **187**(1): p. 65-75.

62. Singh, M., A. Hawtrey, and M. Ariatti, *Lipoplexes with biotinylated transferrin accessories: Novel, targeted, serum-tolerant gene carriers.* International Journal of Pharmaceutics, 2006. **321**(1-2): p. 124-137.

63. Tros de Ilarduya, C. and N. Düzgünes, *Efficient gene transfer by transferrin lipoplexes in the presence of serum.* Biochimica et Biophysica Acta (BBA) - Biomembranes, 2000. **1463**(2): p. 333-342.

64. Khalil, I.A., et al., *Octaarginine-modified liposomes: Enhanced cellular uptake and controlled intracellular trafficking.* International Journal of Pharmaceutics, 2008. **354**(1-2): p. 39-48.

65. Fretz, M.M., et al., *OVCAR-3 cells internalize TAT-peptide modified liposomes by endocytosis.* Biochimica et Biophysica Acta (BBA) - Biomembranes, 2004. **1665**(1-2): p. 48-56.

66. Vandenbroucke, R.E., et al., *Cellular entry pathway and gene transfer capacity of TAT-modified lipoplexes.* Biochimica et Biophysica Acta (BBA) - Biomembranes, 2007. **1768**(3): p. 571-579.

67. Mudhakir, D., et al., *A novel IRQ ligand-modified nano-carrier targeted to a unique pathway of caveolar endocytic pathway.* Journal of Controlled Release, 2008. **125**(2): p. 164-173.

68. Fujita, S., et al., *Highly efficient reverse transfection with siRNA in multiple wells of microtiter plates.* Journal of Bioscience and Bioengineering, 2007. **104**(4): p. 329-333.

69. Yoshikawa, T., et al., *Transfection microarray of human mesenchymal stem cells and on-chip siRNA gene knockdown.* Journal of Controlled Release, 2004. **96**(2): p. 227-232.

70. Bengali, Z., et al., *Gene delivery through cell culture substrate adsorbed DNA complexes.* Biotechnol Bioeng, 2005. **90**(3): p. 290-302.

71. Okazaki, A., J.-I. Jo, and Y. Tabata, *A Reverse Transfection Technology to Genetically Engineer Adult Stem Cells.* Tissue Engineering, 2007. **13**(2): p. 245-251.

72. Bengali, Z., et al., *Efficacy of Immobilized Polyplexes and Lipoplexes for Substrate-Mediated Gene Delivery.* Biotechnology and Bioengineering, 2009. **102**(6): p. 1679-1691.

73. Luo, D. and W.M. Saltzman, *Enhancement of transfection by physical concentration of DNA at the cell surface.* Nature Biotechnology, 2000. **18**(8): p. 893-895.

74. Tseng, S.j., C.-J. Chuang, and S.-C. Tang, *Electrostatic immobilization of DNA polyplexes on small intestinal submucosa for tissue substrate-mediated transfection.* Acta Biomaterialia, 2008. **4**(4): p. 799-807.

75. Delehanty, J.B., K.M. Shaffer, and B. Lin, *A comparison of microscope slide substrates for use in transfected cell microarrays.* Biosensors and Bioelectronics, 2004. **20**(4): p. 773-779.

76. Rea, J.C., et al., *Self-assembling peptide-lipoplexes for substrate-mediated gene delivery.* Acta Biomaterialia, 2009. **5**(3): p. 903-912.

77. Zhou, Y.-M., et al., *Deposition transfection technology using a DNA complex with a thermoresponsive cationic star polymer.* Journal of Controlled Release, 2007. **123**(3): p. 239-246.

78. Segura, T. and L.D. Shea, *Surface-tethered DNA complexes for enhanced gene delivery.* Bioconjug Chem, 2002. **13**(3): p. 621-9.

79. Mehrotra, S., I. Lee, and C. Chan, *Multilayer mediated forward and patterned siRNA transfection using linear-PEI at extended N/P ratios.* Acta Biomaterialia, 2009. **5**(5): p. 1474-1488.

80. Pannier, A.K., B.C. Anderson, and L.D. Shea, *Substrate-mediated delivery from self-assembled monolayers: Effect of surface ionization, hydrophilicity, and patterning.* Acta Biomaterialia, 2005. **1**(5): p. 511-522.

81. Pannier, A.K., J.A. Wieland, and L.D. Shea, *Surface polyethylene glycol enhances substrate-mediated gene delivery by nonspecifically immobilized complexes.* Acta Biomaterialia, 2008. **4**(1): p. 26-39.

82. ffrench-Constant, C. and H. Colognato, *Integrins: versatile integrators of extracellular signals.* Trends in Cell Biology, 2004. **14**(12): p. 678-686.

83. Uchimura, E., et al., *Reverse transfection using antibodies against a cell surface antigen in mammalian adherent cell lines.* Journal of Bioscience and Bioengineering, 2007. **104**(2): p. 152-155.

84. Segura, T., P.H. Chung, and L.D. Shea, *DNA delivery from hyaluronic acid-collagen hydrogels via a substrate-mediated approach.* Biomaterials, 2005. **26**(13): p. 1575-1584.

85. Bengali, Z., J.C. Rea, and L.D. Shea, *Gene expression and internalization following vector adsorption to immobilized proteins: dependence on protein identity and density.* Journal of Gene Medicine, 2007. **9**(8): p. 668-678.

86. Boyd, N.D., B.M.C. Chan, and N.O. Petersen, *beta(1) integrins are distributed in adhesion structures with fibronectin and caveolin and in coated pits.*

Biochemistry and Cell Biology-Biochimie Et Biologie Cellulaire, 2003. **81**(5): p. 335-348.

87. De Laporte, L., et al., *Patterned transgene expression in multiple-channel bridges after spinal cord injury.* Acta Biomaterialia. **In Press, Corrected Proof**.

88. De Laporte, L., A. Lei Yan, and L.D. Shea, *Local gene delivery from ECM-coated poly(lactide-co-glycolide) multiple channel bridges after spinal cord injury.* Biomaterials, 2009. **30**(12): p. 2361-2368.

89. Biggs, M.J.P., R.G. Richards, and M.J. Dalby, *Nanotopographical modification: a regulator of cellular function through focal adhesions.* Nanomedicine: Nanotechnology, Biology and Medicine. **In Press, Uncorrected Proof**.

90. Chao, W.T. and J. Kunz, *Focal adhesion disassembly requires clathrin-dependent endocytosis of integrins.* FEBS Lett, 2009. **583**(8): p. 1337-43.

91. Lord, M.S., M. Foss, and F. Besenbacher, *Influence of nanoscale surface topography on protein adsorption and cellular response.* Nano Today. **5**(1): p. 66-78.

92. Carpenter, J., D. Khang, and T.J. Webster, *Nanometer polymer surface features: the influence on surface energy, protein adsorption and endothelial cell adhesion.* Nanotechnology, 2008. **19**(50): p. -.

93. Gonzalez-Garcia, C., et al., *Effect of nanoscale topography on fibronectin adsorption, focal adhesion size and matrix organisation.* Colloids Surf B Biointerfaces. **77**(2): p. 181-90.

94. Chen, H., et al., *The effect of surface microtopography of poly(dimethylsiloxane) on protein adsorption, platelet and cell adhesion.* Colloids and Surfaces B: Biointerfaces, 2009. **71**(2): p. 275-281.

95. Koh, L.B., I. Rodriguez, and S.S. Venkatraman, *The effect of topography of polymer surfaces on platelet adhesion.* Biomaterials, 2010. **31**(7): p. 1533-1545.

96. Hovgaard, M.B., et al., *Fibronectin Adsorption on Tantalum: The Influence of Nanoroughness.* The Journal of Physical Chemistry B, 2008. **112**(28): p. 8241-8249.

97. Lord, M.S., et al., *The effect of silica nanoparticulate coatings on serum protein adsorption and cellular response.* Biomaterials, 2006. **27**(28): p. 4856-4862.

98. Denis, F.A., et al., *Protein Adsorption on Model Surfaces with Controlled Nanotopography and Chemistry.* Langmuir, 2002. **18**(3): p. 819-828.

99. Galli, C., et al., *Protein adsorption on topographically nanostructured titanium.* Surface Science, 2001. **474**(1-3): p. L180-L184.

100. Vertegel, A.A., R.W. Siegel, and J.S. Dordick, *Silica Nanoparticle Size Influences the Structure and Enzymatic Activity of Adsorbed Lysozyme.* Langmuir, 2004. **20**(16): p. 6800-6807.

101. Roach, P., D. Farrar, and C.C. Perry, *Surface Tailoring for Controlled Protein Adsorption: Effect of Topography at the Nanometer Scale and Chemistry.* Journal of the American Chemical Society, 2006. **128**(12): p. 3939-3945.

102. Stephansson, S.N., B.A. Byers, and A.J. García, *Enhanced expression of the osteoblastic phenotype on substrates that modulate fibronectin conformation and integrin receptor binding.* Biomaterials, 2002. **23**(12): p. 2527-2534.

103. Garcia, A.J., M.D. Vega, and D. Boettiger, *Modulation of cell proliferation and differentiation through substrate-dependent changes in fibronectin conformation.* Molecular Biology of the Cell, 1999. **10**(3): p. 785-798.

104. Bae, Y.H., et al., *Minute changes in composition of polymer substrates produce amplified differences in cell adhesion and motility via optimal ligand conditioning.* Acta Biomaterialia, 2006. **2**(5): p. 473-482.

105. Fasbender, A., et al., *A low rate of cell proliferation and reduced DNA uptake limit cationic lipid-mediated gene transfer to primary cultures of ciliated human airway epithelia.* Gene Therapy, 1997. **4**(11): p. 1173-1180.

106. Park, J.S., et al., *Down-regulation of amphiphysin-1 is responsible for reduced receptor-mediated endocytosis in the senescent cells.* Faseb Journal, 2001. **15**(7): p. 1625-+.

107. Park, S.C., *Functional recovery of senescent cells through restoration of receptor-mediated endocytosis.* Mechanisms of Ageing and Development, 2002. **123**(8): p. 917-926.

108. Martinez, E., et al., *Effects of artificial micro- and nano-structured surfaces on cell behaviour.* Annals of Anatomy-Anatomischer Anzeiger, 2009. **191**(1): p. 126-135.

109. Yim, E.K., et al., *Nanopattern-induced changes in morphology and motility of smooth muscle cells.* Biomaterials, 2005. **26**(26): p. 5405-13.

110. Berry, C.C., et al., *The influence of microscale topography on fibroblast attachment and motility.* Biomaterials, 2004. **25**(26): p. 5781-8.

111. Kim, E.J., et al., *Post microtextures accelerate cell proliferation and osteogenesis.* Acta Biomater. **6**(1): p. 160-9.

112. Yim, E.K., S.W. Pang, and K.W. Leong, *Synthetic nanostructures inducing differentiation of human mesenchymal stem cells into neuronal lineage.* Experimental Cell Research, 2007. **313**(9): p. 1820-1829.

113. Engler, A.J., et al., *Matrix Elasticity Directs Stem Cell Lineage Specification.* Cell, 2006. **126**(4): p. 677-689.

114. Markert, L.D., et al., *Identification of Distinct Topographical Surface Microstructures Favoring Either Undifferentiated Expansion or Differentiation of Murine Embryonic Stem Cells.* Stem Cells and Development, 2009. **18**(9): p. 1331-1342.

115. Lovmand, J., et al., *The use of combinatorial topographical libraries for the screening of enhanced osteogenic expression and mineralization.* Biomaterials, 2009. **30**(11): p. 2015-2022.

116. Washbourne, P. and A.K. McAllister, *Techniques for gene transfer into neurons.* Current Opinion in Neurobiology, 2002. **12**(5): p. 566-573.

117. Van De Parre, T.J.L., et al., *mRNA but not plasmid DNA is efficiently transfected in murine J774A.1 macrophages.* Biochemical and Biophysical Research Communications, 2005. **327**(1): p. 356-360.

118. Lenz, P., et al., *Nucleoporation of dendritic cells: efficient gene transfer by electroporation into human monocyte-derived dendritic cells.* FEBS Letters, 2003. **538**(1-3): p. 149-154.

119. Qureshi, H.Y., R. Ahmad, and M. Zafarullah, *High-efficiency transfection of nucleic acids by the modified calcium phosphate precipitation method in chondrocytes.* Analytical Biochemistry, 2008. **382**(2): p. 138-140.

120. Jiang, Z.Y., et al., *Insulin signaling through Akt/protein kinase B analyzed by small interfering RNA-mediated gene silencing.* Proceedings of the National Academy of Sciences of the United States of America, 2003. **100**(13): p. 7569-7574.

121. Cho, K.A. and S.C. Park, *Caveolin-1 as a prime modulator of aging: a new modality for phenotypic restoration?* Mechanisms of Ageing and Development, 2005. **126**(1): p. 105-110.

122. Perdue, N. and Q. Yan, *Caveolin-1 is up-regulated in transdifferentiated lens epithelial cells but minimal in normal human and murine lenses.* Experimental Eye Research, 2006. **83**(5): p. 1154-1161.

123. Prawitt, J., et al., *Characterization of lipid metabolism in insulin-sensitive adipocytes differentiated from immortalized human mesenchymal stem cells.* Experimental Cell Research, 2008. **314**(4): p. 814-824.

124. McFarland, D.C., et al., *Variation in fibroblast growth factor response and heparan sulfate proteoglycan production in satellite cell populations.* Comparative Biochemistry and Physiology C-Toxicology & Pharmacology, 2003. **134**(3): p. 341-351.

125. Loesberg, W.A., et al., *The threshold at which substrate nanogroove dimensions may influence fibroblast alignment and adhesion.* Biomaterials, 2007. **28**(27): p. 3944-3951.

126. Dalby, M.J., et al., *Nucleus alignment and cell signaling in fibroblasts: response to a micro-grooved topography.* Exp Cell Res, 2003. **284**(2): p. 274-82.

127. Dalby, M.J., et al., *Use of nanotopography to study mechanotransduction in fibroblasts - methods and perspectives.* European Journal of Cell Biology, 2004. **83**(4): p. 159-169.

128. Chalut, K.J., et al., *Label-free, high-throughput measurements of dynamic changes in cell nuclei using angle-resolved low coherence interferometry.* Biophysical Journal, 2008. **94**(12): p. 4948-4956.

129. Chalut, K.J., et al., *Deformation of stem cell nuclei by nanotopographical cues.* Soft Matter, 2010. **6**(8): p. 1675-1681.

130. Le Beyec, J., et al., *Cell shape regulates global histone acetylation in human mammary epithelial cells.* Experimental Cell Research, 2007. **313**(14): p. 3066-3075.

131. Dalby, M.J., et al., *Nucleus alignment and cell signaling in fibroblasts: response to a micro-grooved topography.* Experimental Cell Research, 2003. **284**(2): p. 272-280.

132. Collinet, C., et al., *Systems survey of endocytosis by multiparametric image analysis.* Nature. **464**(7286): p. 243-249.

133. Dalby, M.J., et al., *Fibroblast signaling events in response to nanotopography: a gene array study.* IEEE Trans Nanobioscience, 2002. **1**(1): p. 12-7.

134. Dalby, M.J., et al., *Increasing fibroblast response to materials using nanotopography: morphological and genetic measurements of cell response to 13-nm-high polymer demixed islands.* Experimental Cell Research, 2002. **276**(1): p. 1-9.

135. Seabra, M.C., *Nucleotide Dependence of Rab Geranylgeranylation.* Journal of Biological Chemistry, 1996. **271**(24): p. 14398-14404.

136. Dalby, M.J., et al., *Attempted endocytosis of nano-environment produced by colloidal lithography by human fibroblasts.* Experimental Cell Research, 2004. **295**(2): p. 387-394.

137. Dalby, M.J., N. Gadegaard, and C.D.W. Wilkinson, *The response of fibroblasts to hexagonal nanotopography fabricated by electron beam lithography.* Journal of Biomedical Materials Research Part A, 2008. **84A**(4): p. 973-979.

138. Chen, H., et al., *The Interaction of Epsin and Eps15 with the Clathrin Adaptor AP-2 Is Inhibited by Mitotic Phosphorylation and Enhanced by Stimulation-dependent Dephosphorylation in Nerve Terminals.* Journal of Biological Chemistry, 1999. **274**(6): p. 3257-3260.

139. Barbieri, M.A., et al., *Epidermal Growth Factor and Membrane Trafficking.* The Journal of Cell Biology, 2000. **151**(3): p. 539-550.

140. Tzanakakis, G.N., N.K. Karamanos, and A. Hjerpe, *Effects on glycosaminoglycan synthesis in cultured human mesothelioma cells of transforming, epidermal, and fibroblast growth factors and their combinations with platelet-derived growth factor.* Exp Cell Res, 1995. **220**(1): p. 130-7.

141. Chen, S.L., et al., *Characterization of topographical effects on macrophage behavior in a foreign body response model.* Biomaterials, 2010. **31**(13): p. 3479-3491.

142. Xia, W., et al., *TGF-[beta]3 and TNF[alpha] perturb blood-testis barrier (BTB) dynamics by accelerating the clathrin-mediated endocytosis of integral membrane proteins: A new concept of BTB regulation during spermatogenesis.* Developmental Biology, 2009. **327**(1): p. 48-61.

143. Martinez, I., et al., *Differential Cytokine-Mediated Modulation of Endocytosis in Rat Liver Endothelial Cells.* Biochemical and Biophysical Research Communications, 1995. **212**(1): p. 235-241.

144. Decuzzi, P. and M. Ferrari, *Modulating cellular adhesion through nanotopography.* Biomaterials, 2010. **31**(1): p. 173-179.

145. Ranella, A., et al., *Tuning cell adhesion by controlling the roughness and wettability of 3D micro/nano silicon structures.* Acta Biomater.

146. Dalby, M.J., et al., *Polymer-demixed nanotopography: control of fibroblast spreading and proliferation.* Tissue Eng, 2002. **8**(6): p. 1099-108.

147. Dalby, M.J., et al., *In vitro reaction of endothelial cells to polymer demixed nanotopography.* Biomaterials, 2002. **23**(14): p. 2945-2954.

148. Cavalcanti-Adam, E.A., et al., *Cell spreading and focal adhesion dynamics are regulated by spacing of integrin ligands.* Biophysical Journal, 2007. **92**(8): p. 2964-2974.

149. Wary, K.K., et al., *A requirement for caveolin-1 and associated kinase Fyn in integrin signaling and anchorage-dependent cell growth.* Cell, 1998. **94**(5): p. 625-634.

150. Echarri, A., O. Muriel, and M.A. Del Pozo, *Intracellular trafficking of raft/caveolae domains: Insights from integrin signaling.* Seminars in Cell & Developmental Biology, 2007. **18**(5): p. 627-637.

151. Echarri, A. and M.A. Del Pozo, *Caveolae internalization regulates integrin-dependent signaling pathways.* Cell Cycle, 2006. **5**(19): p. 2179-82.

152. del Pozo, M.A., et al., *Integrins regulate Rac targeting by internalization of membrane domains.* Science, 2004. **303**(5659): p. 839-842.

153. Gallagher, J.O., et al., *Interaction of animal cells with ordered nanotopography.* IEEE Trans Nanobioscience, 2002. **1**(1): p. 24-8.

154. Dalby, M.J., et al., *Osteoprogenitor response to defined topographies with nanoscale depths.* Biomaterials, 2006. **27**(8): p. 1306-15.

155. Yim, E.K., et al., *Nanotopography-induced changes in focal adhesions, cytoskeletal organization, and mechanical properties of human mesenchymal stem cells.* Biomaterials. **31**(6): p. 1299-306.

156. Cukierman, E., et al., *Taking Cell-Matrix Adhesions to the Third Dimension.* Science, 2001. **294**(5547): p. 1708-1712.

157. Mao, Y. and J.E. Schwarzbauer, *Stimulatory effects of a three-dimensional microenvironment on cell-mediated fibronectin fibrillogenesis.* J Cell Sci, 2005. **118**(Pt 19): p. 4427-36.

158. Sottile, J. and J. Chandler, *Fibronectin matrix turnover occurs through a caveolin-1-dependent process.* Molecular Biology of the Cell, 2005. **16**(2): p. 757-768.

159. Wiesner, S., A. Lange, and R. Fassler, *Local call: from integrins to actin assembly.* Trends Cell Biol, 2006. **16**(7): p. 327-9.

160. Jeng, R.L. and M.D. Welch, *Cytoskeleton: Actin and endocytosis - no longer the weakest link.* Current Biology, 2001. **11**(17): p. R691-R694.

161. Bader, M.F., et al., *Coupling actin and membrane dynamics during calcium-regulated exocytosis: a role for Rho and ARF GTPases.* Biochimica Et Biophysica Acta-Molecular Cell Research, 2004. **1742**(1-3): p. 37-49.

162. McPherson, P.S., *The endocytic machinery at an interface with the actin cytoskeleton: a dynamic, hip intersection.* Trends in Cell Biology, 2002. **12**(7): p. 312-315.

163. Kopatz, I., J.-S. Remy, and J.-P. Behr, *A model for non-viral gene delivery: through syndecan adhesion molecules and powered by actin.* The Journal of Gene Medicine, 2004. **6**(7): p. 769-776.

164. Singec, I., *Cell Therapy for Neurodegenerative Disorders*, in *Regenerative Medicine and Cell Therapy*, H. Baharvand and N. Aghdami, Editors. 2013, Humana Press. p. 1-22.

165. Lunn, J.S., et al., *Stem cell technology for neurodegenerative diseases.* Ann Neurol, 2011. **70**(3): p. 353-61.

166. 4/19/2014]; Alzheimer's Facts and Figures]. Available from: https://www.alz.org/alzheimers_disease_facts_and_figures.asp.

167. Eby, D.W., et al., *Driving behaviors in early stage dementia: a study using in-vehicle technology.* Accident Analysis & Prevention, 2012. **49**: p. 330-337.

168. Molsa, P.K., R.J. Marttila, and U.K. Rinne, *Survival and cause of death in Alzheimer's disease and multi-infarct dementia.* Acta Neurol Scand, 1986. **74**(2): p. 103-7.

169. Gu, H., *Stem Cell-Derived Dopamine Neurons for the Treatment of Neurodegenerative Diseases.* Clinical Pharmacology & Biopharmaceutics.

170. Glat, M.J. and D. Offen, *Cell and gene therapy in Alzheimer's disease.* Stem Cells Dev, 2013. **22**(10): p. 1490-6.

171. Gao, A., et al., *Potential therapeutic applications of differentiated induced pluripotent stem cells (iPSCs) in the treatment of neurodegenerative diseases.* Neuroscience, 2013. **228**: p. 47-59.

172. Dorsey, E., et al., *Projected number of people with Parkinson disease in the most populous nations, 2005 through 2030.* Neurology, 2007. **68**(5): p. 384-386.

173. Poewe, W., *The natural history of Parkinson's disease.* J Neurol, 2006. **253 Suppl 7**: p. VII2-6.

174. Ma, V.Y., L. Chan, and K.J. Carruthers, *The Incidence, Prevalence, Costs and Impact on Disability of Common Conditions Requiring Rehabilitation in the US:*

Stroke, Spinal Cord Injury, Traumatic Brain Injury, Multiple Sclerosis, Osteoarthritis, Rheumatoid Arthritis, Limb Loss, and Back Pain. Archives of Physical Medicine and Rehabilitation, (0).

175. Minden, S.L., et al., *The Sonya Slifka Longitudinal Multiple Sclerosis Study: methods and sample characteristics.* Mult Scler, 2006. **12**(1): p. 24-38.

176. Tsang, B.K. and R. Macdonell, *Multiple sclerosis- diagnosis, management and prognosis.* Aust Fam Physician, 2011. **40**(12): p. 948-55.

177. Jacobs, L.D., et al., *Intramuscular interferon beta ‐1a for disease progression in relapsing multiple sclerosis.* Annals of neurology, 1996. **39**(3): p. 285-294.

178. O'Connor, P., et al., *Randomized trial of oral teriflunomide for relapsing multiple sclerosis.* New England Journal of Medicine, 2011. **365**(14): p. 1293-1303.

179. Kappos, L., et al., *A placebo-controlled trial of oral fingolimod in relapsing multiple sclerosis.* New England Journal of Medicine, 2010. **362**(5): p. 387-401.

180. El-Etr, M., et al., *Hormonal influences in multiple sclerosis: new therapeutic benefits for steroids.* Maturitas, 2011. **68**(1): p. 47-51.

181. Kimiskidis, V. and A. Fassas, *Stem Cell-based Therapies in Multiple Sclerosis.* J Genet Syndr Gene Ther S, 2013. **3**: p. 2.

182. Geerts, H., *Of mice and men: bridging the translational disconnect in CNS drug discovery.* CNS Drugs, 2009. **23**(11): p. 915-26.

183. Mingozzi, F. and K.A. High, *Therapeutic in vivo gene transfer for genetic disease using AAV: progress and challenges.* Nat Rev Genet, 2011. **12**(5): p. 341-355.

184. Ginn, S.L., et al., *Gene therapy clinical trials worldwide to 2012 - an update.* J Gene Med, 2013. **15**(2): p. 65-77.

185. Cartier, N., et al., *Hematopoietic stem cell gene therapy with a lentiviral vector in X-linked adrenoleukodystrophy.* Science, 2009. **326**(5954): p. 818-823.

186. Simonelli, F., et al., *Gene therapy for Leber's congenital amaurosis is safe and effective through 1.5 years after vector administration.* Molecular Therapy, 2010. **18**(3): p. 643-650.

187. Testa, F., et al., *Three-year follow-up after unilateral subretinal delivery of adeno-associated virus in patients with Leber congenital Amaurosis type 2.* Ophthalmology, 2013. **120**(6): p. 1283-91.

188. Weinberg, M.S., R.J. Samulski, and T.J. McCown, *Adeno-associated virus (AAV) gene therapy for neurological disease.* Neuropharmacology, 2013. **69**: p. 82-8.

189. Kaplitt, M.G., et al., *Safety and tolerability of gene therapy with an adeno-associated virus (AAV) borne< i> GAD</i> gene for Parkinson's disease: an open label, phase I trial.* The Lancet, 2007. **369**(9579): p. 2097-2105.

190. Bakay, R.A., et al., *Analyses of a phase 1 clinical trial of adeno-associated virus-nerve growth factor (CERE-110) gene therapy in Alzheimer's disease: 866.* Neurosurgery, 2007. **61**(1): p. 216.

191. Marks Jr, W.J., et al., *Gene delivery of AAV2-neurturin for Parkinson's disease: a double-blind, randomised, controlled trial.* The Lancet Neurology, 2010. **9**(12): p. 1164-1172.

192. During, M.J., et al., *Subthalamic GAD gene transfer in Parkinson disease patients who are candidates for deep brain stimulation.* Hum Gene Ther, 2001. **12**(12): p. 1589-91.

193. Eberling, J., et al., *Results from a phase I safety trial of hAADC gene therapy for Parkinson disease.* Neurology, 2008. **70**(21): p. 1980-1983.

194. Tuszynski, M.H., *Nerve growth factor gene therapy in Alzheimer disease.* Alzheimer Dis Assoc Disord, 2007. **21**(2): p. 179-89.

195. Tuszynski, M.H., et al., *A phase 1 clinical trial of nerve growth factor gene therapy for Alzheimer disease.* Nature medicine, 2005. **11**(5): p. 551-555.

196. Hacein-Bey-Abina, S., et al., *Insertional oncogenesis in 4 patients after retrovirus-mediated gene therapy of SCID-X1.* The Journal of clinical investigation, 2008. **118**(9): p. 3132-3142.

197. Therapy, E.S.o.G., *One of three successfully treated CGD patients in a Swiss-German gene therapy trial died due to his underlying disease: A position statement from the European Society of Gene Therapy (ESGT).* The Journal of Gene Medicine, 2006. **8**(12): p. 1435.

198. Cavazzana-Calvo, M., et al., *Transfusion independence and hmga2 activation after gene therapy of human [bgr]-thalassaemia.* Nature, 2010. **467**(7313): p. 318-322.

199. Manno, C.S., et al., *Successful transduction of liver in hemophilia by AAV-Factor IX and limitations imposed by the host immune response.* Nature medicine, 2006. **12**(3): p. 342-347.

200. Shimamura, M., et al., *Plasmid DNA-based gene therapy in neurological disorders.* Plasmid, 2013: p. 46-56.

201. Garren, H., et al., *Phase 2 trial of a DNA vaccine encoding myelin basic protein for multiple sclerosis.* Annals of neurology, 2008. **63**(5): p. 611-620.

202. Edelstein, M.L., M.R. Abedi, and J. Wixon, *Gene therapy clinical trials worldwide to 2007—an update.* The Journal of Gene Medicine, 2007. **9**(10): p. 833-842.

203. Ropper, A.H., et al., *Vascular endothelial growth factor gene transfer for diabetic polyneuropathy: a randomized, double-blinded trial.* Ann Neurol, 2009. **65**(4): p. 386-93.

204. Yan, J., et al., *Extensive neuronal differentiation of human neural stem cell grafts in adult rat spinal cord.* PLoS medicine, 2007. **4**(2): p. e39.

205. Moghadam, F.H., et al., *Transplantation of primed or unprimed mouse embryonic stem cell-derived neural precursor cells improves cognitive function in Alzheimerian rats.* Differentiation, 2009. **78**(2): p. 59-68.

206. Gage, F.H., et al., *Intrahippocampal septal grafts ameliorate learning impairments in aged rats.* Science, 1984. **225**(4661): p. 533-6.

207. Xuan, A.G., et al., *Effects of engrafted neural stem cells in Alzheimer's disease rats.* Neurosci Lett, 2009. **450**(2): p. 167-71.

208. Freed, C.R., et al., *Transplantation of embryonic dopamine neurons for severe Parkinson's disease.* N Engl J Med, 2001. **344**(10): p. 710-9.

209. Mendez, I., et al., *Simultaneous intrastriatal and intranigral fetal dopaminergic grafts in patients with Parkinson disease: a pilot study. Report of three cases.* J Neurosurg, 2002. **96**(3): p. 589-96.

210. Peschanski, M., et al., *Bilateral motor improvement and alteration of L-dopa effect in two patients with Parkinson's disease following intrastriatal transplantation of foetal ventral mesencephalon.* Brain, 1994. **117 (Pt 3)**: p. 487-99.

211. Lindvall, O., et al., *Grafts of fetal dopamine neurons survive and improve motor function in Parkinson's disease.* Science, 1990. **247**(4942): p. 574-7.

212. Astradsson, A., et al., *Recent advances in cell-based therapy for Parkinson disease.* Neurosurg Focus, 2008. **24**(3-4): p. E6.

213. Olanow, C.W., et al., *A double-blind controlled trial of bilateral fetal nigral transplantation in Parkinson's disease.* Ann Neurol, 2003. **54**(3): p. 403-14.

214. Wernig, M., et al., *Neurons derived from reprogrammed fibroblasts functionally integrate into the fetal brain and improve symptoms of rats with Parkinson's disease.* Proc Natl Acad Sci U S A, 2008. **105**(15): p. 5856-61.

215. Ben-Hur, T., N. Fainstein, and Y. Nishri, *Cell-Based Reparative Therapies for Multiple Sclerosis.* Current neurology and neuroscience reports, 2013. **13**(11): p. 1-7.

216. Ben‐Hur, T., et al., *Transplanted multipotential neural precursor cells migrate into the inflamed white matter in response to experimental autoimmune encephalomyelitis.* Glia, 2003. **41**(1): p. 73-80.

217. Ben‐Hur, T., et al., *Serial in vivo MR tracking of magnetically labeled neural spheres transplanted in chronic EAE mice.* Magnetic Resonance in Medicine, 2007. **57**(1): p. 164-171.

218. Keirstead, H., et al., *Polysialylated neural cell adhesion molecule-positive CNS precursors generate both oligodendrocytes and Schwann cells to remyelinate the CNS after transplantation.* The Journal of neuroscience, 1999. **19**(17): p. 7529-7536.

219. Duncan, I., *Remyelination and restoration of axonal function by glial cell transplantation*, in *Opportunities and Challenges of the Therapies Targeting CNS Regeneration*. 2005, Springer. p. 115-132.

220. Wang, S., et al., *Human iPSC-derived oligodendrocyte progenitor cells can myelinate and rescue a mouse model of congenital hypomyelination.* Cell Stem Cell, 2013. **12**(2): p. 252-264.

221. Nussbaum, J.M., M.E. Seward, and G.S. Bloom, *Alzheimer disease: A tale of two prions.* Prion. **7**(1): p. 14.

222. Olanow, C.W. and S.B. Prusiner, *Is Parkinson's disease a prion disorder?* Proceedings of the National Academy of Sciences, 2009. **106**(31): p. 12571-12572.

223. Prineas, J., et al., *Multiple sclerosis: Remyelination of nascent lesions: Remyelination of nascent lesions.* Annals of neurology, 1993. **33**(2): p. 137-151.

224. Scolding, N., et al., *Oligodendrocyte progenitors are present in the normal adult human CNS and in the lesions of multiple sclerosis.* Brain, 1998. **121**(12): p. 2221-2228.

225. Wolswijk, G., *Oligodendrocyte precursor cells in the demyelinated multiple sclerosis spinal cord.* Brain, 2002. **125**(2): p. 338-349.

226. Blakemore, W. and K. Irvine, *Endogenous or exogenous oligodendrocytes for remyelination.* Journal of the neurological sciences, 2008. **265**(1): p. 43-46.

227. Takahashi, K. and S. Yamanaka, *Induction of pluripotent stem cells from mouse embryonic and adult fibroblast cultures by defined factors.* Cell, 2006. **126**(4): p. 663-76.

228. Amariglio, N., et al., *Donor-derived brain tumor following neural stem cell transplantation in an ataxia telangiectasia patient.* PLoS medicine, 2009. **6**(2): p. e1000029.

229. Roy, N.S., et al., *Functional engraftment of human ES cell–derived dopaminergic neurons enriched by coculture with telomerase-immortalized midbrain astrocytes.* Nature medicine, 2006. **12**(11): p. 1259-1268.

230. Lane, E.L., et al., *Neural grafting in Parkinson's disease unraveling the mechanisms underlying graft-induced dyskinesia.* Prog Brain Res, 2010. **184**: p. 295-309.

231. Barker, R.A. and W.-L. Kuan, *Graft-induced dyskinesias in Parkinson's disease: what is it all about?* Cell Stem Cell, 2010. **7**(2): p. 148-149.

232. Ohnishi, K., et al., *Premature Termination of Reprogramming In Vivo Leads to Cancer Development through Altered Epigenetic Regulation.* Cell, 2014. **156**(4): p. 663-677.

233. Chen, Y., et al., *Genome-wide CNV analysis in mouse induced pluripotent stem cells reveals dosage effect of pluripotent factors on genome integrity.* BMC Genomics, 2014. **15**: p. 79.

234. McCarroll, S.A. and D.M. Altshuler, *Copy-number variation and association studies of human disease.* Nature genetics, 2007. **39**: p. S37-S42.

235. Lee, J.A. and J.R. Lupski, *Genomic rearrangements and gene copy-number alterations as a cause of nervous system disorders.* Neuron, 2006. **52**(1): p. 103-121.

236. Biasco, L., C. Baricordi, and A. Aiuti, *Retroviral Integrations in Gene Therapy Trials.* Mol Ther, 2012.

237. Zhao, T., et al., *Immunogenicity of induced pluripotent stem cells.* Nature, 2011. **474**(7350): p. 212-5.

238. Park, H.J., et al., *Nonviral delivery for reprogramming to pluripotency and differentiation.* Arch Pharm Res, 2014. **37**(1): p. 107-19.

239. Yu, J., et al., *Human induced pluripotent stem cells free of vector and transgene sequences.* Science, 2009. **324**(5928): p. 797-801.

240. Kim, D., et al., *Generation of human induced pluripotent stem cells by direct delivery of reprogramming proteins.* Cell Stem Cell, 2009. **4**(6): p. 472-6.

241. Okita, K., et al., *Generation of mouse induced pluripotent stem cells without viral vectors.* Science, 2008. **322**(5903): p. 949-953.

242. Montserrat, N., et al., *Simple Generation of Human Induced Pluripotent Stem Cells Using Poly-β-amino Esters As the Non-viral Gene Delivery System.* Journal of Biological Chemistry, 2011. **286**(14): p. 12417-12428.

243. Gonzalez, F., et al., *Generation of mouse-induced pluripotent stem cells by transient expression of a single nonviral polycistronic vector.* Proc Natl Acad Sci U S A, 2009. **106**(22): p. 8918-22.

244. Drews, K., et al., *The cytotoxic and immunogenic hurdles associated with non-viral mRNA-mediated reprogramming of human fibroblasts.* Biomaterials, 2012. **33**(16): p. 4059-68.

245. Warren, L., et al., *Highly efficient reprogramming to pluripotency and directed differentiation of human cells with synthetic modified mRNA.* Cell Stem Cell, 2010. **7**(5): p. 618-30.

246. Kues, W.A., et al., *Derivation and characterization of sleeping beauty transposon-mediated porcine induced pluripotent stem cells.* Stem Cells Dev, 2013. **22**(1): p. 124-35.

247. Woltjen, K., et al., *piggyBac transposition reprograms fibroblasts to induced pluripotent stem cells.* Nature, 2009. **458**(7239): p. 766-70.

248. Kaji, K., et al., *Virus-free induction of pluripotency and subsequent excision of reprogramming factors.* Nature, 2009. **458**(7239): p. 771-5.

249. Ivics, Z., et al., *Targeted Sleeping Beauty Transposition in Human Cells.* Mol Ther, 2007. **15**(6): p. 1137-1144.

250. Owens, J.B., et al., *Transcription activator like effector (TALE)-directed piggyBac transposition in human cells.* Nucleic acids research. **41**(19): p. 9197-9207.

251. Vierbuchen, T., et al., *Direct conversion of fibroblasts to functional neurons by defined factors.* Nature, 2010. **463**(7284): p. 1035-41.

252. Pang, Z.P.P., et al., *Induction of human neuronal cells by defined transcription factors.* Nature, 2011. **476**(7359): p. 220-U122.

253. Pfisterer, U., et al., *Direct conversion of human fibroblasts to dopaminergic neurons.* Proceedings of the National Academy of Sciences of the United States of America, 2011. **108**(25): p. 10343-10348.

254. Caiazzo, M., et al., *Direct generation of functional dopaminergic neurons from mouse and human fibroblasts.* Nature, 2011. **476**(7359): p. 224-U151.

255. Liu, X., et al., *Direct reprogramming of human fibroblasts into dopaminergic neuron-like cells.* Cell Res, 2012. **22**(2): p. 321-32.

256. Kim, J., et al., *Functional Integration of Dopaminergic Neurons Directly Converted from Mouse Fibroblasts.* Cell Stem Cell, 2011. **9**(5): p. 413-419.

257. Addis, R.C., et al., *Efficient conversion of astrocytes to functional midbrain dopaminergic neurons using a single polycistronic vector.* PLoS One, 2011. **6**(12): p. e28719.

258. Son, E.Y., et al., *Conversion of Mouse and Human Fibroblasts into Functional Spinal Motor Neurons.* Cell Stem Cell, 2011. **9**(3): p. 205-218.

259. Qiang, L., et al., *Directed conversion of Alzheimer's disease patient skin fibroblasts into functional neurons.* Cell, 2011. **146**(3): p. 359-71.

260. Marro, S., et al., *Direct Lineage Conversion of Terminally Differentiated Hepatocytes to Functional Neurons.* Cell Stem Cell, 2011. **9**(4): p. 374-382.

261. Karow, M., et al., *Reprogramming of pericyte-derived cells of the adult human brain into induced neuronal cells.* Cell Stem Cell, 2012. **11**(4): p. 471-476.

262. Ambasudhan, R., et al., *Direct Reprogramming of Adult Human Fibroblasts to Functional Neurons under Defined Conditions.* Cell Stem Cell, 2011. **9**(2): p. 113-118.

263. Yoo, A.S., et al., *MicroRNA-mediated conversion of human fibroblasts to neurons.* Nature, 2011. **476**(7359): p. 228-31.

264. Xue, Y., et al., *Direct conversion of fibroblasts to neurons by reprogramming PTB-regulated microRNA circuits.* Cell, 2013. **152**(1): p. 82-96.

265. Sharp, J., et al., *Derivation of oligodendrocyte progenitor cells from human embryonic stem cells.* Methods Mol Biol, 2011. **767**: p. 399-409.

266. Lujan, E., et al., *Direct conversion of mouse fibroblasts to self-renewing, tripotent neural precursor cells.* Proc Natl Acad Sci U S A. **109**(7): p. 2527-32.

267. Lujan, E. and M. Wernig, *The many roads to Rome: induction of neural precursor cells from fibroblasts.* Curr Opin Genet Dev, 2012. **22**(5): p. 517-22.

268. Yang, N., et al., *Generation of oligodendroglial cells by direct lineage conversion.* Nat Biotechnol, 2013. **31**(5): p. 434-9.

269. Najm, F.J., et al., *Transcription factor-mediated reprogramming of fibroblasts to expandable, myelinogenic oligodendrocyte progenitor cells.* Nat Biotechnol. **31**(5): p. 426-33.

270. Singec, I. and A. Quiñones-Hinojosa, *7 Neurospheres.* Cold Spring Harbor Monograph Archive, 2008. **52**: p. 119-134.

271. Chanda, S., et al., *Neurons generated by direct conversion of fibroblasts reproduce synaptic phenotype caused by autism-associated neuroligin-3 mutation.* Proceedings of the National Academy of Sciences, 2013. **110**(41): p. 16622-16627.

272. Amamoto, R. and P. Arlotta, *Development-inspired reprogramming of the mammalian central nervous system.* Science, 2014. **343**(6170): p. 1239882.

273. Guo, Z., et al., *In Vivo Direct Reprogramming of Reactive Glial Cells into Functional Neurons after Brain Injury and in an Alzheimer's Disease Model.* Cell Stem Cell, 2013.

274. Torper, O., et al., *Generation of induced neurons via direct conversion in vivo.* Proc Natl Acad Sci U S A, 2013. **110**(17): p. 7038-43.

275. Rouaux, C. and P. Arlotta, *Direct lineage reprogramming of post-mitotic callosal neurons into corticofugal neurons in vivo.* Nature cell biology, 2013. **15**(2): p. 214-221.

276. De la Rossa, A., et al., *In vivo reprogramming of circuit connectivity in postmitotic neocortical neurons.* Nat Neurosci, 2013. **16**(2): p. 193-200.

277. Lu, J., et al., *Generation of integration-free and region-specific neural progenitors from primate fibroblasts.* Cell Rep, 2013. **3**(5): p. 1580-91.

278. Shi, Z., et al., *Retinoic acid receptor gamma (Rarg) and nuclear receptor subfamily 5, group A, member 2 (Nr5a2) promote conversion of fibroblasts to functional neurons.* J Biol Chem, 2014.

279. Addis, R.C., *Emerging Cell Therapies.* Cell, 2012. **2012**.

280. Maucksch, C., et al., *Non-viral generation of neural precursor-like cells from adult human fibroblasts.* J Stem Cells Regen Med, 2012. **8**: p. 162-170.

281. Adler, A.F., Grigsby, C.L., Kulangara, K., Wang, H., Yasuda, R., Leong K.W., *Nonviral Direct Conversion of Primary Mouse Embryonic Fibroblasts to Neuronal Cells.* Molecular Therapy-Nucleic Acids, 2012. **1**(e32).

282. Wapinski, O.L., et al., *Hierarchical mechanisms for direct reprogramming of fibroblasts to neurons.* Cell, 2013. **155**(3): p. 621-635.

283. Vierbuchen, T. and M. Wernig, *Molecular roadblocks for cellular reprogramming.* Mol Cell, 2012. **47**(6): p. 827-38.

284. Gaetz, J., et al., *Evidence for a critical role of gene occlusion in cell fate restriction.* Cell Res, 2012. **22**(5): p. 848-858.

285. Ladewig, J., P. Koch, and O. Brustle, *Leveling Waddington: the emergence of direct programming and the loss of cell fate hierarchies.* Nat Rev Mol Cell Biol, 2013. **14**(4): p. 225-36.

286. Tursun, B., et al., *Direct Conversion of C. elegans Germ Cells into Specific Neuron Types.* Science, 2011. **331**(6015): p. 304-308.

287. Chiu, C.P. and H.M. Blau, *5-Azacytidine permits gene activation in a previously noninducible cell type.* Cell, 1985. **40**(2): p. 417-24.

288. Lassar, A.B., B.M. Paterson, and H. Weintraub, *Transfection of a DNA locus that mediates the conversion of 10T12 fibroblasts to myoblasts.* Cell, 1986. **47**(5): p. 649-656.

289. Davis, R.L., H. Weintraub, and A.B. Lassar, *Expression of a single transfected cDNA converts fibroblasts to myoblasts.* Cell, 1987. **51**(6): p. 987-1000.

290. Weintraub, H., et al., *Activation of muscle-specific genes in pigment, nerve, fat, liver, and fibroblast cell lines by forced expression of MyoD.* Proc Natl Acad Sci U S A, 1989. **86**(14): p. 5434-8.

291. Feng, B., et al., *Molecules that promote or enhance reprogramming of somatic cells to induced pluripotent stem cells.* Cell Stem Cell, 2009. **4**(4): p. 301-312.

292. Nie, B., et al., *Cellular reprogramming: a small molecule perspective.* Curr Opin Cell Biol, 2012. **24**(6): p. 784-92.

293. Armond, J.W., et al., *A stochastic model dissects cell states in biological transition processes.* Sci Rep, 2014. **4**: p. 3692.

294. Guo, S., et al., *Nonstochastic reprogramming from a privileged somatic cell state.* Cell, 2014. **156**(4): p. 649-62.

295. Liu, M.-L., et al., *Small molecules enable neurogenin 2 to efficiently convert human fibroblasts into cholinergic neurons.* Nature communications, 2013. **4**.

296. Bertrand, N., D.S. Castro, and F. Guillemot, *Proneural genes and the specification of neural cell types.* Nature Reviews Neuroscience, 2002. **3**(7): p. 517-530.

297. Webb, A.E., et al., *FOXO3 shares common targets with ASCL1 genome-wide and inhibits ASCL1-dependent neurogenesis.* Cell Rep, 2013. **4**(3): p. 477-91.

298. Perez-Pinera, P., et al., *RNA-guided gene activation by CRISPR-Cas9-based transcription factors.* Nat Methods, 2013. **10**(10): p. 973-6.

299. Lin, J., et al., *Microenvironment-evoked cell lineage conversion: Shifting the focus from internal reprogramming to external forcing.* Ageing Res Rev, 2013. **12**(1): p. 29-38.

300. Millet, C., et al., *A negative feedback control of TGF-beta signaling by GSK3-mediated Smad3 linker phosphorylation at Ser204.* Journal of Biological Chemistry, 2009.

301. Ladewig, J., et al., *Small molecules enable highly efficient neuronal conversion of human fibroblasts.* Nature methods, 2012. **9**(6): p. 575-578.

302. Ichida, J.K., et al., *A small-molecule inhibitor of tgf-Beta signaling replaces sox2 in reprogramming by inducing nanog.* Cell Stem Cell, 2009. **5**(5): p. 491-503.

303. Wang, H., et al., *Small Molecules Enable Cardiac Reprogramming of Mouse Fibroblasts with a Single Factor, Oct4.* Cell reports, 2014.

304. Ifkovits, J.L., et al., *Inhibition of TGFβ Signaling Increases Direct Conversion of Fibroblasts to Induced Cardiomyocytes.* PLoS One, 2014. **9**(2): p. e89678.

305. Girard, M. and M. Goossens, *Sumoylation of the SOX10 transcription factor regulates its transcriptional activity.* FEBS Lett, 2006. **580**(6): p. 1635-41.

306. Fukuda, I., et al., *Ginkgolic acid inhibits protein SUMOylation by blocking formation of the E1-SUMO intermediate.* Chem Biol, 2009. **16**(2): p. 133-40.

307. Kawasaki, H., et al., *Induction of midbrain dopaminergic neurons from ES cells by stromal cell-derived inducing activity.* Neuron, 2000. **28**(1): p. 31-40.

308. Wichterle, H., et al., *Directed Differentiation of Embryonic Stem Cells into Motor Neurons.* Cell, 2002. **110**(3): p. 385-397.

309. Rhinn, M. and P. Dolle, *Retinoic acid signalling during development.* Development, 2012. **139**(5): p. 843-58.

310. Osakada, F., et al., *In vitro differentiation of retinal cells from human pluripotent stem cells by small-molecule induction.* J Cell Sci, 2009. **122**(Pt 17): p. 3169-79.

311. Grande, A., et al., *Environmental impact on direct neuronal reprogramming in vivo in the adult brain.* Nat Commun, 2013. **4**: p. 2373.

312. Davila, J., et al., *Acute reduction in oxygen tension enhances the induction of neurons from human fibroblasts.* J Neurosci Methods, 2013. **216**(2): p. 104-9.

313. Bortone, D. and F. Polleux, *KCC2 expression promotes the termination of cortical interneuron migration in a voltage-sensitive calcium-dependent manner.* Neuron, 2009. **62**(1): p. 53-71.

314. Spitzer, N.C., L.N. Borodinsky, and C.M. Root, *Homeostatic activity-dependent paradigm for neurotransmitter specification.* Cell Calcium, 2005. **37**(5): p. 417-423.

315. Deisseroth, K., et al., *Excitation-neurogenesis coupling in adult neural stem/progenitor cells.* Neuron, 2004. **42**(4): p. 535-52.

316. Aumann, T. and M. Horne, *Activity-dependent regulation of the dopamine phenotype in substantia nigra neurons.* J Neurochem. **121**(4): p. 497-515.

317. He, X.B., et al., *Prolonged membrane depolarization enhances midbrain dopamine neuron differentiation via epigenetic histone modifications.* Stem Cells. **29**(11): p. 1861-73.

318. Franklin, J.L. and E.M. Johnson, Jr., *Suppression of programmed neuronal death by sustained elevation of cytoplasmic calcium.* Trends Neurosci, 1992. **15**(12): p. 501-8.

319. Oppenheim, R.W., *Cell death during development of the nervous system.* Annual review of neuroscience, 1991. **14**(1): p. 453-501.

320. Baker, R.E., J.M. Ruijter, and D. Bingmann, *Elevated potassium prevents neuronal death but inhibits network formation in neocortical cultures.* Int J Dev Neurosci, 1991. **9**(4): p. 339-45.

321. KoIKE, T., D.P. Martin, and E.M. Johnson, *Role of Ca2+ channels in the ability of membrane depolarization to prevent neuronal death induced by trophic-factor deprivation: evidence that levels of internal Ca2+ determine nerve growth factor dependence of sympathetic ganglion cells.* Proceedings of the National Academy of Sciences, 1989. **86**(16): p. 6421-6425.

322. Collins, F. and J.D. Lile, *The role of dihydropyridine-sensitive voltage-gated calcium channels in potassium-mediated neuronal survival.* Brain research, 1989. **502**(1): p. 99-108.

323. Michel, P.P. and Y. Agid, *Chronic activation of the cyclic AMP signaling pathway promotes development and long-term survival of mesencephalic dopaminergic neurons.* J Neurochem, 1996. **67**(4): p. 1633-42.

324. Johnson Jr, E.M., T. Koike, and J. Franklin, *A "calcium set-point hypothesis" of neuronal dependence on neurotrophic factor.* Experimental Neurology, 1992. **115**(1): p. 163-166.

325. Song, B., et al., *Inhibitory phosphorylation of GSK-3 by CaMKII couples depolarization to neuronal survival.* J Biol Chem, 2010. **285**(52): p. 41122-34.

326. Elmi, M., et al., *Mechanism of MASH1 induction by ASK1 and ATRA in adult neural progenitors.* Mol Cell Neurosci, 2007. **36**(2): p. 248-59.

327. Downing, T.L., et al., *Biophysical regulation of epigenetic state and cell reprogramming.* Nat Mater, 2013. **12**(12): p. 1154-62.

328. Hsieh, J., et al., *Histone deacetylase inhibition-mediated neuronal differentiation of multipotent adult neural progenitor cells.* Proc Natl Acad Sci U S A, 2004. **101**(47): p. 16659-64.

329. Pan, F., et al., *Topographic effect on human induced pluripotent stem cells differentiation towards neuronal lineage.* Biomaterials, 2013. **34**(33): p. 8131-9.

330. Purcell, E.K., et al., *Combining topographical and genetic cues to promote neuronal fate specification in stem cells.* Biomacromolecules, 2012. **13**(11): p. 3427-38.

331. Yim, E.K., et al. *Effect of Spatial Arrangement of Substrate Topography on Neuronal Differentiation of Stem Cells*. in *The 15th International Conference on Biomedical Engineering*. 2014: Springer.

332. Christopherson, G.T., H. Song, and H.-Q. Mao, *The influence of fiber diameter of electrospun substrates on neural stem cell differentiation and proliferation.* Biomaterials, 2009. **30**(4): p. 556-564.

333. Gertz, C.C., et al., *Accelerated neuritogenesis and maturation of primary spinal motor neurons in response to nanofibers.* Developmental neurobiology, 2010. **70**(8): p. 589-603.

334. Hynes, R.O., *The extracellular matrix: not just pretty fibrils.* Science, 2009. **326**(5957): p. 1216-1219.

335. Nakajima, M., et al., *Combinatorial protein display for the cell-based screening of biomaterials that direct neural stem cell differentiation.* Biomaterials, 2007. **28**(6): p. 1048-1060.

336. Chen, Y.C., et al., *Induction and regulation of differentiation in neural stem cells on ultra-nanocrystalline diamond films.* Biomaterials, 2010. **31**(21): p. 5575-87.

337. Du, J., et al., *Integrin activation and internalization on soft ECM as a mechanism of induction of stem cell differentiation by ECM elasticity.* Proceedings of the National Academy of Sciences, 2011. **108**(23): p. 9466-9471.

338. Delcroix, G.J., et al., *Adult cell therapy for brain neuronal damages and the role of tissue engineering.* Biomaterials. **31**(8): p. 2105-20.

339. Rodnitzky, R.L., *Upcoming treatments in Parkinson's disease, including gene therapy.* Parkinsonism Relat Disord, 2012. **18 Suppl 1**: p. S37-40.

340. Feng, R., et al., *PU.1 and C/EBPalpha/beta convert fibroblasts into macrophage-like cells.* Proc Natl Acad Sci U S A, 2008. **105**(16): p. 6057-62.

341. Kajimura, S., et al., *Initiation of myoblast to brown fat switch by a PRDM16-C/EBP-beta transcriptional complex.* Nature, 2009. **460**(7259): p. 1154-8.

342. Ieda, M., et al., *Direct Reprogramming of Fibroblasts into Functional Cardiomyocytes by Defined Factors.* Cell, 2010. **142**(3): p. 375-386.

343. Sekiya, S. and A. Suzuki, *Direct conversion of mouse fibroblasts to hepatocyte-like cells by defined factors.* Nature, 2011. **475**(7356): p. 390-3.

344. Huang, P., et al., *Induction of functional hepatocyte-like cells from mouse fibroblasts by defined factors.* Nature, 2011. **475**(7356): p. 386-9.

345. Cim, A., et al., *In vivo studies on non-viral transdifferentiation of liver cells towards pancreatic beta cells.* J Endocrinol, 2012.

346. Roessler, R., E. Boddeke, and S. Copray, *Induced Pluripotent Stem Cell Technology and Direct Conversion: New Possibilities to Study and Treat Parkinson's Disease.* Stem Cell Rev.

347. Brennand, K.J. and F.H. Gage, *Modeling psychiatric disorders through reprogramming.* Dis Model Mech. **5**(1): p. 26-32.

348. Montserrat, N., et al., *Simple Generation of Human Induced Pluripotent Stem Cells Using Poly-beta-amino Esters As the Non-viral Gene Delivery System.* Journal of Biological Chemistry, 2011. **286**(14).

349. Lee, C.H., et al., *The generation of iPS cells using non-viral magnetic nanoparticle based transfection.* Biomaterials, 2011. **32**(28): p. 6683-6691.

350. Okita, K., et al., *Generation of Mouse Induced Pluripotent Stem Cells Without Viral Vectors.* Science, 2008. **322**(5903): p. 949-953.

351. Jia, F., et al., *A nonviral minicircle vector for deriving human iPS cells.* Nat Methods, 2010. **7**(3): p. 197-9.

352. Nathanson, J.L., et al., *Preferential labeling of inhibitory and excitatory cortical neurons by endogenous tropism of adeno-associated virus and lentivirus vectors.* Neuroscience, 2009. **161**(2): p. 441-50.

353. Lin, C., et al., *Novel bioreducible poly(amido amine)s for highly efficient gene delivery.* Bioconjug Chem, 2007. **18**(1): p. 138-45.

354. Wheeler, D.G. and E. Cooper, *Depolarization strongly induces human cytomegalovirus major immediate-early promoter/enhancer activity in neurons.* Journal of Biological Chemistry, 2001. **276**(34): p. 31978-85.

355. Kugler, S., E. Kilic, and M. Bahr, *Human synapsin 1 gene promoter confers highly neuron-specific long-term transgene expression from an adenoviral vector in the adult rat brain depending on the transduced area.* Gene Ther, 2003. **10**(4): p. 337-47.

356. Hioki, H., et al., *Efficient gene transduction of neurons by lentivirus with enhanced neuron-specific promoters.* Gene Ther, 2007. **14**(11): p. 872-82.

357. Jordan, M. and F.M. Wurm, *Co-transfer of multiple plasmids/viruses as an attractive method to introduce several genes in mammalian cells*, in *New Comprehensive Biochemistry*, S.C. Makrides, Editor. 2003, Elsevier. p. 337-348.

358. Vierbuchen, T. and M. Wernig, *Direct lineage conversions: unnatural but useful?* Nat Biotechnol, 2011. **29**(10): p. 892-907.

359. Yang, N., et al., *Induced Neuronal Cells: How to Make and Define a Neuron.* Cell Stem Cell, 2011. **9**(6): p. 517-525.

360. Citri, A., et al., *Comprehensive qPCR profiling of gene expression in single neuronal cells.* Nat Protoc, 2012. **7**(1): p. 118-27.

361. Kaji, K., et al., *Virus-free induction of pluripotency and subsequent excision of reprogramming factors.* Nature, 2009. **458**(7239): p. 771-U112.

362. Bormuth, I., et al., *Neuronal Basic Helix–Loop–Helix Proteins Neurod2/6 Regulate Cortical Commissure Formation before Midline Interactions.* The Journal of neuroscience, 2013. **33**(2): p. 641-651.

363. Lauret, E. and R. Baserga, *Inhibition of gene expression at the translational level by cotransfection with competitor plasmids.* DNA, 1988. **7**(3): p. 151-6.

364. Ladewig, J., et al., *Small molecules enable highly efficient neuronal conversion of human fibroblasts.* Nat Methods, 2012.

365. Seko, Y., et al., *Derivation of human differential photoreceptor-like cells from the iris by defined combinations of CRX, RX and NEUROD.* PLoS One, 2012. **7**(4): p. e35611.

366. Liu, X., et al., *Direct reprogramming of human fibroblasts into dopaminergic neuron-like cells.* Cell Res, 2011. **22**(2): p. 321-32.

367. Ladewig, J., et al., *Small molecules enable highly efficient neuronal conversion of human fibroblasts.* Nat Methods.

368. Chambers, S.M., et al., *Highly efficient neural conversion of human ES and iPS cells by dual inhibition of SMAD signaling.* Nature Biotechnology, 2009. **27**(3): p. 275-280.

369. Mak, S.K., et al., *Small molecules greatly improve conversion of human-induced pluripotent stem cells to the neuronal lineage.* Stem Cells Int, 2012. **2012**: p. 140427.

370. Becker, D., et al., *Functional electrical stimulation helps replenish progenitor cells in the injured spinal cord of adult rats.* Experimental Neurology, 2010. **222**(2): p. 211-218.

371. Mennerick, S. and C.F. Zorumski, *Neural activity and survival in the developing nervous system.* Mol Neurobiol, 2000. **22**(1-3): p. 41-54.

372. Dulcis, D., et al., *Neurotransmitter switching in the adult brain regulates behavior.* Science, 2013. **340**(6131): p. 449-53.

373. Cho, A., et al., *Calcineurin Signaling Regulates Neural Induction through Antagonizing the BMP Pathway.* Neuron, 2014. **82**(1): p. 109-124.

374. Liedtke, W., et al., *Highly conductive carbon nanotube matrix accelerates developmental chloride extrusion in central nervous system neurons by increased expression of chloride transporter KCC2.* Small, 2013. **9**(7): p. 1066-75.

375. Chambers, S.M., et al., *Highly efficient neural conversion of human ES and iPS cells by dual inhibition of SMAD signaling.* Nat Biotechnol, 2009. **27**(3): p. 275-80.

376. Chen, Z.-L., J.A. Indyk, and S. Strickland, *The hippocampal laminin matrix is dynamic and critical for neuronal survival.* Molecular Biology of the Cell, 2003. **14**(7): p. 2665-2676.

377. Szymczak, A.L. and D.A.A. Vignali, *Development of 2A peptide-based strategies in the design of multicistronic vectors.* Expert Opinion on Biological Therapy, 2005. **5**(5): p. 627-638.

378. Szymczak-Workman, A.L., K.M. Vignali, and D.A. Vignali, *Design and construction of 2A peptide-linked multicistronic vectors.* Cold Spring Harb Protoc. **2012**(2): p. 199-204.

379. Carey, B.W., et al., *Reprogramming of murine and human somatic cells using a single polycistronic vector.* Proceedings of the National Academy of Sciences, 2009. **106**(1): p. 157-162.

380. Pang, Z.P., et al., *Induction of human neuronal cells by defined transcription factors.* Nature, 2011
476(7359): p. 220-223.

381. Chen, H., et al., *Induced DNA demethylation by targeting Ten-Eleven Translocation 2 to the human ICAM-1 promoter.* Nucleic Acids Res, 2014. **42**(3): p. 1563-74.

382. de Groote, M.L., P.J. Verschure, and M.G. Rots, *Epigenetic Editing: targeted rewriting of epigenetic marks to modulate expression of selected target genes.* Nucleic Acids Res, 2012. **40**(21): p. 10596-613.

383. Kulangara, K., et al., *The effect of substrate topography on direct reprogramming of fibroblasts to induced neurons.* Biomaterials, 2014.

384. Konsavage, W.M., Jr. and G.S. Yochum, *Intersection of Hippo/YAP and Wnt/beta-catenin signaling pathways.* Acta Biochim Biophys Sin (Shanghai), 2013. **45**(2): p. 71-9.

385. Chakraborty, S., et al., *Electrohydrodynamics: A facile technique to fabricate drug delivery systems.* Advanced Drug Delivery Reviews, 2009. **61**(12): p. 1043-1054.

386. Yang, Y., et al., *Neurotrophin releasing single and multiple lumen nerve conduits.* J Control Release, 2005. **104**(3): p. 433-46.

387. De Laporte, L. and L.D. Shea, *Matrices and scaffolds for DNA delivery in tissue engineering.* Advanced Drug Delivery Reviews, 2007. **59**(4-5): p. 292-307.

388. Lovmand, J., et al., *The use of combinatorial topographical libraries for the screening of enhanced osteogenic expression and mineralization.* Biomaterials, 2009. **30**(11): p. 2015-2022.

389. Riedl, J., et al., *Lifeact mice for studying F-actin dynamics.* Nat Meth. **7**(3): p. 168-169.

390. Edlund, M., M.A. Lotano, and C.A. Otey, *Dynamics of alpha-actinin in focal adhesions and stress fibers visualized with alpha-actinin-green fluorescent protein.* Cell Motility and the Cytoskeleton, 2001. **48**(3): p. 190-200.

391. Yim, E.K., S.W. Pang, and K.W. Leong, *Synthetic nanostructures inducing differentiation of human mesenchymal stem cells into neuronal lineage.* Exp Cell Res, 2007. **313**(9): p. 1820-9.

392. Kong, H.J., et al., *Non-viral gene delivery regulated by stiffness of cell adhesion substrates.* Nat Mater, 2005. **4**(6): p. 460-464.

393. Kong, H.J., S. Hsiong, and D.J. Mooney, *Nanoscale Cell Adhesion Ligand Presentation Regulates Nonviral Gene Delivery and Expression.* Nano Letters, 2006. **7**(1): p. 161-166.

394. Bailey, S.N., R.Z. Wu, and D.M. Sabatini, *Applications of transfected cell microarrays in high-throughput drug discovery.* Drug Discov Today, 2002. **7**(18 Suppl): p. S113-8.

395. Sher, I., et al., *Targeting perlecan in human keratinocytes reveals novel roles for perlecan in epidermal formation.* J Biol Chem, 2006. **281**(8): p. 5178-87.

396. Hayashi, K., J.A. Madri, and P.D. Yurchenco, *Endothelial-Cells Interact with the Core Protein of Basement-Membrane Perlecan through Beta-1 and Beta-3 Integrins - an Adhesion Modulated by Glycosaminoglycan.* Journal of Cell Biology, 1992. **119**(4): p. 945-959.

397. Kopatz, I., J.S. Remy, and J.P. Behr, *A model for non-viral gene delivery: through syndecan adhesion molecules and powered by actin.* J Gene Med, 2004. **6**(7): p. 769-76.

398. Memmo, L.M. and P. McKeown-Longo, *The alpha v beta 5 integrin functions as an endocytic receptor for vitronectin.* Journal of Cell Science, 1998. **111**: p. 425-433.

399. Panetti, T.S., et al., *Alpha(V)Beta(5) Integrin Receptor-Mediated Endocytosis of Vitronectin Is Protein-Kinase C-Dependent.* Journal of Biological Chemistry, 1995. **270**(31): p. 18593-18597.

400. Paris, S., A. Burlacu, and Y. Durocher, *Opposing roles of syndecan-1 and syndecan-2 in polyethyleneimine-mediated gene delivery.* J Biol Chem, 2008. **283**(12): p. 7697-704.

401. McQuade, K.J., et al., *Syndecan-1 regulates alphavbeta5 integrin activity in B82L fibroblasts.* J Cell Sci, 2006. **119**(Pt 12): p. 2445-56.

402. Beauvais, D.M. and A.C. Rapraeger, *Syndecan-1-mediated cell spreading requires signaling by alphavbeta3 integrins in human breast carcinoma cells.* Exp Cell Res, 2003. **286**(2): p. 219-32.

403. Smith, R.A. and T.D. Giorgio, *Quantitation and kinetics of CD51 surface receptor expression: Implications for targeted delivery.* Annals of Biomedical Engineering, 2004. **32**(5): p. 635-644.

404. Kolind, K., et al., *A combinatorial screening of human fibroblast responses on micro-structured surfaces.* Biomaterials. **31**(35): p. 9182-9191.

405. Liu, Z., et al., *The tumourigenicity of iPS cells and their differentiated derivates.* J Cell Mol Med, 2013. **17**(6): p. 782-91.

406. Liu, J., et al., *Epigenetic modifiers are necessary but not sufficient for reprogramming non-myelinating cells into myelin gene-expressing cells.* PLoS One, 2010. **5**(9): p. e13023.

407. Sun, T., et al., *Cross-repressive interaction of the Olig2 and Nkx2.2 transcription factors in developing neural tube associated with formation of a specific physical complex.* J Neurosci, 2003. **23**(29): p. 9547-56.

408. Zhou, Q., G. Choi, and D.J. Anderson, *The bHLH transcription factor Olig2 promotes oligodendrocyte differentiation in collaboration with Nkx2.2.* Neuron, 2001. **31**(5): p. 791-807.

409. Castro, D.S., et al., *A novel function of the proneural factor Ascl1 in progenitor proliferation identified by genome-wide characterization of its targets.* Genes Dev, 2011. **25**(9): p. 930-45.

410. Imayoshi, I., et al., *Oscillatory control of factors determining multipotency and fate in mouse neural progenitors.* Science, 2013. **342**(6163): p. 1203-8.

411. Deloulme, J.C., et al., *Nuclear expression of S100B in oligodendrocyte progenitor cells correlates with differentiation toward the oligodendroglial lineage and modulates oligodendrocytes maturation.* Molecular and Cellular Neuroscience, 2004. **27**(4): p. 453-465.

412. Rehberg, S., et al., *Sox10 is an active nucleocytoplasmic shuttle protein, and shuttling is crucial for Sox10-mediated transactivation.* Molecular and cellular biology, 2002. **22**(16): p. 5826-5834.

413. Wang, Y., et al., *Reprogramming of mouse and human somatic cells by high-performance engineered factors.* EMBO Rep, 2011. **12**(4): p. 373-8.

414. Lee, S., et al., *A culture system to study oligodendrocyte myelination processes using engineered nanofibers.* Nature methods, 2012. **9**(9): p. 917-922.

Biography

Andrew Adler was born on March 22, 1986, in St. Louis Park, Minnesota. He spent the first 18 years of life in Fridley, MN, where he was a: public school student, fisherman, trumpet/football/baseball player, unlicensed freelance pyrotechnicist, preschool soccer coach, busboy, and paid puppeteer. In 2004 Andrew enrolled in the Biomedical Engineering undergraduate program at Northwestern University in Evanston, IL, where he worked with Prof. Lonnie Shea to develop implantable bioerodible gene-eluting polyester scaffolds for spinal cord regeneration. While at Northwestern, Andrew also interned at Medtronic, Inc., in the implantable intrathecal infusion systems group, and visited Prof. Balaji Narasimhan's lab at Iowa State University in Ames, IA, to develop a high-throughput polyanhydride synthesis and biological characterization system. Andrew graduated from Northwestern in 2008, *summa cum laude*, and joined Prof. Kam Leong's lab as a PhD student in The Department of Biomedical Engineering at Duke University in Durham, NC. His doctoral research focused on the development of efficient virus-free methods to directly reprogram fibroblasts to functional neurons. While at Duke, Andrew visited Prof. Kristin Baldwin's lab at The Scripps Research Institute in La Jolla, CA, where he supported various direct neuronal reprogramming efforts to deepen his knowledge of neurobiology. After graduation, he plans to build on his love for neuroengineering and neuroscience as a postdoctoral researcher, or become a semi-professional surfer.